

STIMULI RESPONSIVE FUNCTIONAL POLYMERIC MATERIALS FOR
BIOMEDICAL APPLICATIONS

by

Hatice Betül Bingöl

B.S., Chemistry, Boğaziçi University, 2010

M.S., Chemistry, Boğaziçi University, 2012

Submitted to the Institute for Graduate Studies in
Science and Engineering in partial fulfillment of
the requirements for the degree of
Doctor of Philosophy

Graduate Program in Chemistry

Boğaziçi University

2019

Dedicated to my beloved daughter Zeynep Ece

ACKNOWLEDGEMENTS

Firstly I would wish to express my sincere gratitude to my thesis supervisor Prof. Duygu Avcı Semiz for her endless attention, encouraging attitude, scientific guidance and support throughout this work. It was a great pleasure to complete my thesis under her supervision.

I would like to express my thanks to Assoc. Prof. Funda Yağcı Acar, Prof. Seda Kızılel and Prof. Oğuz Okay for their valuable discussions and recommendations regarding my research. I would wish to extend my thanks to the members of my examining comitee Prof. İlknur Doğan, Assoc. Prof. Gökhan Çaylı, Assoc. Prof Funda Yağcı Acar and Assoc. Prof. Ersin Acar for their careful and constructive review of the final manuscript of the thesis.

I am so much thankful to my current and former labmates Seçkin, Tuğçe, Melek, Türkan, Aylin, Miraç, Sesil, Ece, Fulya and Belgin for their intimate friendship, support and sharing the joy of making research. I would also like to thank all the members of the faculty in my department.

I would also like to thank Dr. Ayla Türkekul Bıyık, Dr. Bilge Gedik Uluocak , Dr. Barış Yağcı and Dr. Ümit Gülyüz for structural characterization of my samples through NMR, SEM, Raman spectroscopy and rheometry; Dr. Fatma Demir Duman, Assist. Prof. Ayşe Ak, Dr. Tuğba Bal and Dilem Ceren Oran for their contribution in mineralization, cytotoxicity and photodynamic therapy studies.

Last but not least, my deepest thanks go to my family for their love and support. I am grateful to my father who arised the question “Why?” in my mind during my early childhood, which made me curious about life and nature, and opened my way to pursue a career as a scientist. My mother is my first teacher who always supported me with her generous love and dedicated so much for me during all my life. I owe thanks to a very special person, my

husband, for his endless love, support and understanding. He was there standing by me during all happy or hard moments whenever I need him. And my lovely daughter Zeynep Ece shining so bright, always gave me joy and happiness throughout this journey.

I acknowledge The Scientific and Technological Research Council of Turkey (TUBITAK-BIDEB) for financial support through graduate student scholarship programme and The Council of Higher Education (YÖK) for giving financial support for research and scientific activities through ÖYP Programme. I also acknowledge financial support of Boğaziçi University Research Fund (BAP-13842).

ABSTRACT

STIMULI RESPONSIVE FUNCTIONAL POLYMERIC MATERIALS FOR BIOMEDICAL APPLICATIONS

This work consists of synthesis, structural characterization and evaluation of stimuli-responsive functional polymers and hydrogels designed for biomedical applications. In the first project pH and redox responsive degradable gels and cryogels were synthesized from phosphonate-functionalized poly(β -aminoester) macromers as potential materials for tissue engineering applications. Then injectable poly(β -aminoester) based hydrogels were fabricated by a facile one-step method and a photosensitizer released from these hydrogels showed promising activity in photodynamic therapy. Phosphonic acid containing acrylamides were synthesized and evaluated as self-etching dental adhesives. Furthermore, these acrylamides were used to make hydrogels which were then successfully mineralized to make bone-like composite materials. Lastly carboxylic acid-functional crosslinkers were fabricated into hydrogels, and the pH/redox response of these hydrogels were demonstrated through controlled release studies of R6G dye and resorcinol.

ÖZET

BİYOMEDİKAL UYGULAMALAR İÇİN ETKİ-DUYARLI FONKSİYONLANDIRILMIŞ POLİMERİK MALZEMELER

Bu çalışma biyomedikal uygulamalar için tasarlanan etki-duyarlı fonksiyonel polimer ve hidrojellerin sentezi, yapısal karakterizasyonu ve değerlendirmesinden oluşmaktadır. İlk bölümde doku mühendisliği uygulamaları için potansiyel malzemeler olan pH ve redoks duyarlı bozunabilir jeller ve kriyojeller fosfonat-fonksiyonlandırılmış poli(β -aminoester) makromerler kullanılarak sentezlenmiştir. İkinci bölümde enjekte edilebilir poli(β -aminoester) hidrojeller tek basamaklı basit bir metod ile üretilmiş ve bu hidrojellerden salımı gerçekleşen ışıkduyarlı bir molekül fotodinamik terapide umut verici bir etki göstermiştir. Üçüncü bölümde dental yapıştırıcı olarak tasarlanan fosfonik asit-fonksiyonlandırılmış akrilamit monomerleri sentezlenmiş ve özellikleri incelenmiştir. Ayrıca bu monomerlerden elde edilen hidrojeller başarılı bir şekilde mineralize olarak kemik benzeri kompozit malzemeler oluşturmuştur. Son olarak karboksilik asit-fonksiyonlandırılmış çapraz bağlayıcılar sentezlenerek hidrojel yapımında kullanılmıştır. Bu hidrojellerin pH ve redoks duyarlılığı R6G ve resorcinol moleküllerinin kontrollü salım çalışmaları ile gösterilmiştir.

TABLE OF CONTENTS

ABSTRACT.....	vi
ÖZET	vii
TABLE OF CONTENTS.....	viii
LIST OF FIGURES	xiii
LIST OF TABLES	xx
LIST OF SYMBOLS	xxi
LIST OF ACRONYMS/ABBREVIATIONS	xxii
1. INTRODUCTION	1
1.1. Polymers and Hydrogels for Biomedical Applications	1
1.1.1. Drug Delivery Applications.....	2
1.1.2. Tissue Engineering Applications	8
1.1.3. Gene Delivery Applications.....	10
1.1.4. Dental Applications	12
1.2. Stimuli Responsive Polymers and Hydrogels.....	14
1.2.1 pH Responsive Systems.....	15
1.2.2. Redox Responsive Systems	17
1.2.3. Thermoresponsive Systems	18
1.2.4. Multiple Responsive Systems.....	20
1.3. Poly(β -amino ester)s for Biomedical Applications	23
1.3.1. PBAEs for Tissue Engineering Applications.....	24
1.3.2. PBAEs for Gene Delivery Applications	27
1.3.3. PBAEs for Drug Delivery Applications	31
1.4. (Bis)phosphonate/(Bis)phosphonic Acid Functionalized Biomaterials.....	35
1.4.1. Bone Targeted Drug Delivery Applications	35

1.4.2. Bone Tissue Engineering Applications.....	39
1.4.3. Dental Applications	42
2. OBJECTIVES AND SCOPE.....	45
3. REDOX-RESPONSIVE PHOSPHONATE-FUNCTIONALIZED POLY(β -AMINO ESTER) GELS AND CRYOGELS	46
3.1. Introduction.....	46
3.2. Experimental.....	47
3.2.1. Materials and Methods.....	47
3.2.2. Synthesis of Phosphonate-Functionalized Diamines	48
3.2.2.1. Synthesis of tetraethyl ((hexane-1,6-diylbis(azanediyl))bis(ethane- 2,1-diyl))bis(phosphonate) (A1).	48
3.2.2.2. Synthesis of tetraethyl (((disulfanediylbis(ethane-2,1- diyl))bis(azanediyl)) bis(ethane-2,1-diyl))bis(phosphonate) (A2).	48
3.2.3. Synthesis of PBAE Macromers	49
3.2.4. pH Sensitivity of PBAE Macromer	49
3.2.5. Synthesis of PBAE Gels	49
3.2.6. Synthesis of PBAE Cryogels	50
3.2.7. SEM Characterization.....	50
3.2.8. Swelling Studies	51
3.2.9. Degradation Studies	51
3.2.10. <i>In vitro</i> Cytotoxicity Assay.....	52
3.2.11. Statistical Analysis.....	52
3.3. Results and Discussion	53
3.3.1. Synthesis of Phosphonate-Functionalized Diamines	53
3.3.2. Synthesis and Characterization of Poly(β -amino ester) Macromers	56
3.3.3. Synthesis of PBAE Gels and Cryogels	60
3.3.4. Swelling Studies	63

3.3.5. Degradation Studies	64
3.3.6. <i>In Vitro</i> Cytotoxicity of Polymer Degradation Products	70
3.4. Conclusions.....	71
4. ONE-STEP INJECTABLE AND BIOREDUCIBLE POLY(β -AMINO ESTER) HYDROGELS AS CONTROLLED DRUG DELIVERY PLATFORMS.....	72
4.1. Introduction.....	72
4.2. Experimental.....	75
4.2.1. Materials and Methods.....	75
4.2.2. One-step Synthesis of PBAE Hydrogels	76
4.2.3. One-step Synthesis of Drug Loaded PBAE Hydrogels	76
4.2.4. Rheological Experiments	77
4.2.5. Swelling Studies	77
4.2.6. Degradation of Hydrogels.....	78
4.2.7. <i>In Vitro</i> Release Studies.....	78
4.2.8. Determination of <i>In Vitro</i> Cytotoxicity and PDT Studies	78
4.2.9. Statistical Analysis.....	79
4.3. Results and Discussion	80
4.3.1. One-Step Synthesis and Characterization of PBAE Hydrogels.....	80
4.3.2. Swelling and Degradation Studies	85
4.3.3. Redox Response.....	87
4.3.4. Drug Loading and <i>in vitro</i> Release Studies	88
4.3.5. <i>In Vitro</i> Cytotoxicity and Photodynamic Therapy.....	90
4.4. Conclusions.....	94
5. MINERALIZED HYDROGELS AND DENTAL ADHESIVES FROM PHOSPHONIC ACID-FUNCTIONALIZED ACRYLAMIDES.....	95
5.1. Introduction.....	95
5.2. Experimental.....	97

5.2.1. Materials and Methods.....	97
5.2.2. Synthesis of Monomers	98
5.2.2.1. Diethyl acrylamidomethylphosphonate (1).	98
5.2.2.2. Diethyl 2-acrylamidobutan-2-ylphosphonate (2).....	98
5.2.2.3. Diethyl 2-acrylamidooctan-2-ylphosphonate (3).....	99
5.2.2.4. Diethyl acrylamidomethylphosphonic acid (1a).....	99
5.2.2.5. Diethyl 2-acrylamidobutan-2-ylphosphonic acid (2a).....	99
5.2.2.6. Diethyl 2-acrylamidooctan-2-ylphosphonic acid (3a).	100
5.2.3. Interactions of Monomers with Hydroxyapatite	100
5.2.4. Hydrolytic Stability.....	100
5.2.5. Photopolymerizations	101
5.2.6. Synthesis of Hydrogels	101
5.2.7. Swelling Studies	102
5.2.8. Cell Viability on Hydrogels	102
5.2.9. Mineralization of Hydrogels.....	103
5.2.10. Characterization of Mineralized Hydrogels.....	103
5.2.11.1. SEM-EDX.....	103
5.2.11.2. Determination of Ca ²⁺ Content.	103
5.3. Results and Discussion	104
5.3.1. Synthesis and Characterization of Monomers	104
5.3.2. Acidity, Interactions with HAP, and Stability of Acid Monomers.....	108
5.3.3. Photopolymerizations	111
5.3.4. Synthesis, Characterization and Mineralization of Hydrogels	113
5.4. Conclusions.....	118
6. STIMULI RESPONSIVE HYDROGELS FROM CARBOXYLIC ACID- FUNCTIONALIZED CROSSLINKERS	120
6.1. Introduction.....	120

6.2. Experimental.....	121
6.2.1. Materials and Methods.....	121
6.2.2. Synthesis of Monomers	122
6.2.2.1. Monomer 1.....	122
6.2.2.2. Monomer 1a.....	123
6.2.3. Titration Studies.....	123
6.2.4. Photopolymerization Studies	123
6.2.5. Synthesis of Hydrogels	124
6.2.6. Rheology Studies	125
6.2.7. Swelling Studies	125
6.2.8. Degradation of Hydrogels.....	126
6.2.9. Dye Loading and Release Studies of H3a Hydrogels.....	127
6.2.10. Cell Viability on Hydrogels	127
6.3. Results and Discussion	128
6.3.1. Synthesis and Characterization of Monomers	128
6.3.2. Photopolymerizations	131
6.3.3. Synthesis and Characterization of Hydrogels.....	134
6.3.4. Swelling Studies	136
6.3.5. Degradation of Hydrogels.....	138
6.3.6. Dye Loading and Release Studies	141
6.3.7. Cell Viability on Hydrogels	144
6.4. Conclusions.....	144
7. CONCLUDING REMARKS.....	146
REFERENCES	148

LIST OF FIGURES

Figure 1.1.	Polymers and hydrogels for biomedical applications.....	1
Figure 1.2.	Structure of polymer chains and hydrogels.	2
Figure 1.3.	Model of polymer based drug delivery.	3
Figure 1.4.	Structure of polymers used for controlled drug delivery.	4
Figure 1.5.	Multiscale properties of hydrogels for controlled drug delivery.....	6
Figure 1.6.	Mechanisms of drug release from hydrogels.	7
Figure 1.7.	Mouse with an engineered ear on its back.	8
Figure 1.8.	Process of tissue engineering.	10
Figure 1.9.	Gene transfection mechanism.	11
Figure 1.10.	Components of self-etching enamel-dentin adhesives.....	12
Figure 1.11.	Components of self-etching enamel-dentin adhesives.....	13
Figure 1.12.	Internal and external triggers for controlled release of small molecules from polymers or hydrogels.....	14
Figure 1.13.	pH responsive hydrogels.	15
Figure 1.14.	pH responsive hybrid nano/hydrogel.	16
Figure 1.15.	Reduction of disulfide linkages by glutathione.	17
Figure 1.16.	Temperature dependant transition change of a polymer in aqueous environment.	19
Figure 1.17.	Temperature/redox dual responsive hydrogel.	21

Figure 1.18.	pH/redox dual responsive hydrogel.....	21
Figure 1.19.	Insulin loaded pH/temperature dual responsive polymers and hydrogels..	22
Figure 1.20.	Synthesis of poly(β -aminoester)s.....	23
Figure 1.21.	Development and degradation of PBAE network polymers.	24
Figure 1.22.	Chemical structures of amines and diacrylates used for the development of the combinatorial library.	26
Figure 1.23.	Superelastic PBAE cryogels with ultralight weight.....	27
Figure 1.24.	Structure of highly branched PBAEs.	29
Figure 1.25.	Structure of photoresponsive PBAEs.....	30
Figure 1.26.	DOX/SQ-loaded PBAE micelles.....	32
Figure 1.27.	Hyaluronic acid coated PBAE nanoparticles.	34
Figure 1.28.	Dopamine functionalized PBAE microspheres.....	34
Figure 1.29.	Phosphonate and bisphosphonate based materials for biomedical applications.	35
Figure 1.30.	Structure of pyrophosphate and its synthetic analogue bisphosphonate. ...	36
Figure 1.31.	Design of bisphosphonate prodrugs.....	36
Figure 1.32.	Bisphosphonate containing nanoparticles.	37
Figure 1.33.	PEG-alendronate conjugates for bone targeted drug delivery.....	38
Figure 1.34.	Engineering of the cell membrane for bone targeting.	39
Figure 1.35.	Biomimetic mineralization of hydrogels.....	40
Figure 1.36.	Structure of phosphonic acid containing monomers used for tissue engineering applications.	41

Figure 1.37.	In situ forming hybrid hydrogels.....	42
Figure 1.38.	Structures of phosphonic acid based self-etching adhesive monomers.	43
Figure 1.39.	Adhesion-Decalcification concept.	44
Figure 3.1.	Synthesis of A1 and A2.....	53
Figure 3.2.	FTIR spectra of A1 and A2.	54
Figure 3.3.	¹ H-NMR spectra of A1 and A2.	55
Figure 3.4.	¹³ C-NMR and ³¹ P NMR spectra of A1 and A2.	55
Figure 3.5.	Structure of macromers A1-PEGDA, A2-PEGDA, A1-HDDA and A2-HDDA.....	56
Figure 3.6.	¹ H NMR spectra of HDDA, A2 and the A2-HDDA macromer.....	58
Figure 3.7.	¹ H NMR spectra of the A1-PEGDA and A1-HDDA macromers.	58
Figure 3.8.	FTIR spectra of the A2-PEGDA and A2-HDDA macromers.....	59
Figure 3.9.	Titration curves of PBAE macromers.	60
Figure 3.10.	Synthesis of PBAE gels and cryogels.	61
Figure 3.11.	(a) Raman spectra and (b) DSC curves of PBAE gels.	62
Figure 3.12.	Water uptake profile of PBAE gels and cryogels.....	64
Figure 3.13.	Degradation behaviour of PBAE gels (a) in PBS, (b) in 25 mM DTT (Degradation % is determined at day 1 for A2-PEGDA and day 7 for A2-HDDA), (c) Images of A2-PEGDA in 25 mM DTT at 0 h, 2 h, 6 h and 24 h, (d) Degradation behaviour of PBAE cryogels in PBS.....	66
Figure 3.14.	(a) Degradation behaviour of PBAE cryogels in PBS (b) Degradation behaviour of mix-and-match A1-PEGDA:A1-HDDA cryogels in PBS. ..	68

Figure 3.15.	Representative SEM micrographs of PBAE gels (a) A1-PEGDA, (b) A1-PEGDA after 4h degradation, (c) A1-HDDA, (d) A1-HDDA after 3d degradation. Representative SEM micrographs of PBAE cryogels (e) A1-PEGDA, (f) A1-HDDA, (g) A2-PEGDA, (h) A2-HDDA.	69
Figure 3.16.	The effect of degradation products on cell viability of NIH 3T3 mouse embryonic fibroblast cells (a) and Saos-2 human osteosarcoma cells (b) Cells were treated with different concentrations of the products for 24 h The cell viability test was performed by MTT assay (\pm SD; n = 5; p < 0.05 compared with all concentrations)	70
Figure 4.1.	Design of one-step PBAE hydrogels.....	74
Figure 4.2.	One-step synthesis of H1 from the aza-Michael reaction of PEGDA and cystamine.	81
Figure 4.3.	(a, b) Storage modulus G' (filled symbols), loss modulus G'' (open symbols), and $\tan \delta$ (lines in b) as a function of the reaction time. The solid curves in (a) were calculated using equation (4.6). $\omega = 6.3$ rad/s. $\gamma_o = 0.01$ Temperature = 37 °C. (c) Frequency dependences of G' (filled symbol and G'' (open symbols) of H2 (triangles up) and H3 hydrogels (triangles down) at 37 °C. $\gamma_o = 0.01$	84
Figure 4.4.	(a) DSC profiles of the H1 and H2 hydrogels under nitrogen at a scanning rate of 10 °C/min, (b) Raman spectra of one-step PBAE hydrogels.....	84
Figure 4.5.	(a) pH dependent swelling profile of one-step PBAE hydrogels at pH 5 and pH 7.4, (b) pH dependent degradation profile of one-step PBAE hydrogels at pH 5 and pH 7.4. (Dry hydrogel thickness is 3 mm and dry hydrogel diameter is 8 mm).	86
Figure 4.6.	(a) Visual images of H1, H2 and H3 at the beginning and after 3 h and 6 h incubation in DTT at 37 °C. (b) Redox dependent degradation profiles of H1, H2 and H3 in PBS or DTT at 37 °C.	87

Figure 4.7.	SEM images of hydrogels before and after redox-triggered degradation a) H1 before degradation, b) H1 after 6 h degradation, c) H2 before degradation, d) H2 after 6 h degradation, e) H3 before degradation, f) H3 after 6 h degradation (Scale bar represents 50 μm).....	89
Figure 4.8.	pH-dependent release kinetics of MB from H1 and H2 at 37 °C and two different pH values.....	90
Figure 4. 9.	The effect of degradation products of the hydrogels on cell viability of MCF 7 human breast cancer cells. Cells were treated with different concentrations of the degradation products for 24 h. Untreated cells were used as the control. The cell viability test was performed by MTT assay ($\pm\text{SD}$; n = 5; p < 0.05 (*) compared with all concentrations).	91
Figure 4.10.	(a) The effect of released MB and degradation products on viability of A549 cells after 24 h exposure. Untreated cells were used as a control. (b) The effect of released MB and degradation products on cell viability of A549 cells after laser treatment (365 nm, 100 sec, 30 J/cm ²). Untreated cell were used as a control. Cells were not treated with MB- hydrogel degradation products but subjected to laser irradiation were used as the laser control. ($\pm\text{SD}$; n = 6; p < 0.05 (*) compared with all concentrations).....	93
Figure 5.1.	Phosphonic acid-functionalized acrylamides for fabrication of mineralized hydrogels and dental adhesive monomers.....	96
Figure 5.2.	Structure of monomers.	104
Figure 5.3.	Synthesis of α -aminophosphonates.....	105
Figure 5.4.	Synthesis of monomers.	107
Figure 5.5.	¹³ C NMR spectra of monomers 1 and 2.	107
Figure 5.6.	¹ H NMR spectra of monomers 1a and 2a.....	108

Figure 5.7.	FTIR spectra of (a) HAP, (b) HAP-2a/EtOH/H ₂ O (HAP phase), (c) 2a, (d) HAP-2a/EtOH/H ₂ O (solvent phase).....	110
Figure 5.8.	XRD patterns of HAP, MDP-HAP, 1a-HAP, 2a-HAP, and 3a-HAP.	110
Figure 5.9.	Rate-time and conversion-time plots for copolymerizations of 1a, 2a, and 3a with HEMA at 40 °C using BAPO.....	112
Figure 5.10.	Rate-time and conversion-time plots for copolymerizations of 1a, 2a, and 3a with GDMA and HEMA at 40 °C using DMPA.....	113
Figure 5.11.	Degree of swelling of H0, H1a, H2a, and H3a.....	115
Figure 5.12.	Viability of human dermal fibroblasts (20000/cm ²) on hydrogel scaffolds containing Ca ²⁺ binding sites.....	115
Figure 5.13.	SEM images of hydrogels (a) H1a, (b) H2a, (c) H3a, (d) mineralized H1a, (e) mineralized H2a, (f) mineralized H3a.	116
Figure 5.14.	(a) SEM image of mineralized H1a for EDX, (b) representative EDX spectra of H1a, (c) Ca deposition assay measured as the total Ca ²⁺ content in the mineralized hydrogels and expressed as µg of Ca/mg of dry gel weight.	118
Figure 6.1.	Synthesis of monomers.	129
Figure 6.2.	¹ H NMR spectra of 1 and 1a.	130
Figure 6.3.	¹³ C NMR spectra of 1 and 1a.	130
Figure 6.4.	FT-IR spectra of 1a.....	131
Figure 6.5.	Titration curve of 1a.	131
Figure 6.6.	Rate-time and conversion-time plots for the copolymerizations of (a) HEMA and 1a under nitrogen at 37 °C using DMPA (1 mol%), (b) HEMA with 1a in water under nitrogen at 37 °C using BAPO (1 mol%).	133

Figure 6.7.	Rate-time and conversion-time plots for copolymerizations of 1a with HEMA at 37 °C, 60 °C, 80 °C and 100 °C using DMPA.	134
Figure 6.8.	Fabrication of acid-functional pHEMA hydrogels.....	135
Figure 6.9.	Storage and loss moduli of hydrogels versus photopolymerization time for H1a-10%.	136
Figure 6.10.	Water uptake profile of hydrogels (a) H1a-10%, (b) H1a-30%, (c) H1a-50% in H ₂ O and (d) H1a-10% in CaCl ₂	138
Figure 6.11.	(a) Degradation of H1a-10% by 25 mM DTT at days 0, 1 and 6, (b) Relative mass of hydrogel during degradation (c) Raman spectra of H1a-10% before and after degradation with 25 mM DTT.	139
Figure 6.12.	SEM micrographs of (a) H1a-10%, (b) H1a-30%, (c) H1a-10% after 24h degradation with 25 mM DTT, b) H1a-30% after 6h degradation with 25 mM DTT (Scale bar represents 20 μm).	140
Figure 6.13.	(a) pH-sensitive, (b) redox sensitive release kinetics of R6G dye from H1a- 10% hydrogel, (c) redox sensitive release kinetics of resorcinol from H1a-10% and H1a-30% hydrogels.	143
Figure 6.14.	Viability of HUVECs on hydrogels.	144

LIST OF TABLES

Table 1.1.	Hydrogel based drug delivery systems used in clinic.	5
Table 3.1.	Solubility of A1 and A2 in selected solvents.	54
Table 3.2.	Solubility of PBAE macromers in selected solvents.	57
Table 3.3.	Properties of PBAE macromers.	59
Table 3.4.	Thermal properties of PBAE macromers and gels.	62
Table 4.1.	Properties of one step PBAE hydrogels.	82
Table 5.1.	Solubility of monomers.	107
Table 5.2.	Properties of hydrogels.	115
Table 6.1.	Solubility of monomers.	130
Table 6.2.	Properties of hydrogels.	136

LIST OF SYMBOLS

G'	Storage modulus
G''	Loss modulus
J	Coupling constant
M_n	Number average molecular weight
pH	Power of hydrogen
pK_a	Acid dissociation constant
pK_b	Base dissociation constant
R_p	Rate of polymerization
T_g	Glass transition temperature

LIST OF ACRONYMS/ABBREVIATIONS

ATRP	Atom transfer radical polymerization
BAPO	Bis(2,4,6-trimethylbenzoyl)- phenylphosphine oxide
BP	Bisphosphonate
DCM	Dichloromethane
DMEM	Dulbecco's modified eagle medium
DMPA	2,2-Dimethoxy-2-phenylacetophenone
DMSO	Dimethyl sulfoxide
DNA	Deoxyribonucleic acid
DOX	Doxorubicin
DSC	Differential scanning calorimetry
DTT	Dithiothreitol
EDTA	Ethylenediaminetetraacetic acid
EDX	Energy-dispersive X-ray spectroscopy
FBS	Fetal bovine serum
FT-IR	Fourier transform infrared spectroscopy
GDMA	Glycerol dimethacrylate
GPC	Gel permeation chromatography
GSH	Glutathione
HAP	Hydroxyapatite
HDDA	1,6-Hexane diol diacrylate
HEMA	2-Hydroxyethyl methacrylate
HPMA	N-(2-Hydroxypropyl) methacrylamide

HUVEC	Human umbilical vein endothelial cells
Irgacure 2959	2-Hydroxy-1-[4-(2-hydroxyethoxy)phenyl]-2-methyl-1-
LBL	Layer-by-layer
LCST	Lower critical solution temperature
MB	Methylene blue
MDP	10-Methacryloyloxydecyl dihydrogen phosphate
MTT	Thiazolyl blue tetrazolium bromide
NIPAM	N-isopropyl acrylamide
NMR	Nuclear magnetic resonance spectroscopy
PBAE	Poly(β -amino ester)
PBS	Phosphate buffered saline
PDI	Polydispersity index
PEG	Poly(ethylene) glycol
PEGDA	Poly(ethylene glycol) diacrylate
PEI	Polyethylene imine
RAFT	Reversible addition-fragmentation chain transfer
RGD	Arginylglycylaspartic acid peptide
R6G	Rhodamine 6G dye
RNA	Ribonucleic acid
Saos-2	Human osteogenic sarcoma cells
SBF	Simulated body fluid
SEM	Scanning electron microscope
TBBr	<i>Tert</i> -butyl α -bromomethacrylate
TBHMA	<i>Tert</i> -butyl α -hydroxymethacrylate

TEA	Triethylamine
TFA	Trifluoroacetic acid
TMS	Tetramethylsilane
TMSBr	Trimethylsilyl bromide
UV	Ultraviolet
V-50	2,2-azobis(2-methylpropionamide)-dihydrochloride
XRD	X-ray diffraction

1. INTRODUCTION

1.1. Polymers and Hydrogels for Biomedical Applications

Polymers are very large molecules made of small repeating units called monomers. They can be of natural or synthetic origin. Polymers are light in weight but on the other hand have high mechanical strength. They are relatively cheap and can be easily processed into products with limitless range of characteristics and distinct properties which span a wide field of applications. Polymers are used as biomaterials for many biomedical applications such as coatings of vascular stents and orthopedic implants, artificial organs, theranostic agents, and controlled drug delivery systems (Figure 1.1) [1].

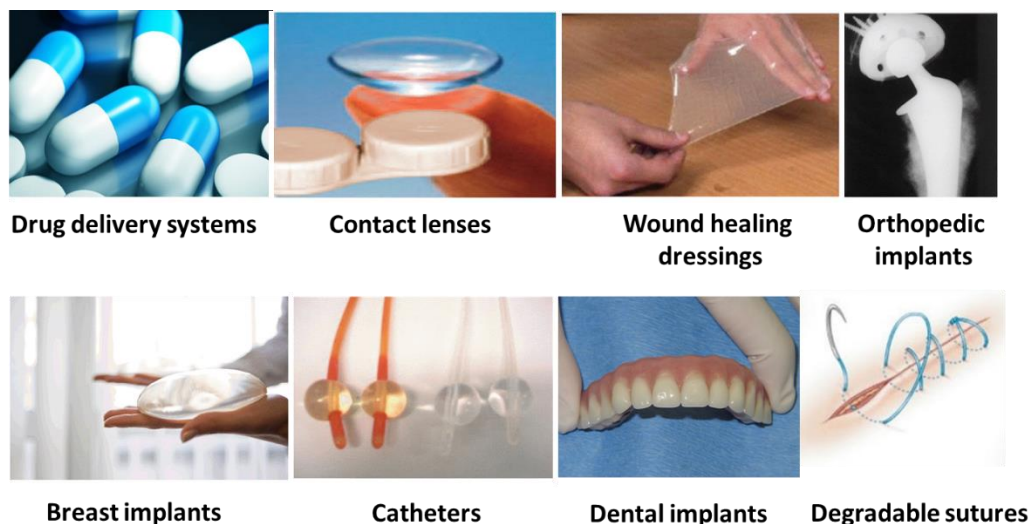


Figure 1.1. Polymers and hydrogels for biomedical applications [2].

Hydrogels are crosslinked hydrophilic polymer networks which are capable of absorbing high amounts of water (Figure 1.2) [3]. They resemble soft tissues in terms of physical properties due the porous structure and high water content which provides the

transfer of nutrients and waste [4]. Hydrogels have been the subject of intensive research in a variety of biomedical applications such as hygiene products, contact lenses, wound healing dressings, delivery of therapeutic agents, tissue engineering and regenerative medicine [5].

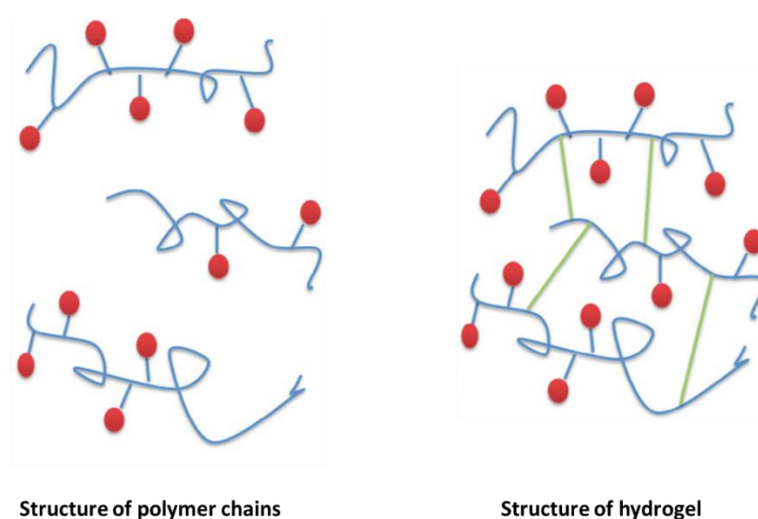


Figure 1.2. Structure of polymer chains and hydrogels [6].

1.1.1. Drug Delivery Applications

The idea of conjugating small molecule drugs to polymers originated from the attempts to improve the efficacy and reduce the systemic toxicity of drugs, especially chemotherapy drugs [7]. Conventional drug administration suffers from low solubility of common drugs which reduces bioavailability, short half-life due to rapid elimination from bloodstream and toxicity caused to healthy cells. Furthermore high dosages of repeated administration is required to obtain a therapeutic effect which reduces patient compliance.

The recent advances in synthetic polymer chemistry aided to overcome the cited problems of small molecule drugs by an innovative and interdisciplinary concept called as “Polymer Therapeutics” [8]. According to Ringsdorf’s model introduced in 1975, the drug should be attached through a cleavable linker onto a polymer which is biocompatible and

biodegradable (Figure 1.3) [9]. The presence of solubilizing groups and targeting moieties on the polymer backbone enhances the therapeutic effect of the system. For example, a polymer-drug conjugate having a targeting group like an antibody specific for the receptors overexpressed on tumor cells, will accumulate at the tumor site and provide an effective cure.

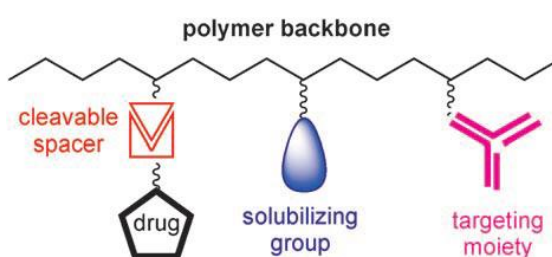


Figure 1.3. Model of polymer based drug delivery [10].

In their pioneering work Maeda *et al.* showed that even in the absence of targeting groups, polymeric drug delivery systems tend to accumulate in tumor site due to structural differences between the anatomy of healthy and tumor tissues. The tumor tissue has a defective structure which is disordered and permeable to macromolecules. The lack of lymphatic drainage also supports the accumulation. The concept of passive accumulation of polymers/macromolecules at tumor tissue was named as “enhanced permeability and retention effect” [11].

Poly(ethylene glycol) (PEG), Poly(hydroxy propyl methacrylate) and Poly(hydroxyl ethyl methacrylate) are widely chosen polymers for therapeutic applications due to their relevant properties such as biocompatibility, nonimmunogenicity, and water solubility. Different polymeric constructs such as polymer-drug protein conjugates, polymer-protein conjugates, and polymeric micelles can be used for therapeutic and diagnostic purposes (Figure 1.4).

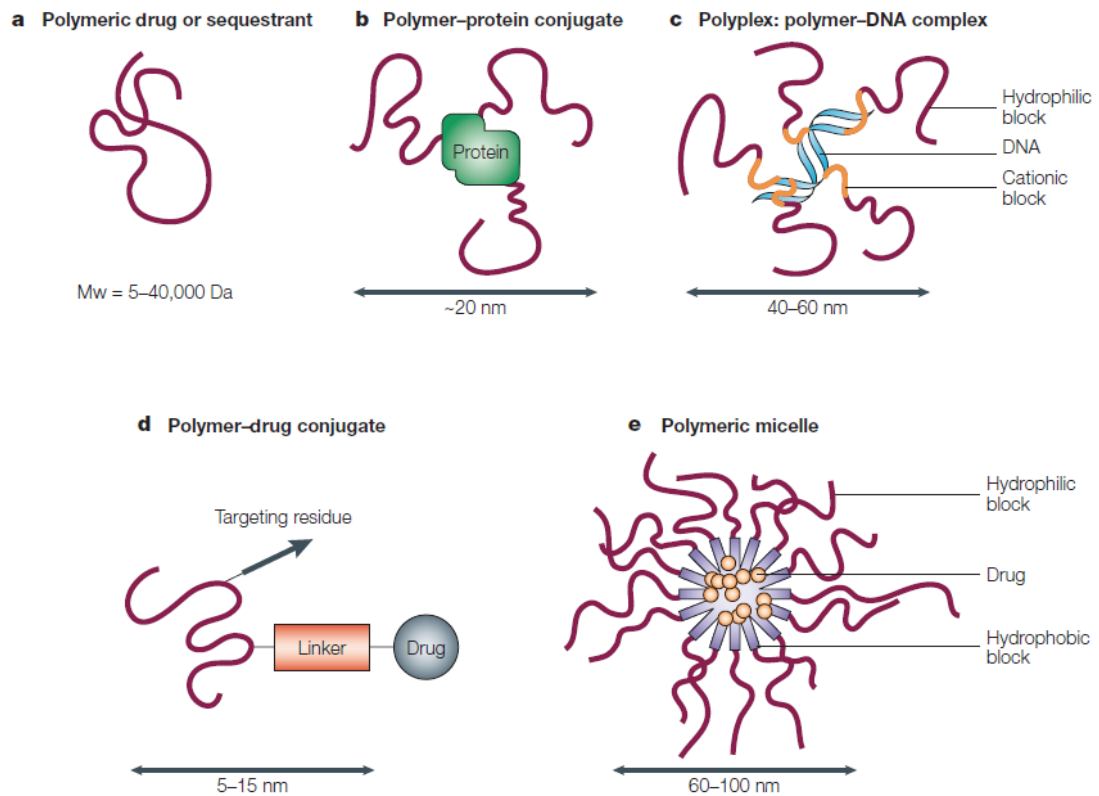


Figure 1.4. Structure of polymers used for controlled drug delivery [8].

Hydrogels are appealing platforms for drug delivery which can provide spatial and temporal control over release of encapsulated therapeutic molecules. Their similarity to natural tissues based on porous structure and high water content provide them biocompatibility which is essential for drug release applications. Collagen, gelatin, alginate, poly(acrylic acid), poly(ethylene glycol) and poly(2-hydroxy ethyl) methacrylate have been used as drug delivery platforms in clinic successfully in various cases including induction of labor and treatment of diseases such as acne vulgaris, diabetic foot ulcer, bacterial conjunctivitis etc (Table 1.1.). Hydrogels have tunable chemical and physical properties which enable the precise design of their structure for various bioapplications (Figure 1.5).

Table 1.1. Hydrogel based drug delivery systems used in clinic [12].

Product	Type of Hydrogel	Drug	Therapeutic Application
INFUSE	Collagen	Recombinant human BMP2	Bone fracture Oral maxillofacial reconstruction Spinal fusion
VANTAS	Poly(2-hydroxyethyl methacrylate)	Histrelin acetate	Subdermal implant for the treatment of prostate cancer
Azasite	Poly(acrylic acid)	Azithromycin	Bacterial Conjunctivitis
Cervidil	PEG or urethane polymer	Dinoprostone	Vaginal insert for servical ripening to induce labour
Differin	Carbomer 940	Adapalene	Topical treatment of Acne Vulgaris
Calamine-zinc gelatin	Gelatin	Calamine zinc oxide	Wound dressing to lessen pain and itching
ALGICELL Suprasorb	Alginate	Silver	Wound dressing with antimicrobial silver
REGRANEX	Carboxymethyl cellulose	Becaplermin	Topical gel for the treatment of diabetic foot ulcers

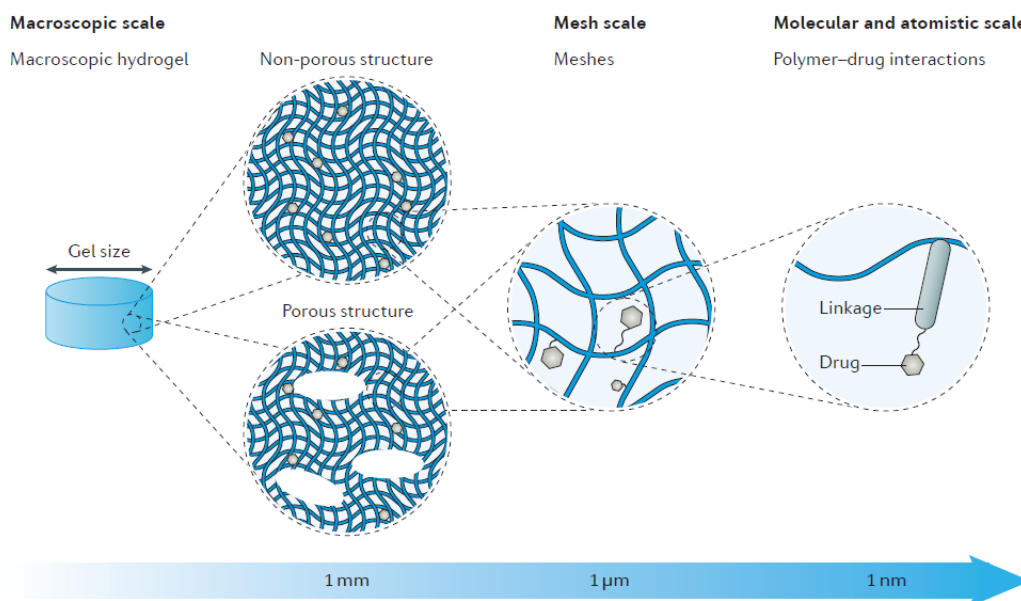


Figure 1.5. Multiscale properties of hydrogels for controlled drug delivery [12] .

The delivery route of hydrogels depends on chemical design and includes surgical implantation or local needle injection for in situ gelling systems [13]. It is very important to design the system in a way that the drug molecules retain their physical stability and biological activity during encapsulation, transport and storage. The degradability of the hydrogel is another factor to take into consideration since it prevents a second surgical operation to remove the hydrogel after treatment.

The pharmacokinetic profile of drug release is largely governed by properties at molecular and atomistic scale. The drugs can be encapsulated into hydrogels either *via* physical or chemical interactions. The commonly used physical interactions for drug encapsulation are electrostatic interactions based on oppositely charged groups or hydrophobic associations. It is possible to load the drug molecules into the hydrogel by swelling the hydrogel network in a concentrated drug solution. In these types of systems the release depends on the size of the drug molecule and meshes which are void spaces between polymer chains. Drug molecules smaller than mesh size easily diffuse through the hydrogel and gets released rapidly. When the dimensions of the drug molecule and meshes are similar

the diffusion is dramatically slowed. If the drug molecule is larger than the mesh size the diffusion is sterically hindered and the drug molecules are immobilized and physically entrapped in the network (Figure 1.6). In this case the controlled release of drug molecules can be mediated by swelling or degradation of the hydrogel network. The typical degradation mechanisms of hydrogels involve hydrolysis and enzyme activity. It is also possible to trigger degradation by external stimuli such as pH or UV light. The other approach to mediate drug release is by swelling. The entrance of water into the hydrogels expands the structure and the mesh size increases allowing for release of drug molecules. Swelling can be induced by alteration of external conditions such as pH, temperature, ionic strength, light, electric field etc.

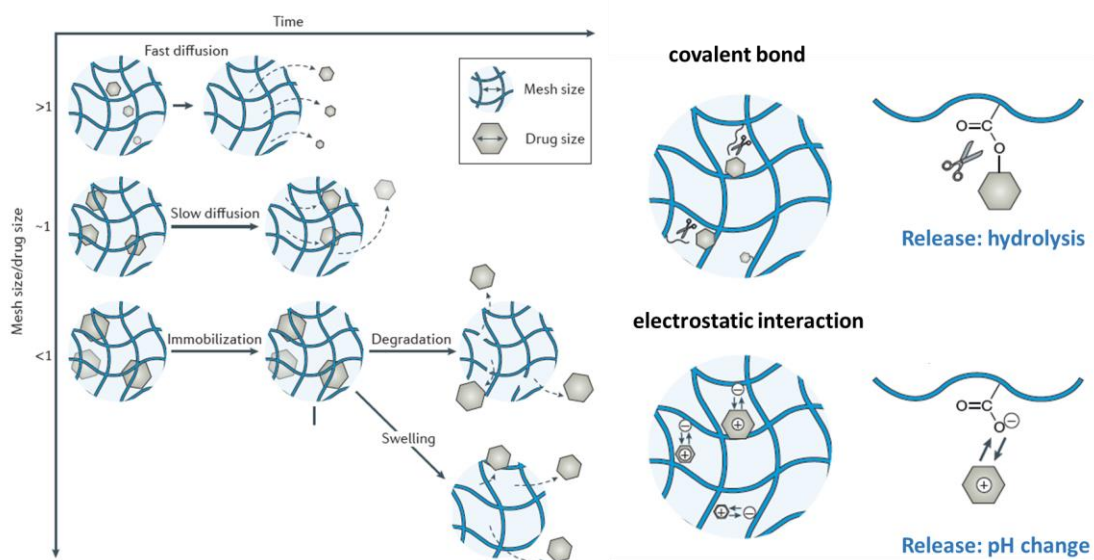


Figure 1.6. Mechanisms of drug release from hydrogels [12] .

Macroscopic hydrogels respond to external triggers very slowly in a time scale of minutes which can limit their use practically. To achieve faster response, hydrogels with interconnected pores have been prepared by different techniques such as cryogelation, gas foaming or using porogens [14] . Water can diffuse rapidly into these macroporous systems and a fast response is observed.

Reducing the dimensions of the hydrogel is another possibility to enhance the response time. For this purpose various types of microgels and nanogels have been designed [15, 16]. Fast response to external triggers, delivery by minimally invasive methods and easy elimination by either kidney filtration or phagocytization by macrophages makes these systems advantageous over macroscopic hydrogels with large dimensions.

1.1.2. Tissue Engineering Applications

Many patients suffer from organ failure due to diseases of organ loss caused by accidents. The treatment of these cases can be by means of tissue or organ transplantation, but unfortunately this strategy has some limitations such as donor shortage or rejection of the transplanted tissue by the immune system of the patient. A revolutionary approach to overcome these problems is to develop artificial tissues and organs to augment or restore the original ones [17]. Researchers at University of Massachusetts exploited tissue engineering and regenerative medicine methods to grow an ear on the body of a mouse and captured great attention of the public (Figure 1.7). Many types of tissues including artery, bladder, skin, cartilage, bone, ligament, and tendon have been engineered to date and now some of them are at or near clinical use [18-22].



Figure 1.7. Mouse with an engineered ear on its back [23].

This interdisciplinary approach named as tissue engineering involves chemistry, materials science and biology to design and fabricate such tailor-made complex systems. Firstly a tissue biopsy is made to the patient and the cells are isolated. Then the cells are expanded *in vitro* and incorporated into a 3D polymeric scaffold together with biologic cues such as growth factors to promote cell growth (Figure 1.8). The scaffold is then implanted into the body where it delivers the cells to the relevant site. Scaffolds act as analogues of natural extracellular matrix by supporting and providing space for newly formed tissues. They also allow the diffusion of nutrients essential for cell growth.

The scaffolds can be made from natural or synthetic polymers. Collagen, gelatin hyaluronate, fibrin, alginate, agarose, and chitosan are natural polymers which have been widely used for tissue engineering applications. Natural polymers are highly biocompatible and degradable but lack sufficient mechanical strength. On the other hand synthetic polymers can be precisely tuned to have appropriate mechanical strength but suffer from toxicity and their synthesis requires tedious purification steps. Synthetic polymers commonly used as tissue engineering scaffolds are poly(acrylic acid), poly(ethylene oxide), poly(vinyl alcohol), polyphosphazene and polypeptides. Besides biocompatibility and mechanical properties, degradation profile is another criteria in successful design of tissue engineering scaffolds. Ideally the scaffold should have a degradation rate which matches the formation rate of newly formed tissue. Although tissues or organs which excellently mimic the natural ones have not been fabricated yet, great progress has been made in the last decades and with advances technology such as in 3D printing it is likely that this field will develop much more in near future [24].

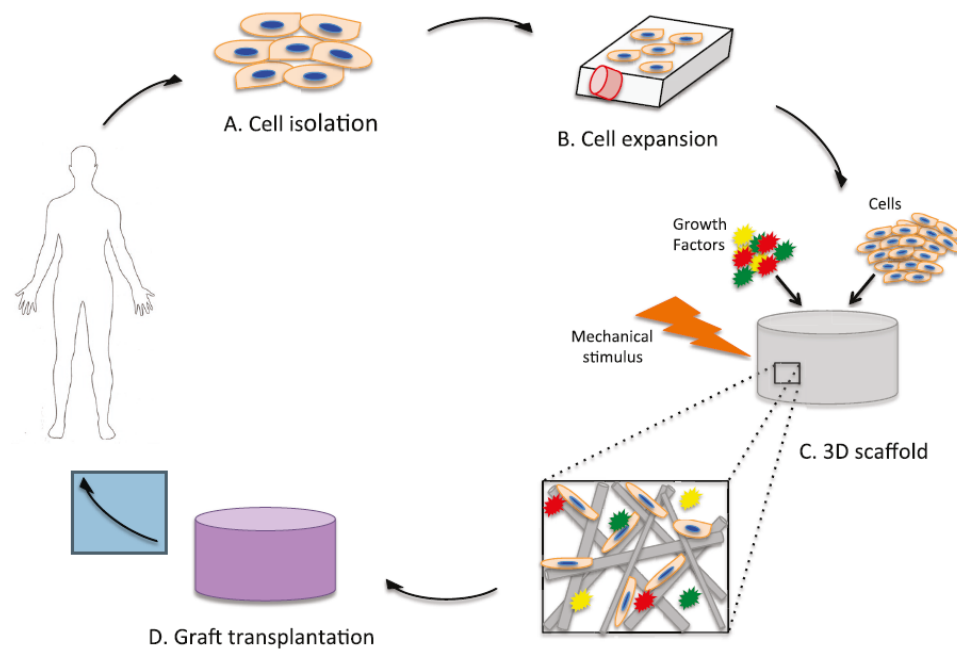


Figure 1.8. Process of tissue engineering [19].

1.1.3. Gene Delivery Applications

Gene delivery is based on the idea of treating certain diseases caused by mutations of genes, by transfer of genetic material to cells [25]. To achieve success, a safe and specific delivery system capable of protecting the genetic material from premature degradation during administration and provide efficient gene transfection should be constructed. Viral vectors have high transfection efficiency but there are concerns regarding their safety in terms of toxicity and immunogenicity. In fact, death of a patient during arthritis gene therapy directed the attention of researchers to non-viral vectors such as polymers, liposomes and inorganic nanoparticles. Thanks to their easy and low cost production, reproducibility, and possibility of tailor-made structural modification, polymers are good candidates as non-viral vectors for gene delivery [26]. Cationic polymers can bind to negatively charged DNA and reduce the size of DNA by forming nano-sized particles called as polyplexes [27]. By forming polyplexes the enzyme-mediated degradation of genetic material is reduced and barriers against gene delivery is passed easily. Polyplexes have an overall positive charge which facilitates their cellular uptake through negatively charged phospholipid bilayers on the cell wall. The most commonly used cationic polymer for gene delivery is poly(ethylene

imine), and other alternatives are poly(β -amino ester)s, poly(amido ethylenimine)s and dendrimers.

Gene delivery process starts with the formation of the polyplex which is then internalized by endocytosis (Figure 1.9) [28]. The polyplex induces endosomal escape *via* proton sponge effect which causes swelling, destabilization and finally rupture of the endosome. The disintegration of polyplex mediates nuclear internalization and gene expression.

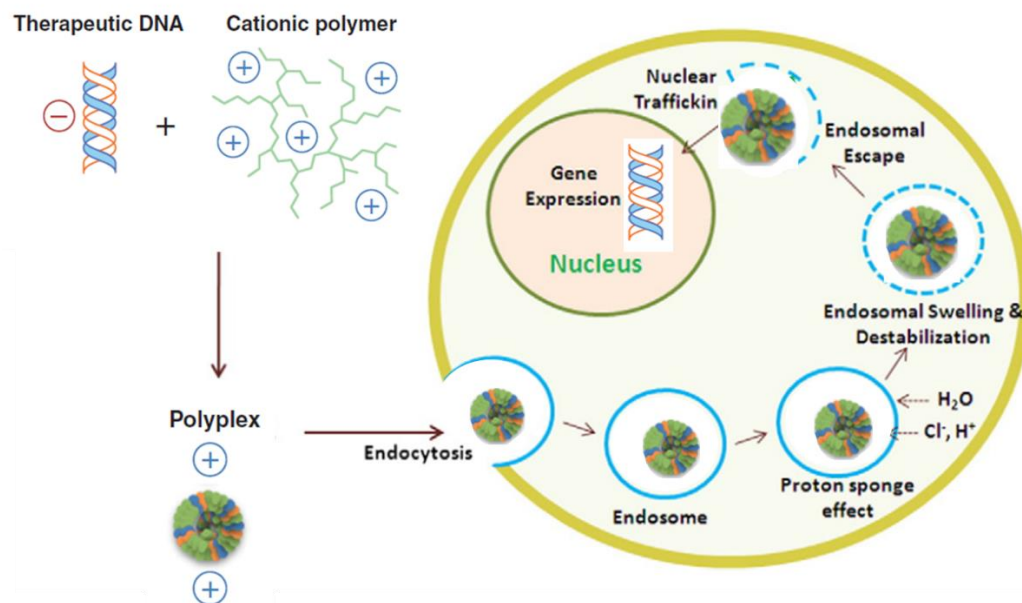


Figure 1.9. Gene delivery mechanism [29].

For an efficient gene therapy, the polyplex should pass through all significant barriers in the body and reach safely to the nucleus. Hence polymer vector should be designed carefully in terms parameters such as charge density, branching and hydrophobic/hydrophilic balance to optimize the process for transation of preclinical studies into successful clinical protocols.

1.1.4. Dental Applications

Tooth contains mineralized tissues, namely enamel and dentin. Enamel is the uppermost layer of the tooth crown and is known as the most highly mineralized tissue in human body consisting of almost entirely hydroxyapatite with organic material content less than 1% [30]. Dentin forms the bulk of tooth and is below the enamel layer. Achieving a good adhesion between these dental tissues and the restorative material is one of the main considerations in dentistry.

Self-etching dental adhesives overcome the problem of insufficient adhesion owing to the fact that they can form strong bonds between the dental hard tissues (dentin and enamel) and the restorative material [31]. They perform by demineralizing the dental tissue as well as forming a strong chemical bond with hydroxyapatite, the major component of dental tissue.

Self-etching dental adhesives consist of monomers, initiator and filler [32]. Based on their function, monomers present in commercial self-etching adhesive formulations are divided into three categories: self-etching adhesive monomers; cross-linking monomers and monofunctional co-monomers (Figure 1.10).

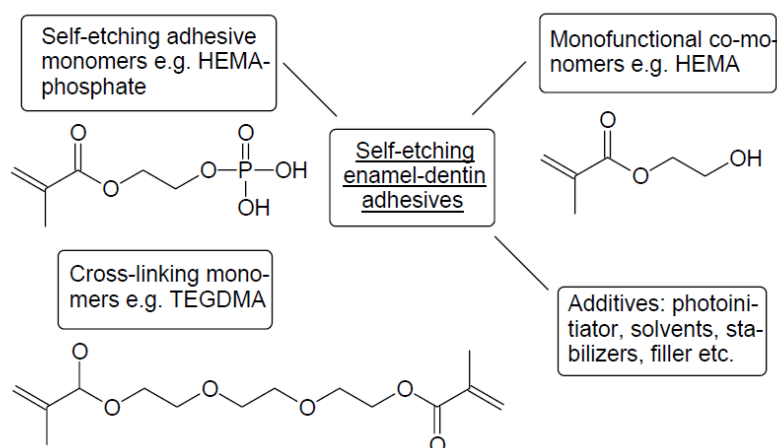


Figure 1.10. Components of self-etching enamel-dentin adhesives [33].

All types of monomers included in commercial self-etching adhesive formulations are expected to satisfy some general requirements such as;

- High rate of free-radical polymerization (homo- or copolymerization),
- Solubility of monomer in the dental composition,
- Low shrinkage upon polymerization,
- Low oral toxicity and cytotoxicity of monomers,
- Stability of both the monomer and polymer in oral conditions

Besides the cited requirements, self-etching adhesive monomers which are acidic monomers responsible for the interaction of the adhesive with dental tissue should meet some additional requirements. Firstly they should be capable of etching the enamel layer on tooth to create a rough surface which enables the bonding of adhesive to enamel. Secondly, optimal film-forming and wetting on tooth surface should be provided. Finally, rapid ionic or covalent interactions with the dental tissue which is characterized by the formation of covalent bonds with collagen or formation of barely soluble calcium salts.

Self-etching adhesive monomers consist of three components; a polymerizable group which copolymerizes with other monomers in the adhesive composition, a spacer group which determines physical properties such as flexibility and solubility, lastly an adhesive group which etches the dental hard tissue hydroxyapatite and interacts with tooth (Figure 1.11).

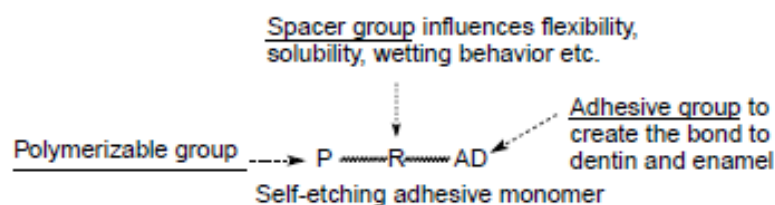


Figure 1.11. Components of self-etching enamel-dentin adhesives [33].

1.2. Stimuli Responsive Polymers and Hydrogels

Precise control over drug delivery to release the payload at the proper site (spatial control) and at the right time (temporal control) is vital for therapeutic success. Recently, sophisticated systems which can respond to external stimuli and mediate on demand release by switching the release on and off have been developed [34, 35]. These systems exhibit changes in their physical and chemical properties such as chain configuration or conformation, solubility and hydrodynamic volume in response to small changes in the external environment. The commonly utilized changing parameters are temperature, magnetism, ultrasound, light, pH, redox state, enzyme concentration etc. The parameters that changes inside the body are called as internal triggers, the ones manipulated from outside the body are called external triggers (Figure 1.12). Stimuli responsive polymers can be used for other applications like sensors, adaptive coatings, and self-healing materials [36].

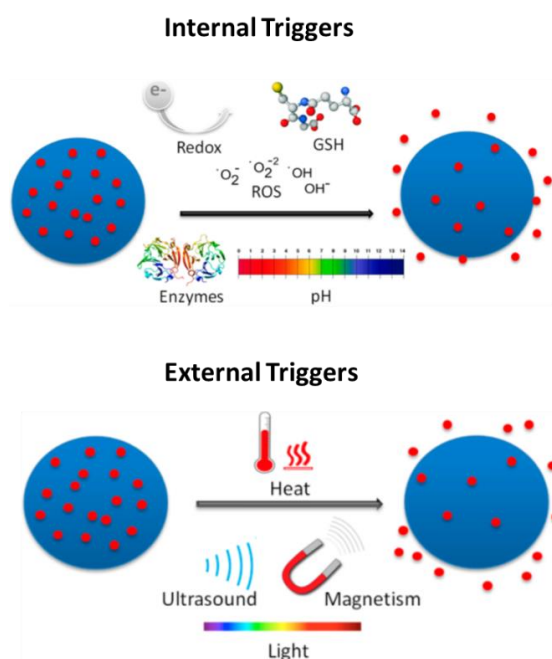


Figure 1.12. Internal and external triggers for controlled release of small molecules from polymers or hydrogels [37].

1.2.1 pH Responsive Systems

pH responsive polymer systems take advantage of the variations in pH throughout the human body [38]. For example the gastrointestinal tract exhibits sharp changes in pH with a strongly acidic (pH 2) environment in the stomach to a basic environment (pH 8) in the intestines. Wound and inflamed or cancerous tissues have an acidic environment (pH 6.5-5.5) when compared to normal tissues and blood (pH 7.4). Subcellular compartments like endosomes (pH 5-6.5) and lysosomes (pH 4.5-5) mediate pH responsive release of drugs or genes [39]. Specific examples on each case is cited in detail below.

In pH responsive hydrogels systems, the hydrogels swell or unswell in the solutions depending on pH (Figure 1.13). For example anionic hydrogels swell in basic solution due to repulsion of negative charges and the expanded hydrogel structure allows for release of encapsulated molecules.

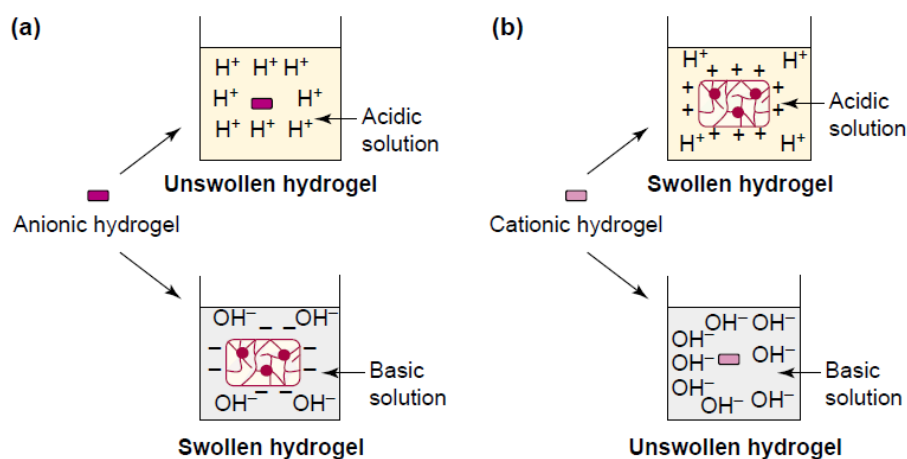


Figure 1.13. pH responsive hydrogels [38].

Ionizable polymers having pH response are commonly made from acrylic acid, methacrylic acid or other monomers containing acid-functional monomers like ones with phosphonic or bisphosphonic acids groups. pH responsive cationic polymers like poly(*N,N*-

dimethylaminoethyl methacrylate), poly(β -aminoester)s, poly(amidoamine)s and poly(ethylene imine)s are widely used for gene delivery.

pH sensitive polymeric microspheres were made from poly(vinyl alcohol) and poly(acrylic acid) to deliver diclofenac sodium, an anti-inflammatory drug, to the intestine. [40]. Modified-cholesterol-bearing pullulan nanogels were embedded into poly(methacrylic acid-*g*-ethylene glycol) hydrogels to form a hybrid controlled delivery system. Pregabalin, an anticonvulsant drug, was used as a model compound to demonstrate pH-sensitive *in vitro* release at pH 2.2 and 7.4 to simulate the conditions of gastric and intestinal media (Figure 1.14).

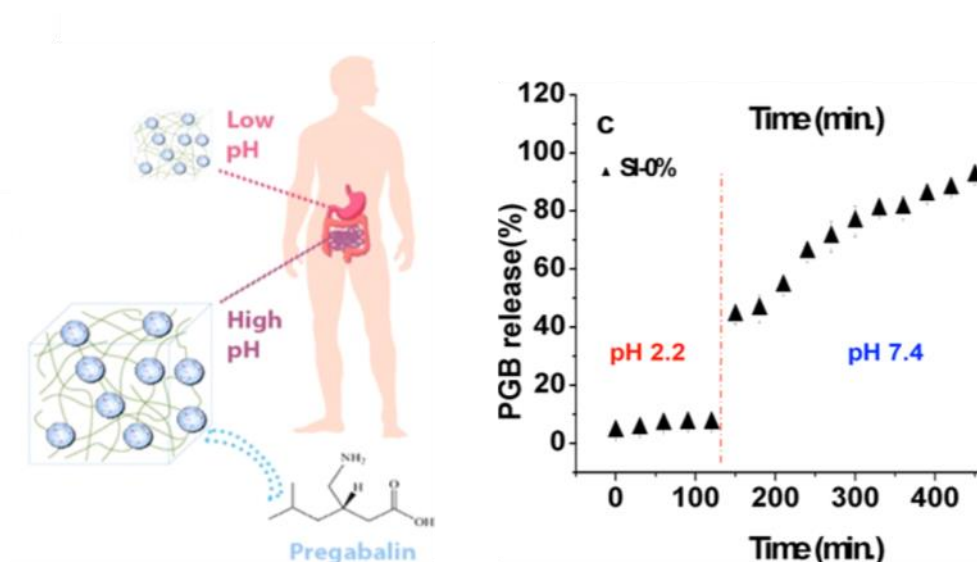


Figure 1.14. pH responsive hybrid nano/hydrogel [41].

Carboxylated agarose hydrogels were prepared as wound healing dressings for release of anti-bacterial and anti-inflammatory agent tannic acid. The release was negligible at neutral and basic pH, but sustained release was observed at acidic pH on acidic wound site [42]. Paclitaxel, a chemotherapy agent, loaded pH sensitive micelles were made from hydrophilic and hydrophobic segments conjugated through an acid sensitive hydrazone

linkage. These micelles were stable under neutral conditions but destabilized and released the drug content due to cleavage of hydrazone linkages [43].

1.2.2. Redox Responsive Systems

Glutathione/glutathione disulfide (GSH/GSSG) couple is responsible for many cellular functions that maintain the redox homeostasis (Figure 1.15) [44]. The intracellular compartments of cells contain 100–1000 times higher concentration of reducing glutathione (GSH) when compared to blood and extracellular fluids (0.5-10 mM vs. 2-20 μ M). Similarly tumor tissues contain 4-fold higher concentration of GSH relative to healthy tissues. The considerable difference in GSH levels leading to a highly reducing environment in intracellular compartments has been exploited to develop redox responsive drug delivery systems [45, 46].

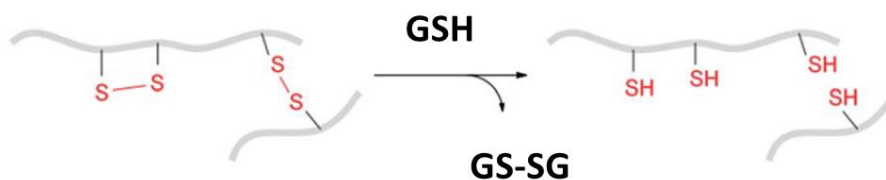


Figure 1.15. Reduction of disulfide linkages by glutathione [47].

Disulfide bonds are incorporated into polymers to serve as redox dependant cleavage sites. The bond is stable in the body during administration and transportation, but gets cleaved selectively in the reducing environment of tumor tissue and intracellular compartments through thiol–disulfide exchange reactions. Other than GSH, synthetic reagents such as 1,4-dithiothreitol (DTT) or tris(2-carboxyethyl)phosphine can also be used for reducing disulfides.

Redox responsive hydrogels were prepared by crosslinking HEMA with varying amounts of disulfide crosslinker. In the presence of GSH, the hydrogel showed enhanced release of encapsulated dye molecules [48]. Bioreducible macroporous HEMA cryogels were synthesized by a novel disulfide crosslinker and the degradation characteristics upon exposure to DTT was studied [49]. Michael addition reaction was used to form PEG based redox-responsive cryogels which were stable under physiological conditions but degraded rapidly in the presence of GSH [50]. These cryogels were evaluated as potential tissue engineering materials and their cell viability and cell attachment properties were investigated.

1.2.3. Thermoresponsive Systems

Thermoresponsive polymers show temperature-dependant solubility change which is ascribed to the balance between hydrophilic and hydrophobic moieties within the structure [51]. The temperature which this phase transformation occurs is defined as critical solution temperature. Even small changes around this temperature result in abrupt changes in solubility due to alterations in interactions between the polymer chains and the surrounding water molecules. At temperatures below the lower critical solution temperature (LCST) the polymer chains interact with water molecules through hydrogen bonding and the polymer chains become soluble, extend and form soluble hydrophilic coils. At temperatures above LCST, hydrogen bonding is favored between the polymer chains compared to solubilisation caused by hydrogen bonding with water. As a result the polymer gets dehydrated, polymer chains collapse and form hydrophobic globules (Figure 1.16). Most widely used thermoresponsive polymers exhibiting LCST are poly(*N*-isopropyl acrylamide) P(NIPAM), poly(*N,N*-diethyl acrylamide), poly(methylvinyl ether), poly(*N*-ethyl oxazoline) and poly(*N*-vinyl caprolactam).

It is possible to shift the LCST of a polymer to meet requirements for a specific application by tuning the hydrophilic/hydrophobic balance. Incorporation of hydrophilic moieties into a thermoresponsive polymer increases the LCST whereas, hydrophobic ones

decrease LCST. Tuning the LCST at physiological temperature (37 °C) makes polymers as potential materials for biomedical applications [52].

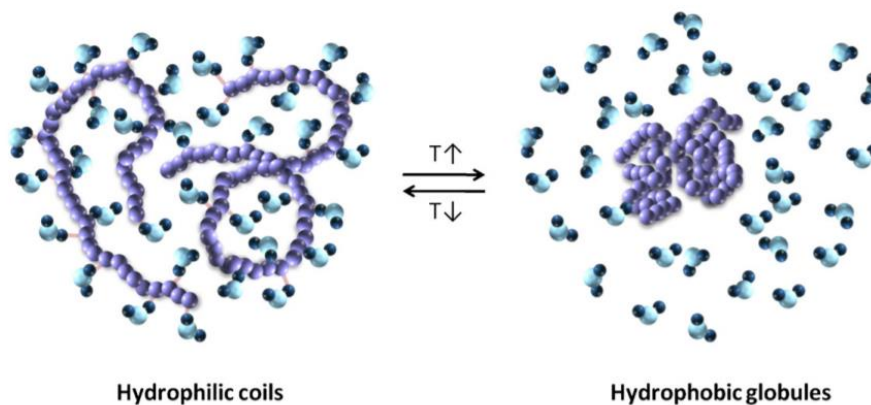


Figure 1.16. Temperature dependant transition change of a polymer in aqueous environment [37].

At the LCST, phase transformation of the polymers and hydrogels make them insoluble, so they volumetrically shrink and squeeze out the absorbed water along with the encapsulated drug. NIPAM was copolymerized with dextran to form biodegradable and thermoresponsive hydrogels. The thermoresponsive behavior was demonstrated by release of hydrophilic model drugs methylene blue and bovine serum albumin [53]. A series of thermoresponsive hydrogels to release antimicrobial agents were prepared and were suggested to be used as coatings for medical devices [54]. A copolymer of NIPAM was investigated for local delivery of anti-mitotic agent colchiconine and proposed to be used as drug-eluting polymer for stent coatings [55]. Poly(lactic acid)-NIPAM star block copolymers were shown to be self-assemble into thermoresponsive micelles with a temperature dependant switching behavior of drug release [56]

Thermoresponsive polymers can be used for tissue engineering applications by manipulating the characteristics of a surface and regulating the cell attachment [57]. Another interesting approach is to mix a soluble thermoresponsive polymer with cells and growth factors and inject it into the relevant site in body with minimal invasion. After the mixture

takes the desired shape it forms an *in situ* 3D scaffold due to increase of temperature above the LCST of polymer at 37 °C [58].

1.2.4. Multiple Responsive Systems

Investigation of sophisticated systems that combine more than one type of stimuli response have been a hot topic in recent years [59]. Dual responsive systems such as pH/temperature, pH/redox, temperature/redox, or multiple responsive systems combining three or more stimuli have been studied widely. The responses may either be simultaneous or in a step-wise fashion.

Dual responsive (temperature/redox) biodegradable hydrogels were prepared by crosslinking NIPAM with poly(ϵ -caprolactone) dimethacrylate and bisacryloylcystamine. The thermal characteristics, morphology, water uptake and mechanical properties of the obtained hydrogels were investigated. The hydrogels showed temperature and redox dependant release of drug (Figure 1.17) [60].

RAFT polymerization and click chemistry was combined to produce disulfide containing poly(N,N-dimethylaminoethyl methacrylate) based pH and redox responsive hydrogels. Ceftriaxone sodium was loaded into these hydrogels and its stimuli dependant release was monitored. The hydrogel shrank and released its drug content at basic environment. The disulfide links were cleaved by DTT to facilitate redox dependant degradation (Figure 1.18) [61].

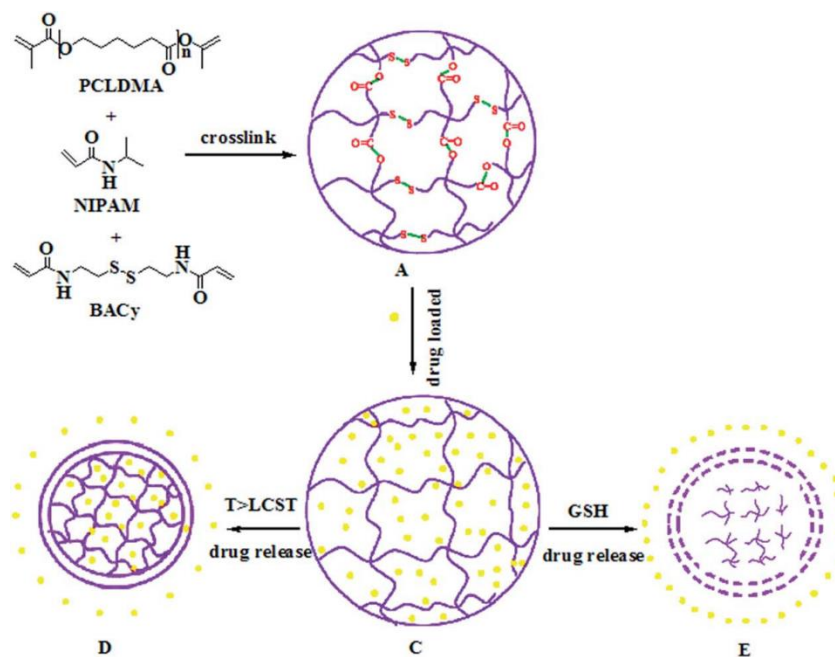


Figure 1.17. Temperature/redox dual responsive hydrogel [60].

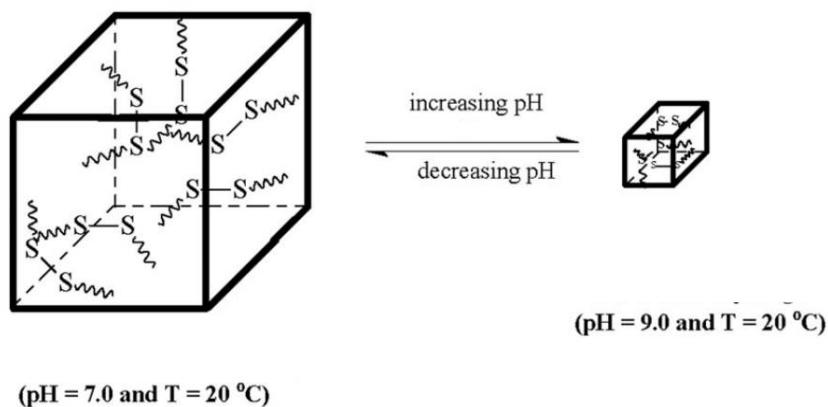


Figure 1.18. pH/redox dual responsive hydrogel [61].

pH and temperature dual-responsive microgels were synthesized from copolymerization of NIPAM and acid monomers with varying pendant chain length. The effect of structure on response rate was systematically evaluated. These microgels were fabricated into optical devices to be used for sensing applications [62]. Polymers and hydrogels which possess dual pH- and temperature-response was synthesized from

copolymerization of NIPAM and acrylic acid derivatives. The LCST of these systems were found to be dependant on both the structure of acrylic acid derivatives and the pH. The physical properties such as morphology and swelling kinetics were investigated. Insulin was selected as a model compound to demonstrate in vitro release. The insulin molecules are retained inside the hydrogel at acidic environment mimicking the stomach but showed an enhanced release in the neutral environment which mimics the intestines (Figure 1.19) [63].

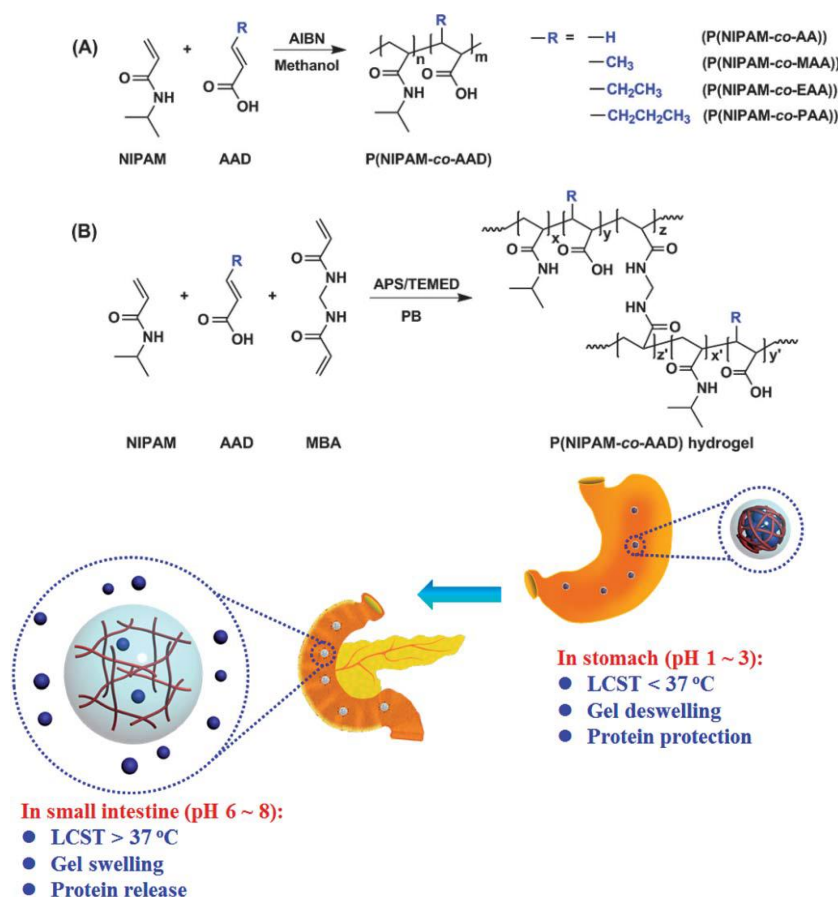


Figure 1.19. Insulin loaded pH/temperature dual responsive polymers and hydrogels [63].

Multiple responsive polymers made of photo-responsive pyrene and temperature/pH-responsive N,N-dimethylaminoethyl methacrylate units were self-assembled into micelles. Nile red and DOX was shown to be controllably released under UV irradiation, and appropriate conditions for pH and temperature [64]. Copolymerization of glucose-sensitive 3-acrylamidophenylboronic acid with pH and temperature-sensitive N,N-dimethylaminoethyl methacrylate gave triple responsive hydrogels. The physical properties

of the hydrogels were investigated and bovine serum albumin was used as a model compound to demonstrate stimuli responsive release [65].

1.3.Poly(β -amino ester)s for Biomedical Applications

Biodegradable polymers have been an extensively studied area of research for a wide scope of bioapplications including tissue engineering, drug delivery and gene delivery [66, 67]. Especially in tissue engineering applications, biodegradability of the polymer into nontoxic materials under physiological conditions is considered a key factor since it prevents the necessity for a second surgery to remove the polymer after the treatment.

Poly(β -aminoester)s (PBAEs) are a class of biodegradable polymers first synthesized by Langer *et al.* [68, 69]. PBAEs are synthesized *via* aza-Michael addition of diamines and diacrylates by step-growth polymerization (Figure 1.20). This versatile procedure is tolerant to many functional groups, does not require complex protection/deprotection steps and does not produce by-products. PBAEs degrade into small molecules like bis(β -aminoacid)s, diols and poly(acrylic acid)s under physiological conditions. Their biodegradability, biocompatibility and pH sensitivity make them suitable candidates for biomedical applications.

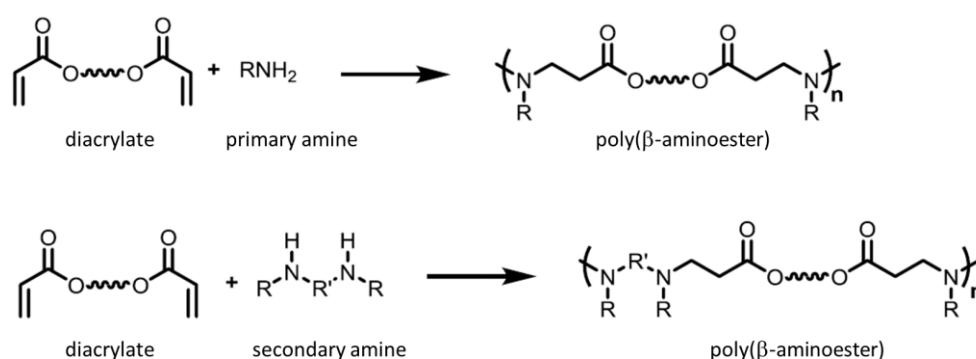


Figure 1.20. Synthesis of poly(β -aminoester)s.

1.3.1. PBAEs for Tissue Engineering Applications

During synthesis of PBAEs using the diacrylate in a slight molar excess ensures that the end groups contain acrylates readily available for polymerization. These PBAE macromers can be polymerized to obtain biodegradable network polymers whose properties such as degradation rate, mechanical strength and cellular interaction can be easily tuned particularly suited for tissue engineering applications. It is possible to adjust the mechanical strength by controlling the molecular weight of the crosslinked PBAEs by changing the amine:acrylate ratio. The chemical structure of the PBAE macromer is also a determining factor for mechanical properties. The relationship between chemical structure of PBAE macromers with mechanical properties and degradation rates by varying the diacrylate structure and amine to acrylate ratio was systematically investigated (Figure 1.21) [70].

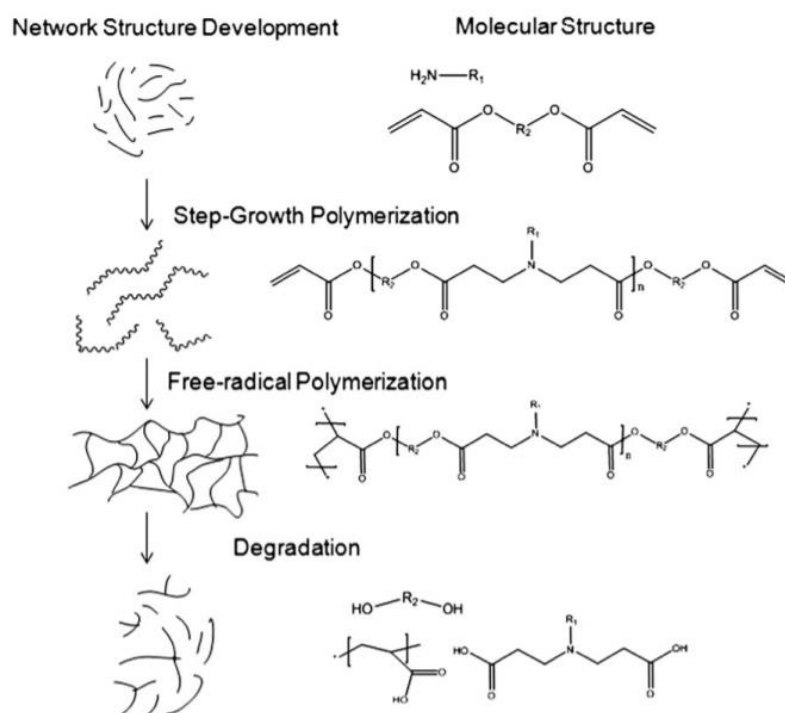


Figure 1.21. Development and degradation of PBAE network polymers [70].

PBAEs were prepared from isobutylamine amine and poly(ethylene glycol) diacrylate (PEGDA) or diethylene glycol diacrylate and the macromer synthesis time on

properties of hydrogels obtained by photopolymerizing them was investigated [71]. In another study the same hydrogels were evaluated as tissue engineering scaffolds [72]. The degradation profiles ranged from 7 h to 4 months and the compressive modulus decreased parallel with degradation as expected. Pluripotent mesenchymal stem cells were seeded on hydrogels showed 98% viability at 24 h showing favorable cell interactions with the material. A library of photocrosslinkable PBAE macromers were produced and the effect of their molecular weight and structure on properties of hydrogels made from them was investigated [73]. The adhesion and spreading behaviour of Saos-2 cells on these hydrogels were also found to be dependant on hydrogel structure. A combinatorial library of 120 PBAE macromers were developed and photopolymerized into degradable networks. The degradation profiles together with mechanical properties of the networks were systematically evaluated to provide a database for rapid screening of properties and to design tailor-made PBAEs for further studies. The relationship between chemical structure of PBAE macromers with mechanical properties and degradation rates by varying the diacrylate and amine structure and amine to acrylate ratio was systematically investigated (Figure 1.22) [74]. The concentration of diacrylate was systematically varied to understand its influence on physical properties and *in vivo* response of PBAEs [75]. The effect of branching on PBAE network properties were investigated by addition of multifunctional monomer during polymerization [76].

Acrylate end-functionalized PBAEs have been used as degradable crosslinkers and incorporated into 2-hydroxyethyl methacrylate for synthesis of biodegradable PBAE based hydrogels. The hydrogels were characterized by swelling and degradation studies [77]. Biswal et al reported a novel one-step method to easily produce PBAE hydrogels from aza-Michael reaction between a diacrylate and tetrafunctional amine [78]. This method eliminates the necessity for photopolymerizing the initially prepared macromers and reaction takes place at mild conditions. Disulfide containing hydrogels with inherent antioxidant property were prepared by a similar method [79]. Hyperbranched PBAEs with fluorescent properties were synthesized by the aforementioned one-step method [80]. Poly(amido)amine dendrimers were reacted with PEGDA through one-step aza-michael reaction to obtain superelastic cryogels with pH response (Figure 1.23) [81].

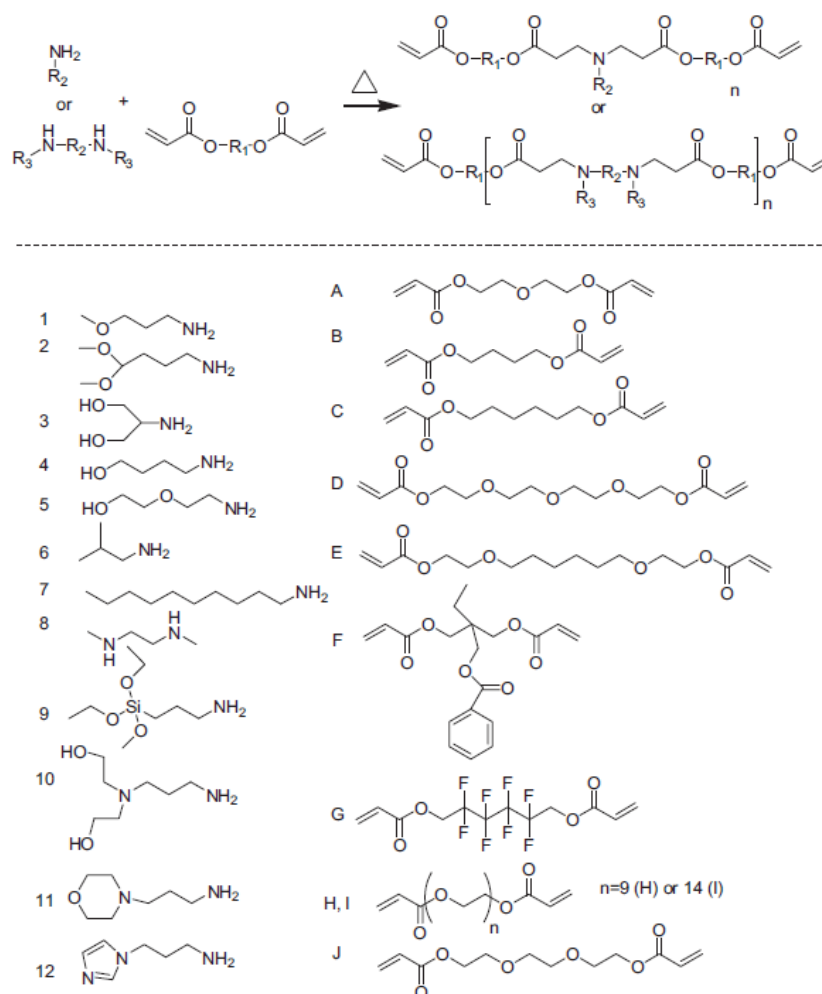


Figure 1.22. Chemical structures of amines and diacrylates used for the development of the combinatorial library [74].

Electrospun scaffolds are similar to components of native extracellular matrix in terms of fiber diameter, hence they are explored as tissue engineering scaffolds especially for musculoskeletal system in the recent years. PBAEs were successfully electrospun into fibrous scaffolds to obtain new materials for tissue engineering applications. The degradation rates and mechanical properties of these scaffolds were investigated [82]. Metter et al produced a combinatorial library of electrospun fibrous scaffolds from PBAEs and investigated their degradation profiles, mechanical properties and interactions with stem cells [83].

Polymers with pendant amine groups were crosslinked with diacrylates *via* aza-Michael reaction to give PBAE based hydrogels [84]. Thermoset networks with tailor-made mechanical and thermal properties were prepared by an environmentally friendly dual curing system based on sequential aza-Michael addition reaction and radical photopolymerization [85]. Retailleau et al prepared PBAEs, photocrosslinked them and then made a second aza-Michael reaction by introducing more amine molecules to consume any leftover C=C double bonds in the network as a postconsolidation step [86]. PBAE macromers were copolymerized with methyl methacrylate to form semi-degradable networks [87, 88]. Recently PBAE based networks have been used for exciting applications such as preparation of semi-interpenetrating networks, shape memory materials, logic gates and optical imaging probes [89-92].

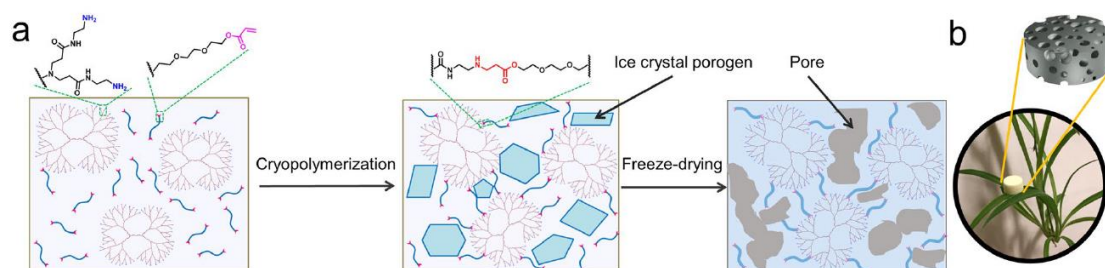


Figure 1.23. Superelastic PBAE cryogels with ultralight weight [81].

Recently we have made phosphonate and bisphosphonate functionalized PBAE network polymers particularly for bone tissue engineering applications. The effect of phosphonate and bisphosphonate group on properties of the networks such as degradation rate, toxicity and cell interaction was investigated [93, 94].

1.3.2. PBAEs for Gene Delivery Applications

PBAEs being cationic polymers have the capability to condense the negatively charged nucleic acids and form complexes called as polyplex through electrostatic interactions. By

this way the nucleic acids get protected from enzyme-mediated degradation and also overcome barriers to gene delivery. The PBAE polyplexes have overall positive charge so the cellular uptake is facilitated *via* electrostatic interactions with negatively charged phospholipid bilayers on the cell. PBAE polyplexes can also act as proton sponges to buffer the endosome and mediate DNA escape. The stated favorable biophysical properties and their low toxicity due to hydrolytic degradation makes PBAEs an important class as non-viral gene delivery vehicles. PBAEs with different structures were used in many *in vitro* studies and transfection efficiency was evaluated on cell types including retinal pigment epithelial cells, neonatal mouse cardiomyocytes, glioblastoma cells, fibroblasts, p53-mutant H446 SCLC cells [95-99]. The effect of PBAE structure on cell uptake profile of PBAE polyplexes were investigated in detail [100]. A study were performed to understand the signalling pathways that PBAEs cause in cells [101].

The effect of properties such as PBAE molecular weight, end group and PBAE/DNA ratio was optimized *via* high throughput methods [69]. *In vitro* studies showed that gene transfer was succesfully mediated by these PBAE polyplexes, even better than common non-viral gene delivery agents poly(ethylene imine) (PEI) and lipofectamine 2000. In a subsequent study, the optimized conditions were used to create a new library and the candidates were tested for toxicity and *in vitro* transfection. The best PBAE/DNA candidate was selected and for *in vivo* transfection experiment and gave promising results [102]. The effect of carbon atom number on gene transfer efficiency was studied to investigate the structure-activity relationship [103].

End-functionalized PBAEs were prepared by end-capping acrylate-terminated PBAEs with amines having different structures. It was shown that variation of end group highly influences the biophysical properties of polyplexes and the transfection efficiency [104]. PBAEs end-capped with oligopeptides were synthesized with the aim of synthesizing gene delivery agents with improved biocompatibility [105]. Mannose end-capped PBAEs were developed to target antigen presenting cells [106]. To enhance transfection efficiency, PEI-terminated PBAEs with increased positive charge were complexed with minicircle DNA. The polyplexes had low cytotoxicity and improved transfection [107].

Trifunctional amines were reacted with diacrylates to form novel PBAEs with branched architecture as efficient gene carrying platforms [108, 109]. In a following study, the effect of terminal amine groups on gene transfection properties of hyperbranched PBAEs was investigated [110]. A series of papers were published on synthesis, characterization and evaluation of highly branched PBAEs for epidermal gene therapy. These highly branched systems were significantly better when compared to linear ones in terms of safety and efficiency (Figure 1.24) [111, 112]. Highly branched PBAEs with high molecular weight showed superior transfection capability over low molecular weight ones [113].

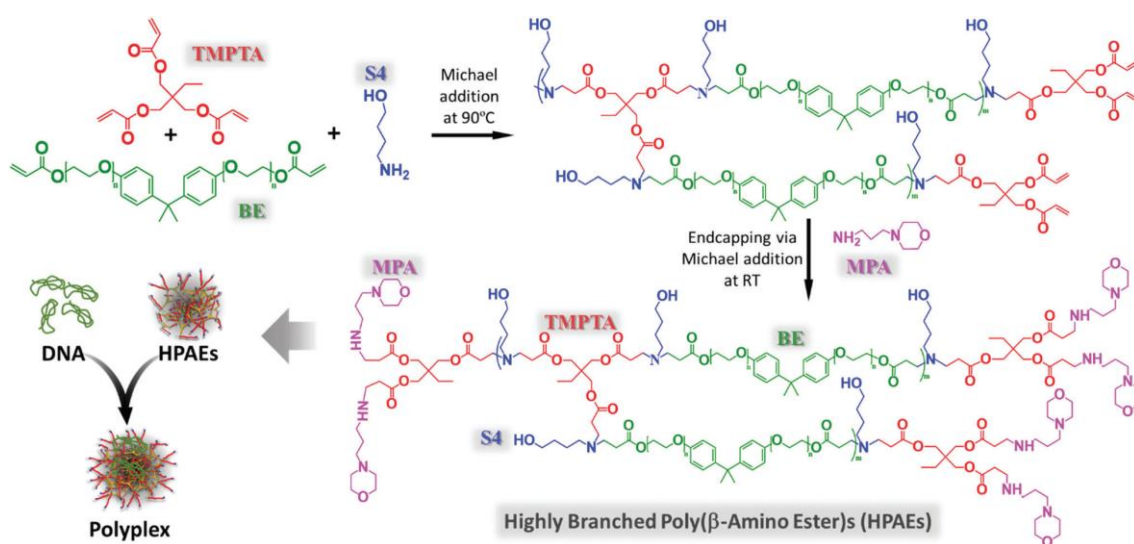


Figure 1.24. Structure of highly branched PBAEs [111].

High molecular weight PBAEs show good transfection efficiency but they are considerably toxic. PBAEs which degrade rapidly in response to an external trigger such as redox state, pH, UV light etc. were developed to overcome this issue. For example acid responsive ketal-containing PBAEs were synthesized as non-viral siRNA delivery systems [114]. The polyplexes were stable under neutral conditions but dissociate at the acidic pH of endosomal compartment to mediate escape of siRNA. Photo-responsive PBAEs, which can be rapidly cleaved upon exposure to external UV light after transfection, were prepared to allow for

enhanced DNA unpackaging and reduced toxicity in various types of cells (Figure 1.25) [115].

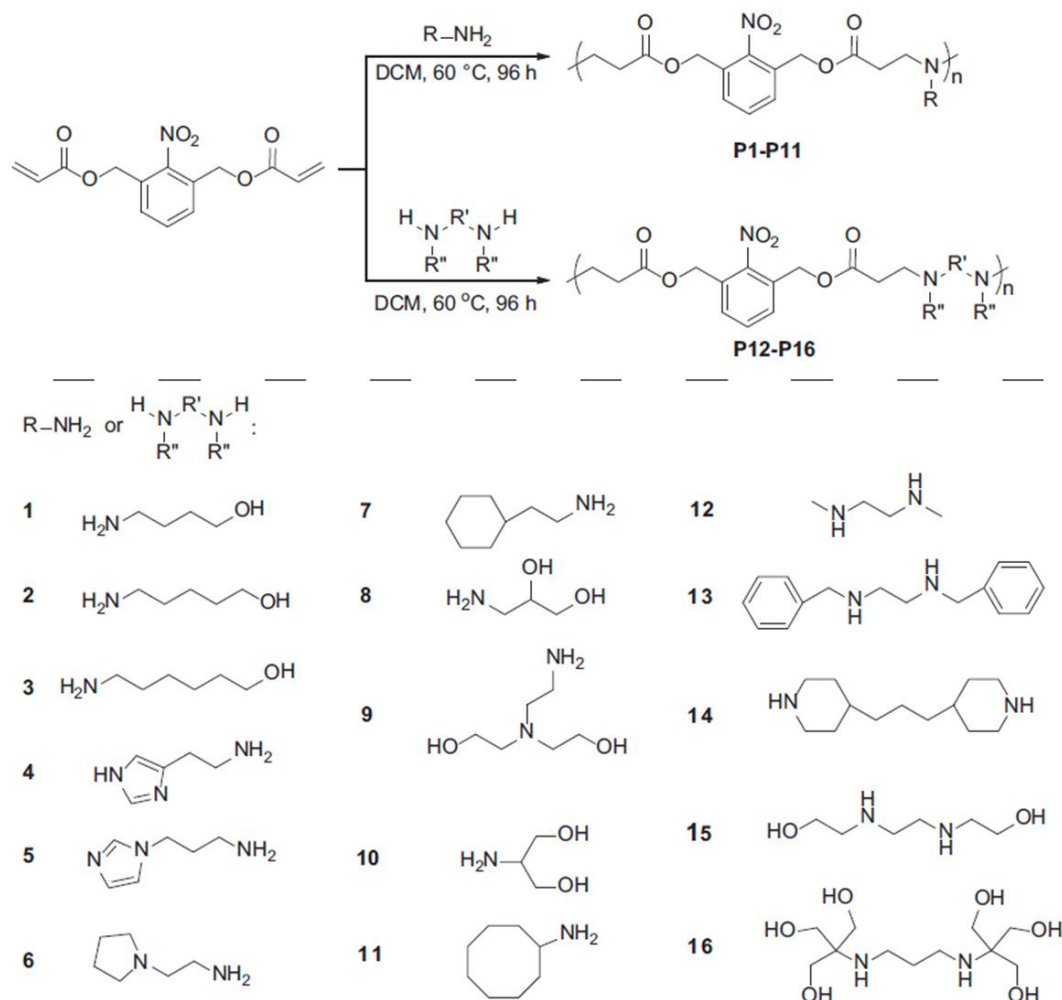


Figure 1.25. Structure of photoresponsive PBAEs [115].

Incorporation of disulfide containing groups into the structure provided redox-responsiveness to the PBAEs. Disulfide bonds are relatively stable in the extracellular environment while rapidly get cleaved in the intracellular environment under reducing conditions. The cleavage of disulfide bonds make the polyplex dissociate and the genetic material is released in the cytoplasm to function efficiently. At the meanwhile, cytotoxicity of the PBAE is reduced due to degradation. Studies demonstrated that using disulfide containing PBAEs for gene delivery increased transfection efficiency and decreased cytotoxicity [116].

Two different kinds of RNA were condensed into a redox-responsive PBAE to obtain a codelivery system with synergistic effect to overcome multidrug resistance which is a major challenge in chemotherapy [117]. PBAEs with pyridyldithio units, which are known to react with thiol groups through a disulfide exchange reaction, were synthesized [118]. The pyridyldithio units in the side chains provided a platform for conjugation to relevant biomolecules and to overcome cellular barriers in gene therapy. Thiol peptide RGD which binds to integrin receptors with high specificity was used as a model compound and conjugated to the PBAEs. Recently disulfide containing branched PBAEs with targeting groups were shown to have high transfection efficiency [119].

1.3.3. PBAEs for Drug Delivery Applications

Amphiphilic copolymers of PBAEs have the ability to form pH sensitive micelles to be used as drug delivery agents. Poly(ethylene)glycol (PEG) is generally used as the hydrophilic block and it is conjugated with pH-sensitive PBAEs to make micelles [120]. A chemotherapy agent, doxorubicin (DOX) loaded PEG-PBAE micelles showed prolonged circulation time in blood-stream and also enhanced cellular uptake [121]. Micelles made from PEG-PLA-PBAE triblock copolymers were used for pH sensitive release of anti-cancer drug curcumin [122]. Cholesterol grafted PBAE as the hydrophobic block was conjugated with hydrophilic PEG to make pH sensitive micelles for cancer therapy [123]. DOX and fluorescence dye squaraine were simultaneously loaded into PBAE micelles and the release was monitored through the change in the photoacoustic signals (Figure 1.26) [124]. RGD peptide which can selectively bind to integrins overexpressed in cancer cells was conjugated to PBAE micelles for targeted cancer therapy by receptor mediated cellular uptake [125].

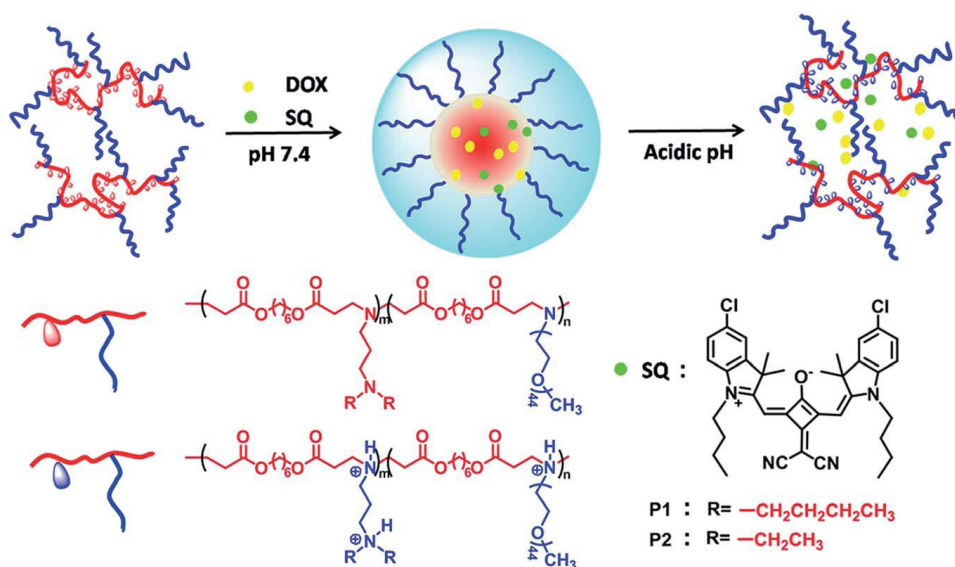


Figure 1.26. DOX/SQ-loaded PBAE micelles [124].

Co-delivery systems based on PBAEs for simultaneous delivery of chemotherapeutic agents, proteins and nucleic acids were also studied. Simultaneous delivery of DOX and shRNA by PBAE nanoparticles showed a synergistic therapy for multidrug resistance of breast cancer [126]. A PBAE was conjugated with peptide drug which then was self-assembled into micellar nanoparticles and loaded with DOX. This co-delivery platform showed accumulation in tumor site and effective suppression of tumor growth [127]. Redox and pH dual responsive PBAE nanoparticle was designed to effectively deliver DOX and pDNA to hepatoma HepG2 cells [128]. The simultaneous delivery of two different RNAs with a chemotherapy drug, paclitaxel, was successfully achieved with a pH sensitive PBAE system [129].

The degradation of PBAEs is influenced by the structure and it is possible to tune the release of payload by incorporation of cleavable trigger responsive domains. Protein encapsulated hydrogels made from disulfide containing PBAEs showed excellent control over the release of the protein [38]. Disulfide containing PBAE micelles showed dual response to pH and redox which enabled the destabilization of micelle and controlled release of anticancer drug [130].

PBAE based structures such as self-assembled nanoparticles, microparticles, microspheres, layer-by-layer (LBL) coatings and hydrogels have been utilized as platforms for drug delivery. Mucoadhesive PBAE nanoparticles were used for ocular drug delivery [131]. The electrostatic interactions between positively charged PBAE nanovehicles and cartilage tissue enhanced the uptake of dexamethasone drug due to prolonged retention of the drug molecules at target site [132]. Mesoporous silica nanoparticles were end-capped with stimuli responsive PBAEs to achieve pH and enzyme triggered release of anticancer drugs [133]. Hybrid PBAE nanoparticles were investigated for nasal vaccination [134]. PEG conjugated PBAE nanoparticles were shown to have superior properties over non-conjugated PBAE nanoparticles in terms of cancer therapy [135, 136]. The effect of polymer structure on drug release properties, cellular uptake and toxicity of PBAE nanoparticles were investigated [137]. PBAE microparticle formulations were demonstrated to be useful in genetic vaccine delivery [138]. PBAE nanogels were developed for sustained delivery of quercetin with the aim of treating oxidative stress [139]. Hyaluronic acid coated PBAE nanoparticles showed promising results for treatment of drug resistance to doxorubicin in breast cancer (Figure 1.27) [140]. Dopamine-functionalized PBAEs were fabricated into microspheres to scavenge reactive oxygen species which are believed to be elevated during neurodegenerative diseases (Figure 1.28) [141]. LBL coatings were prepared utilizing electrostatic interactions between positively charged PBAE and negatively charged alginate for controlled release of gentamicin [142]. Lysine based PBAE macromers were crosslinked to make hydrogels for controlled release of antibiotics [143]. *In situ* forming pH and temperature responsive PBAE hydrogel showed sustained release of DOX over a time period of five weeks [144].

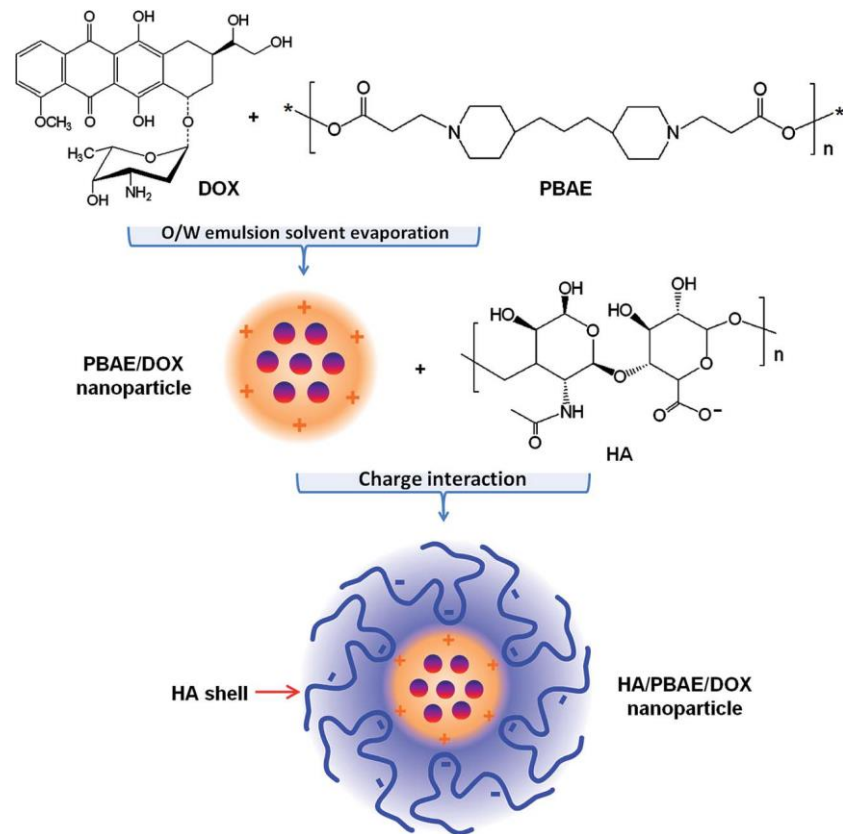


Figure 1.27. Hyaluronic acid coated PBAE nanoparticles [140].

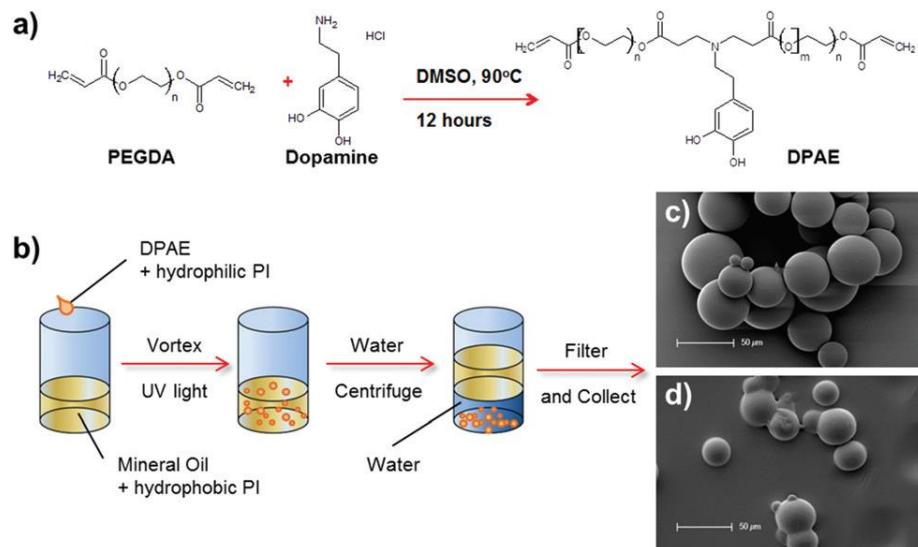


Figure 1.28. Dopamine functionalized PBAE microspheres [141].

1.4. (Bis)phosphonate/(Bis)phosphonic Acid Functionalized Biomaterials

Biomaterials and nanomaterials based on phosphorus-containing building blocks such as phosphonates, phosphonic acids and bisphosphonates have gained much attention due to their specific properties which impart them a great potential for a wide scope of applications [145]. The application areas range from dental materials including dental adhesives and composites to bone targeting systems for the delivery of therapeutic agents such as drugs and proteins or imaging agents for diagnostic applications (Figure 1.29) [146]. Biomineralization of polymeric hydrogel scaffolds, with the aim of mimicking bone structure for tissue engineering applications is another interesting field which phosphorus-containing moieties can be utilized.

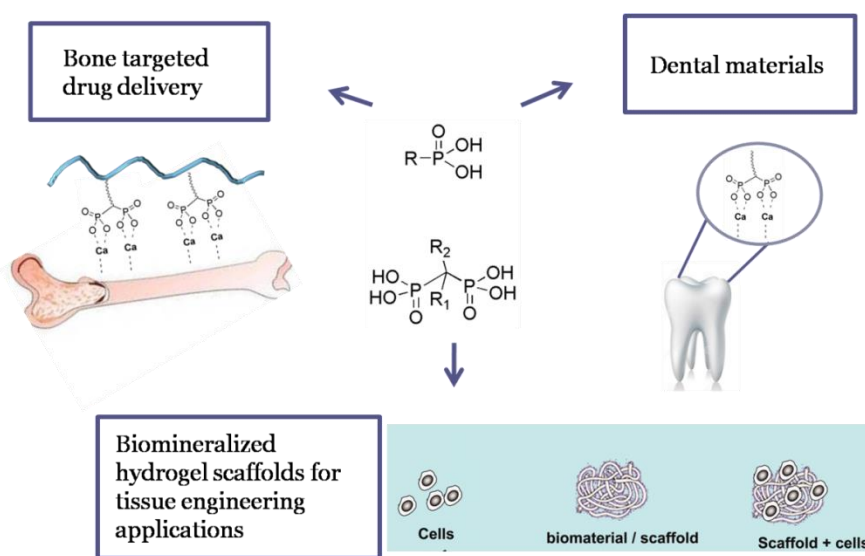


Figure 1.29. Phosphonate and Bisphosphonate based materials for biomedical applications.

1.4.1. Bone Targeted Drug Delivery Applications

Bisphosphonates (BP) are a class of phosphonates which are structural analogues of pyrophosphonate, a naturally existing molecule (Figure 1.30). Bisphosphonates have increased stability due to the replacement of the oxygen atom in the structure with a carbon

atom. Phosphonates have a similar structure to bisphosphonates and are also used for bone-related bioapplications.

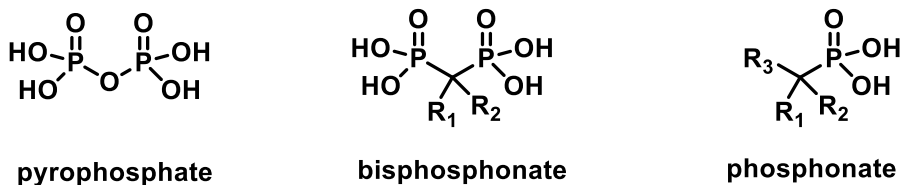


Figure 1.30. Structure of pyrophosphate and its synthetic analogue bisphosphonate.

Bisphosphonates are being prescribed for treatment of several bone diseases including osteoporosis, Paget's disease and bone cancer due to their antiresorptive properties [147]. They have strong affinity towards bone mineral hydroxyapatite (HAP) which makes them considered as targeting agents to deliver imaging agents, proteins or drug molecules to bone [148].

Two prodrugs which contain bisphosphonate group as a bone targeting ligand to selectively release the anticancer drug doxorubicin in site of the skeletal metastases was designed (Figure 1.31) [149]. The bisphosphonate and drug are linked through either an acid sensitive bond or a enzymatically degradable bond. The prodrugs were stable in human plasma and exhibited high affinity for hydroxyapatite. Bifunctional hydrazine-bisphosphonates with spacers of different lengths were synthesized and their affinity to bone was assessed [150]. The hydrazine-bisphosphonates were not cytotoxic and did not affect the proliferation of prosteoblasts. 4-nitrobenzaldehyde was used as a model drug for conjugation to the synthesized bisphosphonates through an acid cleavable hydrazone linkage.

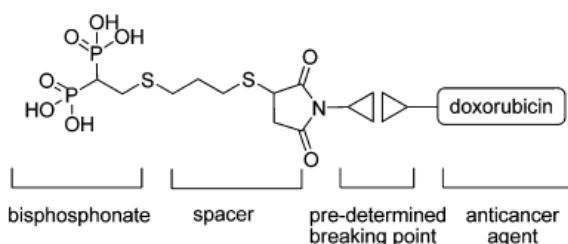


Figure 1.31. Design of bisphosphonate prodrugs [149].

A macrocyclic ligand which contains a bis(phosphonic acid) was designed to be used as an contrast agent which specifically has affinity to bone tissue for magnetic resonance imaging. Lanthanide(III) complexes of the ligand were prepared and their MRI contrast-enhancement abilities were evaluated using hydroxyapatite as a model of bone surface [151]. Recently, the synthesis of a biodegradable bisphosphonate monomer and its near infrared fluorescent nano or microparticles to be used for diagnosis and therapy of bone diseases was reported (Figure 1.32) [152]. Body distribution studies based on fluorescence intensity of nanoparticles indicated that the nanoparticles selectively accumulated in bone tissue rather than the rest of the body. The increased half-life of the nanoparticles in blood has been also demonstrated.

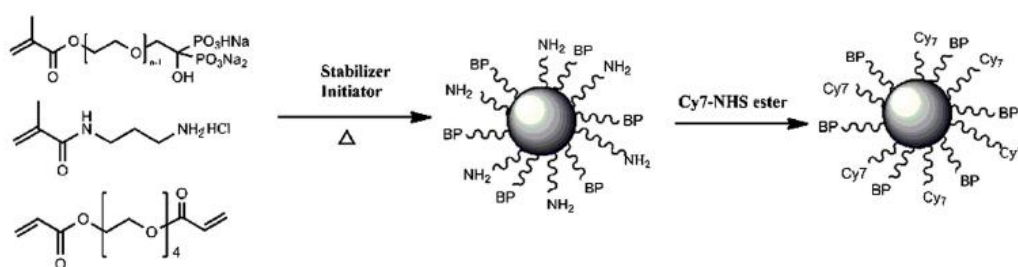


Figure 1.32. Bisphosphonate containing nanoparticles [152] .

Wang *et al.* reported synthesis of bone-targeting conjugates based on PEG (Figure 1.33) [153]. Alendronate (a bisphosphonate containing molecule) and aspartic acid peptide were used as bone-targeting moieties. Fluorescein isothiocyanate was conjugated to the polymer as a model drug for easy detection. The bone-targeting potential of these polymeric systems were evaluated *in vitro* with hydroxyapatite and in mice. The studies demonstrated that these polymer-drug conjugates specifically accumulated in the bone tissue.

The pharmacokinetic properties of polymer-drug conjugates highly depend on the structure and molecular weight of the polymer. It is important for a polymer to have a low polydispersity index for a predictable pharmacokinetic profile. Therefore polymers synthesized by controlled polymerization techniques such as atom transfer radical polymerization (ATRP) and reversible addition-fragmentation chain transfer (RAFT) are preferred for drug delivery applications. Recently, many papers which synthesize

phosphonate or bisphosphonate functionalized polymers by RAFT polymerization have been published [154-156]. For example polymer-drug conjugates consisting of N-(2-hydroxypropyl)-methacrylamide (HPMA) polymer and alendronate was synthesized by RAFT polymerization [157]. Biodistribution and pharmacokinetic behavior of four conjugates with different molecular weight and alendronate content were evaluated. The biodistribution studies in mice showed that alendronate-HPMA copolymer conjugates strongly bind to bone. Recently, water soluble hydroxyapatite-binding polymers with bisphosphonate side chains were prepared by ATRP (Figure 1.34) [158]. These polymers were covalently attached to the surface of both HL-60 and mesenchymal stem cells with the aim of engineering the cell membrane for bone targeting. Surface modification did not cause toxicity to cells but enhanced bone adhesion capacity.

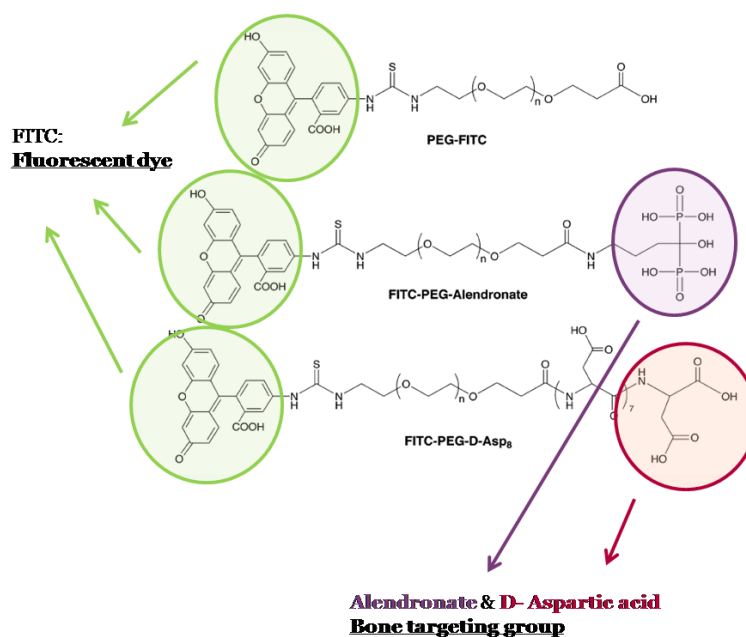


Figure 1.33. PEG-alendronate conjugates for bone targeted drug delivery [153].

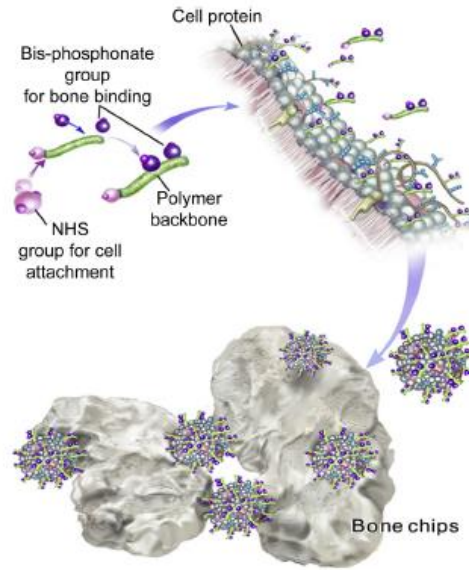


Figure 1.34. Engineering of the cell membrane for bone targeting [158].

1.4.2. Bone Tissue Engineering Applications

Bone has a complex architecture which consists of an organic protein component (collagen, glycoproteins, sialoproteins) and an inorganic mineral component such as hydroxyapatite $[\text{Ca}_{10}(\text{PO}_4)_6(\text{OH})_2]$ crystals [22]. This hybrid structure of bone has a dynamic nature and is constantly being remodeled by osteoclast and osteoblast cells that resorb and form bone tissue respectively [159].

Biom mineralization is a key process for the regeneration of bone in which the organic phase serves as a template for the inorganic mineral phase in order to form a composite material with unique mechanical properties [30]. Inspired from nature, design of polymers possessing Ca^{2+} binding ligands that mimic proteins of natural bone are appealing candidates to be biom mineralized for fabrication of bone-like composite materials for tissue engineering applications. Especially the development of biocompatible hydrogel scaffolds that match the physical and chemical properties of bone is an emerging field of research.

The extracellular matrix of bone contains proteins which are rich in polyaspartic acid and polyglutamic acid residues, therefore have an anionic character. These negatively charged functional groups are believed to play an important role in the mineralization process by serving as Ca^{2+} binding ligands and providing nucleating sites to induce mineralization [160]. Chirila *et al.* discussed the effect of carboxyl, phosphate and phosphonate groups on the enhancement of calcification [161].

Polymethacrylamide and polymethacrylate based hydrogels which contain mineral binding co-monomers with anionic groups similar to glutamate, aspartate, and phosphoserine were synthesized and their ability to template hydroxyapatite formation was evaluated (Figure 1.35) [162]. In another study by same researchers anionic groups which promote mineralization were generated in situ on the surface of hydrogels by a procedure involving thermal decomposition of urea [163]. The decomposition of urea increases the pH which leads to the hydrolysis of the ester groups in the hydrogel into acid groups.

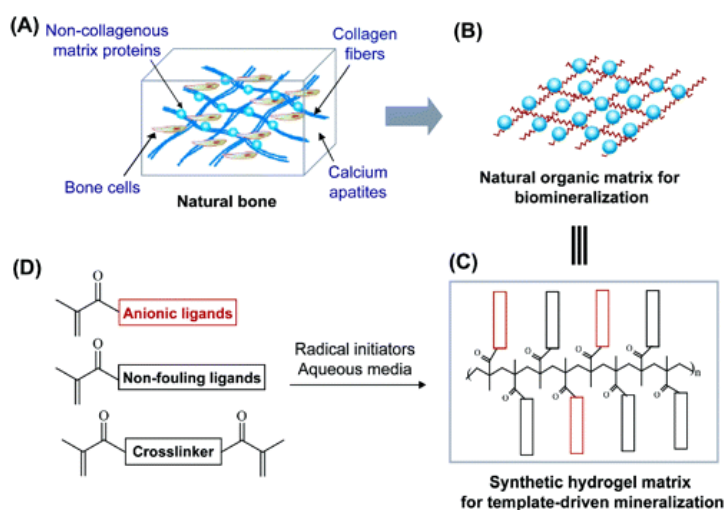


Figure 1.35. Biomimetic mineralization of hydrogels [162].

Polymers containing phosphorus based moieties were investigated for biomimetic mineralization and they were found to be promising candidates for bone tissue engineering applications (Figure 1.36). Non-cytotoxic surfaces grafted with copolymers of poly(vinyl

phosphonic acid) and acrylamide with varying phosphonic acid content were prepared [164]. They found that the surfaces modified by poly(vinyl phosphonic acid) copolymers promoted osteoblast-like cell adhesion, proliferation, differentiation and had enhanced mineralization ability. Vinyl phosphonic acid was copolymerized with N-isopropylacrylamide to prepare an injectable hydrogel system with thermo-responsive behavior [165]. The increase of vinyl phosphonic acid groups in these hydrogels lead to an increase in biomineralization due to enhanced nucleation and growth of calcium phosphate in the hydrogels. Ethylene glycol methacrylate phosphate was incorporated into PEG hydrogels to accomplish improved cell adhesion of human mesenchymal stem cells to these hydrogel systems [166]. Incorporation of ethylene glycol methacrylate phosphate formed a bone-like mineral phase and increased both rate and extent of mineralization. The same monomer, ethylene glycol methacrylate phosphate, was copolymerized with 2-hydroxyethyl methacrylate in order to fabricate hydrogels which facilitate cell adhesion and mineralization [167]. The synthesis of a copolymer series with increasing amounts of ethylene glycol methacrylate phosphate was reported to enhance hydroxyapatite deposition [168]. (Diethylamino) ethyl methacrylate and 1-vinyl-2-pyrrolidinone were used as co-monomers in these polymers. The influence of the phosphate content on mineralization was investigated by incubating the polymers in synthetic body fluid. Recently, poly(ϵ -caprolactone) functionalized with poly(vinyl phosphonic acid-co-acrylic acid) was electrospun to fabricate scaffolds to be used as bone graft substitutes [169].

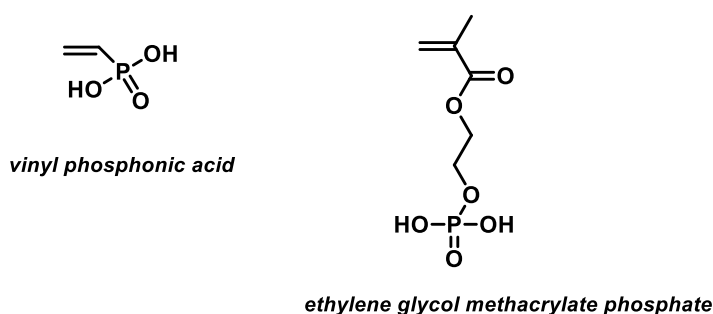


Figure 1.36. Structure of phosphonic acid containing monomers used for tissue engineering applications.

Bisphosphonate based hydrogels were also investigated to be used as scaffolds for bone tissue. For example hydrogels were made from N-isopropylacrylamide and N-acrylpamidronate, a monomer derived from pamidronate which is a bisphosphonate containing drug [170]. The ability of synthesized hydrogels to mineralize was investigated. The synthesis of in situ forming hybrid hydrogels based on hyaluronic acid was reported (Figure 1.37) [171]. The hydrogel was formed by mixing Ca^{2+} ions, a hyaluronic acid derivative functionalized with aldehyde groups, another hyaluronic acid derivative which contains bisphosphonate ligands and is functionalized with hydrazide groups. The mineralization is supported by strong interaction between bisphosphonate moieties and Ca^{2+} ions within the gel which act as nucleation regions for further mineralization.

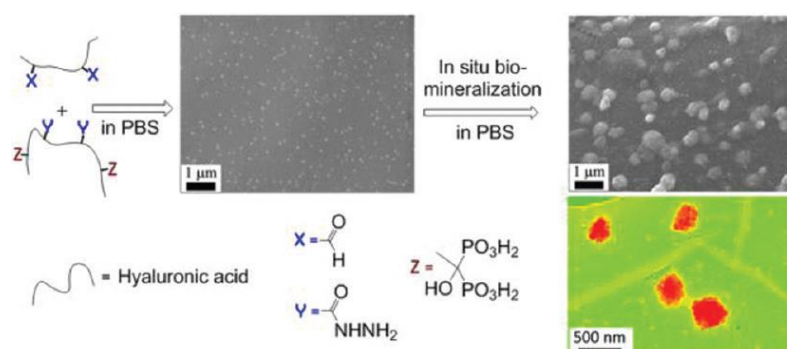


Figure 1.37. In situ forming hybrid hydrogels [171].

1.4.3. Dental Applications

Acidic monomers (carboxylic, phosphonic, phosphoric acids etc.) are particularly important as a component of dental materials because the concept of self-etching adhesives and composites relies on conditioning and priming ability of acidic monomers. Phosphorus-containing monomers with particularly phosphonic acid and mono- or dihydrogen phosphate groups have been explored extensively as components of self-etching dental adhesives [32].

The hydrolytic instability of phosphate monomers makes phosphonic acid monomers a better choice as self-etching adhesive monomers. Anbar *et al.* first showed that vinylphosphonic acid (VPA), 4-vinylbenzylphosphonic acid (VBPA) and their copolymers can improve the adhesion on etched enamel [172, 173]. These monomers were less reactive than methacrylates in radical polymerization. Monomers in which reactive methacrylates are linked to phosphonic acid through stable ether bonds were synthesized to be used as self-etching adhesive monomers [174-177]. Methacrylates of hydroxyalkyl phosphonates have been proposed as self-etching adhesive monomers, but unfortunately they undergo hydrolysis [178]. Structures of cited self-etching adhesive monomers are depicted in Figure 1.38.

Many novel phosphonate / phosphonic acid and bisphosphonate / bisphosphonic acid based monomers have been synthesized in our lab in the past years and evaluated as self-etching adhesive monomers for dental applications [179-185].

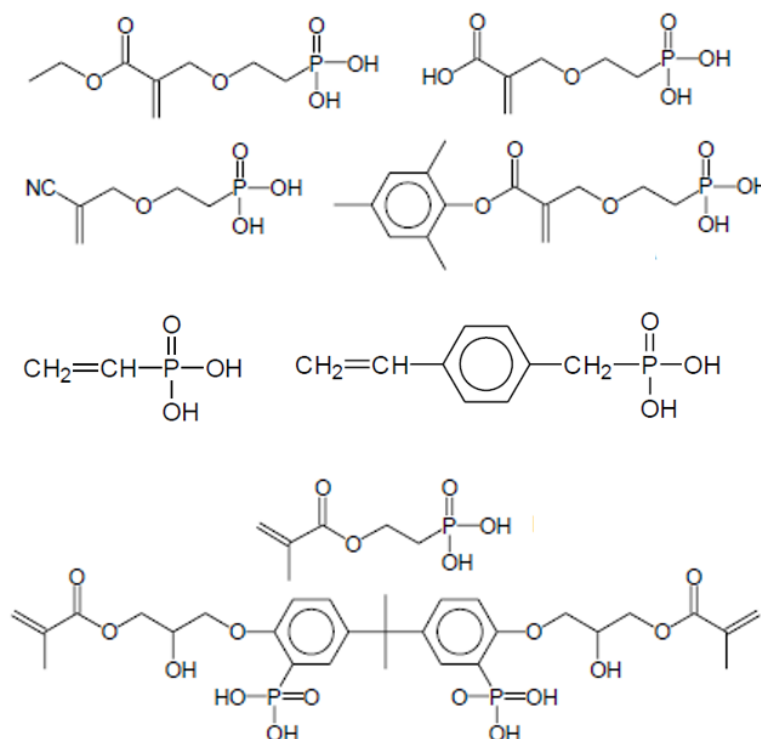


Figure 1.38. Structures of phosphonic acid based self-etching adhesive monomers.

Interaction of acidic monomers with hydroxyapatite based tissues can be explained by the pioneering concept of `Adhesion-Decalcification` introduced by Yoshida *et al.* (Figure 1.39) [186]. According to this concept, the first bonding step (P1) of acidic monomer with hydroxyapatite releases phosphate (PO_4^{3-}) and hydroxide (OH^-) ions and the surface remains electro-neutral. Two routes are possible for the second bonding step depending on the stability of the formed bond to calcium. If the bond is stable, the acidic monomer will prefer to remain bonded to hydroxyapatite which results in chemical adhesion between the monomer and hydroxyapatite of the dental tissue. If the bond is not stable, debonding, decalcification and release of Ca^{2+} and phosphonate ions from tooth surface occurs.

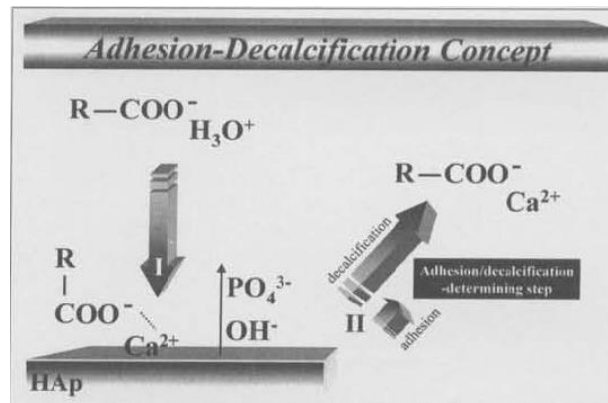


Figure 1.39. Adhesion-Decalcification concept [186].

2. OBJECTIVES AND SCOPE

In this study, stimuli responsive polymers and hydrogels functionalized with various functional groups (phosphonate, phosphonic acid, carboxylate, β -aminoester, disulfide) were designed, synthesized and their properties were evaluated for biomedical applications. These polymers and hydrogels were explored as potential biomaterials with a particular focus on bone tissue engineering and controlled drug release applications.

Phosphonate/phosphonic acid groups have strong interactions with hydroxyapatite which is the main constituent of bone and dental tissues. This feature makes biomaterials functionalized with these groups suitable for dental and bone-related applications. Phosphonic acid and carboxylate groups provide pH response to the materials they are incorporated into, facilitating a means to control properties such as pH dependant swelling, degradation and release. Similarly β -aminoester group is also pH responsive and polymers containing this group in their backbone, namely poly(β -aminoester)s, are used as degradable tissue scaffolds. Disulfide groups have redox-response which is widely used by incorporating them into polymeric drug delivery systems or hydrogels with the aim of controlling the redox-dependent degradation and release kinetics.

In the first chapter pH and redox responsive degradable gels/cryogels were synthesized from disulfide/phosphonate-functionalized poly(β -aminoester) macromers as potential materials for bone tissue engineering applications. Secondly, disulfide functionalized-poly(β -aminoester) hydrogels with pH and redox response were fabricated and used for controlled release of photosensitizers. Thirdly, phosphonic acid-functionalized acrylamides were synthesized and their properties were evaluated to explore their potential to be used as self-etching dental adhesives and building blocks for bone-like composite materials. Lastly, carboxylic acid-functional crosslinkers were fabricated into pH and redox responsive hydrogels which were used for controlled release applications.

3. REDOX-RESPONSIVE PHOSPHONATE-FUNCTIONALIZED POLY(β -AMINO ESTER) GELS AND CRYOGELS

This chapter is published as: Bingol, H. B., F. Demir Duman, H. Yagci Acar, M. B. Yagci, D. Avci, “Redox-responsive phosphonate-functionalized poly(β -amino ester) gels and cryogels”, *Eur. Polym. J.*, Vol. 108, pp. 57-68, 2018.

3.1. Introduction

Poly(β -amino ester) networks have gained attention as a class of degradable polymers for biomedical applications, particularly as scaffolds for tissue engineering. The degradation of PBAEs is largely governed by the chemical structure and it is possible to enhance the degradation by incorporation of trigger responsive domains (pH, UV light and redox) within the structure. Phosphorus based molecules such as phosphates, phosphonates and bisphosphonates provide biodegradability, hemocompatibility and protein adsorption resistance to polymers which they are incorporated into. Strong interactions of these materials with hydroxyapatite (HAP)-based tissues such as dentin, enamel, and bone make them promising candidates for applications in dentistry, bone targeted imaging and drug delivery, and bone tissue engineering applications.

In this work we aim to combine the desirable properties of phosphonate group and redox-responsiveness of disulfide groups to obtain degradable PBAE based network polymers designed for bone tissue engineering applications. Two novel phosphonated diamines (one containing a redox-responsive disulfide group) were reacted with diacrylates *via* aza-Michael addition reaction to form acrylate terminated poly(β -amino ester)s which were subsequently used as macromolecular precursors for fabrication of degradable gels and cryogels. The degradation rates of the gels and cryogels are monitored in phosphate buffer saline (PBS) and dithiothreitol (DTT). The *in vitro* cytotoxicities of the degradation products

are assessed with mouse embryonic fibroblast cells (NIH 3T3) and human osteosarcoma cells (Saos-2).

3.2. Experimental

3.2.1. Materials and Methods

1,6-hexanediamine, cystamine dihydrochloride salt, diethyl vinylphosphonate, triethyl amine (TEA), poly(ethylene glycol) diacrylate (PEGDA, $M_n=575$), 1,6-hexanediol diacrylate (HDDA), 2,2-dimethoxy-2-phenylacetophenone (DMPA), dithiothreitol (DTT) and all solvents were purchased from Sigma-Aldrich and used as received. Roswell Park Memorial Institute (RPMI) 1640 medium (with l-glutamine and 25 mM HEPES), penicillin/streptomycin (pen-strep) and trypsin-EDTA were purchased from Multicell, Wisent (Canada). Fetal bovine serum (FBS) was obtained from Capricorn Scientific GmbH (Germany). Thiazolyl blue tetrazolium bromide (MTT) and phosphate buffered saline (PBS) tablets were provided by Biomatik (Canada). 96-well plates were purchased from Nest Biotechnology (China). NIH 3T3 mouse embryonic fibroblast cells and Saos-2 human osteosarcoma cells were a kind gift of Dr. Halil Kavakli (Department of Molecular Biology and Genetics, Koc University, Istanbul, Turkey).

The chemical structures of phosphonate-functionalized diamines and PBAE macromers were proved by ^1H NMR, ^{13}C NMR, ^{31}P NMR and FTIR spectroscopies. NMR spectra were recorded on Varian Gemini 400 MHz spectrometer using CDCl_3 as solvent and TMS as an internal reference. FTIR spectra were recorded on a Thermo Scientific Nicolet 380 spectrometer. Raman spectra were recorded using Renishaw Invia raman microscope. Glass transition temperature (T_g) of PBAE macromers and gels were analyzed with differential scanning calorimetry (TA Instruments Q100). 5-10 mg sample was placed and sealed inside the pan and heated under nitrogen atmosphere from $-80\text{ }^\circ\text{C}$ to $80\text{ }^\circ\text{C}$ with a

scanning rate of 10 °C min⁻¹. Degradation studies were done using a VWR Incubating Mini Shaker operating at 37 °C and 200 rpm.

3.2.2. Synthesis of Phosphonate-Functionalized Diamines

3.2.2.1. Synthesis of tetraethyl ((hexane-1,6-diylbis(azanediyl))bis(ethane-2,1-diyl))bis(phosphonate) (A1). 1,6-hexanediamine (0.23 g, 2 mmol) and diethyl vinylphosphonate (0.74 mL, 4.8 mmol) were mixed at room temperature for 2 days. The mixture was washed with petroleum ether to remove unreacted diethyl vinylphosphonate and the pure product was obtained as a light yellow viscous liquid in 94 % yield. ¹H NMR (400 MHz, CDCl₃, δ): 1.31 (m, 16H; CH₃ and CH₂CH₂CH₂CH₂), 1.43 (m, 6H; CH₂CH₂CH₂CH₂, NH), 1.93 (dt, *J* = 16 Hz, *J* = 8 Hz, 4H; CH₂-P), 2.57 (t, *J* = 8 Hz, 4H; CH₂CH₂CH₂NH), 2.87 (4H; NHCH₂CH₂P), 4.08 (m, 8H; OCH₂) ppm; ¹³C NMR (100 MHz, CDCl₃, δ): 16.33 (CH₃), 25.72, 27.10 (C-P), 27.20 (CH₂CH₂CH₂CH₂), 29.94 (CH₂CH₂CH₂CH₂), 43.28 (NHCH₂CH₂-P), 49.48 (CH₂CH₂CH₂NH), 61.63 (OCH₂); ³¹P NMR (150 MHz, CDCl₃, δ): 30.55 ppm FTIR (ATR): ν = 3487 (w; N-H), 2980 and 2927 (C-H), 1236 (P=O), 1022 and 951 (P-O) cm⁻¹.

2.3.2.2. Synthesis of tetraethyl (((disulfanediylbis(ethane-2,1-diyl))bis(azanediyl))bis(ethane-2,1-diyl))bis(phosphonate) (A2). First, cystamine dihydrochloride salt was neutralized to cystamine using TEA. Cystamine dihydrochloride salt (0.45 g, 2 mmol) was dissolved in 2 mL of distilled water and TEA (0.62 mL, 4.4 mmol) was added dropwise in an ice bath. The solution was stirred for 15 minutes at room temperature. Diethyl vinylphosphonate (0.74 mL, 4.8 mmol) dissolved in 2 mL of distilled water was added to the reaction mixture which was then stirred at room temperature for 2 days. The mixture was extracted with diethyl ether (3 x 20 mL), the ether phase was dried over sodium sulfate and the solvent was removed under reduced pressure. The residue was finally washed with petroleum ether to remove unreacted diethyl vinylphosphonate. The product was obtained as a light yellow viscous liquid in 27 % yield. ¹H NMR (400 MHz, CDCl₃, δ): 1.31 (t, *J* = 16 Hz, 12H; CH₃), 1.74 (s, 2H; NH), 1.93 (dt, *J* = 16 Hz, *J* = 8 Hz, 4H; CH₂-P), 2.80 (t, *J* =

8 Hz, 4H; S-CH₂), 2.92 (m, 8H; S-CH₂CH₂ and NHCH₂CH₂P), 4.10 (m, 8H; OCH₂); ¹³C NMR (100 MHz, CDCl₃, δ): 16.34 (CH₃), 25.73, 27.12 (C-P), 38.42 (S-CH₂), 42.93 (NHCH₂CH₂-P), 47.62 (S-CH₂CH₂), 61.61 (OCH₂); ³¹P NMR (150 MHz, CDCl₃, δ): 30.20 ppm; FTIR (ATR): ν = 3425 (N-H), 2978 and 2943 (C-H), 1475 (N-H), 1221 (P=O), 1020 and 961 (P-O) cm⁻¹.

3.2.3. Synthesis of PBAE Macromers

The diacrylates (PEGDA or HDDA) and phosphonated diamines A1 or A2 were mixed at a molar ratio of 1.1:1 at room temperature for 4 days while stirring. After the precipitation of the mixtures into diethyl ether (PEGDA-based ones) or petroleum ether (HDDA-based ones) to remove unreacted diacrylates and amines, the macromers were obtained as colorless to light yellow viscous liquids.

3.2.4. pH Sensitivity of PBAE Macromer

50 mg of macromer was dissolved in deionized water with a final concentration of 1.0 mg mL⁻¹ and the pH was adjusted to 2 by HCl. The macromer solution was titrated using 0.1 M NaOH aqueous solution with increments of 50 μ L. The increase in pH was recorded with a pH meter (WTW Inolab pH 720) at room temperature. The pK_b value was determined from the inflection point of the titration curve which responds to the pH value where 50% of protonated amine groups are neutralized.

3.2.5. Synthesis of PBAE Gels

PBAE macromer and initiator (DMPA 1% w) mixtures were placed into glass molds and exposed to UV light (365 nm) at room temperature for 30 minutes in a photoreactor

(Kerman UV/18) containing 12 Philips TL 8W BLB lamps. The obtained PBAE network polymer samples (diameter: 1 cm, thickness: 0.2 cm) were dried under vacuum and weighed (W_i). Then they were immersed in excess ethanol to remove unreacted components, dried in a vacuum oven, and were weighed again (W_f). The percent gelations were calculated according to equation (3.1):

$$Gelation(\%) = \frac{W_f}{W_i} \times 100 \quad (3.1)$$

3.2.6. Synthesis of PBAE Cryogels

0.1 g PBAE macromer is dissolved in 0.75 mL 1,4-dioxane containing initiator (DMPA 1% w), placed into glass molds and exposed to UV light (365 nm) for 15 minutes at subzero temperature in a photoreactor (Kerman UV/18) containing 12 Philips TL 8W BLB lamps. The obtained cryogels were thawed at room temperature and removed from the mold. They were washed with 1,4-dioxane and then immersed into THF to remove unreacted components. Finally the cryogels were dried in vacuum oven. The percent gelations were calculated as described for gels.

3.2.7. SEM Characterization

The morphology of PBAE gels and cryogels was observed by scanning electron microscopy (SEM). The freeze-dried samples were sputter-coated with a gold layer and then examined with a SEM (FEI-Philips XL30), at 1000 x magnification, with an accelerating voltage of 7.0 kV.

3.2.8. Swelling Studies

Dry PBAE gel or cryogel samples were weighed, their diameters were measured and they were immersed into distilled water at room temperature. After reaching equilibrium swelling, the samples were removed from water, blotted on filter paper, and then the swollen weight and swollen diameter were measured. The weight swelling ratio (q_w) and volume swelling ratio (q_v) were calculated using equation (3.2) and (3.3) respectively:

$$q_w = \frac{m_s}{m_d} \times 100 \quad (3.2)$$

$$q_v = \left(\frac{D_s}{D_d}\right)^3 \times 100 \quad (3.3)$$

where m_s and m_d refer to the mass of swollen and dry gel samples; D_s and D_d refer to the gel diameters of swollen and dry gel samples, respectively. The average data obtained from triplicate measurements were reported.

3.2.9. Degradation Studies

Degradation studies were implemented under physiological conditions, at 37 °C and pH = 7.4. All PBAE gels and cryogels were weighed (W_i), immersed in 4 mL PBS solution and placed on an orbital shaker at 200 rpm. Additionally, disulfide containing PBAE gels A2-PEGDA and A2-HDDA were also immersed in 4 mL PBS containing 25 mM DTT solution. Degradation solutions were refreshed every 3 days throughout the study. At predetermined time intervals, the polymers were removed from solution, freeze-dried and weighed (W_f). The average data obtained from triplicate measurements were reported and the degradation % was calculated according to equation (3.4):

$$\text{Degradation (\%)} = \frac{W_i - W_f}{W_i} \times 100 \quad (3.4)$$

3.2.10. *In vitro* Cytotoxicity Assay

Two different cell lines, NIH 3T3 and Saos-2 cells, were used for the assessment of cytotoxicity of the degradation products of the gels. The cells were cultured in RPMI 1640 complete medium supplemented with 10% (v/v) FBS and 1% (v/v) Pen-Strep in a humidified atmosphere of 5% CO₂ in an incubator at 37 °C and passaged in every 2–3 days. The cells were seeded at a density of 104 cells/well into 96-well plates in RPMI 1640 complete medium (37 °C, 5% CO₂) until 60–80% confluency. Then, the cells were treated with the degradation products in 10–200 µg/mL doses and incubated for 24 h. The cell viability was determined with standard MTT colorimetric assay: 50 µL of MTT solution (5 mg/mL in PBS) and 150 µL of culture medium were added into each well and incubated for 4 h. Mitochondrial activity was indicated by the formation of purple formazan crystals which were dissolved in ethanol:DMSO (1:1 v/v) mixture. Absorbance of each sample at 600 nm with a reference reading at 630 nm was recorded using a BioTek ELX800 microplate reader (BioTek Instruments Inc., Winooski, VT, USA). 100% viability is assumed for the control cells which were not treated with the degradation products. The relative cell viability was calculated from equation (3.5):

$$\text{Cell viability (\%)} = \frac{\text{Absorbance}_{\text{sample}}}{\text{Absorbance}_{\text{control}}} \times 100 \quad (n = 4) \quad (3.5)$$

3.2.11. Statistical Analysis

Statistical analysis of the degradation products were conducted by using nonparametric Kruskal–Wallis one-way analysis of variance followed by multiple Dunn’s comparison test of GraphPad Prism 6 software package (GraphPad Software, Inc., USA). All measurements

were expressed as mean values \pm standard deviation (SD). $p < 0.05$ was accepted as statistically significant difference ($n=5$).

3.3. Results and Discussion

3.3.1. Synthesis of Phosphonate-Functionalized Diamines

Phosphonate-functionalized diamines were used as building blocks for the synthesis of PBAE macromers. These diamines A1 and A2 were synthesized by aza-Michael reaction of diethyl vinylphosphonate with 1,6-hexanediamine and cystamine respectively (Figure 3.1). They were highly soluble in polar and weakly polar solvents, but insoluble in non-polar organic solvents (Table 3.1).

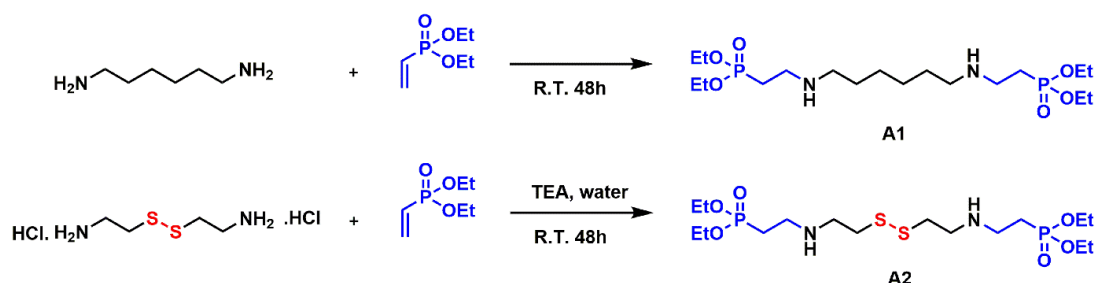


Figure 3.1. Synthesis of A1 and A2.

Table 3.1. Solubility of A1 and A2 in selected solvents.

Amines	Water	Methanol	Dichloromethane	Diethyl ether	Chloroform	Petroleum ether
A1	+	+	+	+	+	-
A2	+	+	+	+	+	-

The diamines were characterized by ^1H , ^{13}C and ^{31}P NMR and FTIR spectroscopies in order to confirm their structure. FTIR spectra of these diamines show NH stretching vibration from 3600 to 3200 cm^{-1} as well as $\text{P}=\text{O}$ stretching vibrations at around 1230 cm^{-1} . $\text{P}-\text{O}-\text{Et}$ stretching peaks are also seen at around 1020 and 950 cm^{-1} (Figure 3.2). Phosphorus-hydrogen coupling caused complex peaks in ^1H NMR spectra of both amines, for example a doublet of triplet at about 1.93 ppm corresponding to the methylene in the α -position of phosphonate group was observed (Figure 3.3). A slight excess of diethyl vinylphosphonate was used to functionalize both ends of the amines, but this led to the formation of trisubstituted amines as a side product in small amount, as can be seen from ^{13}C NMR (Figure 3.4).

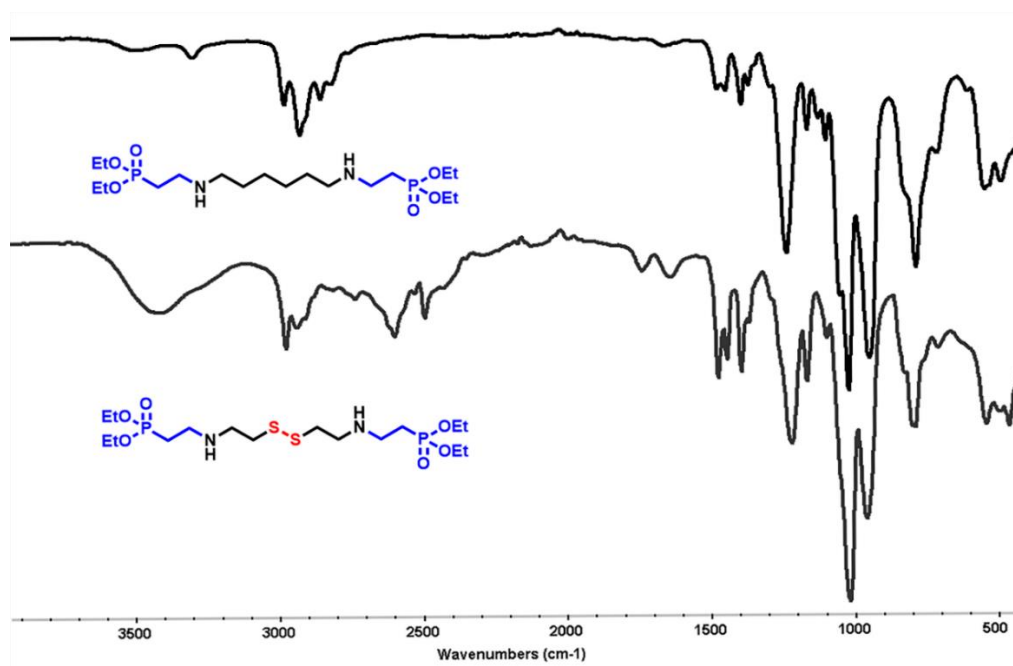
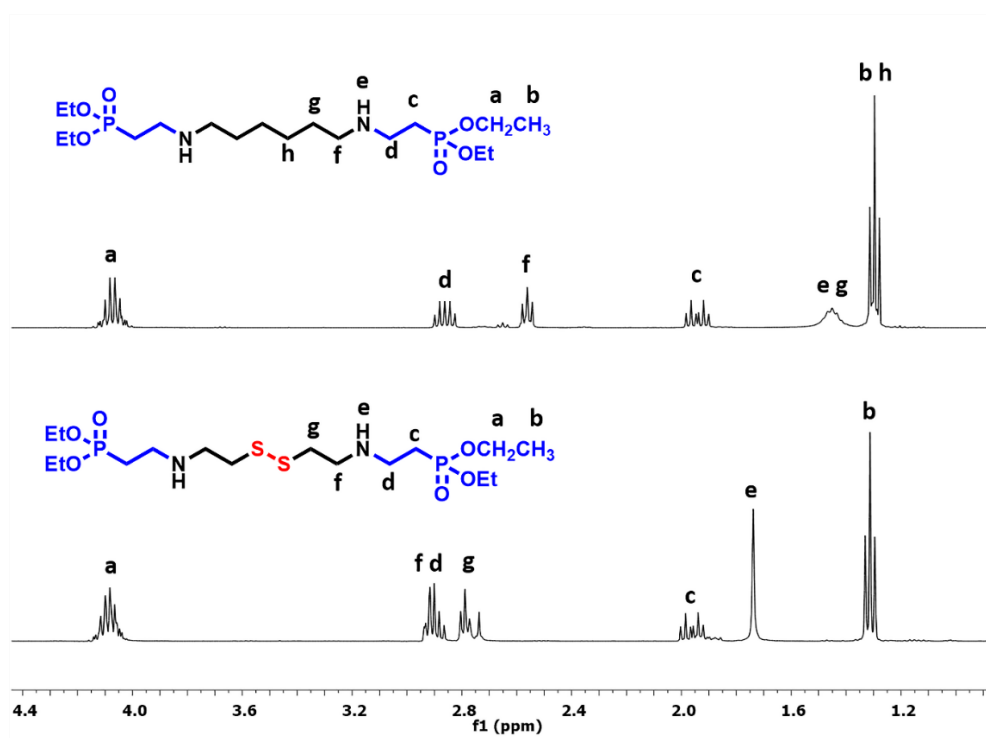
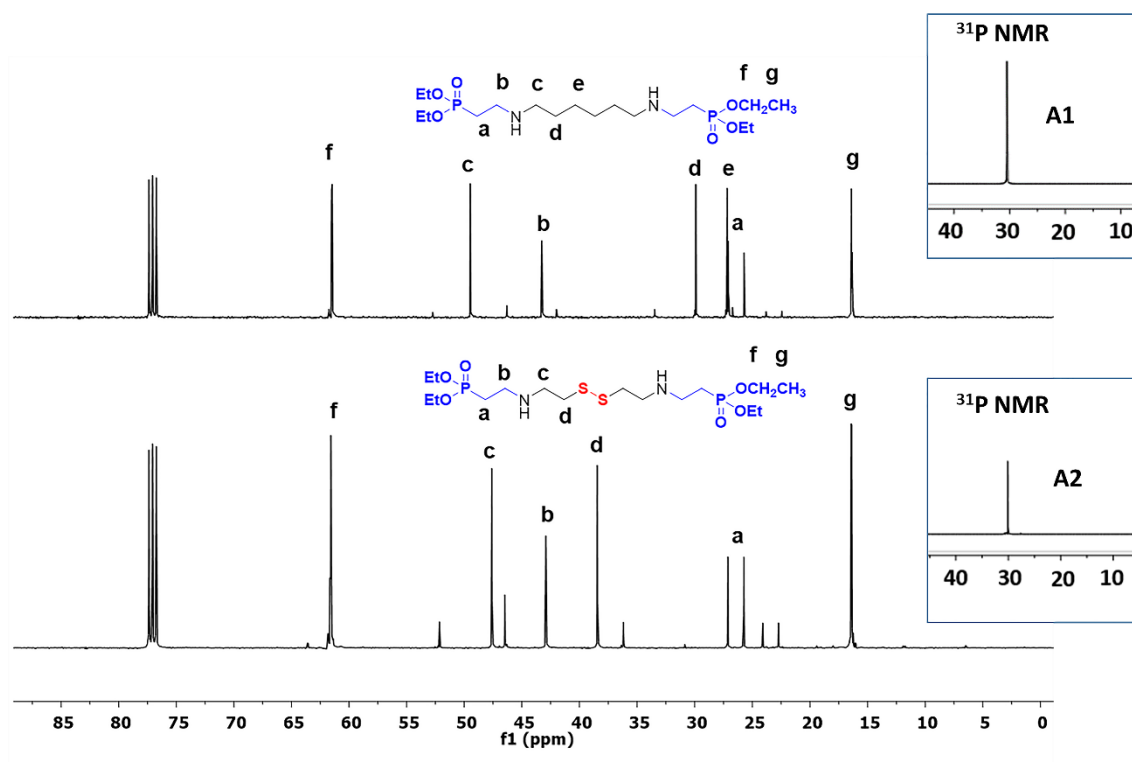


Figure 3.2. FTIR spectra of A1 and A2.

Figure 3.3. $^1\text{H-NMR}$ spectra of A1 and A2.Figure 3.4. $^{13}\text{C-NMR}$ and $^{31}\text{P NMR}$ spectra of A1 and A2.

3.3.2. Synthesis and Characterization of Poly(β -amino ester) Macromers

Biodegradable diacrylate terminated phosphonate-functionalized PBAE macromers were produced using the solvent-free aza-Michael addition of A1 and A2 to diacrylates (HDDA and PEGDA) at room temperature (Figure 3.5). The diamines both contain phosphonate groups to enhance biocompatibility and interactions with hydroxyapatite based tissues such as bone. A2 also contains a bio-reducible disulfide group which can be cleaved in the reductive microenvironment in tumor cells. The disulfide groups in the hydrogel can be used to control its degradation and in our work DTT is used to simulate the said reductive microenvironment.

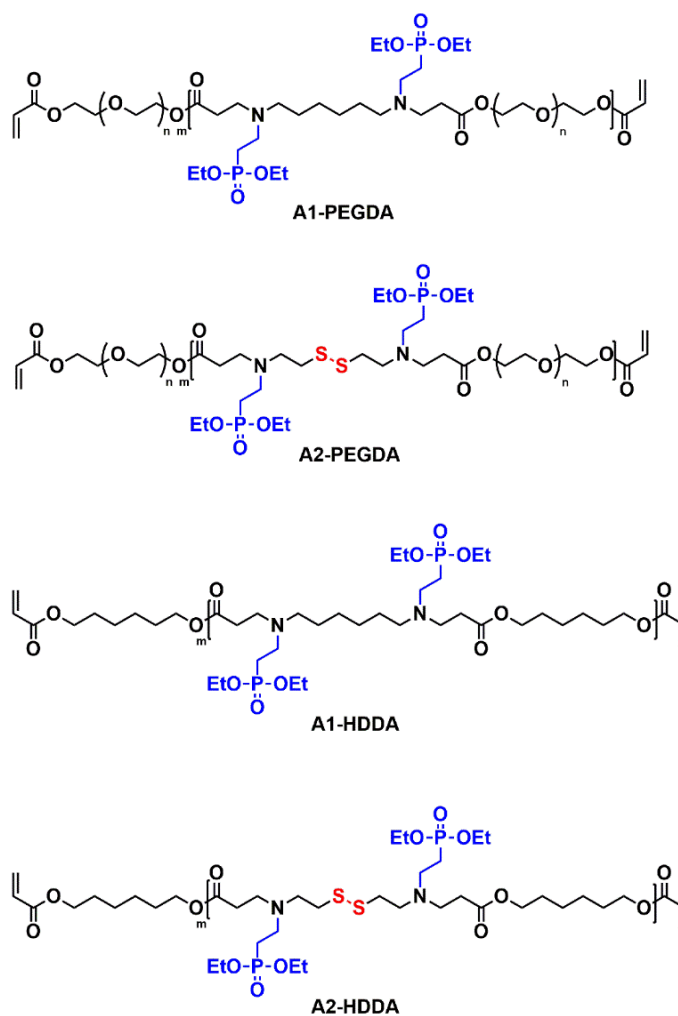


Figure 3.5. Structure of macromers A1-PEGDA, A2-PEGDA, A1-HDDA and A2-HDDA.

Table 3.2. Solubility of PBAE macromers in selected solvents.

Amines	Water	Methanol	Dichloromethane	Diethyl Ether	Ethanol	Hexane
A1-PEGDA	+	+	+	-	+	-
A1-HDDA	+/-	+	+	+/-	+/-	+/-
A2-PEGDA	+	+	+	-	+	-
A2-HDDA	+/-	+	+	+	+	-

The diacrylates PEGDA and HDDA were selected due to their different hydrophilicities, to extend the range of network properties. Diacrylate to amine molar ratio and other reaction conditions such as solvent, temperature and time were adjusted carefully to control the extent of polymerization and to try to avoid formation of crosslinked polymers. Bulk reaction with 1.1:1 diacrylate to amine ratio at room temperature gave the optimal result for synthesis of the diacrylate terminated macromers. The macromers were obtained as pale yellow viscous liquids in high yields (65-96%). The structures of the synthesized macromers were confirmed using ^1H NMR spectroscopy (Figure 3.6 and 3.7). The peaks between 5.7-6.4 ppm indicate that the PBAEs are end-capped with acrylate groups available for further photopolymerization. The characteristic peaks coming from the phosphonate and amine groups are also observed. The appearance of a new triplet at 2.44 ppm proves the reaction has taken place successfully.

The average number of repeat units (n) which can be correlated with the number average molecular weight, was calculated using ^1H NMR spectra. Assuming that all end groups are acrylates, the acrylate protons between 5.7-6.4 ppm were integrated with respect to methylene protons attached to carbonyl at 2.4 ppm or ethyl groups of the phosphonate at 1.3 and 4.1 ppm. The n values calculated for A2-based macromers (3,4) were found to be lower than A1-based ones (8,11), which may be due to the residual trisubstituted amines (Table 3.2). FTIR spectra of macromers showed peaks at 1730, 1630, 1243, 1016 and 966 cm^{-1} due to C=O, C=C, P=O and P-O stretching, respectively (Figure 3.8).

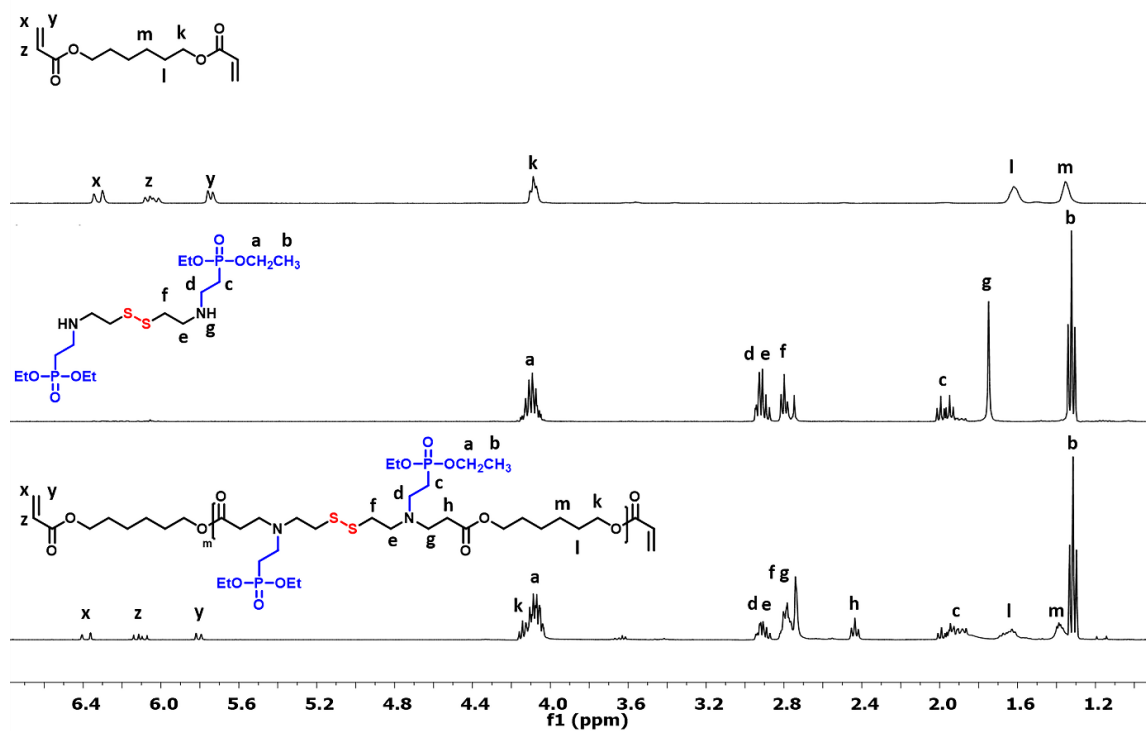


Figure 3.6. ^1H NMR spectra of HDDDA, A2 and the A2-HDDDA macromer.

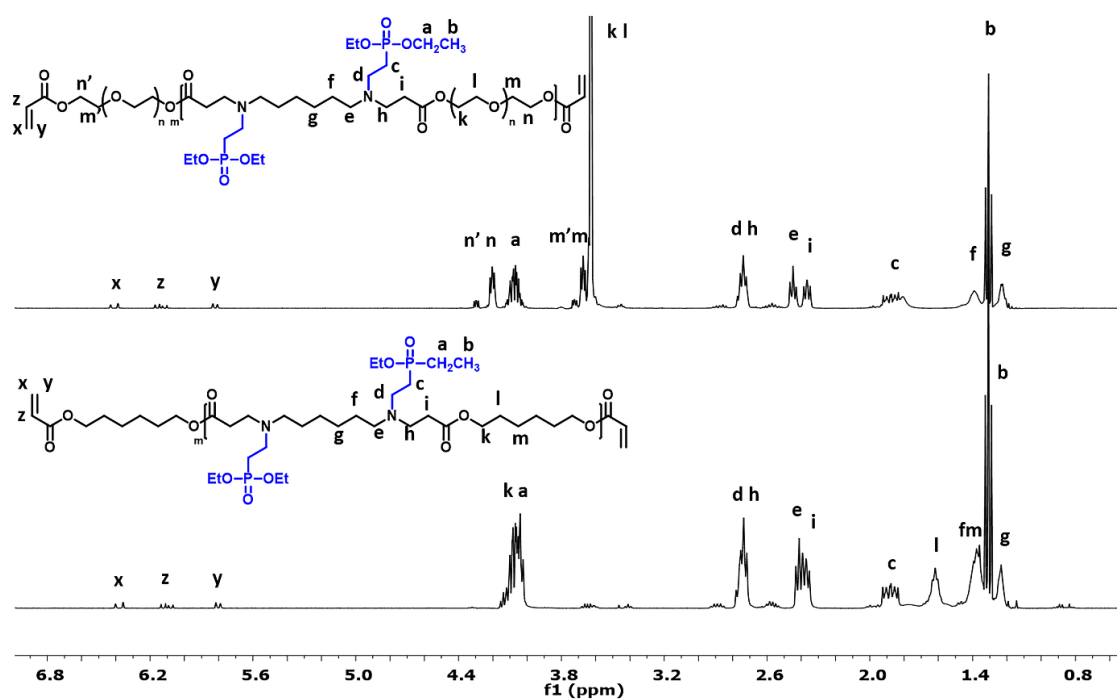


Figure 3.7. ^1H NMR spectra of the A1-PEGDA and A1-HDDDA macromers.

Table 3.3. Properties of PBAE macromers

Macromer	M_n	n
A1-PEGDA	7800	8
A2-PEGDA	4260	4
A1-HDDA	7350	11
A2-HDDA	1800	3

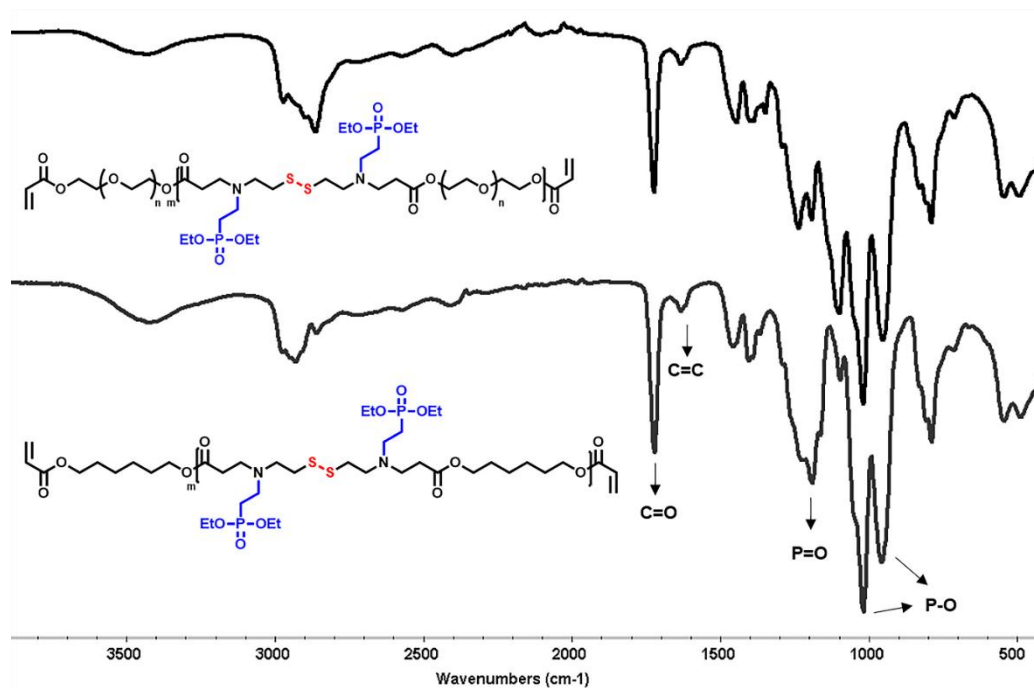


Figure 3.8. FTIR spectra of the A2-PEGDA and A2-HDDA macromers.

The pK_b values of PBAE macromers were determined by titration in order to evaluate their pH-sensitivity. In the acid-base titration profiles presented, macromers showed pH buffering capacities at different regions depending on molecular structure (Figure 3.9).

For macromers with low molecular weight (A2-PEGDA and A2-HDDA) the plateau was hardly observed whereas higher molecular weight ones (A1-PEGDA and A1-HDDA) had longer plateaus indicating a higher buffering capacity. It is reported that pK_b values shift to higher regions with an increase in hydrophilicity [187]. This trend is consistent with A1 based macromers, where the pK_b is 5.86 for A1-HDDA and 6.46 for A1-PEGDA.

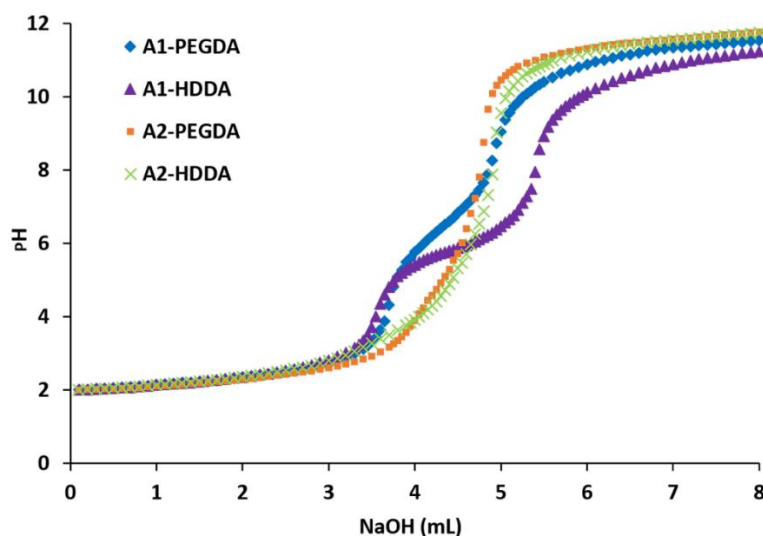


Figure 3.9. Titration curves of PBAE macromers.

3.3.3. Synthesis of PBAE Gels and Cryogels

The macromers were bulk photopolymerized into gels by ultraviolet light exposure in the presence of DMPA (1 w %) as photoinitiator (Figure 3.10). The remaining unreacted monomers and initiator were removed by placing the samples in ethanol. After drying the gelation percentages were found to be ranging from 66% to 77%. To obtain networks with increased porosity, the macromers were also used to fabricate cryogels. Cryogelation is a convenient method to produce a macroporous structure which is especially preferred for tissue engineering applications due to its capability of providing a suitable scaffold for the cells and allowing transfer of nutrients and wastes [188]. Cryogels are formed at temperatures below the freezing point of the solvent where the solvent crystals act as a

template to produce the macroporous structure. The PBAE cryogels were obtained with gelation percentages between 63% and 84%.

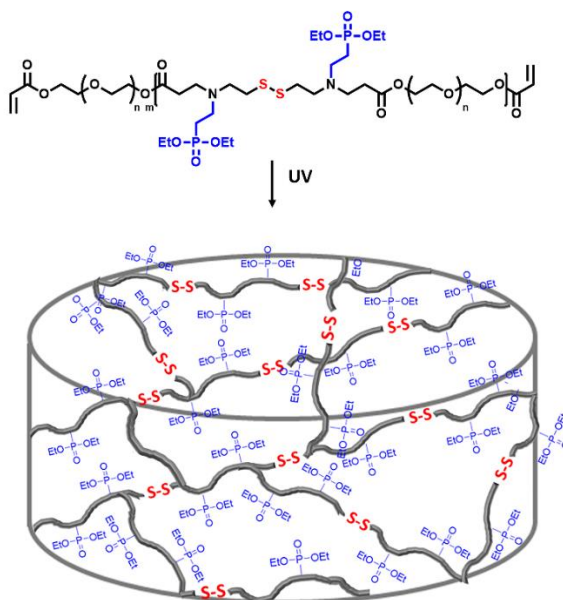


Figure 3.10. Synthesis of PBAE gels and cryogels.

The presence of the disulfide group in the redox-responsive network polymers was verified by Raman spectroscopy (Figure 3.11). The spectrum of A2-HDDA contains ν_{SS} and ν_{CS} bands at 506 cm^{-1} and 644 cm^{-1} respectively. These two bands are not observed in the spectrum of A1-HDDA which does not contain any disulfide group.

The effect of macromer and gel structures on their glass transition temperatures was studied by DSC (Table 3.4). In general, PBAEs have low T_g due to their highly flexible structures resulting from the long ethylene glycol or alkyl chains in their backbones. The T_g ranged from $-54.2\text{ }^\circ\text{C}$ to $-63.7\text{ }^\circ\text{C}$ for the macromers, and from $-35.3\text{ }^\circ\text{C}$ to $-54.4\text{ }^\circ\text{C}$ for the gels (Figure 3.12). Since crosslinking decreases the mobility of PBAE macromer chains, the gels have higher T_g values than the corresponding macromers, as expected. For the gels studied, the T_g values are monotonically decreasing with macromer molecular weight.

Table 3.4. T_g of PBAE macromers and gels

Macromer	T_g of macromers	T_g of gels
A1-PEGDA	-58.7	-54.4
A2-PEGDA	-54.2	-47.3
A1-HDDA	-63.7	-50.1
A2-HDDA	-60.2	-35.3

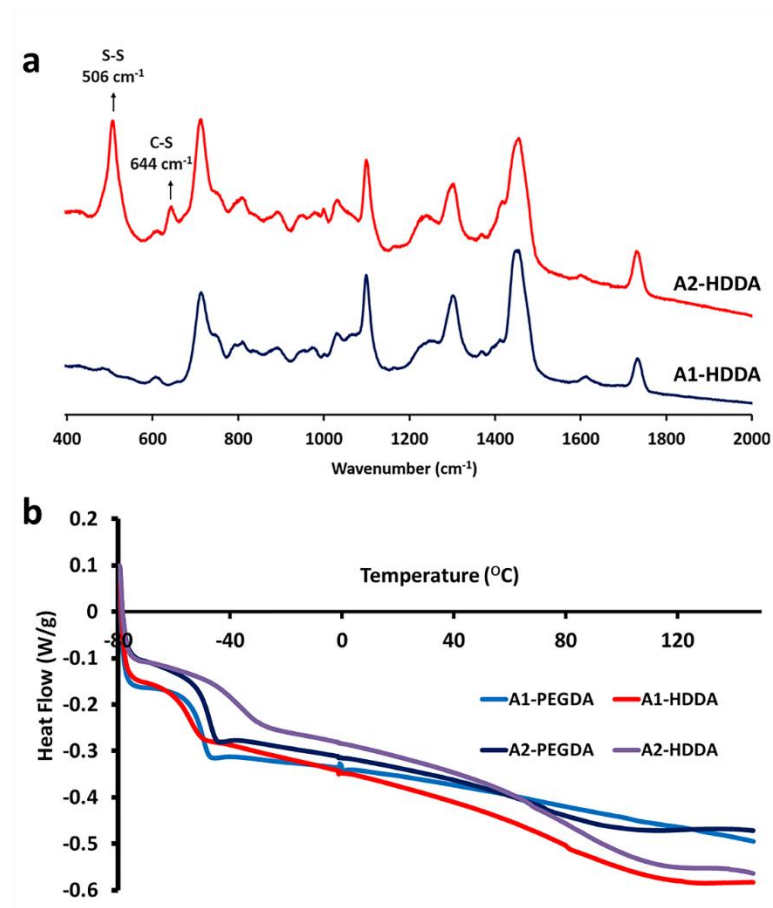


Figure 3.11. (a) Raman spectra and (b) DSC curves of PBAE gels.

This effect can be explained by the denser networks created by the smaller macromers; for example, the T_g of the gel obtained from the lowest molecular weight macromer, A2-HDDA was found to be the highest (-35.3 °C). Other factors expected to affect T_g values are the presence of pendant phosphonate groups (increasing as the number of repeat units increases), polarity differences due to ethylene oxide and S–S units at the backbone. For example, even though monotonicity holds in the four cases, the change in T_g of A1 containing gels relative to the fractional molecular weight change is large compared to that of A2 containing ones. Another observation is, PEGDA based network polymers exhibited well-defined narrow transition peaks, on the other hand HDDA based ones showed broader peaks which implies heterogeneity within the system.

3.3.4. Swelling Studies

As an expected trend for both mass swelling and volume swelling ratios, the hydrophilic gels and cryogels (A1-PEGDA and A2-PEGDA) swelled much more than the hydrophobic ones (A1-HDDA and A2-HDDA) respectively. Swelling profiles indicated that mass swelling ratios were primarily influenced by the method of gelation which in turn determines the pore size (Figure 3.12). The cryogels exhibited mass swelling ratios up to more than a two-fold excess when compared to conventional gels. On the other hand volume swelling ratios were similar for gels and cryogels. This contrast for mass and volume swelling ratios arises from the differences in pore size resulting in the two gelation methods, since the swelling is due to two distinct effects [189]. The pores in the gel are filled with water; at the same time, the walls of the pores, which are made of crosslinked polymer chains, take up water and swell. The volume swelling is determined by the swelling of the walls, whereas the mass swelling is determined by the sum of both effects. If the swelling of the walls is assumed to be similar for standard gels and cryogels, volume swelling ratios would be expected to be similar, and the data show little difference, implying that the similarity assumption is reasonable. However, given their larger pore size, the filling effect is stronger for cryogels, hence their mass swelling is larger.

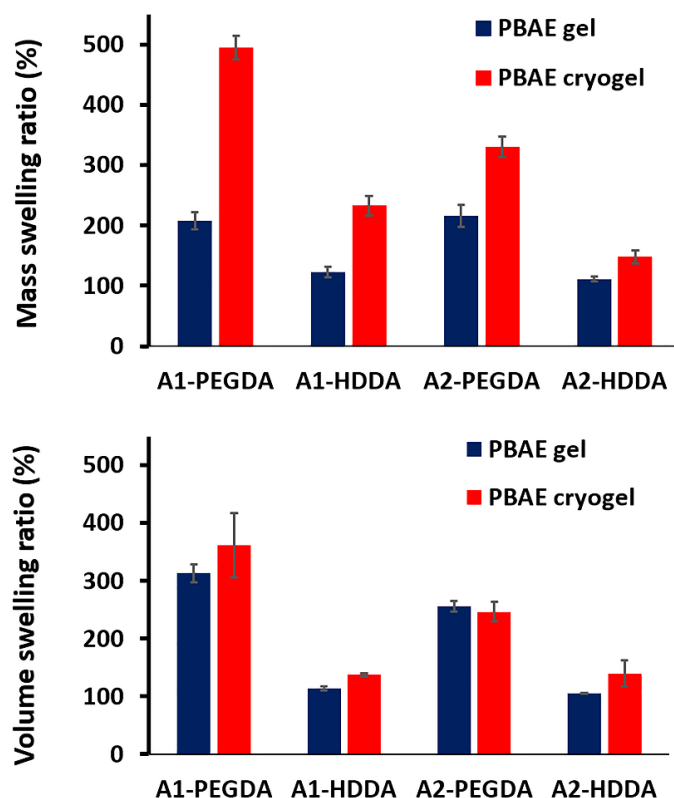


Figure 3.12. Water uptake profile of PBAE gels and cryogels.

3.3.5. Degradation Studies

The degradation profiles of PBAE gels in PBS and DTT were investigated (Figure 3.13). Degradation studies were done by immersing the gels and cryogels into PBS at 37 °C and determining the mass loss by weighing them at certain time intervals. A1-PEGDA gel showed 100% degradation in 24 hours whereas A1-HDDA gel showed only 10% in the same time interval and reached only 70% degradation after 8 weeks. Since their molecular weights are comparable (7800 Da and 7350 Da respectively) the large difference in their degradation behaviour is based on molecular structure. The network polymer made from macromer which contains a hydrophilic diacrylate, PEGDA, degraded much more rapidly than the one which contains a hydrophobic one, HDDA, as expected. Similarly, in the case of A2-PEGDA and A2-HDDA gels hydrophilicity of network polymer enhanced the degradation. But there

is also a contribution of molecular weight since A2-PEGDA macromer has a higher molecular weight (4260 Da) when compared to A2-HDDA macromer (1800 Da). As molecular weight increases, the number of hydrolytically cleavable bonds within a crosslink also increases. Accordingly, it is likely that hydrolysis of multiple bonds will occur and soluble polymer fragments will be released into the solution. Besides degradation in PBS, the degradation of A2-PEGDA and A2-HDDA gels *via* cleavage of disulfide bonds under reducing conditions was also studied. A2-PEGDA gel totally degraded in 25 mM DTT by 24 hours, but only 35% in PBS in the same time interval. After 7 days A2-HDDA gel showed 57% degradation in 25 mM DTT and 29% degradation in PBS. In addition to the hydrophobic nature of A2-HDDA gel which imparts a slower degradation profile to it, another reason for A2-HDDA gel for not reaching complete degradation might be interference of disulfide bond with free radical polymerization, resulting in chain transfer reactions which can cause additional crosslinks within the system [50, 190].

Only A1-PEGDA reached complete degradation in PBS in the duration of the study, but the other ones degraded until a plateau was reached and a part of the network polymer seemed to remain intact indicating the presence of nondegradable crosslinks within the network structure. The degradation profiles ranging from reaching complete degradation within a few hours to a degradation period of months show that the double degradation mechanism based on both hydrolysis of PBAEs into bis(β -aminoacids), diols, and poly(acrylic acid); and cleavage of disulfide bonds by DTT provides an effective tool to tune the rate of degradation.

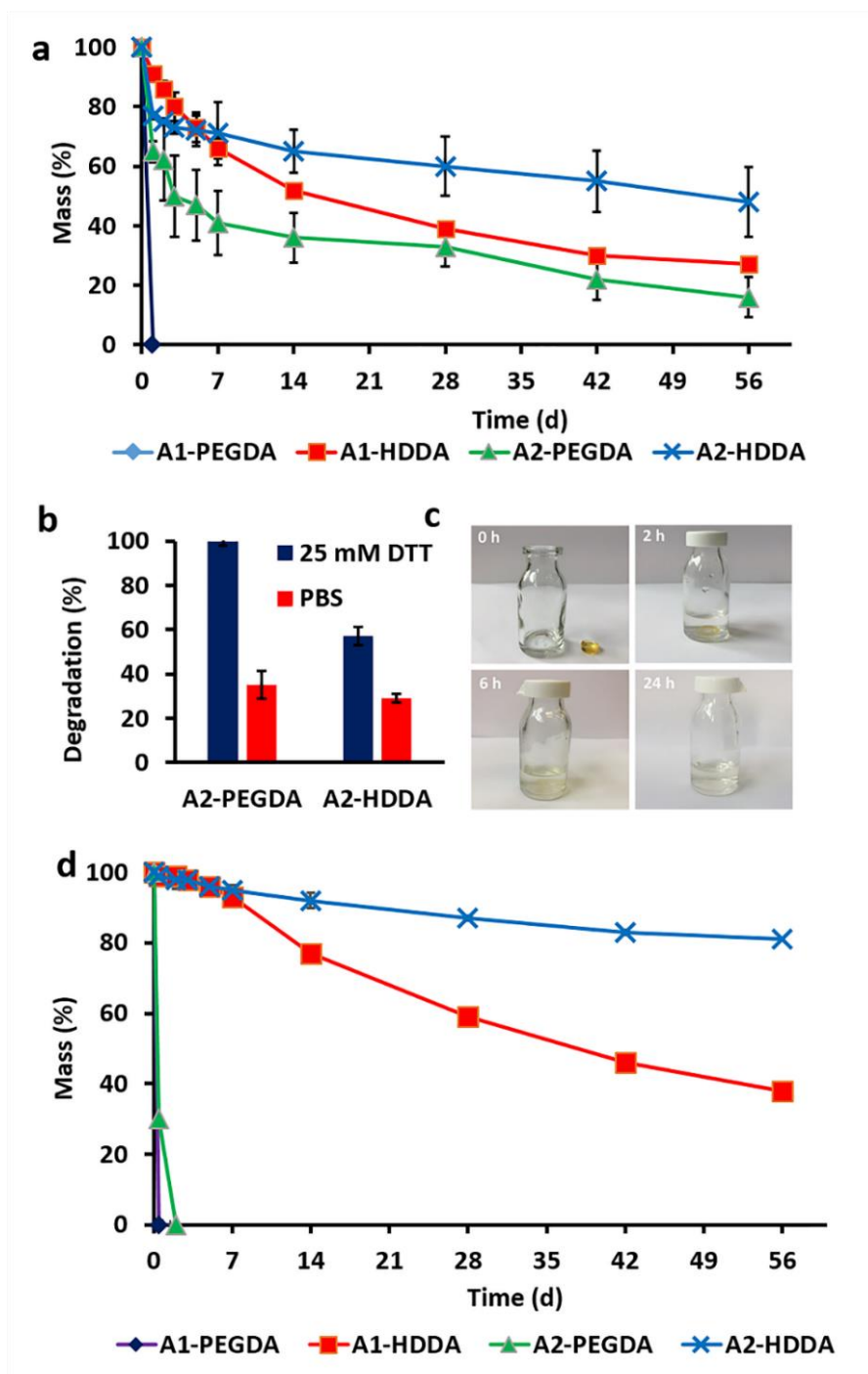


Figure 3.13. Degradation behaviour of PBAE gels (a) in PBS, (b) in 25 mM DTT (Degradation % is determined at day 1 for A2-PEGDA and day 7 for A2-HDDA), (c) Images of A2-PEGDA in 25 mM DTT at 0 h, 2 h, 6 h and 24 h, (d) Degradation behaviour of PBAE cryogels in PBS.

When the degradation behaviour of cryogels are compared with gels, it is seen that the gels degrade with an initial rapid mass loss, which might be due to release of unreacted residual macromers which remain even after a purification step. The gels were previously immersed in ethanol to remove unreacted components, but their nonporous and rubber-like structure, also evident from SEM micrographs, probably hindered the release of unreacted macromers. However an initial rapid mass loss is not observed for cryogels, likely due to their porous structure that enable the removal of any remaining macromer in the purification step. Interestingly, A2-PEGDA cryogel showed a dramatic increase in degradation rate when compared to its analogue network polymer indicating that the porous structure that facilitates the diffusion of water into the interior of the gel has a dominant effect on degradation rate. In the case of hydrophobic macromers A1-HDDA and A2-HDDA, the degradation profile of gels and cryogels are similar to each other except for the initial period of rapid mass loss. Even though water can easily penetrate into the porous cryogels, the hydrophobicity of the gel is the primary determining factor for its degradation.

The PBAE macromers provide a mix-and-match library for further tuning the degradation kinetics. This approach was demonstrated by selecting A1-PEGDA and A1-HDDA macromers and combining them to fabricate cryogels with varying hydrophobic/hydrophilic ratios. A1-PEGDA:A1-HDDA (75:25 w%), A1-PEGDA:A1-HDDA (50:50 w%), and A1-PEGDA:A1-HDDA (25:75 w%) cryogels were prepared and their degradation rates in PBS were monitored (Figure 3.14). As the percent of the hydrophobic macromer A1-HDDA increased, the degradation rate is reduced as expected. In a similar fashion, matching a reducible PBAE macromer with a non-reducible one may allow for control over the concentration of disulfide bonds which mediate redox dependent degradation through thiol–disulfide exchange reactions.

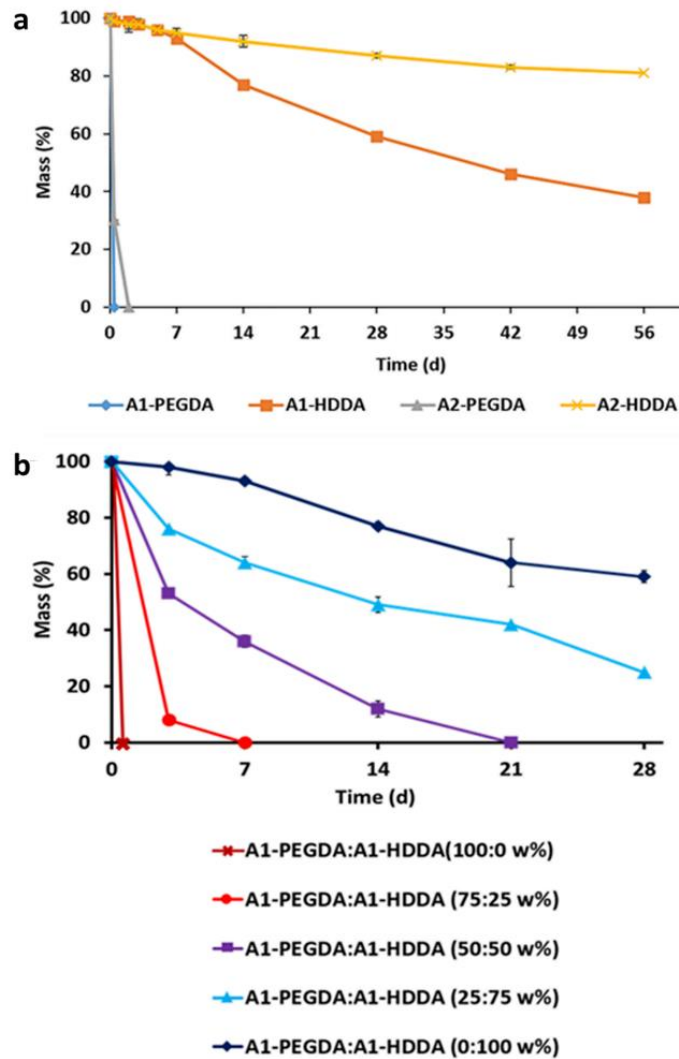


Figure 3.14. (a) Degradation behaviour of PBAE cryogels in PBS (b) Degradation behaviour of mix-and-match A1-PEGDA:A1-HDDA cryogels in PBS.

The surface morphology of the gels were investigated using SEM before and after degradation (Figure 3.15). The initial morphology shows a smooth rubber-like and non-porous surface whereas after degradation formation of pores was observed. Unlike the gels, a porous structure was observed for the cryogels as expected.

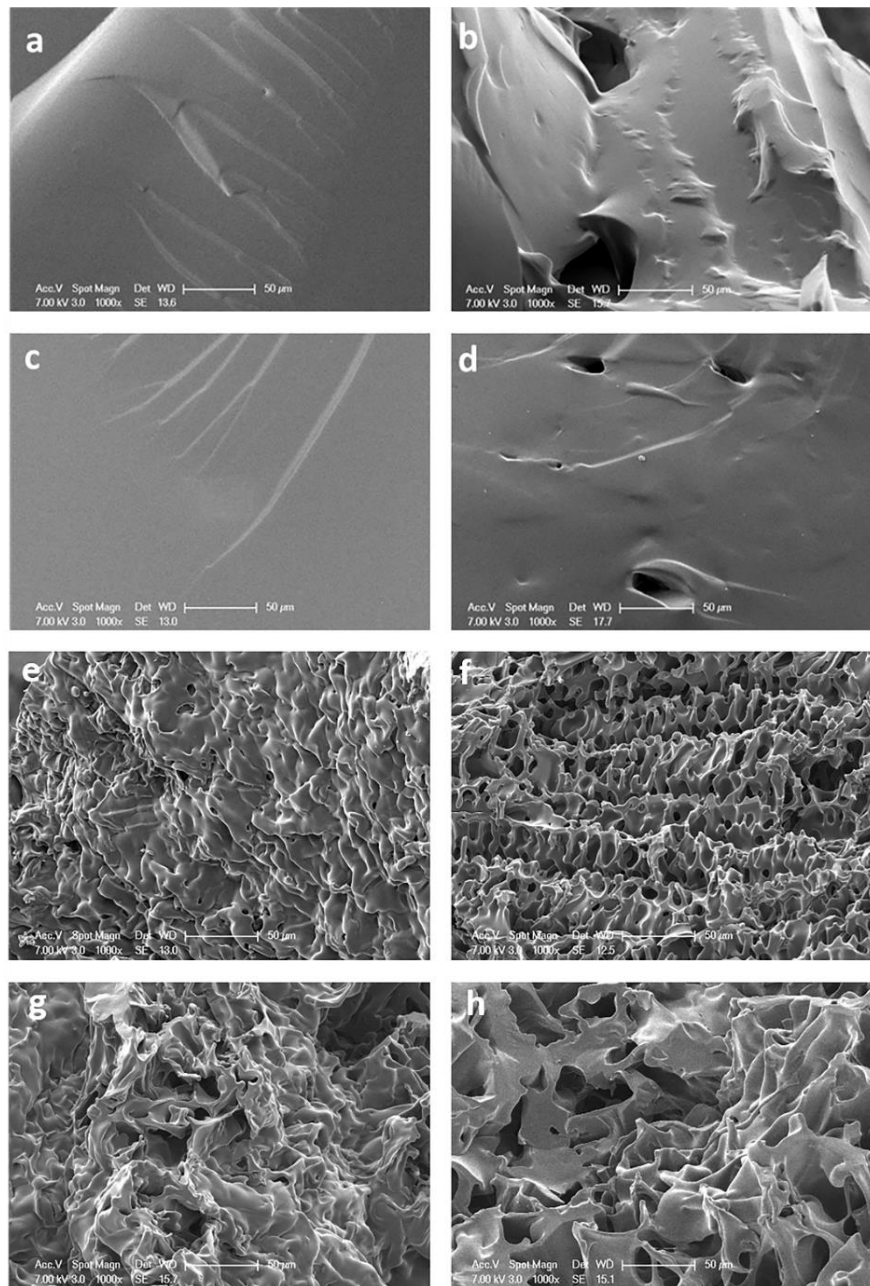


Figure 3.15. Representative SEM micrographs of PBAE gels (a) A1-PEGDA, (b) A1-PEGDA after 4h degradation, (c) A1-HDDA, (d) A1-HDDA after 3d degradation. Representative SEM micrographs of PBAE cryogels (e) A1-PEGDA, (f) A1-HDDA, (g) A2-PEGDA, (h) A2-HDDA.

3.3.6. *In Vitro* Cytotoxicity of Polymer Degradation Products

Potential cytotoxicity of the PBAE gel degradation products was evaluated on NIH 3T3 and Saos-2 cells using the standard MTT assay (Figure 3.16). A dose-dependent study was performed in order to evaluate the influence of concentration of the degradation products as well as to determine the difference in the cytotoxicities of different formulations. Cell viability above 80% is assumed as noncytotoxic according to ISO 10993–5 [191]. Based on this evaluation and statistical analysis of the data, no significant toxicity at any composition and concentration of the degradation products were observed against NIH 3T3 and Saos-2 cells.

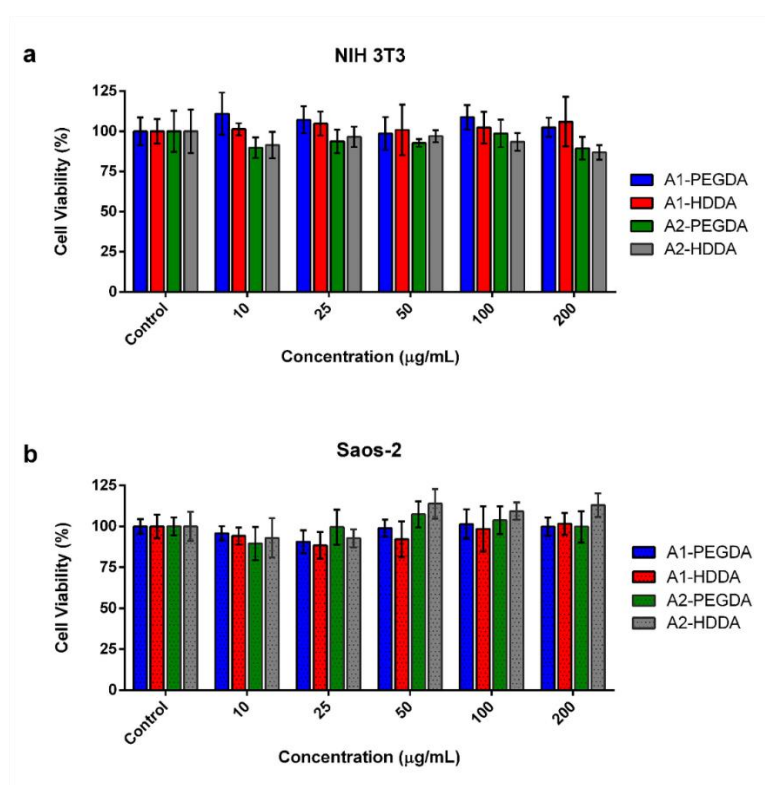


Figure 3.16. The effect of degradation products on cell viability of NIH 3T3 mouse embryonic fibroblast cells (a) and Saos-2 human osteosarcoma cells (b). Cells were treated with different concentrations of the products for 24 h. The cell viability test was performed by MTT assay (\pm SD; $n = 5$; $p < 0.05$ compared with all concentrations)

3.4. Conclusions

In summary, redox-responsive and phosphonate-functionalized degradable PBAE gels and cryogels were synthesized through subsequent step-growth polymerization and photopolymerization reactions of custom PBAEs. The selection of diacrylates and diamines with different chemical structures and use of different gelation methods enabled the tailoring of the degradation profile. The degradation time ranged from reaching complete degradation within a few hours to a degradation period of months. The degradation products were shown to be biocompatible with NIH 3T3 mouse embryonic fibroblast and Saos-2 human osteosarcoma cells. These results demonstrate that, the PBAE gels and cryogels can be regarded as candidates to be used as degradable scaffolds for tissue engineering applications. We are currently evaluating the potential of these systems as platforms for controlled drug release.

4. ONE-STEP INJECTABLE AND BIOREDUCIBLE POLY(β -AMINO ESTER) HYDROGELS AS CONTROLLED DRUG DELIVERY PLATFORMS

This chapter is published as: Bingol, H. B., M. S. Altuncu, A. Ak, F. Demir Duman, Ü. Gülyüz, O. Okay, H. Yagci Acar, D. Avci, “One-step injectable and bio-reducible poly(β -amino ester) hydrogels as controlled drug delivery platforms”, *ACS Appl. Polym. Mater.*, 2019, (doi:10.1021/acsapm.9b00287)

4.1 Introduction

Poly(β -amino ester)'s (PBAEs) are biodegradable and biocompatible polymers which are synthesized by step-growth polymerization *via* aza-Michael reaction of diamines and diacrylates. In many studies PBAEs have been proven to give successful results as potential biomaterials for tissue engineering scaffolds, non-viral vectors for gene delivery, and depots for sustained release of drugs. Biomedical applications of PBAEs have been reported in a detailed review by Liu *et al.* [192]

PBAE based biodegradable 3D networks can be easily prepared by a novel one-step “A2 + B4” Michael addition strategy reported by Biswal *et al* [78]. Hyperbranched PBAEs with fluorescent properties, superelastic PBAE cryogels and PBAE networks with inherent antioxidant property have been synthesized by the aforementioned one-step method [79-81]. The diacrylate and tetrafunctional diamine mixture can be directly injected to target site with minimal surgical invasion where it gels *in situ* under physiological conditions [13, 193]. Recently, Xu *et al.* reported an injectable hyperbranched PBAE/hyaluronic acid hydrogel with on-demand degradation properties for wound healing and a poly(β -hydrazide ester)/hyaluronic acid hydrogel with antioxidative properties by the one-step method [194, 195]. The use of injectable one-step synthesis approach is particularly advantageous for the construction of controlled drug release systems since the therapeutic cargo molecules can be

encapsulated in the hydrogel network by simply adding them into the precursor mixture. Furthermore, this method provides mild encapsulation conditions for cargo molecules, especially for sensitive biomolecules in order to retain their biological activity.

The degradation rate, and hence the mechanical properties of PBAE hydrogels can be tailored through selection of building blocks and design of chemical structure. Recently, incorporation of responsive domains into PBAE networks has been reported to trigger the degradation and release upon changes in pH, UV light, or redox state [114, 115, 119]. Among these triggers redox state is especially convenient for biomedical applications. Disulfide bond is widely utilized *via* incorporation into polymeric drug delivery systems or hydrogels to control the redox-dependent degradation and release kinetics [45].

Photodynamic therapy (PDT) is an effective clinical treatment modality against various cancer types and infections. Its mechanism of action involves activation of a photosensitizer molecule with a light source of appropriate wavelength [196]. Irradiation of the photosensitizer triggers photochemical reactions which generate cytotoxic reactive oxygen species, particularly singlet oxygen, which induce damage to target cells [197]. Application of PDT locally at the target site is very attractive, both to reduce systematic toxicity and to achieve highly effective results. But localizing the photosensitizer at the target site is difficult due to the small molecular nature of most photosensitizers. Some sensitizers also lack sufficient water solubility or stability. From this perspective, hydrogels which remain at the target site due to their low fluidity, are valuable carriers for photosensitizers to enable topical PDT with spatial and temporal control [198]. Hence, many hydrogel-based drug delivery systems for encapsulation of photosensitizers have been designed and explored for their potential use in photodynamic therapy [199-206].

This study describes fabrication of pH and redox responsive PBAE hydrogels as platforms for controlled drug release (Figure 4.1). The hydrogels were fabricated by azo-Michael reaction between cystamine and diacrylates, namely poly(ethylene glycol) diacrylate (PEGDA) and 1,6-hexanediol diacrylate (HDDA) by a facile one-step strategy. In

the literature, one-step reactions were performed in bulk or in solvents such as DMSO or DMF; at high temperatures and for longer periods of time [79, 80, 192]. In our synthesis method, we used water as the solvent to accelerate hydrogel formation and decrease reaction time to less than 1 h. The therapeutic cargo molecules can be encapsulated in the hydrogel network by simply adding them into the precursor mixture under these mild conditions which is significant for sensitive biomolecules in order to retain their biological activity. Besides, the incorporation of the hydrophobic monomer HDDA enables tunable hydrolysis rate, giving degradation times of 1 to more than 10 days for the hydrogels. Real-time dynamic rheological measurements were used in order to probe the formation of the PBAE hydrogel networks. Methylene blue (MB), widely used as an inexpensive and non-toxic photosensitizer for PDT, was selected as a model drug to demonstrate the effect of the hydrophobicity of the network on the release kinetics and evaluate the utility of these hydrogels in local PDT [207-209]. To the best of our knowledge, there is only one report about the usage of PBAE-based micelles encapsulated with protoporphyrin for PDT [210]. The toxicity of hydrogel degradation products was evaluated on MCF-7 human breast cancer cells and A549 adenocarcinomic human alveolar basal epithelial cells. *In vitro* PDT potential of released MB was evaluated on A549 cells.

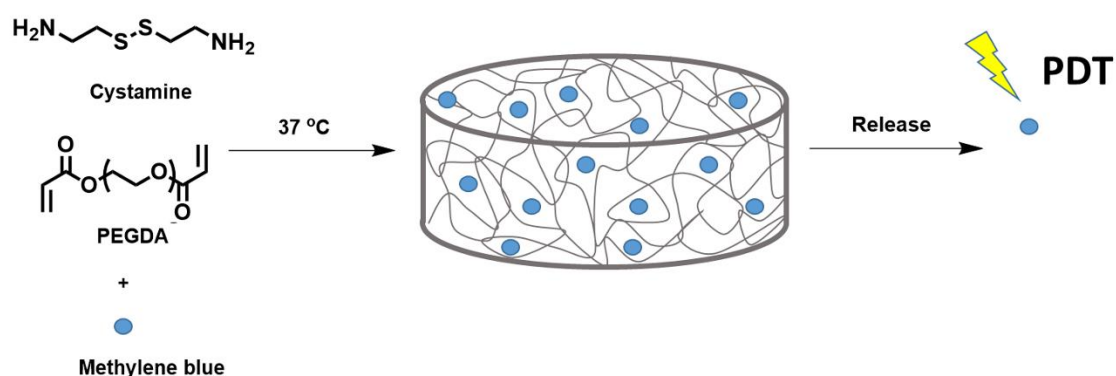


Figure 4.1. Design of one-step PBAE hydrogels.

4.2. Experimental

4.2.1. Materials and Methods

Cystamine dihydrochloride salt, PEGDA ($M_n=575$ g/mol), HDDA, 1,4-dithiothreitol (DTT), MB, Dimethyl sulfoxide Hybri-Max™ and all solvents were purchased from Sigma-Aldrich (St Louis, MO, USA) and used as received. Penicillin-streptomycin and trypsin-EDTA solutions were provided by Multicell, Wisent Inc. (St. Bruno, QC, Canada). Fetal bovine serum (FBS) was obtained from Capricorn Scientific GmbH (Ebsdorfergrund, Germany). Dulbecco's modified Eagle medium (DMEM), phosphate buffer saline (PBS) tablets and thiazolyl blue tetrazolium bromide (MTT) were purchased from Biomatik Corp. (Cambridge, ON, Canada). 96-well plates were obtained from Nest Biotechnology Co. Ltd. (Wuxi, China). MCF-7 human breast cancer cells were given as a gift from Dr. Engin Ulukaya (Department of Medicinal Biochemistry, Faculty of Medicine, University of Istinye, Istanbul, Turkey). A549 was provided by Prof. Devrim Gozuacik (Sabanci University, Istanbul, Turkey).

Thermal analyses were performed with differential scanning calorimetry (DSC) (TA Instruments Q100) under nitrogen atmosphere from -75 °C to 75 °C with a scanning rate of 10 °C min^{-1} . The lyophilized hydrogel samples were sputter coated with a platinum layer and their internal fracture surface was examined with scanning electron microscopy (SEM) (FEI-Philips XL30) with an accelerating voltage of 7.0 kV. Degradation and release studies were done using incubator shaker (VWR) operating at 37 °C and 200 rpm. Raman spectra were obtained using Renishaw InVia Raman Microscope. UV-visible spectra were recorded by Shimadzu UV-1201 spectrophotometer.

4.2.2. One-step Synthesis of PBAE Hydrogels

Cystamine was prepared by neutralization of cystamine dihydrochloride with potassium hydroxide according to a procedure described elsewhere [50]. Briefly, a mixture of cystamine dihydrochloride (2 g, 8.88 mmol), potassium hydroxide (1.1 g, 19.54 mmol), and 20 mL methanol was stirred at room temperature for 24 h. The white precipitate was filtered off and the crude product was obtained by evaporating methanol under reduced pressure. The residue was then dissolved in dichloromethane (50 mL), washed with saturated NaHCO₃ solution (10 mL) and dried over sodium sulfate. Pure cystamine was obtained with 68% yield after evaporation of dichloromethane. To prepare the one-step PBAE hydrogels, cystamine (0.13 mmol, 20 mg) was dissolved in 0.12-0.2 mL distilled water in a vial and a diacrylate (for H1: 0.26 mmol, 150 mg PEGDA, for H2: 0.13 mmol, 75 mg PEGDA and 0.13 mmol, 30 mg HDDA, for H3: 0.065 mmol, 38 mg PEGDA and 0.195 mmol, 45 mg HDDA) was added. The mixture was placed in an orbital shaker at 37 °C and 200 rpm for 1 hour. The obtained hydrogel samples were dried and weighed to obtain (W1). Then the hydrogels were immersed in ethanol (20 mL) for 24 h to remove unreacted starting materials. The swollen samples were dried and weighed again to obtain (W2). The gelation percentage of hydrogel samples, that is, the weight percent of the reactants incorporated into the ethanol-insoluble 3D hydrogel network was calculated by equation (3.1)

4.2.3. One-step Synthesis of Drug Loaded PBAE Hydrogels

The MB loaded hydrogel samples were fabricated as described for unloaded ones, except that 1 wt % MB (with respect to total hydrogel weight) was dissolved in water and the aqueous MB solution was added to the hydrogel precursor mixture instead of water. The dye loaded hydrogels were immersed in ethanol (20 mL) to get rid of unreacted starting materials and excess dye before release studies. The loading capacity (LC %) was calculated using weights of entrapped drug (W_d) and hydrogel (W_h) by equation (4.1)

$$LC (\%) = \frac{W_d}{W_h} \times 100 \quad (4.1)$$

4.2.4. Rheological Experiments

Cystamine (1 mol equiv.) and diacrylate (2 mol equiv.) were dissolved in distilled water in a vial and stirred for a few seconds. The solution was then transferred between the plates of the rheometer (Gemini 150 Rheometer system, Bohlin Instruments) equipped with a cone-and-plate geometry (cone angle = 4°, diameter = 40 mm) to monitor the reaction by oscillatory small-strain shear measurements at 37 °C. The instrument was equipped with a Peltier device for temperature control. During the rheological measurements, a solvent trap was used and the outside of the upper plate was covered with a thin layer of low-viscosity silicone oil to prevent the evaporation of water. An angular frequency ω of 6.3 rad s⁻¹ and a deformation amplitude γ_o of 0.01 were selected to ensure that the oscillatory deformation is within the linear regime. Frequency sweep tests were carried out at 37 °C and $\gamma_o = 0.01$ over the frequency range 0.06 – 300 rad s⁻¹.

4.2.5. Swelling Studies

Swelling studies were performed by immersing dry hydrogel samples into PBS solutions (pH 5 or pH 7.4) at 37 °C. The samples were removed from water, blotted on filter paper, and their swollen weights were measured at different time intervals. The degree of swelling (D_s) was calculated using equation (4.2)

$$D_s = \frac{W_s - W_d}{W_d} \times 100 \quad (4.2)$$

where W_s and W_d refer to the weight of swollen and dry gel samples, respectively. The average values from triplicate measurements were reported.

4.2.6. Degradation of Hydrogels

Hydrogel samples were weighed (W_i) and immersed in 4 mL degradation solution (phosphate buffer solutions of pH 5 and pH 7.4, or 25 mM DTT) at 37 °C. The solution was then placed on an orbital shaker operating at 200 rpm. At predetermined time intervals, the samples were removed from the degradation solution, lyophilized and weighed (W_f). The degradation % was calculated according to equation (3.4).

4.2.7. *In Vitro* Release Studies

MB was selected as a model drug to demonstrate the release kinetics of PBAE hydrogels. MB loaded hydrogels were placed in 50 mL phosphate buffer solutions (pH 7.4 and pH 5) and were shaken at 200 rpm using an incubator shaker at 37 °C. At predetermined time intervals, 2 mL of buffer solution was removed and analyzed by UV–visible spectroscopy. The removed aliquots were replaced by fresh buffer solution to maintain the volume of release medium. The increase in absorbance of the buffer solutions was monitored and the cumulative release of MB was determined using a calibration curve based on the absorbance of MB solutions of known concentrations at 666 nm.

4.2.8. Determination of *In Vitro* Cytotoxicity and PDT Studies

For the cytotoxicity evaluation of the degradation products of the gels and for PDT studies, A549 cells were incubated with the different concentrations of the degradation products (after 6h of degradation at pH 7.4 PBS). After culturing of the cells in DMEM complete medium supplemented with 10% (v/v) FBS and 1% (v/v) penicillin-streptomycin in an incubator under 5% CO₂ atmosphere at 37 °C, the cells were seeded at a density of 1×10^4 cells/well into 96-well plates in complete medium. In the following day, cells at 60-80% confluency were treated between 35-350 and 4.9-49 $\mu\text{g/mL}$ doses for the degradation products of MB loaded hydrogels and incubated for 24 more hours in a 5% CO₂ incubator

at 37 °C. Viability of cells were evaluated with MTT assay. According to the manufacturer's protocol, the medium in each well was replenished with 100 µL fresh medium containing 10 µL of MTT solution (5 mg/mL in PBS) and incubated for 3 h at 37 °C in 5% CO₂. Then, the formed purple formazan crystals were dissolved using 100 µL DMSO solution. Absorbance from each well was determined by a microplate reader (BioTek ELx800 Absorbance Microplate Reader) at 570 nm. Untreated cells were considered as control cells with 100% viability. Each experiment was done in six replicas. Cell viability was calculated according to the equation (3.5).

For the PDT studies, cells cultured and treated as described above were treated with MB containing degradation products hydrogels. After 24 h incubation, the medium was replaced with fresh culture medium to remove un-internalized degradation products and/or MB. A laser beam (635 nm wavelength, 300 mW/cm² power density, 0.5 cm beam diameter, 30 J/cm² energy density) was applied for 100 seconds to the experiment groups. 16 µM free MB was applied as a control, since it corresponds to the highest concentration of MB in release solutions of H1 and H2. Impact of laser treatment on cells which lack the degradation products or MB were also determined. Untreated cells were used as controls. Cell viability was determined before and after laser treatment by MTT assay where cells were incubated at 37 °C for 3 h in 100 µl MTT/DMEM (1:10) solution followed by solubilization of formazan with 100 µl of DMSO and absorbance reading at a 570 nm wavelength.

Cytotoxicity was tested also on MCF-7 human breast cancer cell line to confirm cytocompatibility using the same procedure.

4.2.9. Statistical Analysis

Statistical analyses of the degradation products were assessed by using one-way ANOVA analysis followed by Tukey's b comparison test in SPSS. The data were presented as mean ± standard deviation (SD) ($n=6$). $p < 0.05$ was accepted as statistically significant.

4.3. Results and Discussion

4.3.1. One-Step Synthesis and Characterization of PBAE Hydrogels

PBAE hydrogels were prepared in one-step by mixing a diacrylate or a diacrylate mixture with a primary diamine to form the hydrogels by an aza-Michael reaction (Figure 4.2). Different synthetic procedures for aza-Michael addition reactions have been reported before which mostly require elevated temperatures or catalysts such as transition metal and lanthanide halides, triflates, silica gel, heterogeneous solid salts, ionic liquids or boric acid [211-213]. Here, we used a simple and green approach by conducting the reactions in water at 37 °C without any catalyst. These mild conditions also resulted in high yields within a shorter period of time (15-40 min) when compared to other methods which require catalysts (2-8 h) (Table 4.1). The presence of water facilitates the reaction by activating both the amine and the acrylate through hydrogen bonding [214]. Since the precursor solution is liquid, it is also possible to inject the mixture and obtain the gel in situ [13]. This possibility coupled with the occurrence of gelation at physiological conditions provides the potential of easy administration into the human body and hence great practicality.

The choice of diacrylate and diamine, and their relative ratio determine the physical properties of the hydrogels. Herein we selected PEGDA alone and together with HDDA at different molar ratios to tune the hydrophilicity and accordingly the degradability of the hydrogels. Cystamine was used as the primary diamine due to the redox responsive disulfide bond in its molecular structure. The disulfide group is known to be stable in blood but cleaves rapidly by glutathione in the intracellular environment [45]. Hence, the incorporation of disulfide groups into the hydrogels would render them responsive to the reducing environment. Three hydrogels with different hydrophilicities were thus synthesized: The H1 hydrogel was solely produced from PEGDA, while the H2 and H3 hydrogels were made from a 1:1 and 1:3 mol ratios of PEGDA and HDDA to reduce the hydrophilic nature (Table 4.1). We intended to synthesize a fourth hydrogel, H4, from only HDDA but the HDDA/diamine mixture was not soluble in water and no gelation was observed. Both

hydrogels H1 and H2 were obtained with high gelation percentages, 95% and 92% respectively, whereas H3 resulted in slightly lower gelation percentage probably due to poor solubility of the HDDA-rich mixture in water.

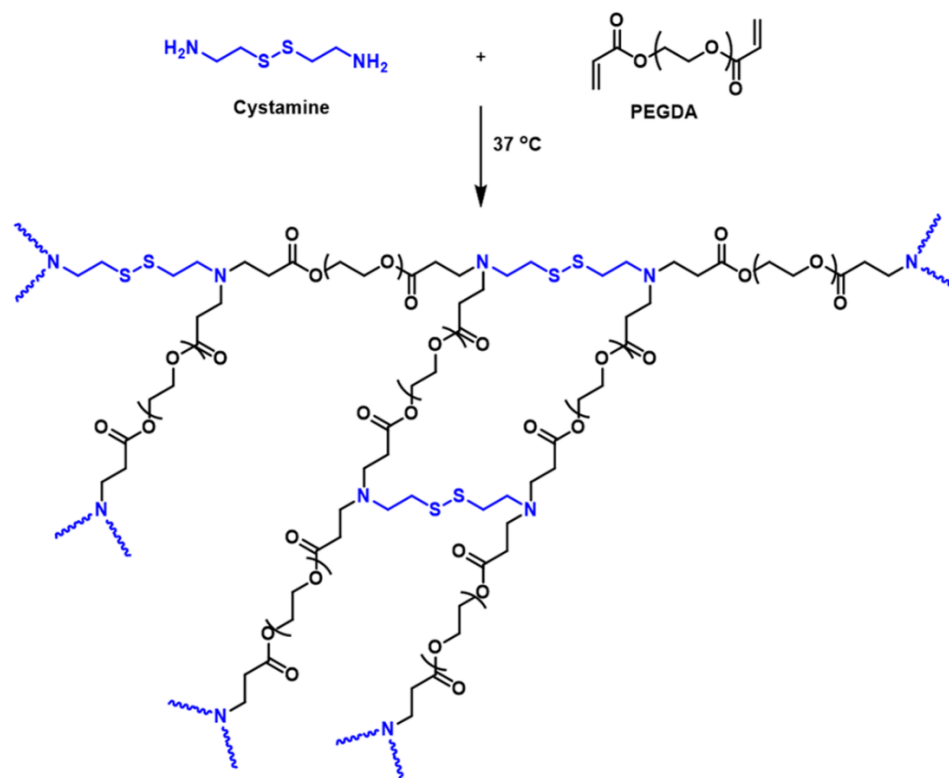


Figure 4.2. One-step synthesis of H1 from the aza-Michael reaction of PEGDA and cystamine.

Table 4.1. Properties of one step PBAE hydrogels.

Hydrogel	PEGDA:HDDA Mole ratio	Gelation (%)	T _g (°C)
H1	1:0	95	-46
H2	1:1	92	-40
H3	1:3	78	-
H4	0:1	No gelation	-

We monitored gelation reactions between cystamine and the diacrylates PEGDA and HDDA by real-time dynamic rheological measurements in order to follow formation of PBAE hydrogel networks. Figure 4.3 shows the storage modulus G' (filled symbols), loss modulus G'' (open symbols), and the loss factor $\tan \delta (= G''/G')$, lines in b) of H1, H2 and H3 reaction solutions at an angular frequency ω of 6.3 rad/s and at a strain amplitude γ_0 of 1% as a function of the reaction time. The inset in (a) shows the same G' vs time data in a semi-logarithmic scale up to 80 min. It is seen that the initial reaction period during which the dynamic moduli remain unchanged, that is, the induction period, varies depending on the composition of the diacrylate mixture. The H1 gelation solution containing PEGDA only exhibits an induction period of 27 ± 5 min, whereas it shortens to 6 ± 2 min and under 1 min in H2 and H3 solutions with PEGDA mole ratios of 1:1 and 1:3, respectively. Thus, the presence of the more hydrophobic HDDA significantly decreases the induction period of the polymerization reactions. This can be explained by the hydrophobic interactions between HDDA segments leading to the formation of temporary cross-links in the gelation solution [215, 216]. Following the induction period, a crossover between G' and G'' occurs after 35 ± 4 , 12 ± 2 and 23 ± 5 min for H1, H2 and H3 hydrogel systems, respectively, which corresponds to the onset of gelation. Eliminating the induction period, this indicates the onset of gelation within 10-20 min for reaction systems. After gelation, G' rapidly increases and $\tan \delta$ decreases until they approach plateau values after about 60 min. The tests could not be conducted for longer times due to the appearance of some scatter in the dynamic moduli data. Therefore, the limiting moduli G'_∞ of the hydrogels were estimated by fitting the experimental G' vs reaction time t data to the modified Hill equation (4.3) [217-219].

$$G'(t) = G'_\infty \frac{t^n}{t^n + \theta^n} \quad (4.3)$$

where θ and n are constants. The solid curves in Figure 4.3 are the best fits of equation (4.3) to the experimental data indicating that equation (4.3) well simulates the gelation process of the solutions. The limiting values of G' obtained from the fits are 35, 56 and 104 kPa for H1, H2 and H3 respectively. Figure 4. 3c shows G' (filled symbols) and G'' (open symbols) of H2 and H3 hydrogels at 37 °C plotted against the frequency ω . G' is 59 ± 2 and

78±4 kPa for H2 and H3, respectively, and independent on the frequency ω while G'' is around 2 orders of magnitude smaller than G' , which is typical behavior of strong gels with a chemically cross-linked network structure. Because G' of such hydrogels corresponds to the equilibrium shear modulus G , one may estimate their effective cross-link densities ν_e by

$$G = 0.5\nu_e RT \quad (4.4)$$

where R is the gas constant and T is the absolute temperature. Equation 4.4 assumes a phantom network behavior and the existence of tetrafunctional cross-links in the hydrogel network. Using equation 4.4 together with limiting values of G' at 37 °C, the cross-link density ν_e was calculated as 27, 43, and 81 mol/m³ for H1, H2, and H3 hydrogels, respectively. The results thus reveal formation of a larger number of effective cross-links after incorporation of hydrophobic HDDA segments into the hydrogel network. An interesting point is a higher loss factor $\tan \delta$ of H2 and H3 as compared to H1, which we attribute to the hydrophobic hexyl segments of HDDA units forming hydrophobic associations and hence creating an energy dissipation mechanism in the gel network [220].

The thermal properties of the hydrogels were studied using differential scanning calorimetry (DSC). The glass transition temperatures T_g of the hydrogels well correlated with their chemical composition (Table 4.1). The H2 hydrogel containing HDDA exhibits a higher T_g at -40 °C as compared to H1 with a T_g of -46 °C due to the lower molecular weight. Moreover, the PEGDA based H1 hydrogel shows well-defined narrow transition peaks whereas incorporation of HDDA into the network leads to broader peaks which imply heterogeneity within the system (Figure 4.4a). The presence of the disulfide group in the hydrogel structure was verified by Raman spectroscopy from the ν_{SS} and ν_{CS} bands observed at 504 and 647 cm⁻¹ for H1, 508 and 644 cm⁻¹ for H2, and 509 and 644 cm⁻¹ for H3, respectively (Figure 4.4b).

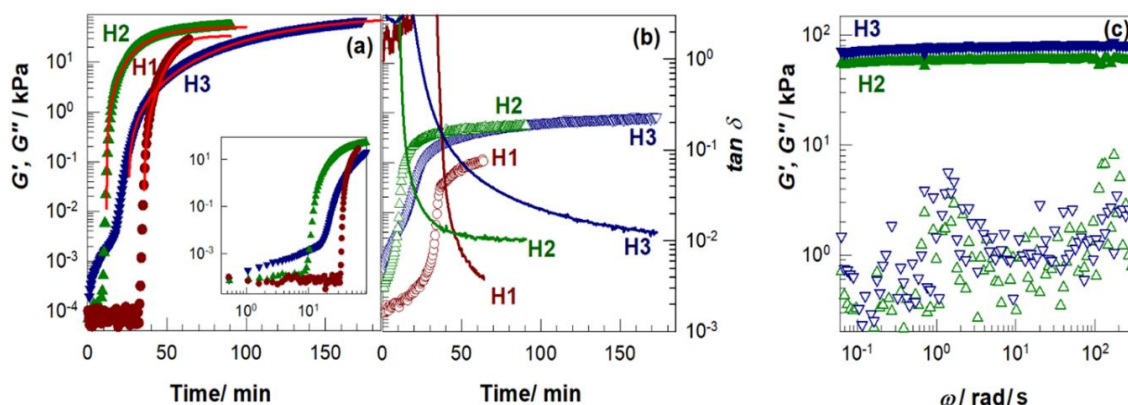


Figure 4.3. (a, b) Storage modulus G' (filled symbols), loss modulus G'' (open symbols), and $\tan \delta$ (lines in b) as a function of the reaction time. The solid curves in (a) were calculated using equation (4.6). $\omega = 6.3$ rad/s. $\gamma_o = 0.01$. Temperature = 37°C . (c) Frequency dependences of G' (filled symbols) and G'' (open symbols) of H2 (triangles up) and H3 hydrogels (triangles down) at 37°C . $\gamma_o = 0.01$.

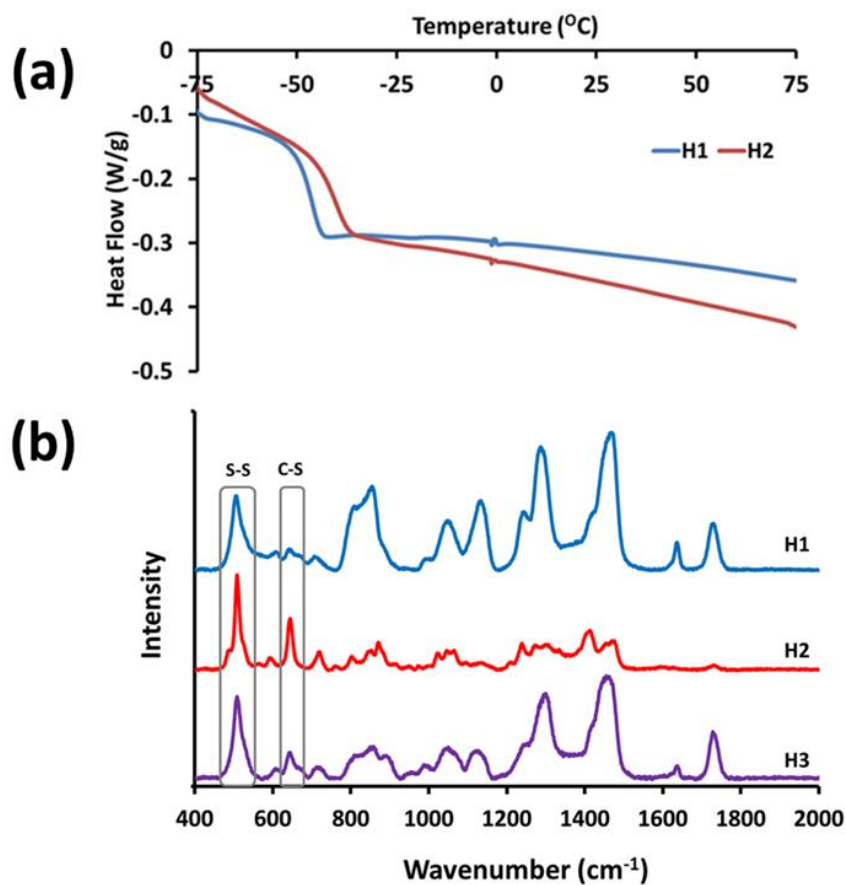


Figure 4.4. (a) DSC profiles of the H1 and H2 hydrogels under nitrogen at a scanning rate of $10^\circ\text{C}/\text{min}$, (b) Raman spectra of one-step PBAE hydrogels.

4.3.2. Swelling and Degradation Studies

The effects of the chemical composition of the hydrogels and the pH of the medium on the swelling and degradation kinetics were evaluated, the swelling studies being conducted for up to 3 hours, since the H1 hydrogel started to degrade due to the hydrolysis of β -aminoesters on the backbone. Figure 4.5 shows time-dependent swelling and degradation profiles, respectively, of H1, H2 and H3 hydrogels at pH = 5.0 and 7.4. It was observed that H1 swells approximately two-fold when compared to H2 after a swelling time of 3 h, the swelling increasing only slightly from pH 7.4 to pH 5; while the swelling of H3 at pH 7.4 is lower, like H2, and at pH 5 higher, like H1.

The degradation rate of H1 is high, reaching complete degradation within 24 h in both buffers; the rate of H2 is lower and pH-dependent, completely degrading in 120 h in the pH 5 buffer, and 144 h in pH 7.4 buffer (15% and 25% at pH 7.4 and pH 5 in 24 h); and the rate of H3 is lowest and also pH-dependent, degrading only by 28% and 55% after 10 days at pH 7.4 and pH 5, respectively (less than 5% at both pH values in 24 h). The higher swelling of H1 compared to H2 can be explained as due to the presence of hydrophilic PEGDA units and the lower crosslink density of H1 hydrogels. The swelling of H3 is comparable to either H1 or H2, depending on the pH, despite the high crosslink density and the higher ratio of the hydrophobic HDDA; which might be explained by the possibly heterogeneous structure of H3, forming microscopic hydrophilic regions that absorb water. The higher swelling of hydrogels in pH 5 buffer compared to those in pH 7.4 probably occurs due to partial protonation of amine groups under acidic conditions creating an electrostatic repulsion of ions expanding the gel network. This effect seems weak for H1 and H2, but strong for H3, possibly due to easier protonation of the amines in the hydrophilic regions hypothesized above.

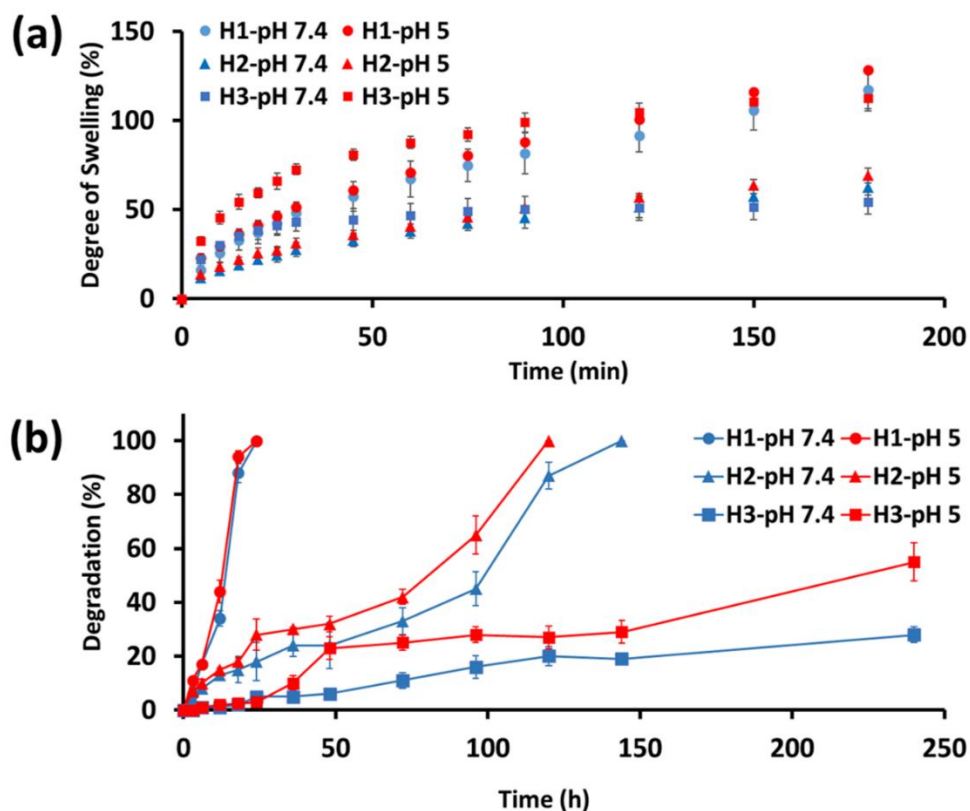


Figure 4.5. (a) pH dependent swelling profile of one-step PBAE hydrogels at pH 5 and pH 7.4, (b) pH dependent degradation profile of one-step PBAE hydrogels at pH 5 and pH 7.4. (Dry hydrogel thickness is 3 mm and dry hydrogel diameter is 8 mm).

When the hydrogels are swollen, there is a larger amount of water in the hydrogel structure; so the degradation behavior is expected to be correlated with the hydrogel's swelling, in addition to the overall hydrophilicity. Hence, the pH of the swelling/degradation medium had a limited effect on degradation kinetics for H1 and H2; whereas it had a significant effect in case of H3 where the degradation also was almost two-fold at pH 5 compared to that of at pH 7.4. (Figure 4.5 b). As for the effect of the hydrogels' hydrophilic/hydrophobic character, the degradation can be seen to proceed faster for the more hydrophilic ones. These studies show that it is possible to tune the degradation rate of these one-step hydrogels by manipulating the hydrophilic/hydrophobic balance by selection of starting materials.

4.3.3. Redox Response

In order to show the redox response, hydrogels were incubated in PBS (pH 7.4) containing 25 mM DTT at 37 °C. Hydrogels were also immersed in pure PBS as a control. Hydrogels exposed to DTT degraded under the reducing conditions *via* cleavage of disulfide bonds. The visual images and the mass loss of the hydrogels were recorded as a function of time during the degradation period (Figure 4.6). When either just PBS or PBS+DTT solutions were used, H3 showed slowest degradation profiles followed by H2 due to the hydrophobic nature of HDDA in their structure. As H2 and H3 degraded, HDDA containing insoluble linear polymer fragments were released into the solution causing turbidity. By the end of 12 h, H1 and H2 completely degraded in DTT, whereas H3 degraded 52%. In the same time interval the hydrogels in PBS degraded 34%, 13% and 2% for H1, H2 and H3, respectively, clearly showing the effect of the redox-state on degradation.

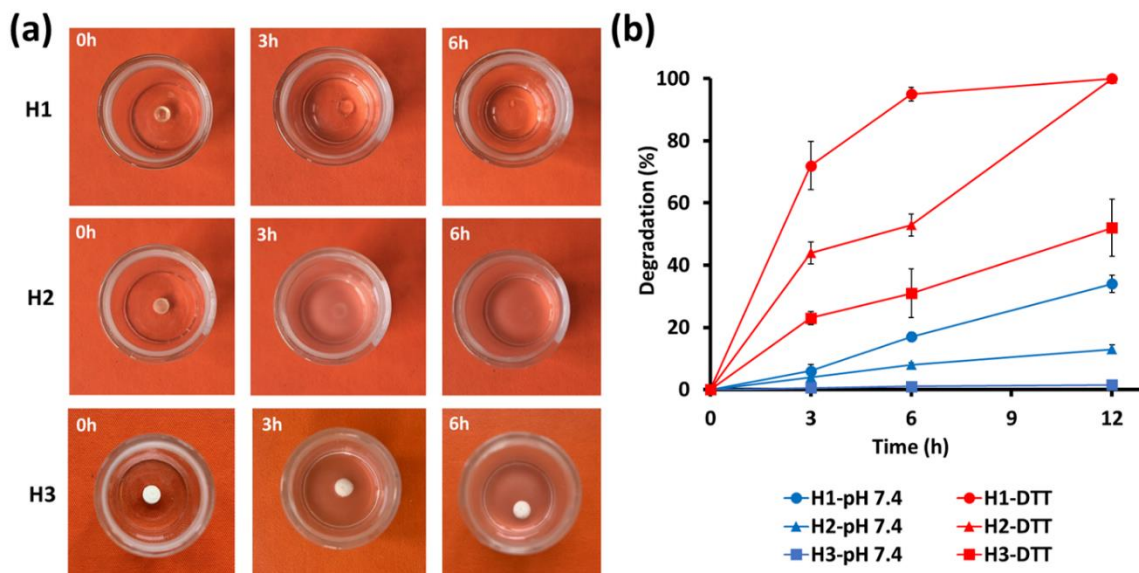


Figure 4.6. (a) Visual images of H1, H2 and H3 at the beginning and after 3 h and 6 h incubation in DTT at 37 °C. (b) Redox dependent degradation profiles of H1, H2 and H3 in PBS or DTT at 37 °C.

The effect of redox-triggered degradation *via* exposure to DTT on the morphology of H1, H2 and H3 was evaluated from the SEM images (Figure 4.7). The initial morphology of H1 and H2 are very similar, and exhibit a smooth rubber-like and non-porous structure (Figure 4.7 a and c) whereas H3 shows an irregular fracture structure (Figure 4.7 e). After degradation, the H1 surface becomes somewhat less smooth (Figure 4.7 b), whereas irregular pores and trenches appear in the H2 fracture surface (Figure 4.7 d). The H3 surface (Figure 4.7 f), on the other hand, develops even more irregular structure, with pores of various sizes. This difference in degradation characteristics can be explained by degradation of hydrophilic PEGDA-containing segments into water soluble polymer chains leaving voids between the hydrophobic-HDDA containing segments.

4.3.4. Drug Loading and *in vitro* Release Studies

MB was selected as a model drug and photosensitizer for photodynamic therapy (PDT) and, it was loaded into the hydrogels during their synthesis process. MB was loaded by 1% wt into the hydrogels and the loading capacity was found to be 0.40 ± 0.03 % for H1 and 0.46 ± 0.04 % for H2 respectively. The effect of the chemical composition, thus hydrophobic/hydrophilic nature of the hydrogels on the release behavior of MB was investigated by UV-visible spectroscopy. The release studies were performed in pH 7.4 and pH 5 buffer solutions to observe the effect of pH on the release profile of the cargo molecule (Figure 4.8). For H1, release of MB is slightly faster at pH 5 than pH 7.4 until 24 h where the cumulative release at each pH becomes equal. Soon after 24 h, both hydrogels release all of their content due to total degradation of the network structure. No significant effect of pH on the release of MB from H2 was observed. At 24 h the cumulative release of MB is approximately 80% from H2 hydrogels in either pH. Considering the slow degradation of H2, we assume that most of MB is released by diffusion due to expansion of hydrogel dimensions as the hydrogel swells. The rest of the MB was probably entrapped in the more hydrophobic domains left behind after the initial degradation of the PEGDA rich regions of H2. Therefore, much slower release of MB was observed after the first 24 h and full release was obtained only after full degradation in 168 h.

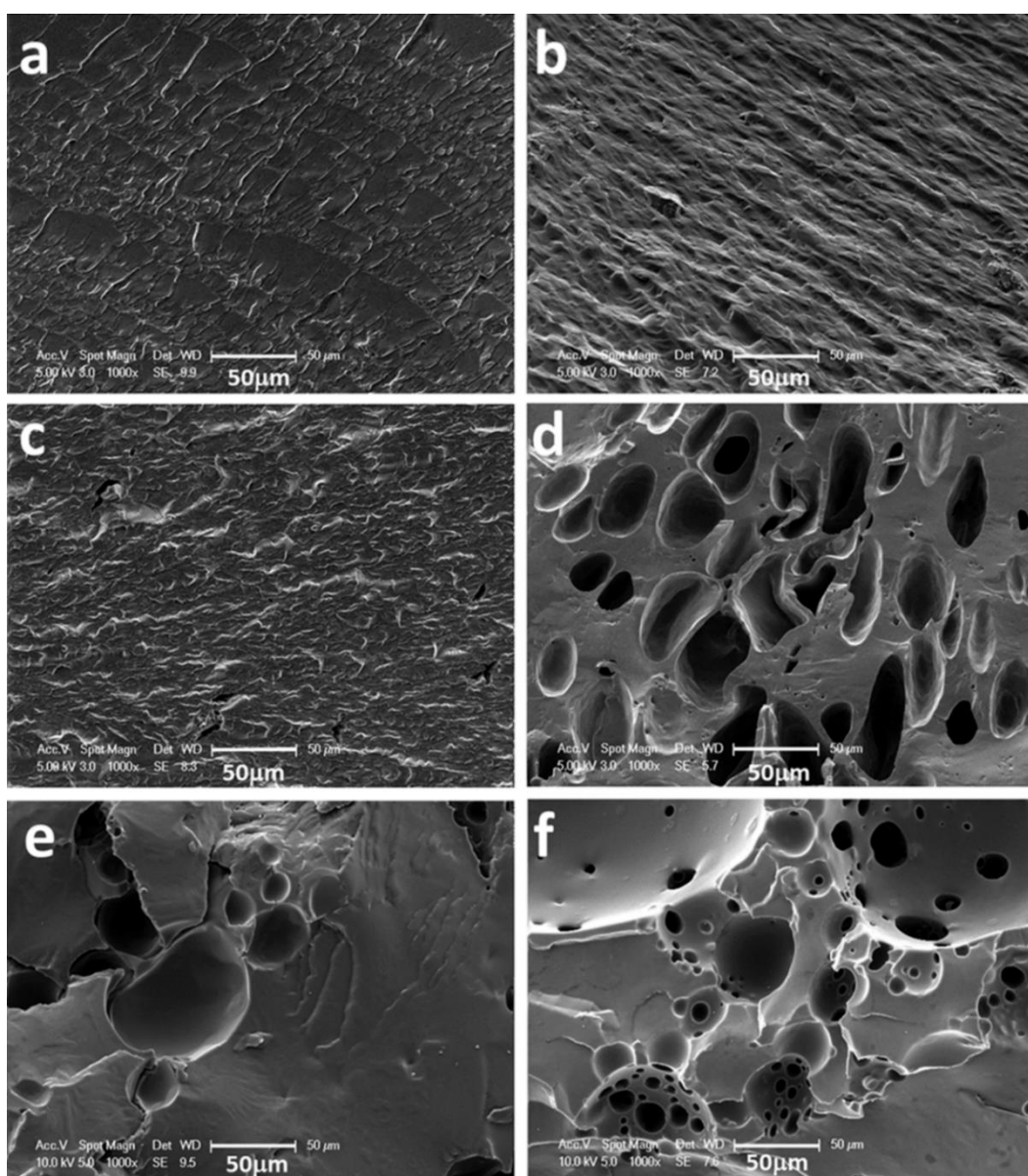


Figure 4.7. SEM images of hydrogels before and after redox-triggered degradation. a) H1 before degradation, b) H1 after 6 h degradation, c) H2 before degradation, d) H2 after 6 h degradation, e) H3 before degradation, f) H3 after 6 h degradation (Scale bar represents 50 μm).

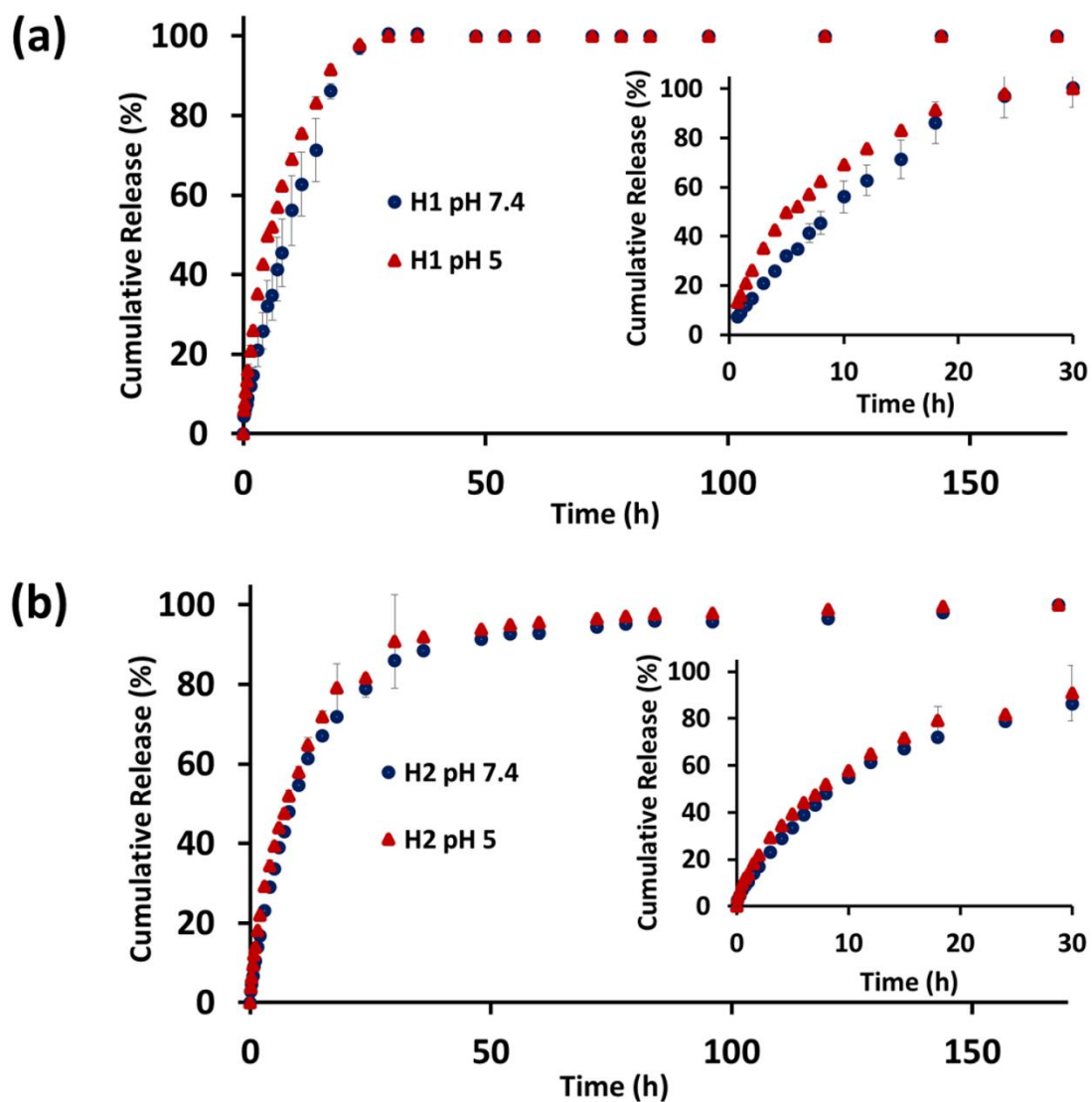


Figure 4.8. pH-dependent release kinetics of MB from H1 and H2 at 37 °C and two different pH values.

4.3.5. *In Vitro* Cytotoxicity and Photodynamic Therapy

The degradability of the hydrogels both *via* hydrolysis and by cleavage of disulfide bonds into non-toxic degradation products can eliminate the need for later surgical removal from the human body, both for tissue scaffold and drug/gene delivery applications. The dose dependent cytotoxicity of degradation products of PBAE hydrogels (after 24 h degradation)

in PBS (pH 7.4) was assessed on MCF-7 cells after 24 h incubation (Figure 4.9). Viability of cells was above 80% at all doses which indicates that degradation products are non-cytotoxic in the range of 1-200 $\mu\text{g/mL}$ in MCF-7 cells according to ISO 10993-5 classification [191]. Overall, looking at the whole concentration range, degradation products of all tested compositions look safe with no dramatic difference between them.

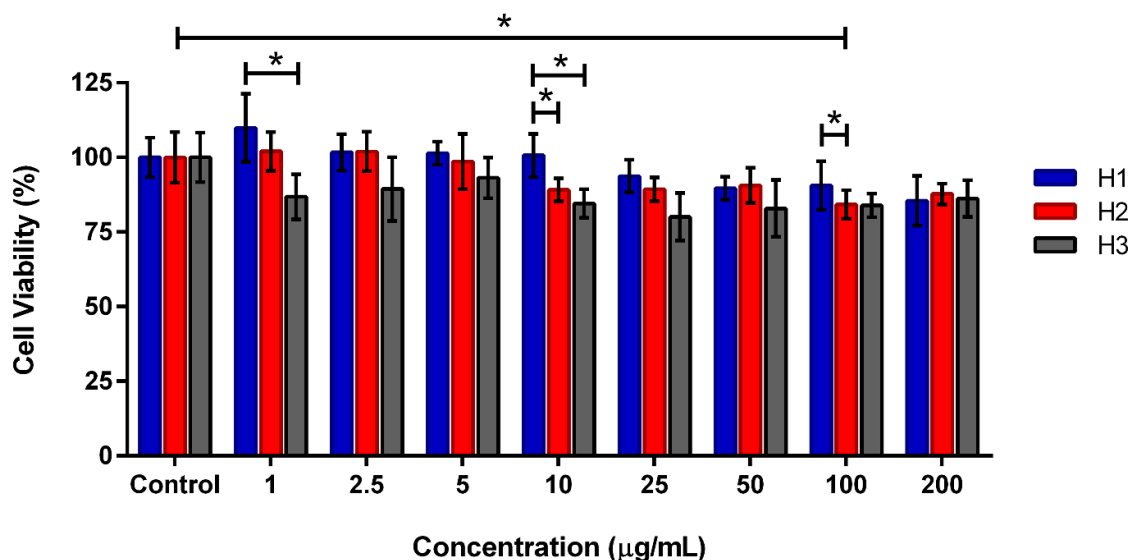


Figure 4.9. The effect of degradation products of the hydrogels on cell viability of MCF-7 human breast cancer cells. Cells were treated with different concentrations of the degradation products for 24 h. Untreated cells were used as the control. The cell viability test was performed by MTT assay ($\pm\text{SD}$; $n = 5$; $p < 0.05$ (*) compared with all concentrations).

To understand whether the released MB retained its biological activity or not, and to demonstrate local drug delivery potential of these PBAE hydrogels, *in vitro* PDT study was performed with the degradation products of the hydrogels (Figure 4.10).

MB loaded H1 and H2 was degraded for 6 h in PBS and then both dark toxicity, impact of laser irradiation on the viability of untreated cells and the influence of PDT on cell viability were tested in a dose dependent manner using A549 cell lines. For this part, a lung cancer cell line was preferred because lung is an appropriate target organ for phototherapies

which can be performed *via* endoscopic methods [209]. Free MB (16 μM) was also applied to cells at the highest concentration of MB in H1 and H2 degradation products.

A549 cells were incubated with MB loaded H1 and H2 degradation products in a dose range of 35-350 $\mu\text{g/ml}$, and 4.9-49 $\mu\text{g/mL}$, respectively, for 24 h. The difference in the dose range originates from degradation rates of H1 and H2 hydrogels. After the medium is replenished, each experiment's groups were treated 100 seconds with 30 J/cm^2 energy density at 635 nm.

As seen in Figure 4.10b, the control (untreated) and laser control (no degradation product but 100 sec laser irradiation) groups showed no decrease in viability. However, cells incubated with MB containing degradation products and treated with laser showed a tremendous drop in cell viability due to cytotoxic effect of photodynamic therapy well established in the literature. [209]. This indicates that there is no significant dark toxicity of MB loaded hydrogels and the laser irradiation does not reduce viability of cells if there is no exposure to photosensitizer, as desired. In addition, the toxicity of released MB was similar to free MB (16 μM), implying that encapsulation and release of MB by one-step PBAE hydrogels did not hamper its function as a photosensitizer and it retained biological activity. Elaborate experiments showing the cell death mechanism is beyond the scope of this study, but the effect is well established as indicated by the references.

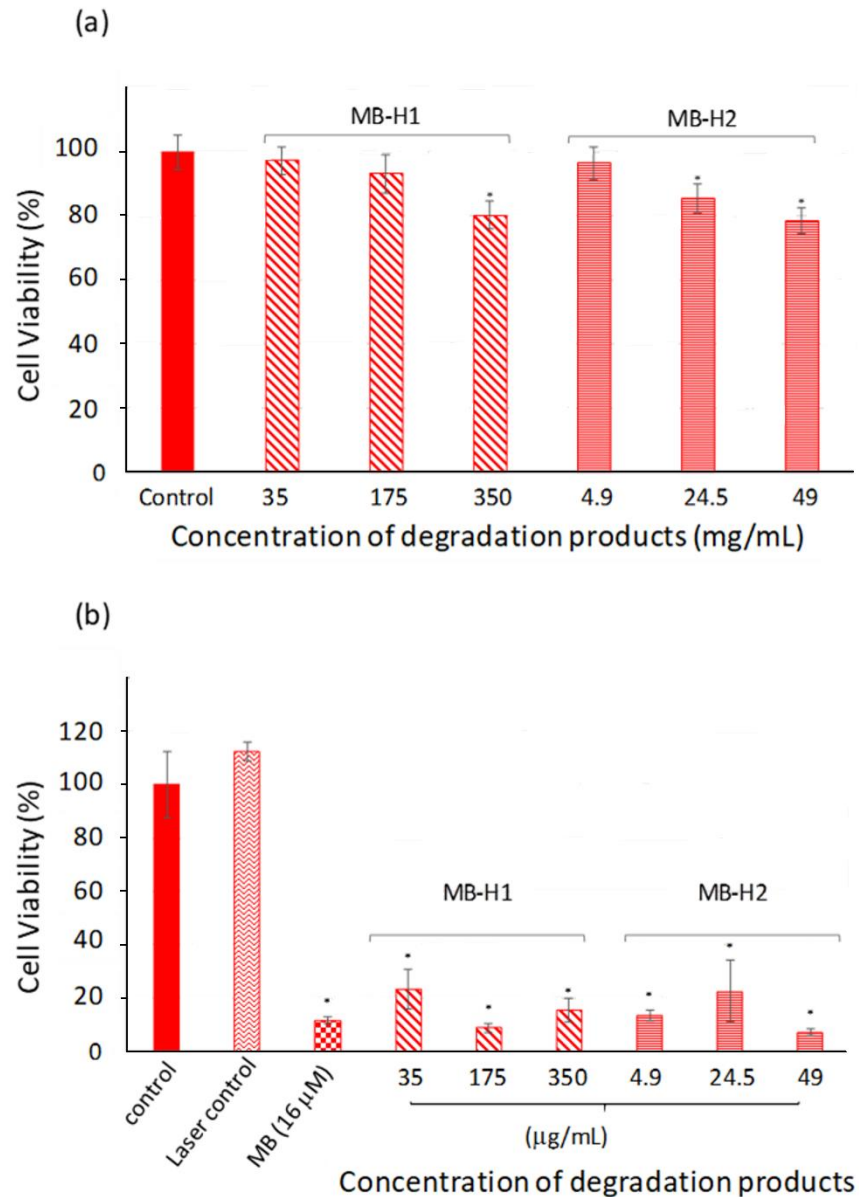


Figure 4.10. (a) The effect of released MB and degradation products on viability of A549 cells after 24 h exposure. Untreated cells were used as a control. (b) The effect of released MB and degradation products on cell viability of A549 cells after laser treatment (365 nm, 100 sec, 30 J/cm²). Untreated cells were used as a control. Cells were not treated with MB-hydrogel degradation products but subjected to laser irradiation were used as the laser control. (\pm SD; $n = 6$; $p < 0.05$ (*)) compared with all concentrations).

4.4. Conclusions

A simple one-step synthesis strategy based on aza-Michael reaction with no by-products was used to prepare novel PBAE hydrogels. By selecting the building blocks the hydrophilicity/hydrophobicity and accordingly the swelling and degradation behavior of the hydrogels were tailored. The hydrogels were loaded with MB as a model drug by simply adding the drug molecule into the precursor mixture. The hydrogels showed response to external triggers such as pH and redox state which served as a tool to facilitate the on-demand degradation of the hydrogel into nontoxic materials and release of the cargo molecule in a controlled manner. The biological activity of the released MB was evaluated by photodynamic therapy. Overall, these systems have the potential to be used as platforms for controlled delivery of therapeutic agents.

5. MINERALIZED HYDROGELS AND DENTAL ADHESIVES FROM PHOSPHONIC ACID-FUNCTIONALIZED ACRYLAMIDES

This chapter is published as: Bingol H. B., A. Altin, T. Bal, S. Agopcan-Cinar, S. Kizilel, D. Avcı, “Synthesis and evaluation of new phosphonic acid-functionalized acrylamides with potential biomedical applications”, *J. Polym. Sci. A*, Vol. 53, pp. 2755–2767, 2015.

5.1 Introduction

Phosphorus based molecules are widely used in bioapplications because they provide biodegradability, hemocompatibility and protein adsorption resistance to polymers which they are incorporated into [145]. Phosphorus-containing acidic monomers are able to interact with the inorganic phase of mineralized tissues such as enamel, dentin, and bone. Strong interactions of these materials with hydroxyapatite (HAP)-based tissues make them promising candidates for bone targeted imaging and drug delivery, bone tissue engineering applications and dentistry.

From this perspective, three phosphonic acid-containing acrylamide monomers with different lengths of alkyl chains were synthesized to be used for both self-etching dental adhesives and mineralized hydrogel scaffolds (Figure 5.1). Monomers were synthesized by the reaction of aminophosphonates (diethyl aminomethylphosphonate, diethyl 2-aminobutan-2-ylphosphonate, and diethyl 2-aminoctan-2-ylphosphonate) with acryloyl chloride followed by the hydrolysis of phosphonate groups by using trimethylsilyl bromide. The properties such as pH in the range of mild self-etching adhesives, hydrolytic stability, high rate of copolymerizations with 2-hydroxyethyl methacrylate (HEMA) and HEMA/glycerol dimethacrylate, giving high-molecular-weight polymers on thermal polymerization, and strong decalcification ability of hydroxyapatite make these monomers

good candidates for self-etching adhesives, although no appreciable effect of the number and size of the α -substituents was observed.

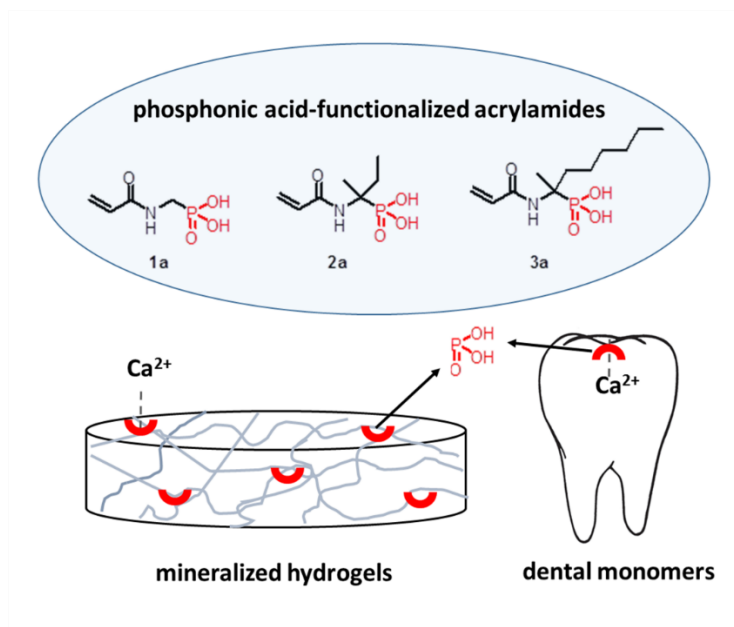


Figure 5.1. Phosphonic acid-functionalized acrylamides for fabrication of mineralized hydrogels and dental adhesive monomers.

To investigate the use of these monomers for tissue engineering applications, they were incorporated into HEMA to fabricate hydrogel scaffolds. The cytotoxicity of these hydrogels were evaluated against fibroblast cells. Mineralization of the hydrogels was performed upon immersion in SBF and mineral deposits were observed in SEM micrographs. EDX was used to show that these minerals contain Ca and P, furthermore Ca deposition assay was performed for the quantitative detection of Ca in mineralized scaffolds. These results imply that the phosphonic acid-containing monomers are good candidates to be used for both dental and tissue engineering applications.

5.2. Experimental

5.2.1. Materials and Methods

Diethyl aminomethylphosphonate, diethyl 2-aminobutan-2-ylphosphonate, and diethyl 2-aminooctan-2-ylphosphonate were prepared according to literature procedures [221, 222]. Trimethylsilyl bromide (TMSBr), acryloyl chloride, triethyl amine (TEA), 2-hydroxyethyl methacrylate (HEMA), poly (ethylene glycol)diacrylate (PEGDA) (M_n 575), glycerol dimethacrylate (GDMA), bis(2,4,6-trimethylbenzoyl)- phenylphosphine oxide (BAPO), 2,2-dimethoxy-2-phenyl acetophenone (DMPA), HAP, and all other reagents and solvents were obtained from Aldrich and used as received. 10-Methacryloyloxydecyl dihydrogen phosphate (MDP) was a gift from Ivoclar Vivadent AG. Dichloromethane was dried over activated molecular sieves (4 Å). DMEM (HG) and fetal bovine serum (FBS) were purchased from Life Technologies, and 10,000 U/mL penicillin–10 mg/mL streptomycin, L-glutamine, and trypsin–EDTA (0.25%) were obtained from Sigma. Sodium pyruvate was purchased from Lonza.

Monomer characterization involved ^1H , ^{13}C , and ^{31}P NMR spectroscopy (Varian Gemini 400 MHz) and FTIR spectroscopy (Thermo Fisher T380). Combi Flash Companion Teledyne ISCO Flash Chromatography with C18 reverse-phase silica gel as a stationary phase was used for purification of monomers. Photopolymerizations were performed using a TA Instruments Q100 differential photocalorimeter. The interactions of monomers with HAP were studied by X-ray diffraction (Rigaku D/max-2200/PC). The images were obtained using Zeiss Ultra Plus FE–SEM. The presence of calcium in mineralized hydrogels was determined by EDX (Bruker X flash 5010 123 eV). Gel permeation chromatography (GPC) was performed on a Malvern Viscotek TDA 302 GPC instrument equipped with a refractive index detector, using PBS (pH 7.0%, 0.05 NaN_3) as a solvent and poly(ethylene oxide) standards.

5.2.2. Synthesis of Monomers

5.2.2.1. Diethyl Acrylamidomethylphosphonate (1). Acryloyl chloride (0.77 mL, 9.57 mmol) was added dropwise, under N₂, to a mixture of diethyl aminomethylphosphonate (1.02 g, 5.98 mmol) and triethylamine (1.13 mL, 8.07 mmol) in anhydrous dichloromethane (15.0 mL) in an ice bath. The mixture was stirred at room temperature for 2 h. The reaction was terminated by addition of distilled water (3.0 mL). After addition of chloroform (40 mL), the organic layer was extracted with 2 M HCl (3 x 10 mL), saturated NaHCO₃ (3 x 10 mL), and distilled water (3 x 10 mL). The organic phase was dried over anhydrous Na₂SO₄, filtered, and evaporated under vacuum to leave the crude product, which was purified by column chromatography on silica gel using MeOH–EtOAc (5:95) as eluent. Monomer 1 was obtained as a yellow viscous liquid in 32% yield. ¹H-NMR (400 MHz, CDCl₃, δ): 1.32 (t, ³J_{HH} = 6.8 Hz, 3H, OCH₂CH₃), 3.76 (dd, ³J_{HH} = 12.2 Hz, ³J_{HH} = 5.8 Hz, 2H, CH₂-P), 4.13 (m, 4H, OCH₂CH₃), 5.67 (d, ³J_{HH} = 10.4 Hz, 1H, CH₁H₂=CH), 6.17 (dd, ³J_{HH} = 16.8 Hz, ³J_{HH} = 10.4 Hz, 1H, CH₁H₂=CH), 6.32 (d, ³J_{HH} = 16.8 Hz, 1H, CH₁H₂=CH), 6.57 (s, 1H, NH) ppm. ¹³C-NMR (400 MHz, CDCl₃, δ): 15.75 (OCH₂CH₃), 38.87, 39.90 (C–P), 63.15 (OCH₂CH₃), 127.26 (CH=CH₂), 130.06 (CH=CH₂), 165.89 (C=O) ppm. FTIR (ATR): 3270 (N-H), 2983, 2926 (C–H), 1664 (C=O), 1634 (C=C), 1549 (NH), 1204 (P=O), 1018 and 975 (P–O) cm⁻¹.

5.2.2.2. Diethyl 2-acrylamidobutan-2-ylphosphonate (2). Monomer 2 was synthesized using the same procedure as for monomer 1 using diethyl 2-aminobutan-2-ylphosphonate instead of diethyl aminomethylphosphonate. The crude product was purified by column chromatography on silica gel using EtOAc-Hexane (90:10) as eluent. Monomer 2 was obtained as a yellow viscous liquid in 83% yield. ¹H-NMR (400 MHz, CDCl₃, δ): 0.95 (t, ³J_{HH} = 7.6 Hz, 3H, CH₂CH₃), 1.33 (t, ³J_{HH} = 7.0 Hz, 6H, OCH₂CH₃), 1.65 (d, ³J_{HH} = 16.4 Hz, 3H, C-CH₃), 1.96, 2.20 (m, 2H, CH₂CH₃), 4.16 (m, 4H, OCH₂CH₃), 5.60 (d, ³J_{HH} = 10.0 Hz, 1H, CH₁H₂=CH), 5.73 (s, 1H, NH) 6.11 (dd, ³J_{HH} = 16.8 Hz, ³J_{HH} = 10.0 Hz, 1H, CH₁H₂=CH), 6.23 (d, ³J_{HH} = 16.8 Hz, 1H, CH₁H₂=CH) ppm. ¹³C-NMR (400 MHz, CDCl₃, δ): 7.80 (CH₂CH₃), 16.46 (OCH₂CH₃), 20.11 (C-CH₃), 27.83 (C-CH₂CH₃), 55.85, 57.39 (C–P), 62.69 (OCH₂CH₃), 126.05 (CH=CH₂), 131.66 (CH=CH₂), 165.15 (C=O) ppm. FTIR

(ATR): 3261 (N-H), 2977, 2937 (C-H), 1683 (C=O), 1631 (C=C), 1553 (NH), 1219 (P=O), 1020 and 946 (P-O) cm^{-1} .

5.2.2.3. Diethyl 2-acrylamidoctan-2-ylphosphonate (3). Monomer 3 was synthesized using the same procedure as for monomer 1 using diethyl 2-aminoctan-2-ylphosphonate instead of diethyl aminomethylphosphonate (Monomer 3 was previously synthesized by Ayşe Altın in TÜBİTAK Project No:112T594).

5.2.2.4. Diethyl acrylamidomethylphosphonic acid (1a). TMSBr (0.77 mL, 5.86 mmol) was added dropwise to a solution of monomer 1 (0.43 g, 1.95 mmol) in dry dichloromethane (6.0 mL) in an ice bath and under N_2 . After stirring for 3 h at room temperature, the volatile components were removed under vacuum. Methanol (15.0 mL) was added and the mixture was stirred at room temperature overnight. The solvent was evaporated and the crude product was purified by flash chromatography on C18 reverse phase silica gel, eluting with H_2O to give monomer 1a as a white waxy solid in 89% yield. $^1\text{H-NMR}$ (400 MHz, MeOD, δ): 3.62 (dd, $^3J_{\text{HH}} = 23.8$ Hz, $^3J_{\text{HH}} = 13.0$ Hz, 2H, $\text{CH}_2\text{-P}$), 5.68 (d, $^3J_{\text{HH}} = 9.8$ Hz, 1H, $\text{CH}_1\text{H}_2=\text{CH}$), 6.23 (d, $^3J_{\text{HH}} = 16.6$ Hz, 1H, $\text{CH}_1\text{H}_2=\text{CH}$), 6.31 (dd, $^3J_{\text{HH}} = 16.6$ Hz, $^3J_{\text{HH}} = 9.8$ Hz, 1H, $\text{CH}_1\text{H}_2=\text{CH}$) ppm. $^{13}\text{C-NMR}$ (400 MHz, MeOD, δ): 34.12, 36.52 (C-P), 126.02 ($\text{CH}=\text{CH}_2$), 130.03 ($\text{CH}=\text{CH}_2$), 166.79 (C=O) ppm. ^{31}P NMR (400 MHz, MeOD, δ): 20.09 ppm. FTIR (ATR): 3249 (N-H), 3000-2600 (OH), 2987, 2926 (C-H), 1648 (C=O), 1619 (C=C), 1548 (NH), 1137 (P=O), 998 and 947 (P-O) cm^{-1} .

5.2.2.5. Diethyl 2-acrylamidobutan-2-ylphosphonic acid (2a). Monomer 2a was synthesized using the same procedure as for monomer 1a using monomer 2 instead of monomer 1. The crude product was purified by flash chromatography on C18 reverse phase silica gel, eluting with $\text{H}_2\text{O-MeOH}$ (45:55) to give monomer 2a as a white waxy solid in 56% yield. $^1\text{H-NMR}$ (400 MHz, MeOD, δ): 0.83 (m, 3H, CH_2CH_3), 1.36 (m, 3H, CCH_3), 1.65, 2.20 (m, 2H, CH_2CH_3), 5.60 (dd, $^3J_{\text{HH}} = 14.7$ Hz, $^3J_{\text{HH}} = 11.4$ Hz, 1H, $\text{CH}_1\text{H}_2=\text{CH}$), 6.16 (d, $^3J_{\text{HH}} = 14.7$ Hz, 1H, $\text{CH}_1\text{H}_2=\text{CH}$), 6.25 (m, 1H, $\text{CH}_1\text{H}_2=\text{CH}$) ppm. $^{13}\text{C-NMR}$ (400 MHz, MeOD, δ): 7.49 (CH_2CH_3), 20.13 (C- CH_3), 27.56 (C- CH_2CH_3), 56.64, 58.09 (C-P), 128.42 ($\text{CH}=\text{CH}_2$), 131.56 ($\text{CH}=\text{CH}_2$), 169.64 (C=O) ppm. ^{31}P NMR (400 MHz, MeOD, δ): 26.81 ppm. FTIR

(ATR): 3249 (N-H), 3000-2600 (OH), 2977, 2940 (C-H), 1652 (C=O), 1626 (C=C), 1539 (NH), 1167 (P=O), 978 and 926 (P-O) cm^{-1} .

5.2.2.6. Diethyl 2-acrylamidoctan-2-ylphosphonic acid (3a). Monomer 3a was synthesized using the same procedure as for monomer 1a using 3 instead of 1. (Monomer 3a was previously synthesized by Ayşe Altın in TÜBİTAK Project No:112T594. In this dissertation the properties of hydrogels made from this monomer is investigated).

5.2.3. Interactions of Monomers with Hydroxyapatite

HAP particles (0.2 g) were dispersed in 1.00 g of monomer/EtOH/H₂O (15/45/40 wt %) solution under stirring [223]. The monomer coated HAP particles were isolated by centrifugation after 24 h and washed. For characterization with FTIR, they were washed first with water and then with ethanol and dried at room temperature. For characterization with XRD, the monomer coated HAP particles were washed first with ethanol and then with water and dried at room temperature. The crystal phases on the monomer-coated HAP particles were identified by a powder XRD operated under 40 kV acceleration, 40 mA current and scanning rate of 2°min^{-1} for $2\theta/\theta$ scan.

5.2.4. Hydrolytic Stability

The hydrolytic stability of monomer 3a was investigated by ¹H NMR measurement of 5 wt % solution of monomer in methanol-*d*₄/D₂O (1/1, v/v) after storage at 37 °C for 20 days.

5.2.5. Photopolymerizations

Reactivities of the synthesized monomers were determined by photopolymerization studies which were performed on a DSC equipped with a mercury arc lamp. The samples containing 2.0 mol % initiator were prepared and irradiated for 10 min with an incident light intensity of 20 mW cm⁻² and a nitrogen flow of 20 mL min⁻¹. Photopolymerization rates were calculated using the equation (5.1):

$$Rate = \frac{(Q/s)M}{n(\Delta H_p)m} \quad (5.1)$$

where Q/s is the heat flow per second, M is the molar mass of the monomer, n is the number of double bonds per monomer molecule, ΔH_p is the heat released per mole of double bonds reacted, and m is the mass of monomer in the sample. The theoretical value that was used for the heat of reaction (ΔH_p) is 20.6 kcal/mol for acrylamide double bonds [224].

5.2.6. Synthesis of Hydrogels

Monomers 1a - 3a (15 wt %), HEMA (50 wt %), and PEGDA (35 wt %) were dissolved in ethanol (30 wt %) to form precursor solutions of hydrogels H1a, H2a, and H3a respectively. DMPA was added (2 wt %) to the mixture of monomers as an initiator. The precursor solutions were then poured into teflon molds and subjected to UV light for 30 minutes. A blank hydrogel H0 that does not contain phosphonic acid monomer was also prepared from HEMA (65 wt %) and PEGDA (35 wt %) under the same conditions. The hydrogel samples (diameter: 1 cm, thickness: 0.2 cm) were dried and weighed to obtain W_1 . Then the hydrogels were immersed in ultrapure water for 48 h, with exchange of fresh water to remove unreacted components. The swollen samples were dried and weighed again to obtain W_2 . The percent gelation of hydrogel samples were calculated by equation (3.1).

5.2.7. Swelling Studies

Swelling studies were conducted by immersing a piece of dry hydrogel into a flask containing excess amount of ultrapurewater at room temperature. The hydrogel samples were removed at pre-determined time intervals, blotted on filter paper and the swollen weight was measured. The increase in the weight of hydrogel sample was recorded as a function of time until equilibration was reached. The degree of swelling (D_s) was calculated using the equation (4.2).

5.2.8. Cell Viability on Hydrogels

Human dermal fibroblasts were grown in DMEM supplemented with 10% FBS, 1% penicillin-streptomycin, 2 mM L-glutamine and 1 mM sodium pyruvate. After reaching 80-90% confluence, cells were passaged with 0.25% trypsin-EDTA and used for seeding experiments. Hydrogels were swollen in growth medium overnight and seeding was performed in 24-well plates. Briefly, swollen hydrogels were seeded with a concentration of 20 000 human dermal fibroblasts/cm². After seeding, 1 ml of growth medium was added to each well and viability of cells was analyzed with alamar blue assay (Invitrogen) on day 1 and day 4. Five hundred microliters of 10% alamar blue reagent was added to each hydrogel and incubated at 37 °C and 5% CO₂ for 3 hours. Following this incubation period, supernatants were collected and fluorescence was measured (Ex: 550, Em: 590 nm) with a microplate reader (Synergy H1 Hybrid Multi-Mode Microplate Reader, Bio-Tek). Cell survival rate measured on day 4 was normalized with respect to day 1 to obtain proliferation rate of cells.

5.2.9. Mineralization of Hydrogels

Simulated body fluid (SBF) was prepared as described by Kokubo and Takadama. [225] 1 L of buffer solution (pH 7.4) containing 142 mM Na⁺, 5 mM K⁺, 1.5 mM Mg²⁺, 2.5 mM Ca²⁺, 147.8 mM Cl⁻, 4.2 mM HCO₃⁻, 1 mM HPO₄²⁻, and 0.5 mM SO₄²⁻ was prepared in ultrapure water. This solution was then filter sterilized (Millipore, sterivex filter unit, 0.22 μm). SBF was stored at 4 °C and used at 37 °C. 40 mM Ca²⁺ / 24 mM HPO₄²⁻ solution was prepared as described by Phadke *et al.* [226]. 2.74 g of K₂HPO₄·3H₂O and 2.22 g CaCl₂ was dissolved in 500 mL ultrapure water. 6 N HCl was added slowly until the turbidity disappeared. Similar to SBF, this solution was filter sterilized and stored at 4 °C until use. 1 M Tris-HCl (pH 7.5) was added dropwise until the pH raised to 5.2 prior to use. Freeze-dried hydrogels were swollen in SBF for 24 h. Hydrogels (3 samples for each monomer) were immersed in 40 mM Ca²⁺ / 24 mM HPO₄²⁻ solution (metastable solution) for 30 min, rinsed with ultrapure water and immersed in simulated body fluid (SBF) for 24 h. Metastable solution treatment followed by SBF was considered as a cycle and this cycle was repeated two times. As a control, hydrogel samples were immersed in water for 72 h and no Ca²⁺ could be detected by Ca²⁺ assay on these samples.

5.2.10. Characterization of Mineralized Hydrogels

5.2.11.1. SEM-EDX. Morphological properties of the hydrogels before and after mineralization were characterized by SEM analysis. The samples were lyophilized and sputter coated with Au prior to analysis. The images were obtained using Zeiss Ultra Plus FE-SEM. The presence of calcium in mineralized hydrogels was determined by using EDX (Bruker X flash 5010 123 eV).

5.2.11.2. Determination of Ca²⁺ Content. Ca²⁺ content was measured according to the procedure described elsewhere [226]. Mineralized hydrogel samples were lyophilized and then homogenized in 0.5 mL of 0.5 N HCl. The homogenate was shaken at 175 rpm for 24 h at 4 °C and mechanical force was applied for complete disruption of the hydrogels. To

achieve complete dissolution, shaking was repeated overnight. The Ca^{2+} concentration in the solution was measured using spectrophotometric analysis. Cresolphthalein complexone and Calcium Reagent (Pointe Scientific) set was used to determine the Ca^{2+} content in the lyophilized sample. Standard solutions in the range of 0.2-0.0136 mg/ml Ca^{2+} were prepared to generate a standard curve and Ca^{2+} content was normalized with the dry weight of sample.

5.3. Results and Discussion

5.3.1. Synthesis and Characterization of Monomers

Firstly, the phosphonic-acid functionalized acrylamide monomers to be used for dental adhesives and hydrogel fabrication with the aim of mineralization was synthesized and characterized. The structure of monomers used in this study is shown in Figure 5.2.

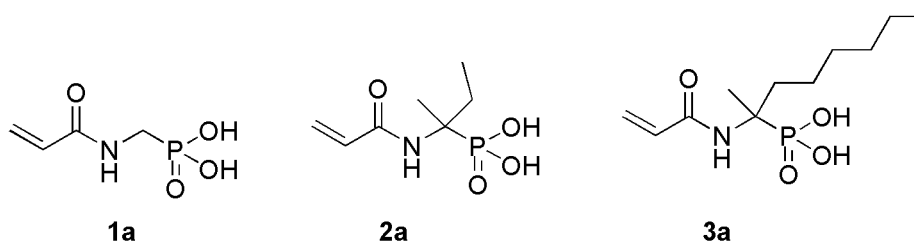


Figure 5.2. Structure of monomers.

The three α -aminophosphonates required for the study were obtained by two different methods (Figure 5.3). Diethyl 2-aminobutan-2-ylphosphonate and diethyl 2-aminooctan-2-ylphosphonate were prepared by a one-pot reaction of butan-2-one or octan-2-one, ammonium carbonate and diethyl phosphite under solvent-free conditions catalyzed by $\text{Al}(\text{OTf})_3$ [221]. Diethyl aminomethylphosphonate was synthesized from diethyl phthalimidomethylphosphonate obtained in the Arbuzov reaction of *N*-bromomethylphthalimide and triethyl phosphate by reaction with hydrazine hydrate [222].

The three acrylamides (1a-3a) with phosphonic acid groups were synthesized in two steps (Figure 5.4). In the first step, the α -aminophosphonates were reacted with acryloyl chloride in the presence of triethyl amine to form phosphonate-containing monomers (1-3) as pale yellow viscous liquids in 32-83% yields. In the second step, the phosphonate-containing monomers were silylated by TMSBr, then the silyl ester groups were removed by methanolysis to obtain the phosphonic acid-containing monomers (1a-3a) which were further purified by C18 reversed-phase flash chromatography. The acidic monomers (1a-3a) were obtained as white colored waxy solids in 33-89% yields.

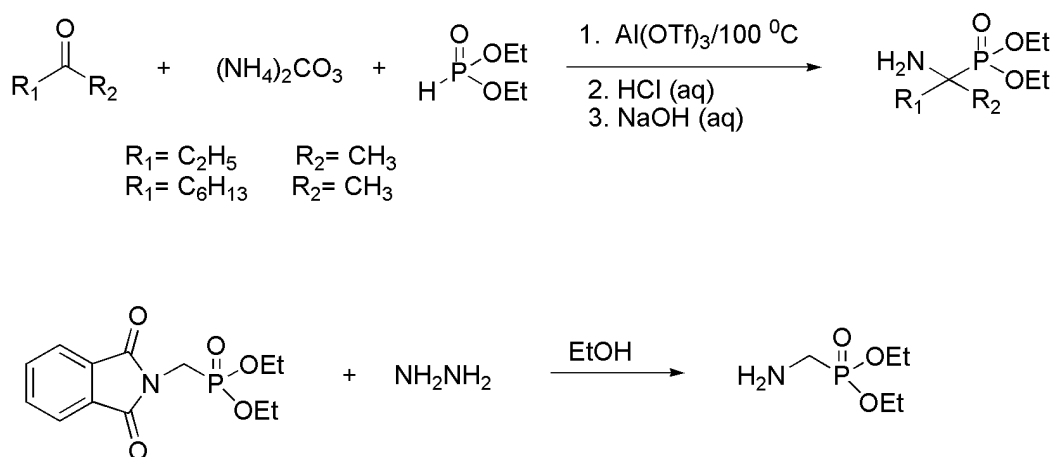


Figure 5.3. Synthesis of α -aminophosphonates.

Monomers 1a and 3a are well soluble in water, whereas 2a has limited solubility in this solvent. Monomer 3a is also soluble in THF and acetone due to its less polar structure compared to 1a and 2a (Table 5.1).

Table 5.1. Solubility of monomers

Monomer	H ₂ O	EtOH	THF	Acetone	Et ₂ O	CH ₂ Cl ₂
1	+	+	+	+	+	+
2	-	+	+	+	+	+
3	-	+	+	+	+	+
1a	+	+/-	-	-	-	-
2a	+/-	+/-	-	-	-	-
3a	+	+	+	+	-	-

The monomers (1-3, 1a-3a) were characterized by FTIR and ¹H, ¹³C, ³¹P NMR spectroscopies to confirm their structures. In the ¹³C NMR spectra of 1 and 2, the doublet seen at 38.87, 39.90 and 55.85 and 57.39 ppm is due to the carbon attached to phosphorus (Figure 5.5). The complexity of ¹H NMR spectra of these monomers are due to phosphorus-hydrogen coupling and the non-equivalence of atoms within the geminal groups attached to the prochiral phosphorus atom. The signals for the olefinic protons appeared as two multiplets between 5.60 and 6.34 ppm (Figure 5.6). We also observed two different multiplets at 1.65 and 2.20 ppm for methylene protons of monomer 2a.

The FTIR spectrum of monomers 1a-3a shows broad peaks in the region of 3000–2600 cm⁻¹ and 2300–2100 cm⁻¹ due to OH stretching, 1670–1600 cm⁻¹ due to OH bending and strong peaks at around 1650, 1630, and 1540 cm⁻¹ due to C=O, C=C, and NH stretching, respectively. Also the strong bands in the range of 920-1000 cm⁻¹ correspond to the symmetric and asymmetric vibrations of P-O.

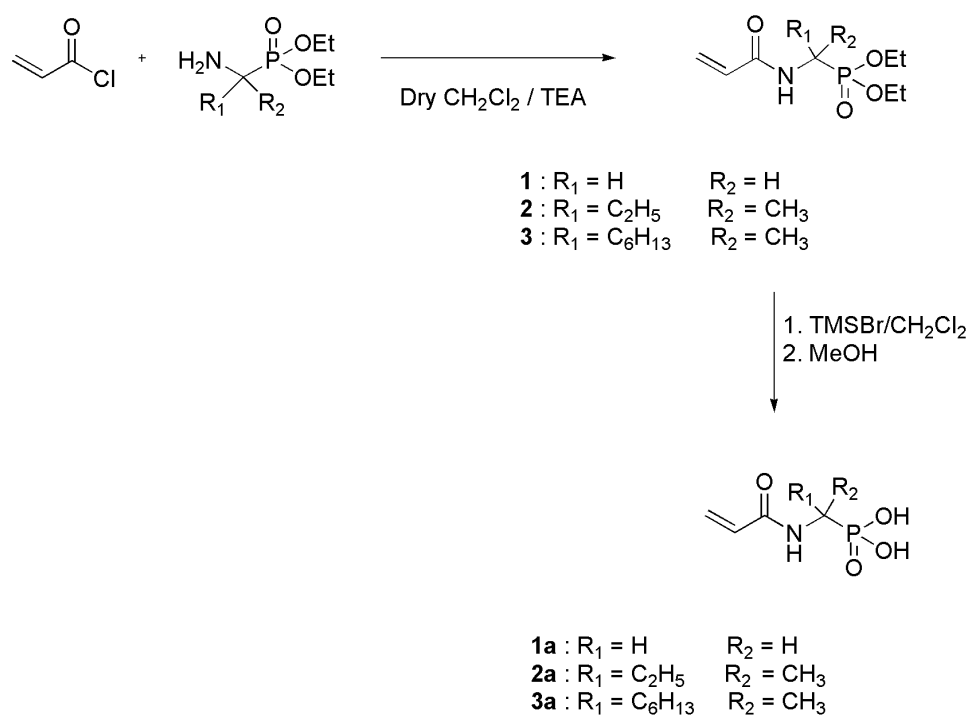
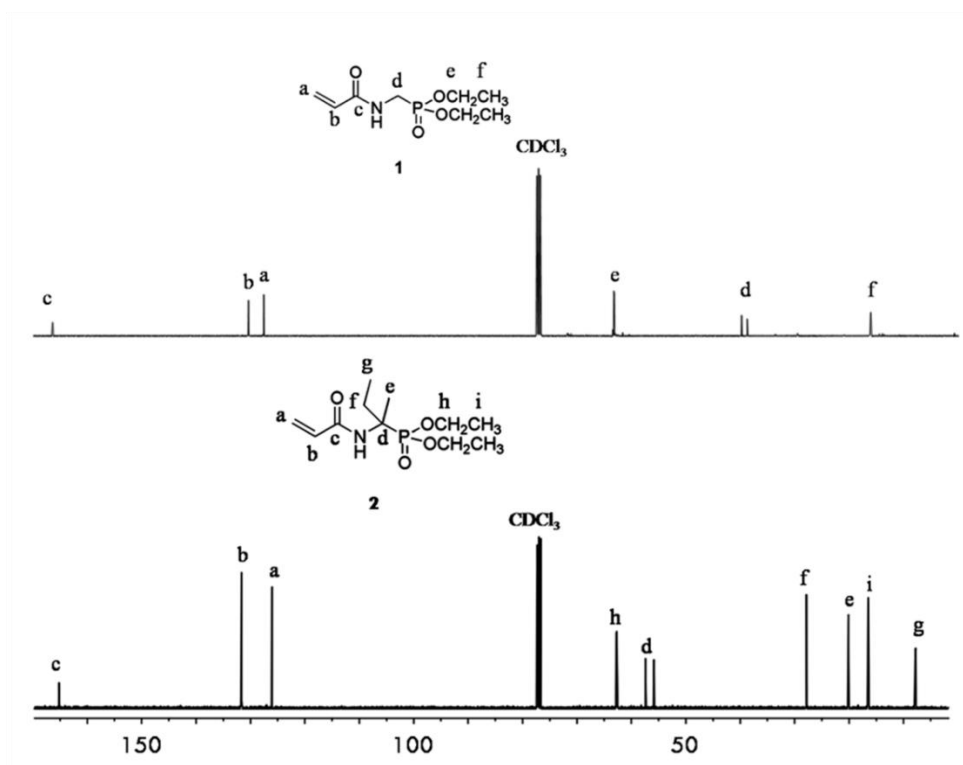


Figure 5.4. Synthesis of monomers.

Figure 5.5. ¹³C NMR spectra of monomers 1 and 2.

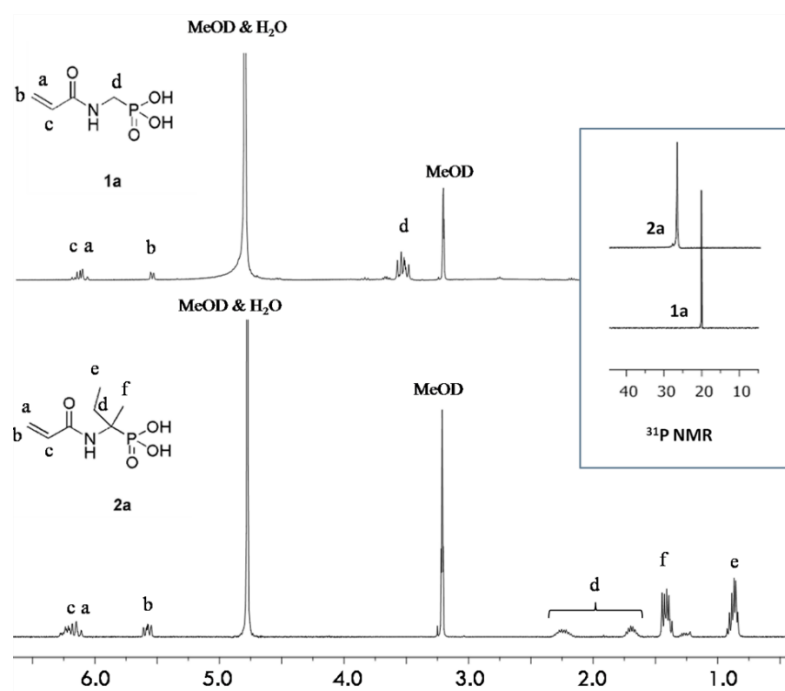


Figure 5.6. ^1H NMR spectra of monomers 1a and 2a.

5.3.2. Acidity, Interactions with HAP, and Stability of Acid Monomers

The enamel-dentin etching ability of the monomers is due to their acidic property. The pH values of aqueous solutions of the monomers (2 wt %) were found to be 1.58, 1.88, and 1.93 for monomers 1a, 2a and 3a, respectively, in the range expected for mild self-etching adhesives. 2a was not completely dissolved in water, the higher pH value of its solution can be partially explained by the incomplete solution, partially due to higher molecular weight. The pH value of 3a solution is too high to be explained solely due to its molecular weight; we believe that the electron donating effect of both methyl and hexyl groups also contributes. The hydrophobicity of the acid monomers were estimated by the logarithm of partition coefficient, using a chemical structure drawing software (ChemDraw Ultra version 8.0.3). These values were found to be 0.07, 1.77 and 3.36 for monomers 1a, 2a, and 3a, respectively. These values correlate well, with expectations from inspection of molecular structures.

The interaction of monomers 1a-3a with dental tissues and bone was demonstrated by investigating their interactions with HAP as a model compound. The solid and liquid phases of monomer-treated HAP solutions were analysed by FTIR (Figure 5.7). The solid phase spectrum indicated some carbonyl groups (at about 1650 cm^{-1}) and the typical stretching of the phosphoric groups (at 1022 cm^{-1}). FTIR spectrum of the liquid part of monomer-treated HAP showed C=O, C=C stretching bands of the monomers as well as some changes of the P-O and P=O peaks when compared to the corresponding monomer. The peaks at 926 cm^{-1} and 978 cm^{-1} corresponding to the symmetric and asymmetric vibration of P-O in monomer 2a decreased and shifted to 918 cm^{-1} and 983 cm^{-1} respectively. Also a new peak which corresponds to the phosphoric groups of HAP appeared at 1046 cm^{-1} . These results imply that monomers 1a-3a can decalcify HAP and are also slightly adsorbed onto HAP surfaces.

The solid phase was further analyzed by XRD to observe the changes in the crystal structure of HAP. The obtained XRD patterns can be interpreted according to the adhesion-decalcification mechanism proposed by Yoshida *et al.* [27]. According to this mechanism, firstly the decalcification of HAP is induced by monomer adsorption from the aqueous solution. Then, calcium salts of monomers and $\text{CaHPO}_4 \cdot 2\text{H}_2\text{O}$ (DCPD) are deposited on HAP depending on their solubilities in water-ethanol solution. XRD spectrum of untreated HAP was used as reference which showed peaks at $2\theta = 26^\circ$ and 32° (Figure 5.8). To compare the performance of the synthesized monomers, MDP, which has been shown to have excellent binding ability, was used as a control monomer. Upon treatment of HAP with monomer/EtOH/ H_2O solutions, a new peak appeared at $2\theta = 11.6^\circ$ which was assigned to deposited DCPD indicating etching and demineralization. No peaks were observed around $2\theta = 5-8^\circ$ which can be assigned to monomer-Ca salts. These results can be explained by (i) decalcification of HAP by the synthesized monomers and (ii) higher solubilities of monomer-Ca salt than DCPD in water-EtOH solution.

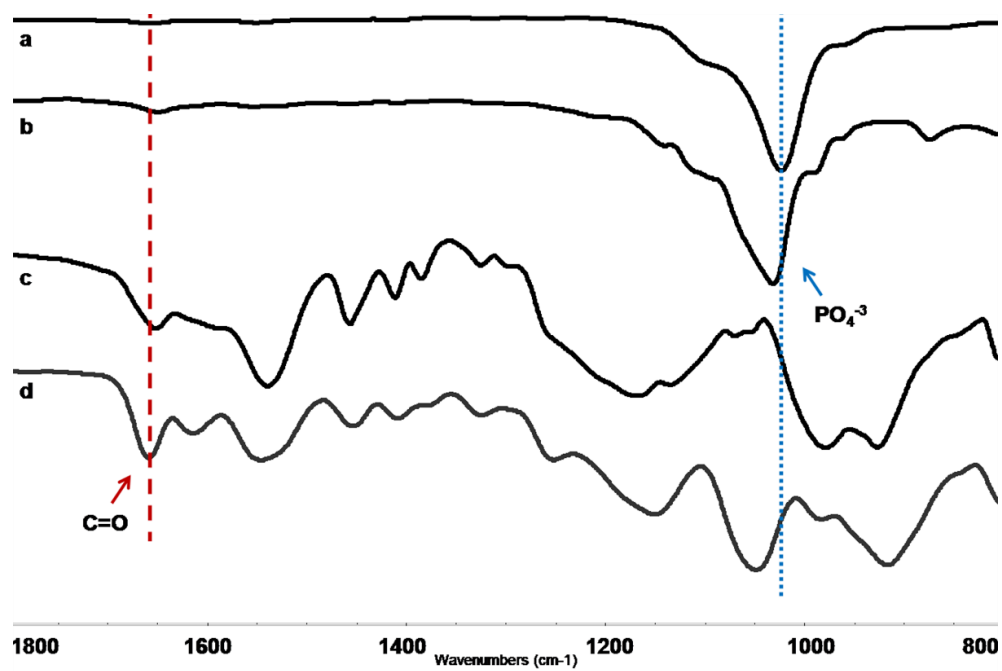


Figure 5.7. FTIR spectra of (a) HAP, (b) HAP-2a/EtOH/H₂O (HAP phase), (c) 2a, (d) HAP-2a/EtOH/H₂O (solvent phase).

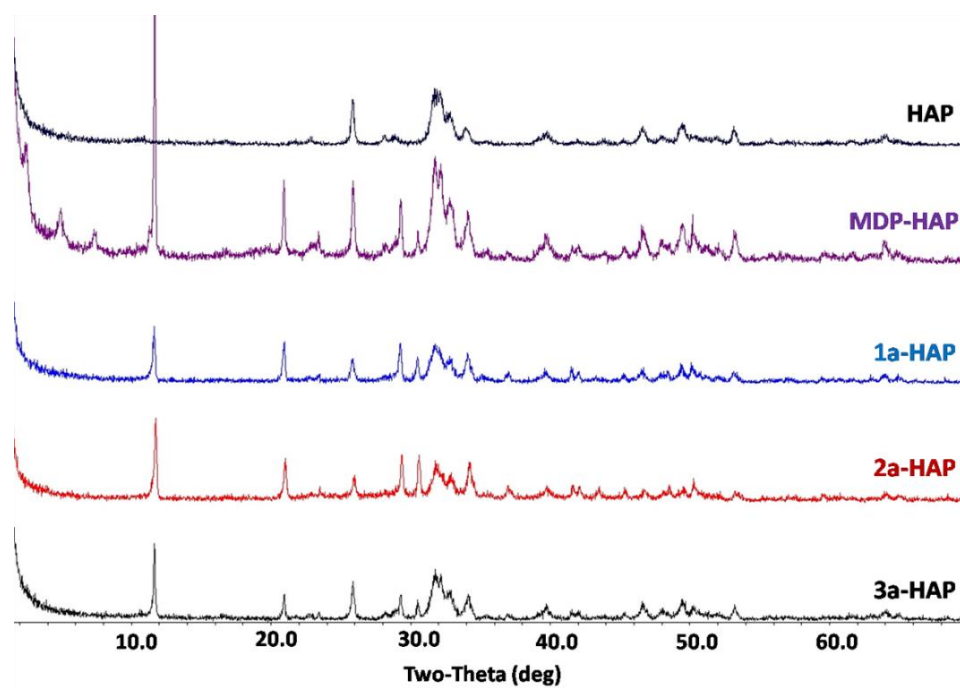


Figure 5.8. XRD patterns of HAP, MDP-HAP, 1a-HAP, 2a-HAP, and 3a-HAP.

As mentioned briefly in the introduction, the recent trend is to use acidic (meth)acryl amide monomers instead of (meth)acryl ester monomers in dental adhesives to address the problem of hydrolysis of the latter, leading to expectations of improvement in both the shelf life and the useful lifetime in oral conditions for the said adhesives. In our study, hydrolytic stability of 3a was examined by recording ^1H NMR spectra of its 5 wt% solution in aqueous methanol. No detectable amide hydrolysis occurred after 20 days of incubation at 37 °C.

5.3.3. Photopolymerizations

In order to investigate the reactivity of the monomers, they were photopolymerized using photodifferential scanning calorimetry. First, the polymerization kinetics of the synthesized phosphonic acid monomers 1a-3a together with HEMA were investigated in order to evaluate their potential to be used as self-etching dental adhesives. Formulations consisting of HEMA/1a-3a/water (45/15/40 wt%) were prepared and photopolymerized using BAPO (2 mol %). Figure 5.9 shows photopolymerization results such as maximum rate of polymerization (R_{pmax}), time to reach maximum polymerization rate (t_{max}) and conversion. The following conclusions can be drawn : i) the time of the maximum polymerization rate (t_{max}) is reduced compared to HEMA, consistent with the trend that acrylates are more reactive than comparable methacrylates; ii) replacement of 15 wt% of HEMA with one of the monomers 1a-3a and two other monosubstituted ones showed no significant effect on both maximum polymerization rate and conversion values; iii) the number of substituents and size of the substituents on the α -position of the phosphonic acid group did not influence the rate of polymerizations and conversions.

Bulk copolymerization of phosphonic acid monomers 1a-3a with a mixture of GDMA and HEMA was studied to compare reactivities (Figure 5.10). The mixtures of HEMA/GDMA (7/3 mol%) and HEMA/1a-3a/GDMA (5/2/3 mol%) were photopolymerized at 40 °C using DMPA (2 mol %) as initiator. The R_{pmax} values followed the order: 0.029, 0.049, 0.056 s^{-1} , and 0.058 s^{-1} for 1a, 2a, 3a, and HEMA respectively. It was observed that mixtures containing 2a and 3a had comparable R_{pmax} values with

HEMA/GDMA system whereas 1a had a lower value. Actually, the lower reactivity of 1a can be explained by low solubility of this monomer in HEMA/GDMA system. Incorporation of phosphonic acid monomers into HEMA/GDMA mixtures slightly lowered the conversions by increasing intermolecular interactions. Also, improvement of t_{\max} values by the addition of phosphonic acid monomers can be clearly seen.

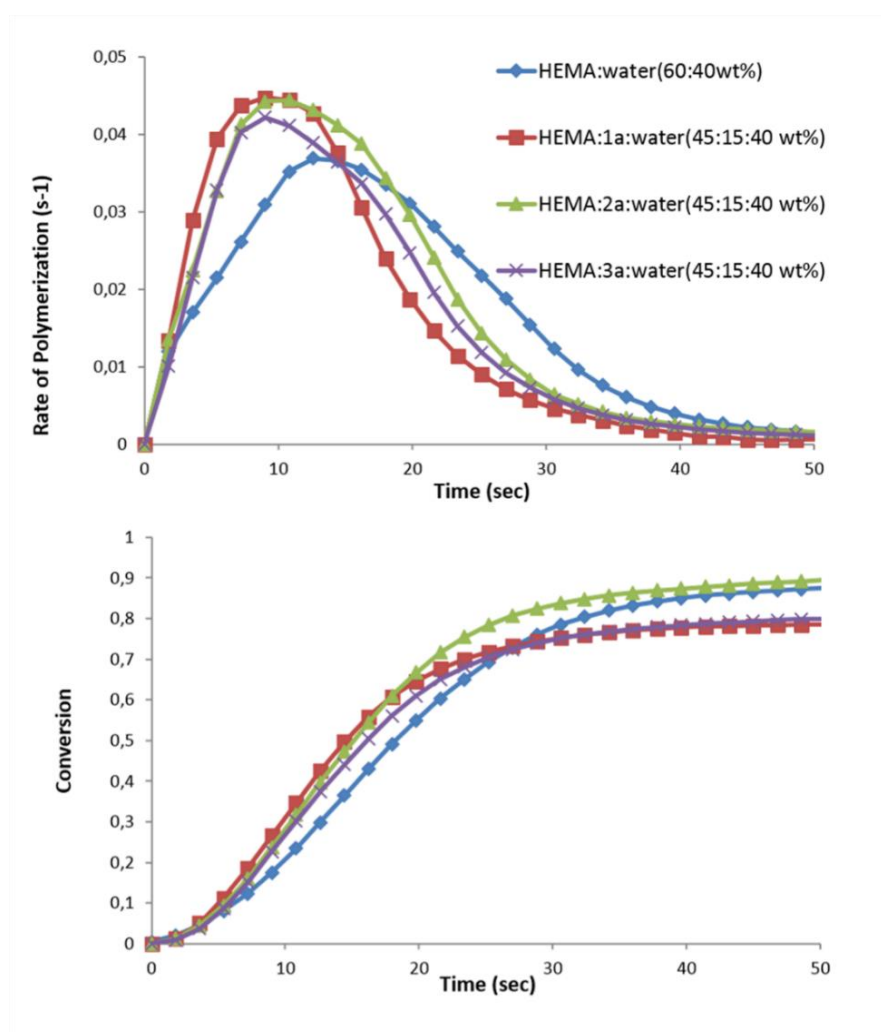


Figure 5.9. Rate-time and conversion-time plots for copolymerizations of 1a, 2a, and 3a with HEMA at 40 °C using BAPO.

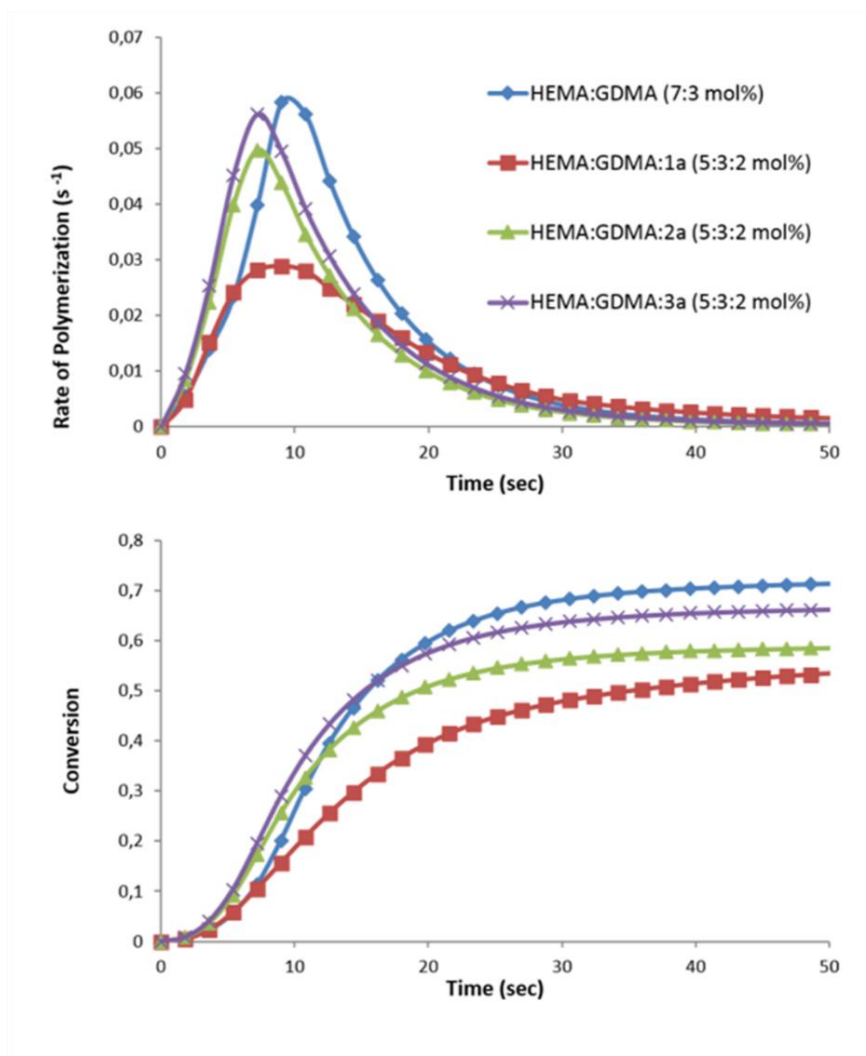


Figure 5.10. Rate-time and conversion-time plots for copolymerizations of 1a, 2a, and 3a with GDMA and HEMA at 40 °C using DMPA.

5.3.4. Synthesis, Characterization and Mineralization of Hydrogels

After evaluating the potential of monomers 1a-3a to be used in self-etching dental adhesives, we proposed that these monomers with calcium affinity may also be used for fabrication of scaffolds with mineralization capability. In this context, we synthesized hydrogel scaffolds H1a, H2a, and H3a by copolymerizing HEMA and PEGDA with phosphonic acid monomers 1a, 2a, and 3a respectively (Table 5.2). A blank hydrogel H0 that does not contain phosphonic acid monomer was also prepared for comparison. HEMA

and PEGDA were chosen for their well-known biocompatibility whereas phosphonic acid-containing monomers were incorporated into the scaffolds to serve as nucleating sites for mineralization.

Table 5.2. Properties of Hydrogels.

Hydrogel	HEMA (wt %)	PEGDA (wt %)	Phosphonic acid monomer (wt %)	Gel Content %
H0	65	35	-	91
H1a	50	35	15	82
H2a	50	35	15	83
H3a	50	35	15	87

The ratio of monomers in the hydrogels was chosen to obtain rigid hydrogels with high crosslink density to be used for hard tissue applications. The highly crosslinked and less flexible nature of the hydrogels resulted in degree of swelling values in the range 49% - 70% (Figure 5.11). Swelling profiles show that the water uptake was enhanced by incorporation of phosphonic acid monomer and the structure of the monomer also influenced the swelling behaviour. As an expected trend, as the hydrophobicity of the monomer increased, the degree of swelling decreased. The hydrogel containing the more hydrophilic monomer H1a had the highest degree of swelling (70%), followed by H2a (64%) and H3a (55%).

Percent viability results demonstrated that the cell proliferation was influenced by alteration of hydrogel composition (Figure 5.12). Fibroblasts seeded on blank hydrogels showed proliferation, as 34% increase in fluorescence was observed on day 4. Cell viability on hydrogel H2a displayed comparable cellular activity with 42% increase during four-day incubation. In contrast, modification of these hydrogels with monomers 1a or 3a provided

unfavorable environment, where 82% and 78% viability were measured for cells on H1a and H3a hydrogels, respectively.

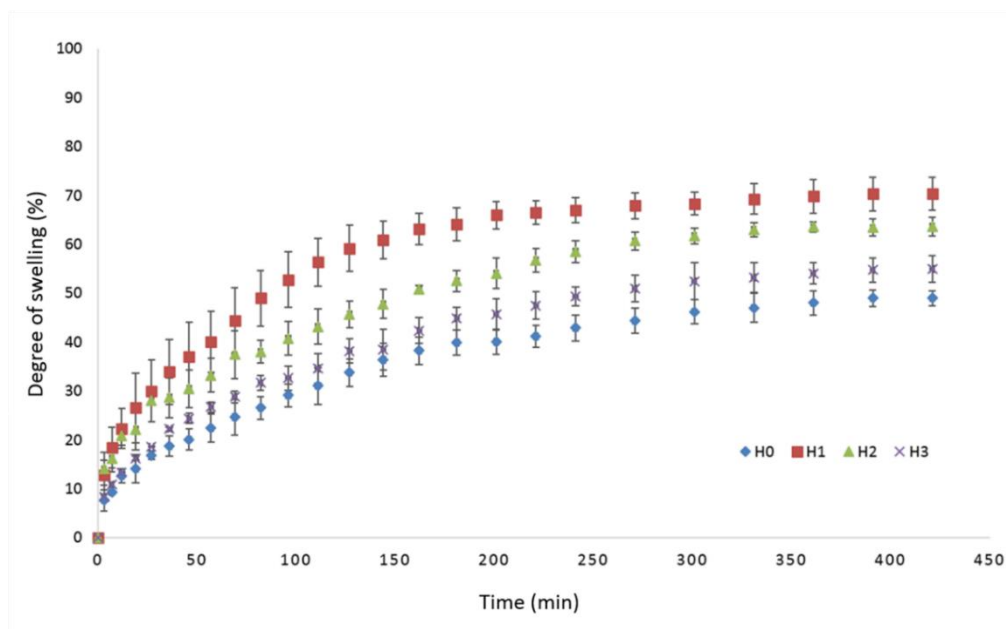


Figure 5.11. Degree of swelling of H0, H1a, H2a, and H3a.

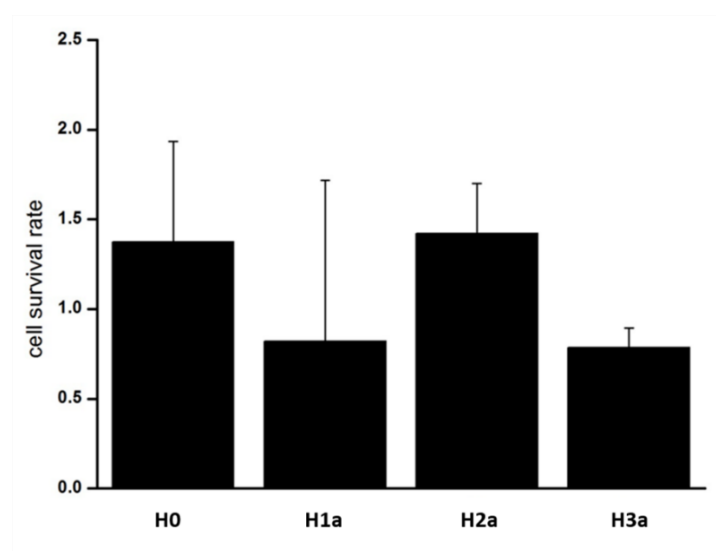


Figure 5.12. Viability of human dermal fibroblasts ($20000/\text{cm}^2$) on hydrogel scaffolds containing Ca^{2+} binding sites.

Simulated body fluid (SBF) mimics the ion concentrations of human blood plasma and is often used for assessing a biomaterials bone-bonding ability based on mineralization upon immersion in it [225]. Since Ca^{2+} and HPO_4^{2-} concentrations are too low in SBF to induce extensive mineralization without plasma proteins, a metastable solution developed by Phadke *et al.* with higher concentrations of Ca^{2+} and HPO_4^{2-} was also used in combination with SBF for mineralization [226].

The ability of the phosphonic-acid containing hydrogel scaffolds to mineralize was evaluated by immersing hydrogel samples in 40 mM Ca^{2+} / 24 mM HPO_4^{2-} solution for 30 minutes followed by immersion in SBF for 24 h. White mineral deposits were observed visually on hydrogel samples after mineralization. SEM micrographs were used to demonstrate the morphological properties of hydrogels before and after mineralization (Figure 5.13).

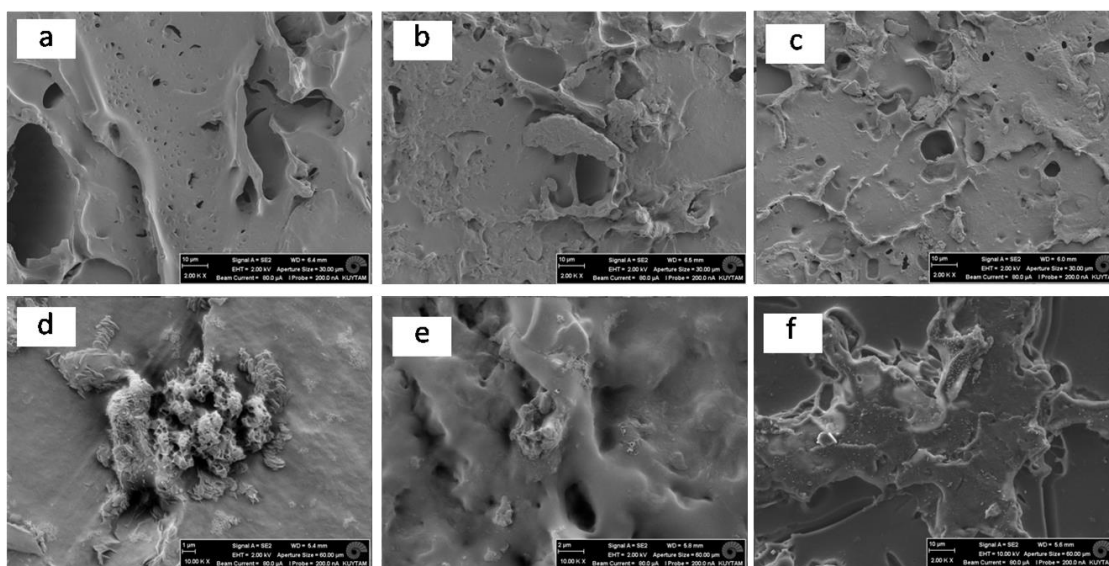


Figure 5.13. SEM images of hydrogels (a) H1a, (b) H2a, (c) H3a, (d) mineralized H1a, (e) mineralized H2a, (f) mineralized H3a.

Before mineralization the hydrogel scaffolds showed porous structure. Mineral deposits were observed on the surface of scaffolds in SEM micrographs obtained after mineralization. The typical cauliflower-like morphology of the apatite layer was not observed, but mineral clusters with irregular shapes were formed instead. The presence of calcium in mineralized hydrogel samples was verified by EDX but the Ca/P ratio was not taken into consideration because the hydrogels already contain phosphorus in their structure.

Besides qualitative analysis by SEM and EDX, a quantitative analysis of mineralization was performed by measuring the Ca^{2+} content (Figure 5.14). The measurement of Ca^{2+} content was conducted with the aim of gaining insight into the influence of monomer structure (based on different alkyl groups) on mineralization. Hydrogel scaffold H0 which lacks phosphonic acid monomer was also examined for mineralization. H0 did not contain any Ca^{2+} at all, indicating that mineralization is likely to be induced by phosphonic acid monomers. H2a (3.2 $\mu\text{g}/\text{mg}$ dry gel weight) exhibited the highest Ca^{2+} content followed by H3a (2.3 $\mu\text{g}/\text{mg}$ dry gel weight) and H1a (1.9 $\mu\text{g}/\text{mg}$ dry gel weight).

It is possible that H2a has an optimal balance between hydrophobic and hydrophilic groups which enhances its ability to induce mineralization. Indeed, two previous studies demonstrated that hydrophobicity of the matrix has a considerable influence on mineralization [226, 227].

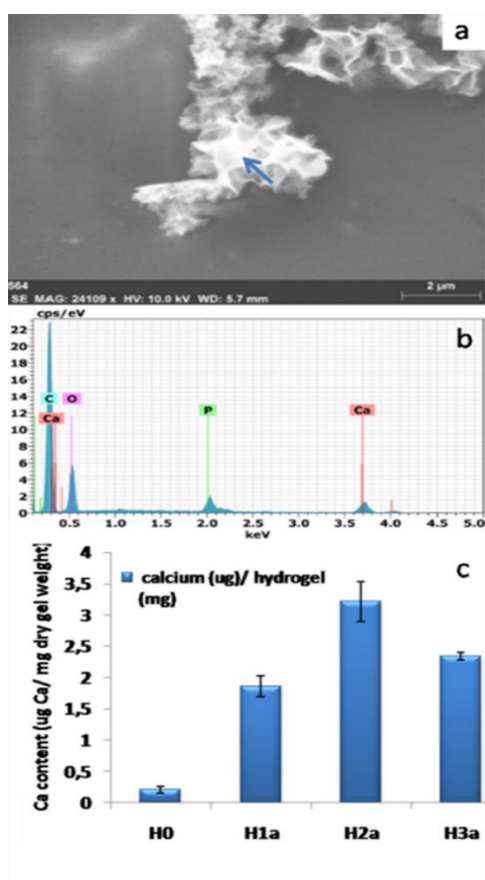


Figure 5.14. (a)SEM image of mineralized H1a for EDX, (b) representative EDX spectra of H1a, (c) Ca deposition assay measured as the total Ca^{2+} content in the mineralized hydrogels and expressed as μg of Ca/mg of dry gel weight.

5.4 Conclusions

We have reported the synthesis, characterization, and polymerization of three novel acrylamide monomers which contain Ca^{2+} binding phosphonic acid groups. These monomers were evaluated for their potential use in self-etching dental adhesives. They were found to be hydrolytically stable, and their interactions with hydroxyapatite was shown by FTIR and XRD. Photopolymerization studies performed by photo-DSC verified their reactivity. In order to investigate the use of these monomers for tissue engineering applications, they were incorporated into hydrogel scaffolds. Mineralization of the hydrogels

were performed upon immersion in SBF. Mineral deposits were observed in SEM micrographs and EDX was used to show that these minerals contain Ca and P. Ca deposition assay was performed for the quantitative detection of Ca in mineralized scaffolds. These results imply that the phosphonic acid containing monomers are good candidates to be used for both dental and tissue engineering applications.

6. STIMULI RESPONSIVE HYDROGELS FROM CARBOXYLIC ACID-FUNCTIONALIZED CROSSLINKERS

This chapter is published as: Bingol H. B., S. Agopcan Cinar, T. Bal, D. C. Oran, N. Kayaman Apohan, S. Kizilel, D. Avci, “Stimuli-responsive hydrogels from carboxylic acid-functionalized crosslinkers”, *J. Biomed. Res. A*, 2019, (doi:10.1002/jbm.a.36714).

6.1. Introduction

Hydrogels have been the subject of intensive research in a variety of biomedical applications such as delivery of theranostic agents, tissue engineering and regenerative medicine. Poly(hydroxyethyl methacrylate) (PHEMA) exhibits low interfacial free energy in contact with body fluids thanks to its hydrophilic surface formed by high density of hydroxyl groups. This restricts the adhesion of proteins and cells to its surface. Despite these relevant properties for biological applications, the usage of PHEMA for delivery of therapeutic agents is limited due to its stability under physiological conditions unless a degradable cross-linker is incorporated within the structure. Introducing a redox-responsive disulfide cross-linker into the hydrogel structure enables controllable on-demand degradation upon exposure to reducing agents such as dithiothreitol (DTT), L-cysteine and glutathione through thiol-disulfide exchange reactions. Indeed, disulfide cross-linked PHEMA hydrogels with tunable degradation and release kinetics under reducing conditions were reported recently [48, 49, 228]. Acid-functionalized polymers and hydrogels have been used in numerous fields ranging from drug delivery and biotechnology to environmental and dental applications. Carboxylic acid groups have been incorporated into hydrogels, thus giving them capability of self-healing which is mediated by hydrogen bonding [229]. Acid-functional hydrogels are particularly useful in environmental applications due to their ability to chelate various metal ions [230-233]. They are widely exploited for biomedical applications including tissue engineering and delivery of therapeutic agents [40-43, 234-239]. Self-etch dental adhesives containing acid groups play an essential role in formation of bonds between the polymer based restorative material and dental tissues [240]. Negatively

ionizable acid groups are believed to facilitate the binding of Ca^{2+} ions and to trigger mineralization. Several studies have demonstrated that it is possible to mimic the process of bone formation by designing synthetic hydrogels decorated with carboxylate groups [162, 225, 226, 241-243].

Commonly, the acid functionality is incorporated into the polymers either by copolymerization with acrylic/methacrylic acid or by exploiting biopolymers containing acid moieties. Herein we describe the synthesis of a novel carboxylic acid-containing difunctional dimethacrylate by using disulfide group as the spacer segment to impart redox response. The synthesized acid functional crosslinker was then characterized and its structure-reactivity relationship was investigated by photopolymerization studies. It was used for fabrication of HEMA based hydrogels with redox and pH sensitivity. Physical properties of hydrogels were characterized by SEM, swelling and rheology studies. The redox-responsive behaviour was demonstrated by degradation of the hydrogel upon exposure to DTT. R6G dye and the drug resorcinol were used as model compounds to demonstrate the redox and pH responsive release behaviour. R6G dye being a positively charged molecule was selected to demonstrate the effect of pH dependent electrostatic interactions between the hydrogel network and dye molecule on release kinetics. Resorcinol being a neutral molecule was used to demonstrate the redox dependent release *via* exposure to DTT. Finally, the toxicity of hydrogels were evaluated against human umbilical vein endothelial cells (HUVECs).

6.2. Experimental

6.2.1. Materials and Methods

tert-Butyl α -bromomethacrylate (TBBr) was synthesized according to the literature procedures [244]. 2-hydroxyethyl disulfide, triethyl amine (TEA), trifluoroacetic acid (TFA), HEMA, poly(ethylene glycol) diacrylate (PEGDA) ($M_n = 575$ Da), 2,2-dimethoxy-

2-phenylacetophenone (DMPA), 2-hydroxy-1-[4-(2-hydroxyethoxy) phenyl]-2-methyl-1-propanone (Irgacure 2959), phenylbis(2,4,6-trimethylbenzoyl)phosphine oxide (BAPO), Rhodamine 6G, resorcinol, DTT and all other reagents and solvents were obtained from Sigma-Aldrich and used without further purification.

CombiFlash Companion flash chromatography system (Teledyne-Isco; Lincoln, NE, USA) with C18 reversed-phase RediSep columns were used for purification of crosslinkers. The chemical structures of crosslinkers were confirmed by ^1H NMR, ^{13}C NMR (Varian Gemini 400 MHz) and FTIR (Thermo Scientific Nicolet 380) spectroscopies. Photopolymerizations were performed on a Discovery DSC 250 (TA Instruments). Degradation studies were carried out at 37 °C using a VWR Incubating Mini Shaker operating at 200 rpm. Rheology experiments were carried out using TA Instruments AR/DHR series rheometer (New Castle, DE, USA) with UV light attachment. Raman spectra were recorded by Perkin Elmer Raman Station 400F. Internal fracture surfaces of lyophilized hydrogels were examined using SEM (FEI-Philips XL30) under an accelerating voltage of 7.0 kV after sputter-coating with a platinum layer. During release studies, the dye concentrations were measured by UV/vis spectrophotometry (Shimadzu, Model UV 1201).

6.2.2. Synthesis of Monomers

6.2.2.1. Monomer 1. TBBr (6 mmol) was added dropwise, under N_2 atmosphere, to 2-hydroxyethyl disulfide (3 mmol) and TEA (12 mmol) in THF (3-4 mL) in an ice bath. The mixture was stirred at 60 °C for 24 h. Then it was diluted with 20 mL of CH_2Cl_2 and extracted with saturated NaCl solution (3 x 5 mL). The organic phase was dried over anhydrous sodium sulfate, filtered and evaporated under reduced pressure to leave the crude product. The crude product was purified by column chromatography on silica gel using ethyl acetate-hexane as eluent. 1 was obtained as a yellow viscous liquid in 32% yield. ^1H NMR (400 MHz, CDCl_3 , δ): 1.43 (s, 18H, CCH_3), 2.80, 2.86 (t, $^3J_{\text{HH}} = 6.2$ Hz, 4H, CH_2S), 3.69, 3.82 (t, $^3J_{\text{HH}} = 6.2$ Hz, 4H, $\text{CH}_2\text{CH}_2\text{O}$), 4.12 (s, 4H, $\text{OCH}_2\text{C}=\text{CH}_2$), 5.74, 6.14 (s, 4H, $\text{CH}_2=\text{C}$) ppm.

^{13}C NMR (100 MHz, CDCl_3 , δ): 28.05 [$\text{C}(\text{CH}_3)_3$], 38.60, 41.35 (S- CH_2), 60.28 ($\text{OCH}_2\text{C}=\text{CH}_2$), 69.02, 69.27 (S- CH_2CH_2), 81.07 [$\text{C}(\text{CH}_3)_3$], 125.07 ($\text{CH}_2=\text{C}$), 138.42 ($\text{CH}_2=\text{C}$), 165.10 (O=C) ppm. FTIR (ATR): 2973, 2928 (C-H), 1706 (C=O), 1638 (C=C), 1099 (C-O-C) cm^{-1} .

6.2.2.2. Monomer 1a. TFA (14 mmol) was added dropwise to 1 (2 mmol) in an ice bath and under N_2 atmosphere. The mixture was stirred at room temperature for 24 h, then excess TFA was removed. The residue was purified on a flash column using water/acetonitrile solvent pair (0.1% TFA is routinely added) as eluent. 1a was obtained as white powdered solid (mp = 79.5 $^\circ\text{C}$) in 87 % yield. ^1H NMR (400 MHz, D_2O , δ): 2.84 (t, $^3J_{\text{HH}} = 5.8$ Hz, 4H, CH_2S), 3.76 (t, $^3J_{\text{HH}} = 5.8$ Hz, 4H, $\text{CH}_2\text{CH}_2\text{O}$), 4.19 (s, 4H, $\text{OCH}_2\text{C}=\text{CH}_2$), 5.88, 6.28 (s, 4H, $\text{CH}_2=\text{C}$) ppm. ^{13}C NMR (100 MHz, MeOD, δ): 39.59 (S- CH_2), 70.01 ($\text{OCH}_2\text{C}=\text{CH}_2$), 70.17 (S- CH_2CH_2), 126.63 ($\text{CH}_2=\text{C}$), 139.14 ($\text{CH}_2=\text{C}$), 169.01 (O=C) ppm. FTIR (ATR): 2921, 2869 (C-H), 1696 (C=O), 1632 (C=C), 1110 (C-O-C) cm^{-1} .

6.2.3. Titration Studies

50 mg of crosslinker 1a was dissolved in deionized water with a concentration of 1.0 mg mL^{-1} and titrated with 0.1M NaOH aqueous solution with increments of 50-100 μL . The increase in pH during titration was recorded with a pH meter (WTW Inolab pH 720) at room temperature.

6.2.4. Photopolymerization Studies

Photopolymerizations were conducted on a DSC equipped with a UV-Vis light (320-500 nm) source, Omnicure 2000 with dual-quartz light guide. The sample mass in the aluminium pans was 3 ± 0.5 mg. Formulations containing 1.0 mol% initiator were irradiated for 10 min with an incident light intensity of 20 mW cm^{-2} under nitrogen flow of 50 mL min^{-1} and in isothermal mode at 37 $^\circ\text{C}$ or 60, 80, 100 $^\circ\text{C}$. The heat flow of the polymerization

reaction was recorded as a function of time. All measurements were performed in duplicate. Total double bond conversions (DBC) was calculated by equation 6.1

$$DBC = \frac{\Delta H_p}{\Delta H_{op}} \quad (6.1)$$

where ΔH_p is the overall heat evolved and ΔH_{op} is the theoretical heat obtained for 100% conversion [224]. Polymerization rates (s^{-1}) were calculated by equation 6.2

$$Rate = \frac{(Q/s)M}{n(\Delta H_{op})m} \quad (6.2)$$

where Q/S is the heat flow per second, M (322 g/mol) is the molar mass of the monomer, n (2) is the number of double bonds per monomer molecule, ΔH_{op} (13.1 kcal/mol for methacrylate double bonds) is the heat released per mole of double bonds reacted, and m (3 ± 0.5 mg) is the mass of monomer in the sample.

6.2.5. Synthesis of Hydrogels

Hydrogels with different formulations were prepared by free radical photopolymerization technique. Monomer 1a (10, 30 or 50 wt %) and HEMA (90, 70, or 50 wt %) were added into distilled water (300 wt% of total monomers) to form precursor solutions of H1a hydrogels. Then, Irgacure 2959 (2 wt % relative to the total monomer mass) was added into these mixtures. The solutions were then poured into glass molds and subjected to UV light (365 nm) at room temperature for 30 minutes. The hydrogel samples (diameter: 1 cm, thickness: 0.2 cm) were dried and weighed (W_1). Then the hydrogels were immersed in ethanol and subsequently in ultrapure water for 24 h each, in order to achieve complete removal of unreacted monomers. The samples were dried and weighed again (W_2).

The percent gelation of hydrogel samples were calculated by equation (3.1). The hydrogels synthesized were designated as H1a-x% (x denote the weight fraction of crosslinker).

6.2.6. Rheology Studies

The synthesis of gels were carried out using a TA Instruments AR/DHR series rheometer (New Castle, DE) with UV light attachment. The crosslinked gels were synthesized in the shape of a disk over a quartz sensor surface covered with a rotating plate with a diameter of 2 cm, and a fixed gap size of 600 μm . Storage modulus (G'), describing the elastic component, and loss modulus (G''), describing the viscous components of the system were monitored during gelation. The 'gelation time' (tg) for the polymer was noted as the time when G' exceeded G'' [245].

For each set of samples, a prepolymer solution was conditioned for 60 s at a shear rate of 100 s^{-1} with the temperature of the system set to $25 \text{ }^\circ\text{C}$. The system was then exposed to UV light at 365 nm, with a flux of 20 mW/cm^{-2} for 1a/HEMA sample under 1% strain, at a frequency of 10 Hz for 2400 s. These sample was obtained with a prepolymer solution containing monomer 1a (10 wt %), HEMA (90 wt %) and Irgacure 2959 (2 wt%) dissolved in water (300 wt%).

6.2.7. Swelling Studies

Swelling properties were studied by immersing dry hydrogel samples into phosphate-buffered salines (PBS) of varying pH values (5.5, 7.4 and 9.0), water or CaCl_2 (2.5m M, 0.1M or 1M) at $37 \text{ }^\circ\text{C}$. The gels were taken out of the solution at predetermined time intervals, blotted carefully with filter paper to remove the surface-adhered solution and weighed. The increase in the weight of hydrogel sample was recorded as a function of time until equilibrium was reached. The degree of swelling (D_s) was calculated by equation (4.2).

Swelling experiments with hydrogels after reaction (at relaxed state) were performed in PBS at pH 7.4 and 37 °C to find volumetric swelling ratios which were calculated from mass swelling ratios by using polymer and solvent densities. The molecular weight between cross-links (M_c) was calculated using Peppas's equation (6.3) for hydrogels prepared in the presence of a solvent [246]:

$$\frac{1}{M_c} = \frac{2}{M_n} - \frac{\bar{v}}{V_1} \frac{[\ln(1-v_{2,s}) + v_{2,s} + \chi v_{2,s}^2]}{v_{2,r} \left[\left(\frac{v_{2,s}}{v_{2,r}} \right)^{\frac{1}{3}} - \left(\frac{v_{2,s}}{2v_{2,r}} \right) \right]} \quad (6.3)$$

where M_n is the chain length of the starting polymer, χ is the polymer–solvent interaction parameter, \bar{v} is the specific volume of PHEMA, $v_{2,r}$ and $v_{2,s}$ are polymer volume fraction of the hydrogels in the relaxed and swollen state, respectively. M_n is assumed to be large enough so that $2/M_n$ may be neglected [247]. M_c values were then used to calculate the mesh size (ξ) of the polymer network by Canal-Peppas equation (6.4) [248]

$$\xi = l \left(2 \frac{M_c}{M_r} \right)^{1/2} C_n^{1/2} v_{2,s}^{-1/3} \quad (6.4)$$

where l is the bond length between C-C bond of polymer backbone (1.54Å), M_r is the molecular weight of HEMA monomer as the repeating unit (130 g/mol), C_n is the Flory characteristic ratio as 6.9.

6.2.8. Degradation of Hydrogels

Fully swollen hydrogels were weighed and immersed in 4 mL PBS containing 25mM and 50 mM DTT or PBS as control. The degradation studies were implemented under physiological conditions at 37 °C with mixing at 200 rpm. At predetermined time intervals the hydrogels were removed from solution, blotted, and weighed. The degradation media was refreshed at each time point. Relative mass of hydrogel (the ratio of the mass of

degrading hydrogel at each time point and its mass at equilibrium swelling prior to degradation) was plotted as a function of time [249].

6.2.9. Dye Loading and Release Studies of H3a Hydrogels

Rhodamine 6G (R6G) and resorcinol were selected as a model compounds to demonstrate the loading and release profile of H1a hydrogels. Calibration curves were prepared from UV-Vis spectra of solutions containing different amount of R6G or resorcinol. Approximately a 50 mg dry hydrogel sample was immersed in an aqueous R6G or resorcinol solution (1 mg/mL) at 37 °C for 24 h. The solution was kept in an orbital shaker at 200 rpm to facilitate the diffusion of the dye/drug into the hydrogel. The dye/drug loaded hydrogels were washed with water to get rid of excess dye/drug on surface before release studies. The amount of loaded dye/drug was calculated by analyzing the concentration of the dye/drug left in the loading and washing solution using UV-vis spectroscopy.

The dye loaded hydrogels were kept in DTT solution (25 mM or 50 mM) or PBS (pH 2.0, 5.5 and 7.4) at 37 °C at a shaking speed of 200 rpm. At predetermined time intervals solution medium was removed and analyzed by UV-vis spectroscopy ($\lambda_{\text{max}} = 527$ nm for R6G, $\lambda_{\text{max}} = 266$ nm for resorcinol). The calibration curve was used to quantify the release of dye.

6.2.10. Cell Viability on Hydrogels

Human Umbilical Vein Endothelial Cells (HUVECs) were maintained in RPMI-1640 Medium (ATCC, 30-2001) supplemented with 10 % (v/v) fetal bovine serum (FBS) (Gibco, 10500-064) and 1 (v/v) % Penicillin Streptomycin (Sigma, P4333), and incubated at 37 °C in a humidified CO₂ (5% v/v) incubator. After HUVECs reach 80–90% confluence, cells were passaged with 0.25% trypsin-EDTA (Sigma, T4049) and used for viability assay. Hydrogels were sterilized under ultraviolet light for approximately 3 hours and then swollen

in growth medium overnight. Diameters of swollen hydrogels were measured by ruler and then area of each hydrogel was calculated. HUVECs were seeded with concentration of 16000 HUVECs per cm^2 in each well of 24 well plate containing hydrogels. As a control, HUVECs with same concentration for each type of hydrogels were seeded in 24 well plate without hydrogels. Viability of cells was analyzed with cell titer glo (Promega, G7572) on day 1 and day 4. Briefly, medium was aspirated and 500 μl fresh growth medium was added on each well. Then, 50 μl of cell titer glo reagent was added to each well and incubated on shaker with 200 rpm at room temperature for 15 min. After that, supernatants were collected, and then luminescence was measured with a microplate reader (Synergy H1 Hybrid Multi-Mode Microplate Reader; Bio-Tek). Survival rate of cells seeded with hydrogels was normalized to control for both day. Then, proliferation rate of cells was calculated as a ratio of cell survival rate on day 4 to day 1.

6.3. Results and Discussion

6.3.1. Synthesis and Characterization of Monomers

The novel acid-functional crosslinker was synthesized using nucleophilic substitution reaction of a diol, namely 2-hydroxyethyl disulfide, with TBBr under basic conditions followed by cleavage of *tert*-butyl groups by TFA (Figure 6.1). Monomer 1a was a solid and was easily purified by flash column chromatography giving typical yields of about 80%. 1a was soluble in water (Table 6.1).

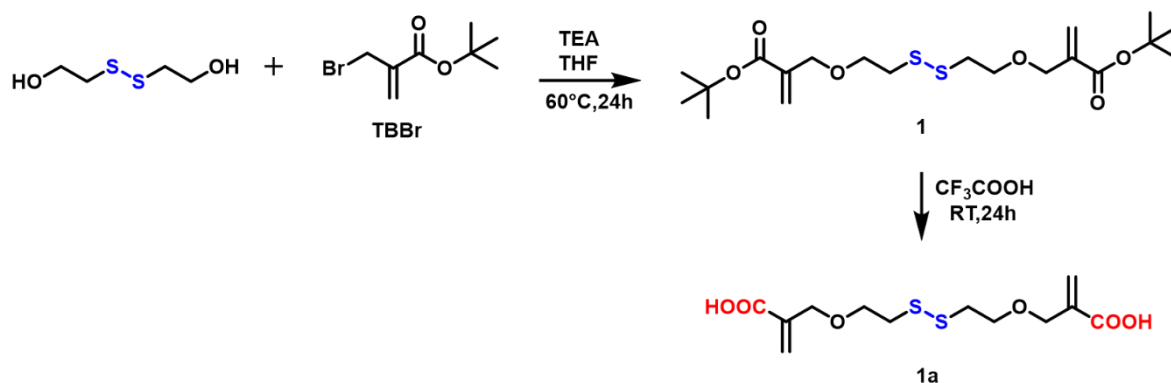
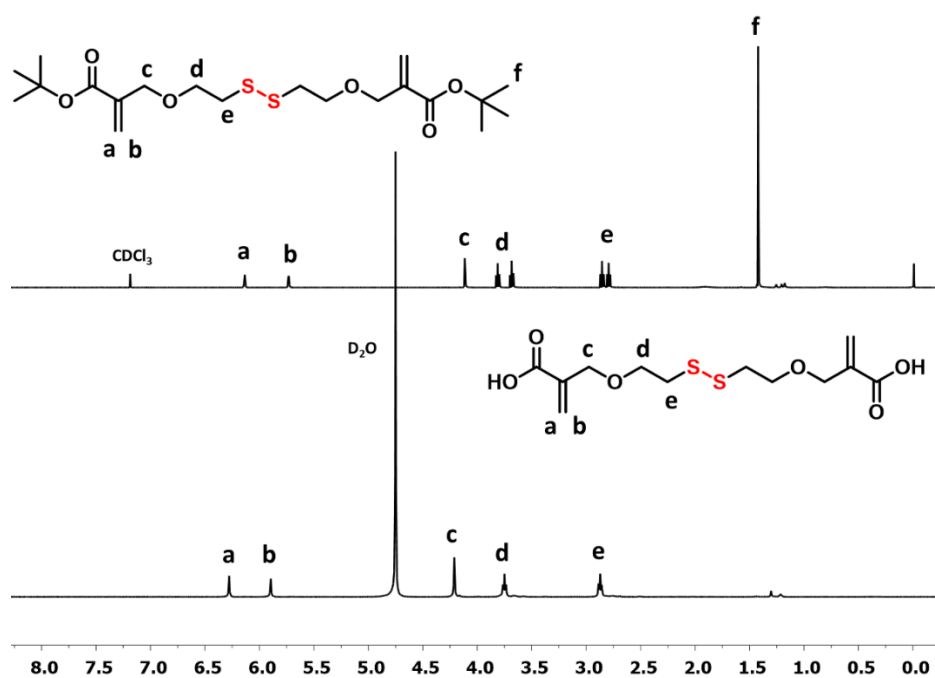
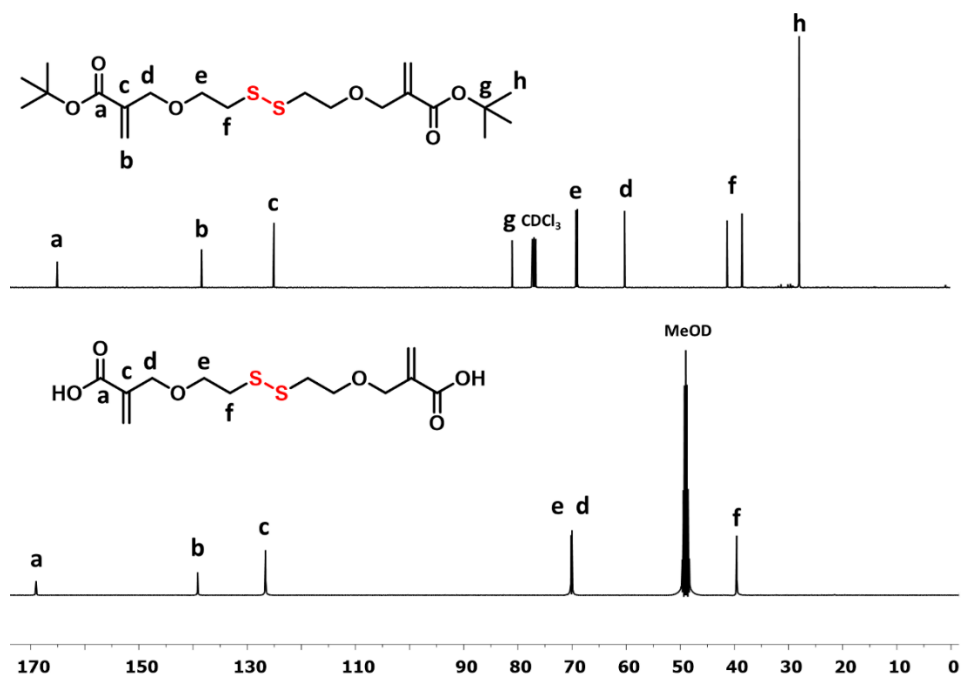


Figure 6.1. Synthesis of monomers.

Table 6.1. Solubility of monomers.

Monomer	H ₂ O	EtOH	THF	Acetone	Et ₂ O	CH ₂ Cl ₂
1	-	+	+	+	+	+
1a	+	+	+	+	-	+/-

The structures of monomers were confirmed by ¹H, ¹³C NMR, and FTIR spectroscopies. The protons of methylene units next to the disulfide bond in **1** are diastereotopic and each appear as two triplets at 2.80, 2.86 and 3.69, 3.82 ppm in the ¹H NMR spectrum (Figure 6.2). This is a result of the bulky *tert*-butyl group which restricts the rotation of the molecule. After removal of this bulky group free rotation is possible, thus the protons became homotopic and ¹H NMR spectrum of **1a** showed only two triplets at 2.84 and 3.76 ppm. A similar trend is also present in the ¹³C NMR spectra of **1** and **1a**, indicating methylene units next to the disulfide as a doublet at approximately 40 ppm (Figure 6.3).

Figure 6.2. ^1H NMR spectra of 1 and 1a.Figure 6.3. ^{13}C NMR spectra of 1 and 1a.

The FTIR spectra of 1a showed broad OH stretching peak at approximately 3500–3000 cm^{-1} . Two C=O stretching peaks, at around 1780 and 1700 cm^{-1} , are characteristic of carboxylic acid dimers (Fig. 6.4). Titration studies were carried out in order to determine the pKa values of carboxylic acid-functionalized crosslinkers. The pKa value was found to be 3.89 for 1a (Figure 6.5).

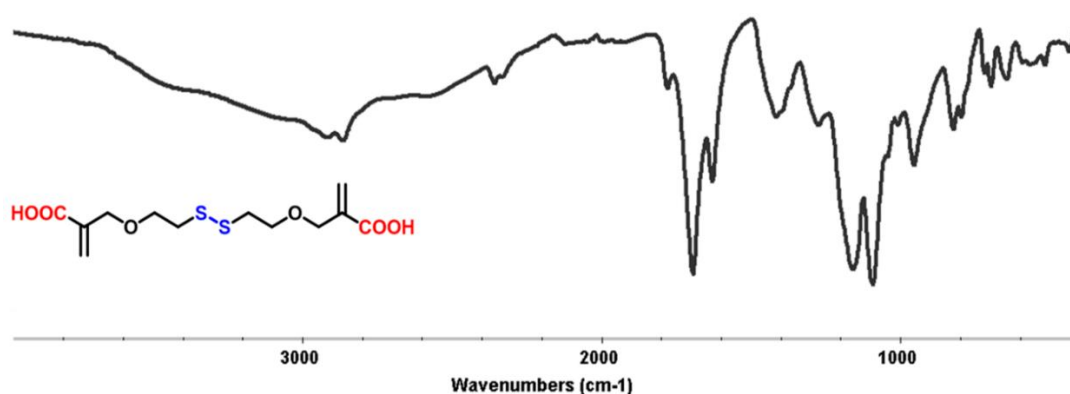


Figure 6.4. FT-IR spectra of 1a.

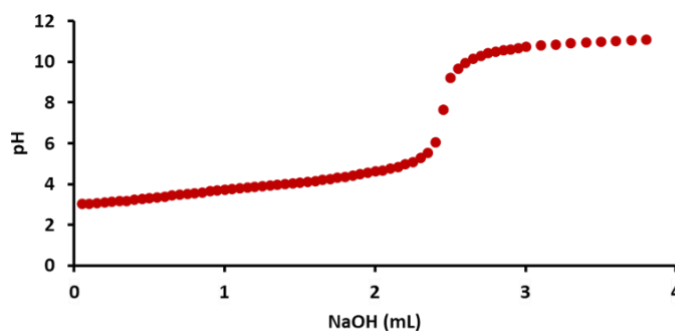


Figure 6.5. Titration curve of 1a.

6.3.2. Photopolymerizations

The photoreactivity for the synthesized crosslinker 1a was analyzed during its copolymerizations with HEMA using photo-DSC. Formulations containing 10 mol% of 1a

in HEMA were polymerized with DMPA (1 mol%) as photoinitiator. DBC, polymerization rate R_p and the time to reach the maximum of the polymerization exotherm (t_{max}) are shown in Figure 6.6. Incorporation of acid-functional crosslinkers by 10 mol% into HEMA reduced t_{max} . The t_{max} value 1a-containing formulations was 11.4 s, and hence lower than HEMA (18.6 s) itself. The DBC (81%) was similar to HEMA (85%). The polymerization rate (0.062 s^{-1}) was slightly higher than that of HEMA (0.047 s^{-1}).

The photoreactivity studies showed improved photoreactivity due to autoacceleration upon incorporation of acid-functional crosslinker which is typical for multifunctional monomers. Autoacceleration arises from a decrease in the mobility of polymer radicals in an extremely viscous environment which reduces diffusion controlled termination in these highly crosslinked systems. When termination is inhibited, the radical concentration increases and the polymerization rates are improved. The capability of these crosslinkers to form hydrogen bonds may be another factor for the enhancement of polymerization rate.

Copolymerization kinetics of 1a with HEMA was also investigated for various concentrations/ratios in aqueous environment using the water-soluble photoinitiator BAPO. A slight shift in t_{max} confirms the successful incorporation of 1a, since this behavior is typical to multifunctional monomers. The rate was increased with 5 mol% incorporation of 1a. Although adding more 1a into the formulations decreased the rate, they were still comparable to HEMA. In aqueous polymerization studies, the DBC was observed to be inversely related to percentage of crosslinker. The observed decrease in the double bond conversions is probably because of both the higher crosslinking tendency of these systems with increasing crosslinker ratio and the increase of hydrogen bonding which reduces the flexibility leading to a highly rigid system. These two factors lead to early gelation.

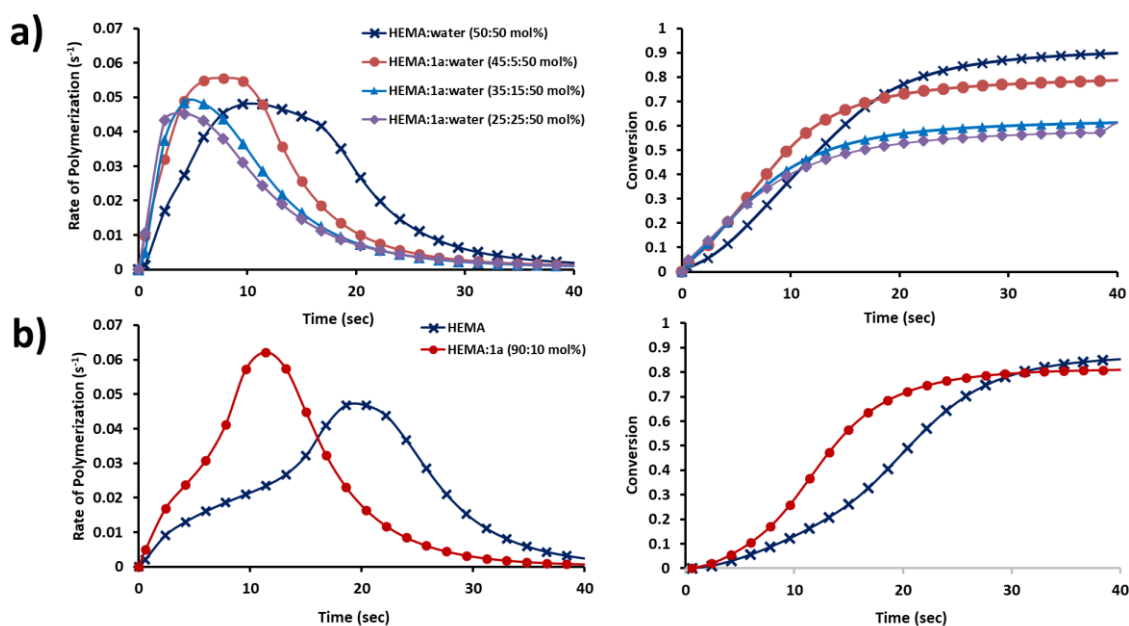


Figure 6.6. Rate-time and conversion-time plots for the copolymerizations of (a) HEMA and 1a under nitrogen at 37 °C using DMPA (1 mol%), (b) HEMA with 1a in water under nitrogen at 37 °C using BAPO (1 mol%).

Monomer 1a was polymerized at different temperatures to observe the effect of hydrogen bonding on polymerization rate. Increasing the temperature from 37 °C to 60 °C slightly increased the rate of polymerization and conversion, however as the temperature was elevated up to 80 °C and 100 °C the rate of polymerization and conversion were reduced dramatically (Figure 6.7). Our results parallel those of Jansen *et al.* and Hoyle and collaborators [250-252]. The former reported that monomers containing functional groups capable of hydrogen bonding polymerize very rapidly at room temperature, and attributed this behaviour to preorganization of monomers to form multimeric aggregates which reduces the termination, thus enhancing polymerization rate. However as the temperature increases, the hydrogen bonds between the monomers undergo dissociation, generally leading to reduction in polymerization rates.

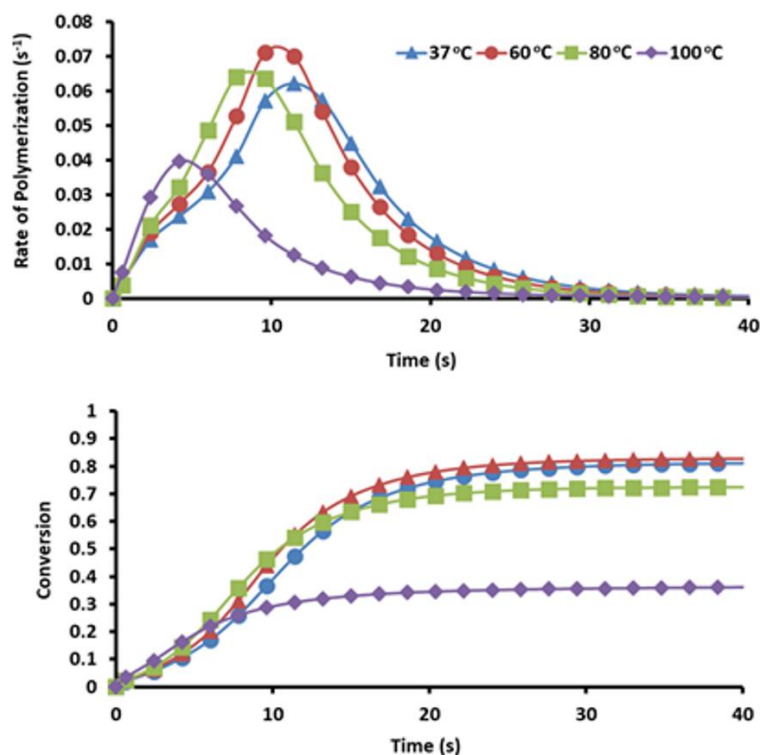


Figure 6.7. Rate-time and conversion-time plots for copolymerizations of 1a with HEMA at 37 °C, 60 °C, 80 °C and 100 °C using DMPA.

6.3.3. Synthesis and Characterization of Hydrogels

Carboxylic acid-functionalized crosslinker 1a was incorporated into HEMA by 10, 30 or 50 wt% to form the hydrogels H1a-10%, H1a-30% and H1a-50% respectively (Figure 6.8). The hydrogels were obtained in moderate to high gelation values between 86% and 89% (Table 6.2). 10 wt% incorporated hydrogels had high gelation values and were stiffer and better-shaped. As crosslinker % increased to 50 wt% the gelation values were reduced, and hydrogels were observed to be sticky and difficult to remove from the mold.

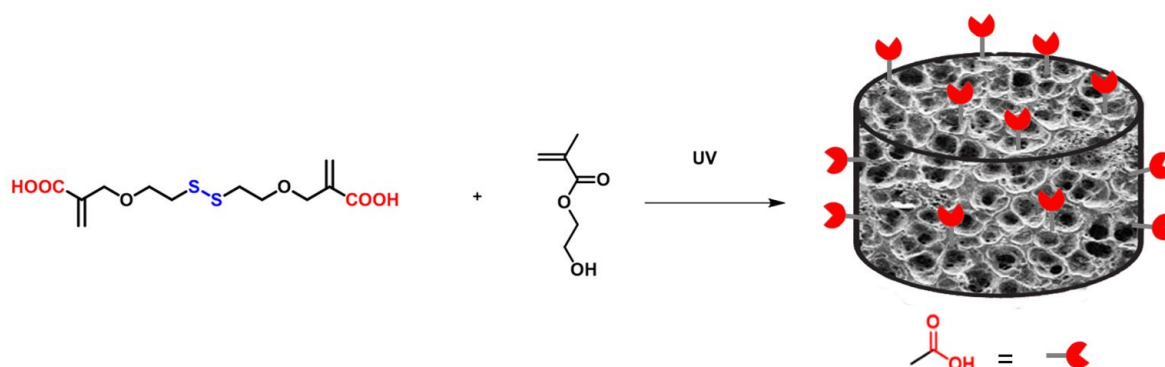


Figure 6.8. Fabrication of acid-functional pHEMA hydrogels

Table 6.2. Properties of Hydrogels

Hydrogel	Crosslinking Monomer Type	Crosslinking Monomer (wt%)	HEMA (wt%)	Gel Content (wt%)
H1a-10%	1a	10	90	88
H1a-30%	1a	30	70	89
H1a-50%	1a	50	50	86

We carried out rheology experiments to characterize mechanical properties using a UV-attached rheometer (Figure 6.9). The storage modulus in viscoelastic materials provides information about the elastic solid-like behavior (G'), and the loss modulus is the viscous response (G''), which is the energy dissipated as heat. As gelation proceeded, the formation of elastic hydrogel due to crosslinking continued, and both moduli increased rapidly. Photopolymerization reactions promoted the formation of a 3D network structure contributing to mechanical properties. This reaction converted prepolymer solution to 3D crosslinked hydrogel networks.

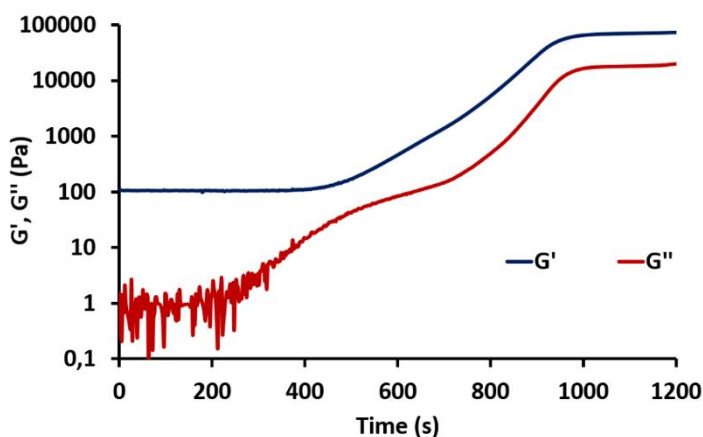


Figure 6.9. Storage and loss moduli of hydrogels versus photopolymerization time for H1a-10%.

The viscous behavior of this gelling system, as was observed through G'' , could be attributed to the non-interacting segments of polymer chains. Continued gelation resulted in the formation of more networks and solid-like behavior dominated the viscoelastic properties of the hydrogels. When crosslinking reactions approached completion, both G' and G'' saturated, suggesting a formation of well-established hydrogel network. During gelation and crosslinking reactions, storage modulus (G') increased significantly, suggesting a decrease in chain mobility. Elastic properties dominated viscous properties where the gel point occurred with a dramatic increase in both G' and G'' around 500 seconds for H1a-10%. Continued UV exposure induced further increases in both elastic (G') and viscous (G'') moduli and reached saturation at around 1200 seconds. The saturation of G' and G'' suggests that crosslinking reactions have approached completion, forming a well-established hydrogel network, where solid-like behavior dominates the viscoelastic properties.

6.3.4. Swelling Studies

The swelling properties of the hydrogels were studied as a function of pH and content of the crosslinker (Figure 6.10). First, the degree of swelling of the hydrogels at pH 5.5, 7.4 and 9.0 at 37 °C was investigated. Figure 6.10a presents the degree of swelling of H1a-10%

hydrogels. It was observed that the degree of swelling is similar at pH 5.5 and 7.4 (406% and 444% respectively), but becomes larger as the pH is increased to 9.0 (594%). In acidic conditions, the hydrogen bonding among the carboxylic acid groups of the hydrogel leads to dense networks, resulting in low degree of swelling. In near-neutral or alkaline conditions, the hydrogen bonds are broken, so negative charges are generated on the carboxylic acid groups. This causes a more hydrophilic network, and both this and the electrostatic repulsion between acid groups contribute to higher water uptake. The comparable swelling of the H2a hydrogels at pH 5.5 and 7.4, can be explained by the pK_a value of the 1a crosslinker being 3.89, indicating that the hydrogels were already in fully ionized form at pH 5.5 and 7.4. However, we are unable to explain the higher swelling at pH 9.

The degree of swelling of the hydrogels decreased with increasing amount of the crosslinkers. For example, the equilibrium degree of swelling of H1a-10%, H1a-30% and H1a-50% hydrogels were found to be 444%, 261% and 153% at pH 7.4. The decrease of the swelling with increasing crosslinker amount can be due to an increase in crosslinking density of the hydrogel and decreasing the pore size. The crosslinkers used in this study are hydrophilic and when their content increases, the hydrophilicity of the hydrogels are also expected to increase. However, the effect of increasing of crosslinker concentration apparently overcomes the extra hydrophilicity brought by the crosslinkers.

Mesh size values, ξ , were obtained as 21Å for H1a-10% and 18Å for H1a-30% respectively, which are similar to ones reported for crosslinked PHEMA hydrogels [246]. H1a hydrogels made with a higher crosslinker ratio of 30% resulted in a higher crosslinking density when compared to ones made with 10% crosslinker as evident from the reduced mesh size.

The ability of carboxylate groups on the hydrogel to chelate Ca^{2+} ions was also investigated by swelling studies. The hydrogels were immersed in 2.5 mM (physiological concentration of Ca^{2+}), 0.1 M or 1 M $CaCl_2$ aqueous solution. Hydrogels immersed in $CaCl_2$ swelled less than ones immersed in pure water. As Ca^{2+} concentration increased, the

hydrogels showed a trend of decrease in swelling values which was most pronounced for the highest CaCl_2 concentration at 1M (Figure 6.10d). The results of the study of the Ca^{2+} chelation ability of carboxylate decorated hydrogels can be explained by interactions between the Ca^{2+} ions in the solution and the carboxylate groups, where Ca^{2+} ions act as physical crosslinking points forming a secondary network based on interactions between the oppositely charged groups [253, 254].

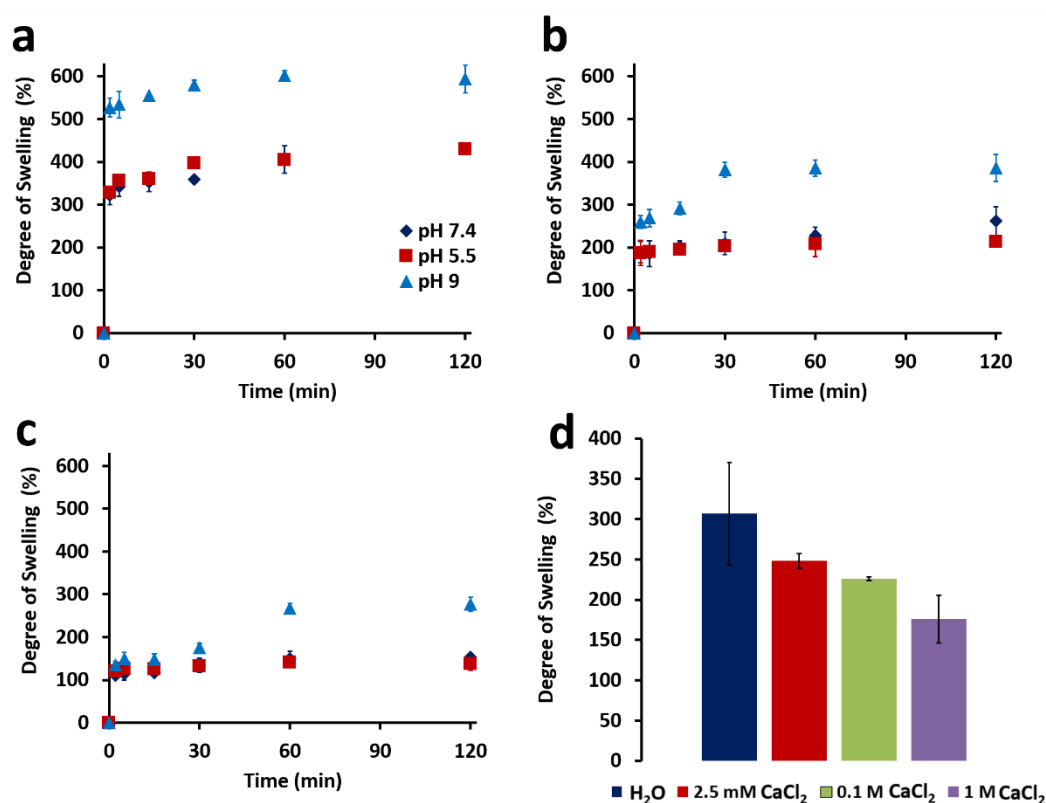


Figure 6.10. Water uptake profile of hydrogels (a) H1a-10%, (b) H1a-30%, (c) H1a-50% in H₂O and (d) H1a-10% in CaCl₂.

6.3.5. Degradation of Hydrogels

Degradation studies were done by incubating H1a-10% in PBS (pH 7.4) containing either 25 mM or 50 mM DTT at 37 °C. The hydrogels initially swelled and gained mass due

to absorption of water. This absorption kept increasing with increased exposure time to DTT. After a point the hydrogels started to lose their shape and finally lost their structural integrity (Figure 6.11). No significant degradation was observed for the hydrogels immersed in PBS as a control. The continuously increasing water absorption and eventual loss of structural integrity of the hydrogel in DTT solution can be explained by water which fills the voids in the network structure formed when the disulfide crosslinks are cleaved. Appearance of a new peak at 2592 cm^{-1} in the Raman spectrum of H1a-10% immersed in DTT confirms the formation of thiol group *via* cleavage of disulfide bonds.

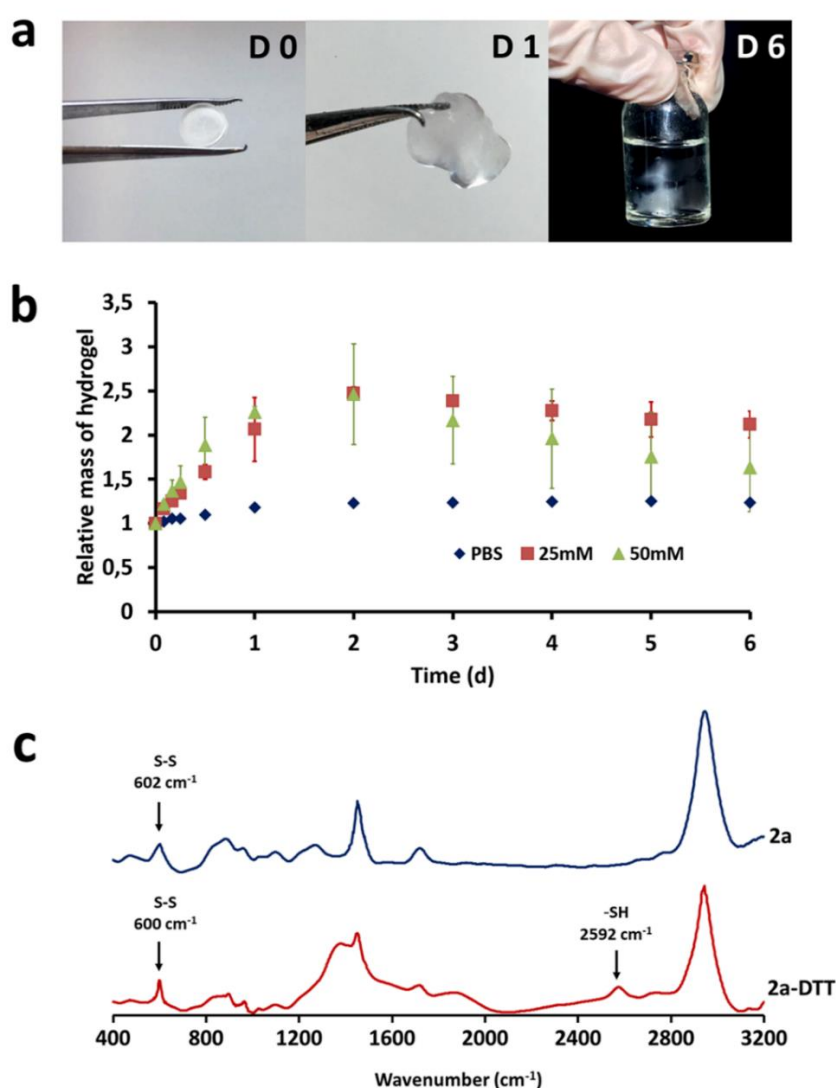


Figure 6.11. (a) Degradation of H1a-10% by 25 mM DTT at days 0, 1 and 6 (b) Relative mass of hydrogel during degradation (c) Raman spectra of H1a-10% before and after degradation with 25 mM DTT.

Morphologies of the hydrogels were investigated by SEM (Fig. 6.12). The network structure was observed to be dependent on crosslinker ratio and incorporation of higher ratios of crosslinker resulted in denser networks. All hydrogels exhibited a homogenous network structure. The change in morphology of H1a-10% and H1a-30% hydrogels exposed to 25 mM DTT can be observed in the SEM images of their internal fracture surface.

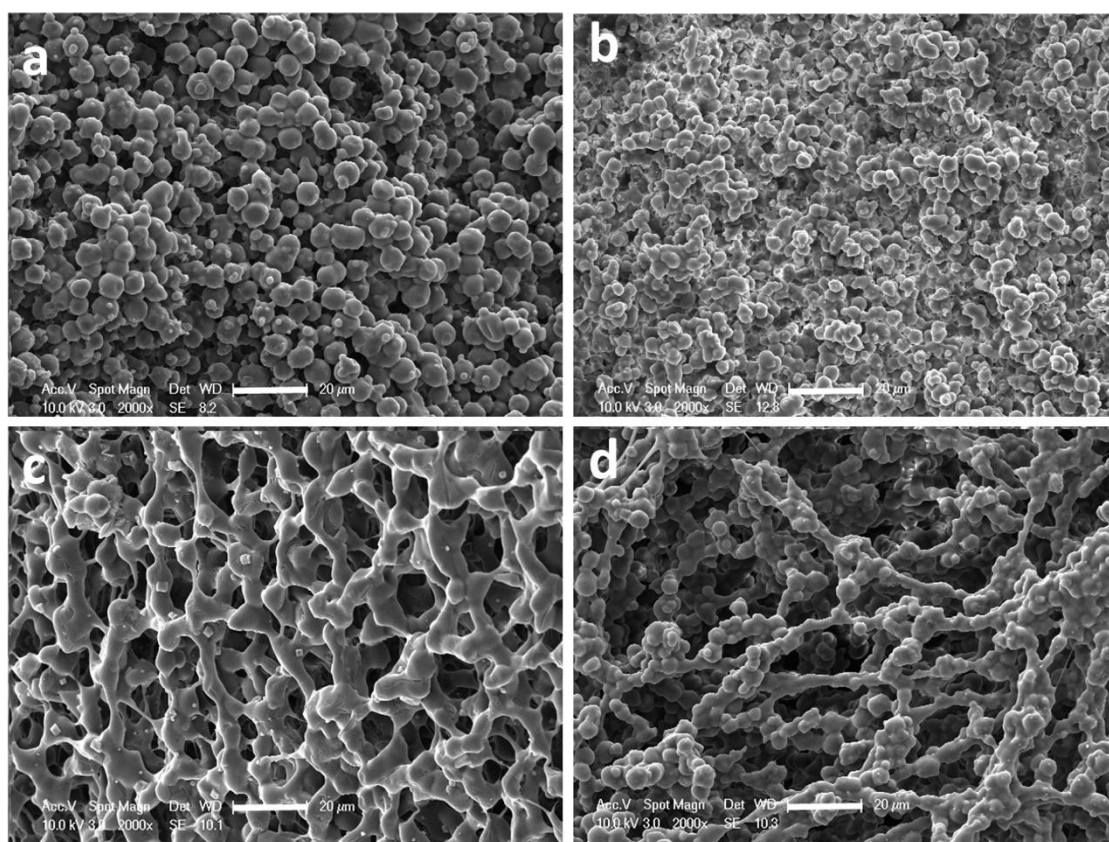


Figure 6.12. SEM micrographs of (a) H1a-10%, (b) H1a-30%, (c) H1a-10% after 24h degradation with 25 mM DTT, (d) H1a-30% after 6h degradation with 25 mM DTT (Scale bar represents 20 μm).

Total degradation of H1a-10% hydrogels in DTT could not be achieved even after one week probably due to interference of the disulfide bond with free radical polymerization resulting in chain transfer reactions which might cause permanent crosslinks within the system [50, 190, 255]. Upon exposure to DTT, the cleavage of disulfide bonds leads to formation of homogeneously distributed pores throughout the structure. H1a-30% hydrogel

which contains a higher percentage of the disulfide crosslinker was more prone to cleavage as evident from the micrographs.

No degradation was observed for both H1a-10% and H1a-30% hydrogels under acidic conditions at pH 2 and pH 5.5 during one week period. H1a-10% and H1a-30% hydrogels did not show any degradation under acidic conditions as expected, since there are no acid labile linkages in the polymer backbone.

6.3.6. Dye Loading and Release Studies

Rhodamine 6G and resorcinol were used as model compounds to demonstrate the trigger responsive release behaviour of H1a hydrogels (Figure 6.13). R6G or resorcinol were loaded into H1a hydrogels by soaking them into a concentrated solution of the dye/drug. The hydrogels swelled in the dye/drug solution and absorbed the molecules. The loading efficiency of R6G into the H1a-10% hydrogel was calculated to be $58\pm 5\%$. Loading efficiency of resorcinol was calculated as $21\pm 3\%$ for H1a-10% and $17\pm 4\%$ for H1a-30% respectively. The loading was observed to reach high percentages for R6G due to electrostatic interactions between the carboxylate groups in the hydrogel and the dye molecules, which facilitate the diffusional post-loading.

Firstly the pH dependent release of R6G from H1a-10% was investigated in PBS at pH 7.4, 5.5 and 2. At pH 7.4, only 1% of the dye was released, however in acidic conditions the released amount of R6G increased to 9% at pH 5.5 and reached 79% at pH 2. During pH dependent release studies, at neutral conditions, the deprotonated carboxylate groups interact with positively charged R6G so strongly that a negligible amount of the dye is released. At slightly acidic conditions some of the carboxylate groups get protonated, and the released amount of R6G is increased. However when the pH is switched to strongly acidic conditions below the pKa, the carboxylates get fully protonated and repel the positively charged R6G molecules within the hydrogel, so R6G slowly diffuses out of the hydrogel at acidic conditions.

The redox dependent release of R6G from H1a-10% was studied by incubating the hydrogels in PBS containing either 25 mM or 50 mM DTT. The release reached only 2% for 25 mM and 4% for 50 mM DTT release media. When immersed into DTT solution to determine the redox dependent release characteristics, R6G hydrogels' water uptake increased due to cleavage of disulfide bonds by thiol exchange reactions due to DTT and the hydrogel was observed to swell. Although the cleavage of some linkages facilitated diffusion based release of R6G dye to a small extent, most of the dye was retained in the hydrogel due to very strong electrostatic interactions. This result indicates that the electrostatic interactions between the carboxylate groups and the positively charged R6G govern the release profile and counteract the diffusion of dye molecules.

Resorcinol was selected to achieve a better demonstration of redox-responsive release from H1a-10% and H1a-30% hydrogels. Resorcinol did not show strong electrostatic interactions with the hydrogels matrix as R6G did, and showed higher percentages of release through diffusion both in PBS (pH 7.4) and DTT solution (25 mM). Resorcinol showed 64% and 68% release at pH 7.4 PBS for H2a-10% and H2a-30% respectively. Under reducing conditions provided by 25 mM DTT, the degradation of the hydrogel matrix increased the release of resorcinol to 88% and 85% for H1a-10% and H1a-30% respectively.

Resorcinol is a smaller molecule than R6G and easily diffuses out of the hydrogel resulting in rapid release. Its diffusion is independent of mesh size in PBS. In the literature it was indicated that when diffusion related release occurs with small molecule drugs, the release is generally completed within a time scale of a few hours to a day [12]. In the presence of DTT, the hydrogel degraded through thiol-exchange mediated cleavage of the disulfide groups, facilitating the release of resorcinol. The initial rate of resorcinol release from H1a-10% was found to be faster compared to H1a-30%. This can be explained by higher mesh size of H1a-10% resulting in easy diffusion of DTT into the interior of the network, hence leading to faster degradation. However, total release of both hydrogels in DTT were found to be similar.

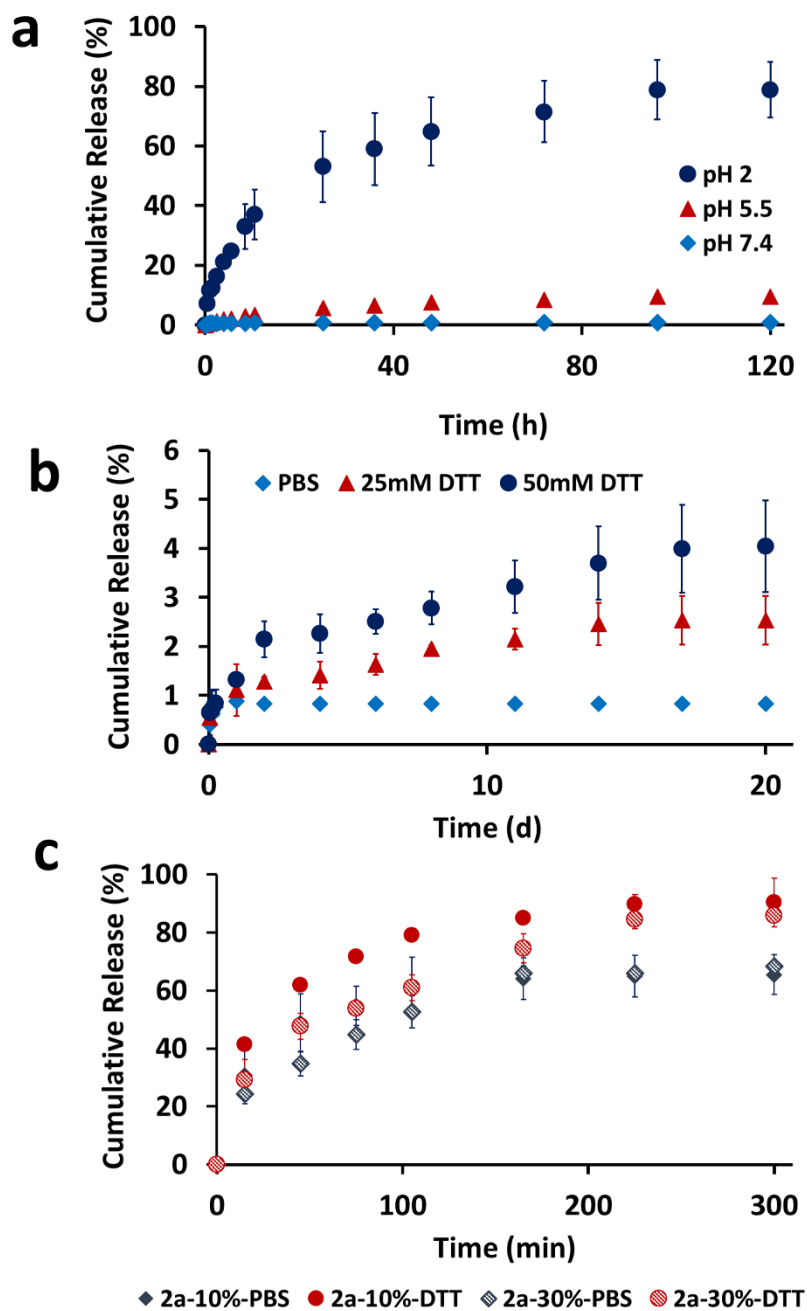


Figure 6.13. (a) pH-sensitive, (b) redox sensitive release kinetics of R6G dye from H1a-10% hydrogel, (c) redox sensitive release kinetics of resorcinol from H1a-10% and H1a-30% hydrogels.

6.3.7. Cell Viability on Hydrogels

HUVECs (human umbilical vein endothelial cells) seeded on H1a-10% showed lower cellular activity when compared to control as can be observed from the decrease in fluorescence on day 4. According to percent viability results, 10% incorporation of acidic crosslinker 1a into HEMA hydrogels result in a moderately favorable environment for HUVECs (Figure 6.14).

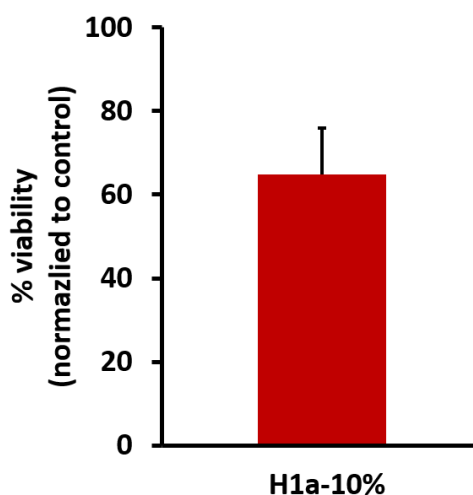


Figure 6.14. Viability of HUVECs on hydrogels.

6.4 Conclusions

We utilized the method of nucleophilic substitution of diols with TBBr followed by cleavage of tert-butyl groups to synthesize a novel disulfide and carboxylic acid-functionalized crosslinker. This synthesis illustrates that using this method, more crosslinkers with versatile structures and properties (for example, hydrophobicity/hydrophilicity) can be obtained starting from various diols. The crosslinker synthesized in this work was used to fabricate HEMA based redox- and pH- responsive hydrogels. En route, structure-reactivity relationship was investigated for copolymerization

with HEMA in bulk and in water using photo-DSC. The morphology of hydrogels was shown by SEM, mechanical properties were investigated by rheology studies. The response of the hydrogels to stimuli such as pH and concentrations of compounds like CaCl_2 or DTT in the solution can be controlled by the crosslinker amount. The pH and redox dependant release were demonstrated by using R6G dye and the drug resorcinol as model compounds, showing that release of small molecules is somewhat dominated by diffusion, and positively charged molecules which interact with the hydrogel network can be released in acidic media, for example targeting the stomach. The hydrogels were found to be moderately cytotoxic to HUVECs. Overall, these hydrogels with dual pH and redox response have potential to be used for different biomedical applications.

7. CONCLUDING REMARKS

Stimuli responsive polymers and hydrogels designed as bone tissue engineering scaffolds and platforms for controlled release were successfully synthesized and evaluated for their potential use in biomedical applications.

Phosphonate-functionalized redox-responsive and degradable PBAE based gels/cryogels were synthesized *via* subsequent step-growth polymerization and photopolymerization reactions. The variation in chemical structure of macromers and use of different gelation methods enabled the tailoring of physical properties. The degradation period ranged from a few hours to months. The degradation products were shown to be biocompatible with NIH 3T3 mouse embryonic fibroblast and Saos-2 human osteosarcoma cells. These results demonstrate that, the PBAE gels and cryogels can be regarded as successful candidates for tissue engineering applications.

Novel pH and redox-responsive PBAE hydrogels were prepared by a simple one-step synthesis strategy based on aza-Michael reaction which was probed by rheology studies. By selecting the building blocks the hydrophilicity/hydrophobicity and accordingly the physical properties including swelling and degradation behavior of the hydrogels were tailored. The hydrogels were easily loaded with a photosensitizer molecule by adding it into the precursor mixture. The hydrogels showed response to external triggers such as pH and redox state which served as a tool to facilitate the on-demand degradation of the hydrogel into nontoxic materials and release of the cargo molecule in a controlled manner. Photodynamic therapy was used to assess the biological activity of the released molecules. These hydrogels showed the potential to be used as platforms for controlled delivery of therapeutic agents.

The synthesis, characterization, and polymerization of three novel acrylamide monomers which contain Ca^{2+} binding phosphonic acid groups were achieved successfully.

These monomers were found to be hydrolytically stable, sufficiently reactive in photopolymerization as verified by photo-DSC and have interactions with hydroxyapatite as shown by FTIR and XRD, indicating their suitable properties to be used as self-etching dental adhesives. These monomers were incorporated into hydrogel scaffolds and immersed in SBF to facilitate mineralization. Mineral deposits were observed in SEM micrographs and EDX was used to verify the Ca and P content. Ca deposition assay was performed for the quantitative detection of Ca in mineralized scaffolds. These results imply that the phosphonic acid containing monomers are good candidates to be used for both dental and tissue engineering applications.

Novel carboxylic acid-functionalized crosslinkers were synthesized, characterized and their structure-reactivity relationship was investigated in bulk and in water using photo-DSC. This crosslinker was then used to fabricate HEMA based redox- and pH- responsive hydrogels. The morphology of hydrogels was shown by SEM, mechanical properties were investigated by rheology studies. The response of the hydrogels to stimuli such as pH and concentrations of compounds like CaCl_2 or DTT in the solution can be controlled by the crosslinker amount. The pH and redox dependant release were demonstrated by using R6G dye and the drug resorcinol as model compounds. The hydrogels were found to be moderately cytotoxic to HUVECs. Overall, these hydrogels with dual pH and redox response have potential to be used for different biomedical applications.

REFERENCES

1. Langer, R. and N. A. Peppas, “Advances in biomaterials, drug delivery, and bionanotechnology”, *AIChE J.*, Vol. 49, pp. 2990–3006, 2003.
2. Wang, Y., A. Guan, I. Isayeva, K. Vorvolakos, S. Das, Z. Li and K. S. Phillips, “Interactions of *Staphylococcus aureus* with ultrasoft hydrogel biomaterials”, *Biomaterials*, Vol. 95, pp. 74–85, 2016.
3. Hoffman, A.S., “Hydrogels for biomedical applications”, *Adv. Drug Deliv. Rev.*, Vol. 64, pp. 18–23, 2012.
4. Buwalda, S. J., K. W. M. Boere, P. J. Dijkstra, J. Feijen, T. Vermonden and W. E. Hennink, “Hydrogels in a historical perspective: From simple networks to smart materials”, *J. Control. Release*, Vol. 190, pp. 254–273, 2014.
5. Peppas, N.A.; J. Z. Hilt, A. Khademhosseini and R. Langer, “Hydrogels in biology and medicine: From molecular principles to bionanotechnology”, *Adv. Mater.*, Vol. 18, pp. 1345–1360, 2006.
6. Caló, E. and V. V. Khutoryanskiy, “Biomedical applications of hydrogels: A review of patents and commercial products”, *Eur. Polym. J.*, Vol. 65, pp. 252–267, 2015.
7. Duncan, R., “Polymer conjugates as anticancer nanomedicines”, *Nat. Rev. Cancer*, Vol. 6, pp. 688–701, 2006.
8. Duncan, R. “The dawning era of polymer therapeutics”, *Nat. Rev. Drug Discov.*, Vol. 2, pp. 347–360, 2003.
9. Ringsdorf, H. “Structure and properties of pharmacologically active polymers”, *J. Polym. Sci. Polym. Symp.*, Vol. 51, pp. 135–153, 2007.
10. Haag, R. and F. Kratz, “Polymer therapeutics: Concepts and applications”, *Angew. Chemie Int. Ed.*, Vol. 45, pp. 1198–1215, 2006.

11. Maeda, H., J. Wu, T. Sawa, Y. Matsumura and K. Hori, "Tumor vascular permeability and the EPR effect in macromolecular therapeutics : a review", *J Control Release*, Vol. 65, pp. 271–284, 2000.
12. Li, J. and D. J. Mooney, "Designing hydrogels for controlled drug delivery", *Nat. Rev. Mater.*, Vol. 1, no. 12, 2016.
13. Yu, L. and J. Ding, "Injectable hydrogels as unique biomedical materials" *Chem. Soc. Rev.*, Vol. 37, pp. 1473–1481, 2008.
14. Murphy, S. M., P. J. Skelly and B. J. Tighe, "Synthetic hydrogels. Part 9 - Preparation and characterisation of macroporous hydrophilic matrices" *J. Mater. Chem.* Vol. 2, pp. 1007–1013, 1992.
15. Oh, J. K., R. Drumright, D. J. Siegwart and K. Matyjaszewski, "The development of microgels/nanogels for drug delivery applications", *Prog. Polym. Sci.*, Vol. 33, pp. 448–477, 2008.
16. Soni, K. S., S. S. Desale and T. K. Bronich, "Nanogels: An overview of properties, biomedical applications and obstacles to clinical translation", *J. Control. Release*, Vol. 240, pp. 109–126, 2016.
17. Lee, K. Y. and D. J. Mooney, "Hydrogels for tissue engineering", *Chem. Rev.*, Vol. 101, pp. 1869–1879, 2001.
18. Abou Neel, E. A., W. Chrzanowski, V. M. Salih, H. W. Kim and J. C. Knowles, "Tissue engineering in dentistry", *J. Dent.*, Vol. 42, pp. 915–928, 2014.
19. Serbo, J. V. and S. Gerecht, "Vascular tissue engineering : biodegradable scaffold platforms to promote angiogenesis", *Stem Cell Res. Ther.*, Vol. 4, pp. 1–8, 2013.
20. Eslahi, N., M. Abdorahim and A. Simchi, "Smart polymeric hydrogels for cartilage tissue engineering: A review on the chemistry and biological functions", *Biomacromolecules*, Vol. 17, pp. 3441–3463, 2016.
21. Dalton, P. D. and T. Woodfi, "Polymeric scaffolds for bone tissue engineering", *Bone*, Vol. 32, pp. 2004–2005, 2008.

22. Salgado, A. J., O. P. Coutinho and R. L. Reis, “Bone tissue engineering: State of the art and future trends”, *Macromol. Biosci.*, Vol. 4, pp. 743–765, 2004.
23. Kaul, H. and Y. Ventikos, “On the genealogy of tissue engineering and regenerative medicine”, *Tissue Eng. Part B Rev.*, Vol. 21, pp. 203–217, 2015.
24. Khademhosseini, A. and R. Langer, “A decade of progress in tissue engineering”, *Nat. Protoc.*, Vol. 11, pp. 1775–1781, 2016.
25. Mulligan, R. C., “The basic science of gene therapy”, *Science*, Vol. 260, pp. 926–932, 1993.
26. Park, T. G., J. H. Jeong and S. W. Kim, “Current status of polymeric gene delivery systems”, *Adv. Drug Deliv. Rev.*, Vol. 58, pp. 467–486, 2006.
27. De Smedt, S. C., J. Demeester and W. E. Hennink, “Cationic polymer based gene delivery systems,” *Pharm. Res.*, Vol. 17, no. 2, pp. 113–126, 2000.
28. Aied, A., U. Greiser, A. Pandit and W. Wang, “Polymer gene delivery: Overcoming the obstacles”, *Drug Discov. Today*, Vol. 18, pp. 1090–1098, 2013.
29. Gajbhiye, V. and S. Gong, “Lectin functionalized nanocarriers for gene delivery”, *Biotechnol. Adv.*, Vol. 31, pp. 552–562, 2013.
30. Palmer, L. C., C. J. Newcomb, S. R. Kaltz, E. D. Spoerke and S. I. Stupp, “Biomimetic systems for hydroxyapatite mineralization inspired by bone and enamel biomimetic systems for hydroxyapatite mineralization inspired by bone and enamel”, *Chem. Rev.*, Vol. 108, pp. 4754–4783, 2008.
31. Milia, E., E. Cumbo, R. J. A. Cardoso and G. Gallina, “Current dental adhesive system: A Narrative Review”, *Curr. Pharm. Des.*, Vol. 18, pp. 5542–5552, 2012.
32. Van Landuyt, K. L., J. Snauwaert, J. De Muncka, M. Peumans, Y. Yoshida, A. Poitevin, E. Coutinho, K. Suzuki, P. Lambrechts and B. Van Meerbeek, “Systematic review of the chemical composition of contemporary dental adhesives”, *Biomaterials*, Vol. 28, pp. 3757–3785, 2007.
33. Moszner, N., U. Salz and J. Zimmermann, “Chemical aspects of self-etching enamel-

- dentin adhesives: A systematic review”, *Dent. Mater.*, Vol. 21, pp. 895–910, 2005.
34. Qiu, Y. and K. Park, “Environment-sensitive hydrogels for drug delivery”, *Adv. Drug Deliv. Rev.*, Vol. 64, pp. 49–60, 2012.
 35. Blum, A. P., J. K. Kammeyer, A. M. Rush, C. E. Callmann, M. E. Hahn and N. C. Gianneschi, “Stimuli-responsive nanomaterials for biomedical applications”, *J. Am. Chem. Soc.*, Vol. 137, no. 6, pp. 2140–2154, 2015.
 36. Hu, J. and S. Liu, “Responsive polymers for detection and sensing applications: Current status and future developments”, *Macromolecules*, Vol. 43, pp. 8315–8330, 2010.
 37. Kamaly, N., B. Yameen, J. Wu and O. C. Farokhzad, “Degradable controlled-release polymers and polymeric nanoparticles: Mechanisms of controlling drug release”, *Chem. Rev.*, Vol. 116, pp. 2602–2663, 2016.
 38. Gupta, P., K. Vermani and S. Garg, “Hydrogels: From controlled release to pH-responsive drug delivery”, *Drug Discov. Today*, Vol. 7, pp. 569–579, 2002.
 39. Schmaljohann, D., “Thermo- and pH-responsive polymers in drug delivery”, *Adv. Drug Deliv. Rev.*, Vol. 58, pp. 1655–1670, 2006.
 40. Kurkuri, M. D. and T. M. Aminabhavi, “Poly(vinyl alcohol) and poly(acrylic acid) sequential interpenetrating network pH-sensitive microspheres for the delivery of diclofenac sodium to the intestine”, *J. Control. Release*, Vol. 96, pp. 9–20, 2004.
 41. Cinay, G. E., P. Erkoc, M. Alipour, Y. Hashimoto, Y. Sasaki, K. Akiyoshi and S. Kizilel, “Nanogel-integrated pH-responsive composite hydrogels for controlled drug delivery”, *ACS Biomater. Sci. Eng.*, Vol. 3, pp. 370–380, 2017.
 42. Ninan, N., A. Forget, V. P. Shastri, N. H. Voelcker and A. Blencowe, “Antibacterial and anti-inflammatory pH-Responsive tannic acid-carboxylated agarose composite hydrogels for wound healing”, *ACS Appl. Mater. Interfaces*, Vol. 8, pp. 28511–28521, 2016.
 43. Zhang, X., Y. Huang, M. Ghazwani, P. Zhang, J. Li, S. H. Thorne and S. Li, “Tunable

- pH-responsive polymeric micelle for cancer treatment”, *ACS Macro Lett.*, Vol. 4, pp. 620–623, 2015.
44. Quinn, J. F., M. R. Whittaker and T. P. Davis, “Glutathione responsive polymers and their application in drug delivery systems”, *Polym. Chem.*, Vol. 8, pp. 97–126, 2017.
 45. Huo, M., M. J. Yuan, L. Tao and Y. Wei, “Redox-responsive polymers for drug delivery: from molecular design to applications”, *Polym. Chem.*, Vol. 5, 1519–1528, 2014.
 46. Meng, F., W. E. Hennink and Z. Zhong, “Reduction-sensitive polymers and bioconjugates for biomedical applications”, *Biomaterials*, Vol. 30, pp. 2180–2198, 2009.
 47. Le Neindre, M. and R. Nicolaÿ, “Polythiol copolymers with precise architectures: a platform for functional materials”, *Polym. Chem.*, Vol. 5, pp. 4601–4611, 2014.
 48. Ejaz, M., H. Yu, Y. Yan, D. A. Blake, R. S. Ayyala and S. M. Grayson, “Evaluation of redox-responsive disulfide cross-linked poly(hydroxyethyl methacrylate) hydrogels”, *Polymer*, Vol. 52, pp. 5262–5270, 2011.
 49. Andac, M., F. M. Plieva, A. Denizli, I. Y. Galaev and B. Mattiasson, “Poly(hydroxyethyl methacrylate)-based macroporous hydrogels with bisulfide cross-linker”, *Macromol. Chem. Phys.*, Vol. 209, pp. 577–584, 2008.
 50. Dispinar, T., W. Van Camp, L. J. De Cock, B. G. De Geest and F. E. Du Prez, “Redox-responsive degradable PEG cryogels as potential cell scaffolds in tissue engineering”, *Macromol. Biosci.*, Vol. 12, pp. 383–394, 2012.
 51. Gandhi, A., A. Paul, S. O. Sen and K. K. Sen, “Studies on thermoresponsive polymers: Phase behaviour, drug delivery and biomedical applications”, *Asian J. Pharm. Sci.*, Vol. 10, pp. 99–107, 2015.
 52. Karimi, M., P. S. Zangabad, A. Ghasemi, M. Amiri, M. Bahrami, H. Malekzad, H. G. Asl, Z. Mahdieh, M. Bozorgomid, A. Ghasemi, M. R. R. T. Boyuk and M. R. Hamblin, “Temperature-responsive smart nanocarriers for delivery of therapeutic agents: Applications and recent advances”, *ACS Appl. Mater. Interfaces*, Vol. 8, pp. 21107–

- 21133, 2016.
53. Huang, X. and T. L. Lowe, “Biodegradable thermoresponsive hydrogels for aqueous encapsulation and controlled release of hydrophilic model drugs”, *Biomacromolecules*, Vol. 6, pp. 2131–2139, 2005.
 54. Jones, D. S., C. P. Lorimer, C. P. McCoy and S. P. Gorman, “Characterization of the physicochemical, antimicrobial, and drug release properties of thermoresponsive hydrogel copolymers designed for medical device applications”, *J. Biomed. Mater. Res. - Part B Appl. Biomater.*, Vol. 85, pp. 417–426, 2008.
 55. Doorty, K. B., T. A. Golubeva, A. V. Gorelov, Y. A. Rochev, L. T. Allen, K. A. Dawson, W. M. Gallagher and A. K. Keenan, “Poly(N-isopropylacrylamide) copolymer films as potential vehicles for delivery of an antimitotic agent to vascular smooth muscle cells”, *Cardiovasc. Pathol.*, Vol. 12, pp. 105–110, 2003.
 56. Wei, H., X. Z. Zhang, W. Q. Chen, S. X. Cheng and R. X. Zhuo, “Self-assembled thermosensitive micelles based on Poly(L-lactide-star block-N-isopropylacrylamide) for drug delivery”, *J. Biomed. Mater. Res. A*, Vol. 83, pp. 980–989, 2007.
 57. Kumashiro, Y., M. Yamato and T. Okano, “Cell attachment-detachment control on temperature-responsive thin surfaces for novel tissue engineering”, *Ann. Biomed. Eng.*, Vol. 38, pp. 1977–1988, 2010.
 58. Ruel-Gariépy, E. and J. C. Leroux, “In situ-forming hydrogels - Review of temperature-sensitive systems”, *Eur. J. Pharm. Biopharm.*, Vol. 58, pp. 409–426, 2004.
 59. Cheng, R., F. Meng, C. Deng, H. A. Klok and Z. Zhong, “Dual and multi-stimuli responsive polymeric nanoparticles for programmed site-specific drug delivery”, *Biomaterials*, Vol. 34, pp. 3647–3657, 2013.
 60. Gan, J., X. Guan, J. Zheng, H. Guo, K. Wu, L. Liang and M. Lu, “Biodegradable, thermoresponsive PNIPAM-based hydrogel scaffolds for the sustained release of levofloxacin”, *RSC Adv.*, Vol. 6, no. 39, pp. 32967–32978, 2016.
 61. Zhang, B. Y., W. D. He, L. I. Y. Li, X. L. I. Sun, W. T. Li and K. E. R. Zhang,

- “Reducibly degradable hydrogels of PNIPAM and PDMAEMA: Synthesis, stimulus-response and drug release”, *J. Polym. Sci. Part A Polym. Chem.*, Vol. 48, pp. 3604–3612, 2010.
62. Ahiabu, A. and M. J. Serpe, “Rapidly responding pH-and temperature-responsive poly (N-isopropylacrylamide)-based microgels and assemblies”, *ACS Omega*, Vol. 2, pp. 1769–1777, 2017.
63. Gao, X., Y. Cao, X. Song, Z. Zhang, C. Xiao, C. He and X. Chen, “pH- and thermo-responsive poly(N-isopropylacrylamide-co-acrylic acid derivative) copolymers and hydrogels with LCST dependent on pH and alkyl side groups”, *J. Mater. Chem. B*, Vol. 1, pp. 5578–5587, 2013.
64. Dong, J., R. Zhang, X. Zhan, H. Yang, S. Zhu and G. Wang, “Triple stimuli-responsive polymers based on pyrene-functionalized poly(dimethylaminoethyl methacrylate): Synthesis, self-assembled nanoparticles and controlled release”, *Colloid Polym. Sci.*, Vol. 292, pp. 2735–2744, 2014.
65. Wang, L., M. Liu, C. Gao, L. Ma and D. Cui, “A pH-, thermo-, and glucose-, triple-responsive hydrogels: Synthesis and controlled drug delivery”, *React. Funct. Polym.*, Vol. 70, pp. 159–167, 2010.
66. Tian, H., Z. Tang, X. Zhuang, X. Chen and X. Jing, “Biodegradable synthetic polymers: Preparation, functionalization and biomedical application”, *Prog. Polym. Sci.*, Vol. 37, pp. 237–280, 2012.
67. Ulery, B. D., L. S. Nair and C. T. Laurencin, “Biomedical applications of biodegradable polymers”, *J. Polym. Sci. Part B Polym. Phys.*, Vol. 49, pp. 832–864, 2011.
68. Lynn, D. M. and R. Langer, “Degradable Poly (β -amino esters): Synthesis, characterization, and self-assembly with plasmid DNA,” *J. Am. Chem. Soc.* Vol. 122, pp. 10761–10768, 2000.
69. Lynn, D. M., D. G. Anderson, D. Putnam and R. Langer, “Accelerated discovery of synthetic transfection vectors: Parallel synthesis and screening of a degradable

- polymer library,” *J. Am. Chem. Soc.* Vol. 123, pp. 8155–8156, 2001.
70. Safranski, D. L., M. A. Lesniewski, B. S. Caspersen, V. M. Uriarte and K. Gall, “The effect of chemistry on the polymerization, thermo-mechanical properties and degradation rate of poly(β -amino ester) networks”, *Polymer*, Vol. 51, pp. 3130–3138, 2010.
 71. Hawkins, A. M., D. A. Puleo and J. Z. Hilt, “Effect of macromer synthesis time on the properties of the resulting poly(β -amino ester) degradable hydrogel”, *J. Appl. Polym. Sci.*, Vol. 122, pp. 1420–1426, 2011.
 72. Hawkins, A. M., T. A. Milbrandt, D. A. Puleo and J. Z. Hilt, “Synthesis and analysis of degradation, mechanical and toxicity properties of poly (β -amino ester) degradable hydrogels”, *Acta Biomater.*, Vol. 7, pp. 1956–1964, 2011.
 73. Brey, D. M., I. Erickson and J. A. Burdick, “Influence of macromer molecular weight and chemistry on poly(β -amino ester) network properties and initial cell interactions”, *J. Biomed. Mater. Res. A*, Vol. 85, pp. 731–741, 2009.
 74. Anderson, D. G., C. A. Tweedie, N. Hossain, S. M. Navarro, D. M. Brey, K. J. Van Vliet, R. Langer and J. A. Burdick, “A combinatorial library of photocrosslinkable and degradable materials”, *Adv. Mater.*, Vol. 18, no. 19, pp. 2614–2618, 2006.
 75. Safranski, D. L., D. Weiss, J. B. Clark, B. S. Caspersen, W. R. Taylor and K. Gall, “Effect of poly(ethylene glycol) diacrylate concentration on network properties and *in vivo* response of poly(β -amino ester) networks”, *J. Biomed. Mater. Res. A*, Vol. 96, pp. 320–329, 2011.
 76. Brey, D. M., J. L. Ifkovits, R. I. Mozia, J. S. Katz and J. A. Burdick, “Controlling poly(β -amino ester) network properties through macromer branching”, *Acta Biomaterialia*, Vol. 4, pp. 207–217, 2008.
 77. McBath, R. A. and D. A. Shipp, “Swelling and degradation of hydrogels synthesized with degradable poly(β -amino ester) crosslinkers”, *Polym. Chem.*, Vol. 1, pp. 860–865, 2010.

78. Biswal, D., P. P. Wattamwar, T. D. Dziubla and J. Z. Hilt, “A single-step polymerization method for poly(β -amino ester) biodegradable hydrogels”, *Polymer*, Vol. 52, pp. 5985–5992, 2011.
79. Lakes, A. L., C. T. Jordan, P. Gupta, D. A. Puleo, J. Z. Hilt and T. D. Dziubla, “Reducible disulfide poly(beta-amino ester) hydrogels for antioxidant delivery”, *Acta Biomater.*, Vol. 68, pp. 178–189, 2018.
80. Du, Y., H. Yan, S. Niu, L. Bai and F. Chai, “Facile one-pot synthesis of novel water-soluble fluorescent hyperbranched poly(amino esters)”, *RSC Adv.*, Vol. 6, pp. 88030–88037, 2016.
81. Wang, J. and H. Yang, “Superelastic and pH-responsive degradable dendrimer cryogels prepared by cryo-aza-Michael addition reaction”, *Sci. Rep.*, Vol. 8, pp. 1–10, 2018.
82. Tan, A. R., J. L. Ifkovits, B. M. Baker, D. M. Brey, R. L. Mauck and J. A. Burdick, “Electrospinning of photocrosslinked and degradable fibrous scaffolds” *J. Biomed. Mater. Res. A*, Vol. 87, pp. 1034–1043, 2008.
83. Metter, R. B., J. L. Ifkovits, K. Hou, L. Vincent, B. Hsu, L. Wang, R. L. Mauck and J. A. Burdick, “Biodegradable fibrous scaffolds with diverse properties by electrospinning candidates from a combinatorial macromer library”, *Acta Biomater.*, Vol. 6, no. 4, pp. 1219–1226, 2010.
84. Southan, A., M. Mateescu, V. Hagel, M. Bach, C. Schuh, C. Kleinhans, P. J. Kluger, S. Tussetschläger, I. Nuss, T. Haraszti, S. V. Wegner, J. P. Spatz, H. Boehm, S. Laschat and G. E. M. Tovar, “Toward controlling the formation, degradation behavior, and properties of hydrogels synthesized by aza-Michael reactions”, *Macromol. Chem. Phys.*, Vol. 214, no. 16, pp. 1865–1873, 2013.
85. González, G., X. Fernández-Francos, À. Serra, M. Sangermano and X. Ramis, “Environmentally-friendly processing of thermosets by two-stage sequential aza-Michael addition and free-radical polymerization of amine–acrylate mixtures”, *Polym. Chem.*, Vol. 6, pp. 6987–6997, 2015.

86. Retailleau, M., A. Ibrahim, C. Croutxé-Barghorn, X. Allonas, C. Ley and D. Le Nouen, “One-pot three-step polymerization system using double click Michael addition and radical photopolymerization”, *ACS Macro Lett.*, Vol. 4, pp. 1327–1331, 2015.
87. Safranski, D. L., J. C. Crabtree, Y. R. Huq and K. Gall, “Thermo-mechanical properties of semi-degradable Poly(β -amino ester)-co-methyl methacrylate networks under simulated physiological conditions”, *Polymer*, Vol. 52, pp. 4920–4927, 2011.
88. Safranski, D. L., D. Weiss, J. B. Clark, W. R. Taylor and K. Gall, “Semi-degradable poly(β -amino ester) networks with temporally controlled enhancement of mechanical properties”, *Acta Biomater.*, Vol. 10, pp. 3475–3483, 2014.
89. Park, H. S., J. E. Lee, M. Y. Cho, Y. W. Noh, M. H. Sung, H. Poo, K. S. Hong and Y. T. Lim, “pH-stimuli-responsive near-infrared optical imaging nanoprobe based on poly(γ -glutamic acid)/poly(β -amino ester) nanoparticles”, *Nanotechnology*, Vol. 22, no. 46, 2011.
90. Retailleau, M., J. Pierrel, A. Ibrahim, C. Croutxé-Barghorn and X. Allonas, “Sequenced click chemistry and photopolymerization: a new approach toward semi-interpenetrating polymer networks”, *Polym. Adv. Technol.*, Vol. 28, pp. 491–495, 2017.
91. Sankaranarayanan, J., E. Mahmoud, G. Kim, M. Morachis and A. Almutairi, “Multiresponse strategies to modulate nanoparticles” *ACS Nano*, Vol. 4, pp. 5930–5936, 2010.
92. Retailleau, M., A. Ibrahim, C. Croutxé-Barghorn and X. Allonas, “New design of highly homogeneous photopolymer networks for shape memory materials”, *RSC Adv.*, Vol. 6, pp. 47130–47133, 2016.
93. Guven, M. N., M. Seckin Altuncu, F. Demir Duman, T. N. Eren, H. Yagci Acar and D. Avci, “Bisphosphonate-functionalized poly(β -amino ester) network polymers”, *J. Biomed. Mater. Res. A*, Vol. 105, pp. 1412–1421, 2017.
94. Akyol, E., M. Tatliyuz, F. Demir Duman, M. N. Guven, H. Y. Acar and D. Avci,

- “Phosphonate-functionalized poly(β -amino ester) macromers as potential biomaterials”, *J. Biomed. Mater. Res. A*, Vol. 106, pp. 1390–1399, 2018.
95. Sunshine, J. C., S. B. Sunshine, I. Bhutto, J. T. Handa and J. J. Green, “Poly(β -amino ester)-nanoparticle mediated transfection of retinal pigment epithelial cells *in vitro* and *in vivo*”, *PLoS One*, Vol. 7, no. 5, 2012.
96. Tzeng, S. Y., H. Guerrero-Cázares, E. E. Martinez, J. C. Sunshine, A. Quiñones-Hinojosa Alfredo and J. J. Green, “Non-viral gene delivery nanoparticles based on Poly(β -amino esters) for treatment of glioblastoma”, *Biomaterials*, Vol. 32, pp. 5402–5410, 2011.
97. Kreuter, J., “Nanoparticles and microparticles for drug and vaccine delivery”, *J. Anat.*, Vol. 189, pp. 503–505, 1996.
98. Bhise, N. S., K. J. Wahlin, D. J. Zack and J. J. Green, “Evaluating the potential of poly(beta-amino ester) nanoparticles for reprogramming human fibroblasts to become induced pluripotent stem cells”, *Int. J. Nanomedicine*, Vol. 8, pp. 4641–4658, 2013.
99. Kamat, C. D., R. B. Shmueli, N. Connis, C. M. Rudin, J. J. Green and C. L. Hann, “Poly(β -amino ester) nanoparticle delivery of TP53 has activity against small cell lung cancer *in vitro* and *in vivo*,” *Mol. Cancer Ther.*, Vol. 12, pp. 405–415, 2013.
100. Kim, J., J. C. Sunshine and J. J. Green, “Differential polymer structure tunes mechanism of cellular uptake and transfection routes of poly(β -amino ester) polyplexes in human breast cancer cells”, *Bioconjug. Chem.*, Vol. 25, pp. 43–51, 2014.
101. Dold, N. M., Q. Zeng, X. Zeng and C. M. Jewell, “A poly(beta-amino ester) activates macrophages independent of NF- κ B signaling”, *Acta Biomater.*, Vol. 68, pp. 168–177, 2018.
102. Anderson, D. G., W. Peng, A. Akinc, N. Hossain, A. Kohn, R. Padera, R. Langer and J. A. Sawicki, “A polymer library approach to suicide gene therapy for cancer”, *Proc. Natl. Acad. Sci.*, Vol. 101, pp. 16028–16033, 2004.
103. Bishop, C. J., T. M. Ketola, S. Y. Tzeng, J. C. Sunshine, A. Urtti, H. Lemmetyinen, E. Vuorimaa-Laukkanen, M. Yliperttula and Jordan J. Green, “The effect and role of

- carbon atoms in poly(β -amino ester)s for DNA binding and gene delivery”, *J. Am. Chem. Soc.* Vol. 135, 6951–6957, 2013
104. Zugates, G. T., N. C. Tedford, A. Zumbuehl, S. Jhunjhunwala, C. S. Kang, L. G. Griffith, D. A. Lauffenburger, R. Langer and D. G. Anderson, “Gene delivery properties of end-modified poly(β -amino ester)s”, *Bioconjugate Chem.*, Vol. 18, 1887–1896, 2007.
 105. Segovia, N., P. Dosta, A. Cascante, V. Ramos and S. Borrós, “Oligopeptide-terminated poly(β -amino ester)s for highly efficient gene delivery and intracellular localization”, *Acta Biomaterialia*, Vol. 10, pp. 2147–2158, 2014.
 106. Jones, C. H., M. Chen, A. Ravikrishnan, R. Reddinger, G. Zhang, A. P. Hakansson and B. A. Pfeifer, “Mannosylated poly(beta-amino esters) for targeted antigen presenting cell immune modulation”, *Biomaterials*, Vol. 37, pp. 333–344, 2015.
 107. Zhao, J., L. Yang, P. Huang, Z. Wang, Y. Tan, H. Liu, J. Pan, C. Y. He and Z. Y. Chen “Synthesis and characterization of low molecular weight polyethyleneimine-terminated Poly(beta-amino ester) for highly efficient gene delivery of minicircle DNA”, *J. Colloid Interface Sci.*, Vol. 463. pp. 93–98, 2016.
 108. Y. Liu, D. Wu, Y. Ma, G. Tang, S. Wang, and C. He, “Novel poly (amino ester)s obtained from Michael addition polymerizations of trifunctional amine monomers with diacrylates : safe and efficient DNA carriers ”, *Chem. Commun.*, pp. 2630–2631, 2003.
 109. Wu, D., Y. Liu, X. Jiang, L. Chen, C. He, S. H. Goh and K. W. Leong, “Evaluation of hyperbranched poly(amino ester)s of amine constitutions similar to polyethlenimine for DNA delivery”, *Biomacromolecules*, Vol. 6, pp. 3166–3173, 2005.
 110. Wu, D., Y. Liu, X. Jiang, C. He and S. H. Goh, “Hyperbranched poly(amino ester)s with different terminal amine groups for DNA delivery”, *Biomacromolecules*, Vol. 7, pp. 1879–1883, 2006.
 111. Huang, J. Y., Y Gao, L. Cutlar, J. O’Keeffe-Ahern, T. Zhao, F. Lin, D. Zhou, S.

- McMahon, U. Greiser, W. Wang and W. Wang, "Tailoring highly branched poly(β -amino ester)s: a synthetic platform for epidermal gene therapy", *Chem. Commun.*, Vol. 51, pp. 8473–8476, 2015.
112. Zhou, D., Y. Gao, A. Aied, L. Cutlar, O. Igoucheva, B. Newland, V. Alexeeve, U. Greiser, J. Uitto and W. Wang "Highly branched poly(β -amino ester)s for skin gene therapy", *J Control Rel.*, Vol. 244, 336–346, 2016.
113. Gao, Y., J. Y. Huang, J. O’Keeffe-Ahern, L. Cutlar, D. Zhou, F. H. Lin and W. Wang, "Highly branched poly(β -amino esters) for non-viral gene delivery: high transfection efficiency and low toxicity achieved by increasing molecular weight", *Biomacromolecules*, Vol. 17, pp. 3640–3647, 2016.
114. Guk, K., H. Lim, B. Kim, M. Hong, G. Khang and D. Lee, "Acid-cleavable ketal containing poly(β -amino ester) for enhanced siRNA delivery", *Int J Pharm.*, Vol. 453, pp. 541–550, 2013.
115. Deng, X., N. Zheng, Z. Song, L. Yin and J. Cheng, *Biomaterials*, Vol. 35, pp. 5006–5015, 2014.
116. Yin, Q., Y. Gao, Z. Zhang, P. Zhang and Y. Li, "Bioreducible poly (β -amino esters)/shRNA complex nanoparticles for efficient RNA delivery", *J Control. Rel.*, Vol. 151, pp. 35–44, 2011.
117. Yin, Q., J. Shen, L. Chen, Z. Zhang, W. Gu and Y. Li, *Biomaterials*, "Overcoming multidrug resistance by co-delivery of Mdr-1 and survivin-targeting RNA with reduction-responsible cationic poly(β -amino esters)", Vol. 33, pp. 6495–6506, 2012.
118. Zugates, G. T., D. G. Anderson, S. R. Little, I. E. B. Lawhorn and R. Langer, "Synthesis of poly(β -amino ester)s with thiol-reactive side chains for DNA delivery", *J Am. Chem. Soc.*, Vol. 128, pp. 12726–12734, 2006.
119. Liu, S., Y. Gao, S. A. D. Zhou, U. Greiser, T. Guo, R. Guo and W. Wang, "Biodegradable highly branched poly(β -amino ester)s for targeted cancer cell gene transfection", *ACS Biomater. Sci. Eng.*, Vol. 3, pp. 1283–1286, 2017.
120. Hwang, S. J., M. S. Kim, J. K. Han, D. S. Lee, B. S. Kim, E. K. Choi, H. J. Park and

- J. S. Kim, "pH-Sensitivity control of PEG-poly(β -amino ester) block copolymer micelle", *Macromolecular Research*, Vol. 15, no. 5. pp. 437–442, 2007.
121. Cheng, T., R. Ma, Y. Zhang, Y. Ding, J. Liu, H. Ou, Y. An, J. Liu and L. Shi, "A surface-adaptive nanocarrier to prolong circulation time and enhance cellular uptake", *Chem. Commun.*, Vol. 51, pp. 14985–14988, 2015.
122. Yu, Y., X. Zhang and L. Qiu, "The anti-tumor efficacy of curcumin when delivered by size/charge-changing multistage polymeric micelles based on amphiphilic poly(β -amino ester) derivatives", *Biomaterials*, Vol. 35, pp. 3467–3479, 2014.
123. Huang, X., W. Liao, G. Zhang, S. Kang and C. Y. Zhang, "pH-sensitive micelles self-assembled from polymer brush (PAE-g-cholesterol)-b-PEG-b-(PAE-g-cholesterol) for anticancer drug delivery and controlled release", *Int. J. Nanomedicine*, Vol. 12, pp. 2215–2226, 2017.
124. Duan, Z., Y. J. Gao, Z. Y. Qiao, G. Fan, Y. Liu, D. Zhang and H. Wang, "A photoacoustic approach for monitoring the drug release of pH-sensitive poly(β -amino ester)s", *J. Mater. Chem. B*, Vol. 2, pp. 6271–6282, 2014.
125. Qiao, Z. Y., S.L. Qiao, G. Fan, Y.S. Fan, Y. Chen and H. Wang, "One-pot synthesis of pH-sensitive poly(RGD-co- β -amino ester)s for targeted intracellular drug delivery", *Polym. Chem.*, Vol. 5, pp. 844–853, 2014.
126. Tang, S., Q. Yin, Z. Zhang, W. Gu, L. Chen, H. Yu, Y. Huang, X. Chen, M. Xu and Y. Li, "Co-delivery of doxorubicin and RNA using pH-sensitive poly (β -amino ester) nanoparticles for reversal of multidrug resistance of breast cancer", *Biomaterials*, Vol. 35, pp. 6047–6059, 2014.
127. Qiao, Z. Y., C. Y. Hou, D. Zhang, Y. Liu, Y. X. Lin, H. W. An, X. J. Lib and H. Wang, "Self-assembly of cytotoxic peptide conjugated poly(β -amino ester)s for synergistic cancer chemotherapy", *J. Mater. Chem. B*, Vol. 3, pp. 2943–2953, 2015.
128. Wang, H., G. Wan, Y. Liu, B. Chen, H. Chen, S. Zhang, D. Wang, Q. Xiong, N. Zhang and Y. Wang, "Dual-responsive nanoparticles based on oxidized pullulan and a disulfide-containing poly(β -amino) ester for efficient delivery of genes and

- chemotherapeutic agents targeting hepatoma”, *Polym. Chem.*, Vol. 7, pp. 6340–6353, 2016.
129. Tang, S., Q. Yin, J. Su, H. Sun, Q. Meng, Y. Chen, L. Chen, Y. Huang, W. Gu, M. Xu, H. Yu, Z. Zhang and Y. Li. “Inhibition of metastasis and growth of breast cancer by pH-sensitive poly (β -amino ester) nanoparticles co-delivering two siRNA and paclitaxel”, *Biomaterials*, Vol. 48, pp. 1–15, 2015.
130. Bui, Q. N., Y. Li, M. S. Jang, D. P. Huynh, J. H. Lee and D. S. Lee, “Redox- and pH-sensitive polymeric micelles based on poly(β -aminoester)-grafted disulfide methylene oxide poly(ethylene glycol) for anticancer drug delivery”, *Macromolecules*, 48, 4046-4054, 2015.
131. Sabzevari A., K. Adibkia, H. Hashemi, B G. De Geest, N. Mohsenzadeh, F. Atyabi, M. H. Ghahremani, M. R. Khoshayand and R. Dinarvand, “Improved anti-inflammatory effects in rabbit eye model using biodegradable poly beta-amino ester nanoparticles of triamcinolone acetonide”, *Investig. Ophthalmol. Vis. Sci.*, Vol. 54, pp. 5520–5526, 2013.
132. Perni, S. and P. Prokopovich, “Poly-beta-amino-esters nano-vehicles based drug delivery system for cartilage,” *Nanomedicine Nanotechnology, Biol. Med.*, Vol. 13, pp. 539–548, 2017.
133. Fernando, I. R., D. P. Ferris, M. Frasconi, D. Malin, E. Strelakova, M. D. Yilmaz, M. W. Ambrogio, M. M. Algaradah, M. P. Hong, X. Chen, M. S. Nassar, Y. Y. Botros, V. L. Cryns and J. F. Stoddart, “Esterase- and pH-responsive poly(β -amino ester)-capped mesoporous silica nanoparticles for drug delivery”, *Nanoscale*, Vol. 7, 7178–7183, 2015
134. Sinani, G., M. Sessevmez , M. Koray-Gök, S. Özgümüş, A. Okyar, H. Oya-Alpar and E. Cevher, “Nasal vaccination with poly(β -amino ester)-poly(D,L-lactide-co-glycolide) hybrid nanoparticles”, *Int. J. Pharm.*, Vol. 529, pp. 1–14, 2017.
135. Shen, Y., H. Tang, Y. Zhan, E. A. Van Kirk and W. J. Murdoch, “Degradable Poly(β -amino ester) nanoparticles for cancer cytoplasmic drug delivery”, *Nanomedicine*, Vol. 5, pp. 192–201, 2009.

136. Devalapally, H., D. Shenoy, S. Little, R. Langer and M. Amiji, "Poly(ethylene oxide)-modified poly(beta-amino ester) nanoparticles as a pH-sensitive system for tumor-targeted delivery of hydrophobic drugs: Part 3. Therapeutic efficacy and safety studies in ovarian cancer xenograft model", *Cancer Chemother. Pharmacol.*, Vol. 59, no. 4, pp. 477–484, 2007.
137. Fang, C., F. M. Kievit, Y.-C. Cho, H. Mok, O. W. Press and M. Zhang, "Effect of cationic side-chains on intracellular delivery and cytotoxicity of pH sensitive polymer–doxorubicin nanocarriers", *Nanoscale*, Vol. 4, pp. 7012–7020, 2012.
138. Little, S. R., D. M. Lynn, S. V. Puram and R. Langer, "Formulation and characterization of poly (β amino ester) microparticles for genetic vaccine delivery", *J. Control. Release*, Vol. 107, pp. 449–462, 2005.
139. Gupta, P., S. P. Authimoolam, J. Z. Hilt and T. D. Dziubla, "Quercetin conjugated poly(β -amino esters) nanogels for the treatment of cellular oxidative stress", *Acta Biomaterialia*, Vol. 27, pp.194–204, 2015.
140. An, T., C. Zhang, X. Han, G. Wan, D. Wang, Z. Yang, Y. Wang, L. Zhang and Y. Wang "Hyaluronic acid-coated poly(β -amino) ester nanoparticles as carrier of doxorubicin for overcoming drug resistance in breast cancer cells", *RSC Adv.*, Vol. 6, pp. 38624–38636, 2016.
141. Newland, B., P. Wolff, D. Zhou, W. Wang, H. Zhang, A. Rosser, W. Wang and C. Werner, "Synthesis of ROS scavenging microspheres from a dopamine containing poly(β -amino ester) for applications for neurodegenerative disorders", *Biomater. Sci.*, Vol. 4, pp. 400–404, 2016.
142. Al Thaher, Y., S. Latanza, S. Perni and P. Prokopovich, "Role of poly-beta-amino-esters hydrolysis and electrostatic attraction in gentamicin release from layer-by-layer coatings", *J. Colloid Interface Sci.*, Vol. 526, pp. 35–42, 2018.
143. Tamer, Y. and B. Chen, "Lysine-derived, pH-sensitive and biodegradable poly(beta-aminoester urethane) networks and their local drug delivery behaviour", *Soft Matter*, Vol. 14, pp. 1195–1209, 2018.

144. Huynh, C. T., M. K. Nguyen, J. H. Kim, S. W. Kang, B. S. Kim and D. S. Lee, "Sustained delivery of doxorubicin using biodegradable pH/temperature-sensitive poly(ethylene glycol)-poly(β -amino ester urethane) multiblock copolymer hydrogels", *Soft Matter*, Vol. 7, pp. 4974–4982, 2011.
145. Monge, S., B. Canniccioni, A. Grailot and J. J. Robin, "Phosphorus-containing polymers : A great opportunity for the biomedical field", *Biomacromolecules*, Vol. 126, pp. 1973–1982, 2011.
146. Monge, S. and G. David, *Phosphorus-based polymers: From synthesis to applications*, The Royal Society of Chemistry, Cambridge, UK, 2014.
147. Russell, R. G., N. B. Watts, F. H. Ebetino and M. J. Rogers, "Mechanisms of action of bisphosphonates : similarities and differences and their potential influence on clinical efficacy", *Osteoporos Int.*, Vol. 19, pp. 733–759, 2008.
148. Ossipov, D. A., "Bisphosphonate-modified biomaterials for drug delivery and bone tissue engineering", *Expert Opin. Drug Deliv.*, Vol. 12, pp. 1443–1458, 2015.
149. Hochdörffer, K., K. Abu Ajaj, C. Schäfer-Obodozie and F. Kratz, "Development of novel bisphosphonate prodrugs of doxorubicin for targeting bone metastases that are cleaved pH dependently or by cathepsin B: Synthesis, cleavage properties, and binding properties to hydroxyapatite as well as bone matrix", *J. Med. Chem.*, Vol. 55, pp. 7502–7515, 2012.
150. Yewle, J. N., D. A. Puleo and L. G. Bachas, "Enhanced affinity bifunctional bisphosphonates for targeted delivery of therapeutic agents to bone", *Bioconjug Chem.*, Vol. 22, pp. 2496-2506, 2011.
151. Kubiček, V., J. Rudovský, J. Kotek, P. Hermann, L. V. Elst, R. N. Muller, Z. I. Kolar, H. T. Wolterbeek, J. A. Peters and I. Lukeš, "A bisphosphonate monoamide analogue of DOTA : A potential agent for bone targeting", *J. Am. Chem. Soc.*, Vol.127, pp. 16477–16485, 2005.
152. Gluz, E., S. Rudnick-glick, D. M. Mizrahi, R. Chen and S. Margel, "New biodegradable bisphosphonate vinylic monomers and near infrared fluorescent

- nanoparticles for biomedical applications”, *Polym. Adv. Technol.*, Vol. 25, pp. 499–506, 2014.
153. Wang, D., S. Miller, M. Sima and P. Kopec, “Synthesis and evaluation of water-soluble polymeric bone-targeted drug delivery systems”, *Bioconjug Chem.*, Vol. 14, pp. 853–859, 2003.
154. Travelet, C., A. Graillot and S. Monge, “Polymer chemistry synthesis of fatty phosphonic acid based polymethacrylamide by RAFT polymerization and self-assembly in solution”, *Polym. Chem.*, Vol. 5, pp. 2756–2767, 2014.
155. Blidi, I., O. Coutelier and M. Destarac, “Well-defined phosphonate-functional copolymers through RAFT copolymerization of dimethyl-p-vinylbenzylphosphonate”, *J. Polym. Sci. A*, Vol. 52, pp. 1–9, 2014.
156. Graillot, A., S. Monge, C. Faur and J. Robin, “Synthesis by RAFT of innovative well-defined (co)polymers from a novel phosphorus-based acrylamide monomer”, *Polym. Chem.*, Vol. 4 pp. 795–803, 2013.
157. Pan, H., M. Sima, P. Kopečková, K. Wu, S. Gao, J. Liu, D. Wang, S. C. Miller and J. Kopeček, “Biodistribution and pharmacokinetic studies of bone-targeting N-(2-hydroxypropyl)methacrylamide copolymer-alendronate conjugates.”, *Mol Pharm.*, Vol. 5, 548–558, 2008.
158. D'Souza, S., H. Murata, M. V. Jose, S. Askarova, Y. Yantsen, J. D. Andersen, C. D. Edington, W. P. Clafshenkel, R. R. Koepsel and A. J. Russell, “Biomaterials engineering of cell membranes with a bisphosphonate-containing polymer using ATRP synthesis for bone targeting”, *Biomaterials*, Vol. 35, pp. 1–12, 2014.
159. Sikavitsas, V. I., J. S. Temeno and A. G. Mikos, “Biomaterials and bone mechanotransduction”, *Biomaterials*, Vol. 22, pp. 2581–2593, 2001.
160. Agents, P. P., “Mimicking the nanostructure of bone: Comparison of polymeric process-directing agents”, *Polymers*, Vol. 3, pp. 10–35, 2011.
161. Chirila, T. V., “Calcification of synthetic polymers functionalized with negatively ionizable groups : A critical review”, *React. Func. Polm.*, Vol. 67, pp. 165–172, 2007.

162. Song, J., V. Malathong and C. R. Bertozzi, “Mineralization of synthetic polymer scaffolds: A bottom-up approach for the development of artificial bone”, *J. Am. Chem.*, Vol. 127, pp. 3366–3372, 2005.
163. Song, J., E. Saiz and C. R. Bertozzi, “A new approach to mineralization of biocompatible hydrogel scaffolds: An efficient process toward 3-dimensional bonelike composites”, *Am. Chem. Soc.*, Vol. 125, pp. 1236–1243, 2003.
164. Gemeinhart, R. A., C. M. Bare, R. T. Haasch and E. J. Gemeinhart, “Osteoblast-like cell attachment to and calcification of novel phosphonate-containing polymeric substrates”, *J Biomed. Mater. Res. A.*, Vol. 78, pp. 433-440, 2006.
165. Kim, S. Y. and S. C. Lee, “Thermo-responsive injectable hydrogel system based on poly (n-isopropylacrylamide-co-vinylphosphonic acid) I: Biomineralization and protein delivery”, *J App. Polym. Sci.*, Vol. 113, pp. 3460-3469, 2009.
166. Nuttelman, C. R., D. S. W. Benoit, M. C. Tripodi and K. S. Anseth, “The effect of ethylene glycol methacrylate phosphate in PEG hydrogels on mineralization and viability of encapsulated hMSCs”, *Biomaterials*, Vol. 27, pp. 1377–1386, 2006.
167. E. Kemal, K. O. Adesanya and S. Deb, “Phosphate based 2-hydroxyethyl methacrylate hydrogels for biomedical applications”, *J. Mater. Chem.*, Vol. 21, pp. 2237–2245, 2011.
168. Stancu, I. C., R. Filmon, C. Cincu, B. Marculescu, C. Zaharia and Y. Tourmen, “Synthesis of methacryloyloxyethyl phosphate copolymers and *in vitro* calcification capacity”, *Biomaterials*, Vol. 25, pp. 205–213, 2004.
169. Ghag, A. K., J. E. Gough and S. Downes, “The osteoblast and osteoclast responses to phosphonic acid containing poly(ϵ -caprolactone) electrospun scaffolds”, *Biomater. Sci.*, Vol. 2, pp. 233–241, 2014.
170. Wang, L., M. Zhang and B. Xu, “The first pamidronate containing polymer and copolymer”, *Chem. Commun.*, Vol. 42, pp. 2795–2797, 2006.
171. Yang, X., S. Akhtar, S. Rubino, K. Leifer, J. Hilborn and D. Ossipov, “Direct click synthesis of hybrid bisphosphonate-hyaluronic acid hydrogel in aqueous solution for

- biomineralization”, *Chem. Mater.*, Vol. 24, pp. 1690–1697, 2012.
172. Anbar, M., G. A. S. T. John and A. C. Scott, “Organic polymeric polyphosphonates as potential preventive agents of dental caries : *in vitro* experiments”, *J Dent Res.*, Vol. 53, pp. 867–878, 1974.
173. Farley, E. P., R. L. Jones and M. Anbar, “Improved adhesion of acrylic restorative materials to dental enamel by precoating with monomers containing phosphonate groups” *J. Dent. Res.*, Vol. 56, pp. 943–952, 1977.
174. Salz, U., F. Zeuner, N. Moszner and I. Vivadent, “Hydrolytic stability of self-etching adhesive systems”, *J Adhes Dent.*, Vol. 7, pp. 107–116, 2005.
175. Moszner, N., F. Zeuner, U. K. Fischer, V. Rheinberger, I. Ag and F. Schaan, “Monomers for adhesive polymers, 2a synthesis and radical polymerisation of hydrolytically stable acrylic phosphonic acids”, *Macromol. Chem. Phys.*, Vol. 200, pp. 1062–1067, 1999.
176. Moszner, N., F. Zeuner, S. Pfeiffer, I. Schurte, V. Rheinberger and M. Drache, “Monomers for adhesive polymers, 3a synthesis, radical polymerization and adhesive properties of hydrolytically stable phosphonic acid monomers”, *Macromol. Mater. Eng.*, Vol. 286, pp. 225–231, 2001.
177. Catel, Y., M. Degrange, L. Le Pluart, P. J. Madec, T. N. Pham, F. Chen and W. D. Cook, “Synthesis , photopolymerization , and adhesive properties of new bisphosphonic acid monomers for dental application”, *J. Polym. Sci. A*, Vol. 47, pp. 5258–5271, 2009.
178. Mou, L. and J. W. Nicholson, “Synthesis of a hydrophilic phosphonic acid monomer for dental materials”, *Chem. Commun.*, Vol. 5, pp. 345–346, 2000.
179. Sahin, G., D. Avci, O. Karahan and N. Moszner, “Synthesis and photopolymerizations of new phosphonated methacrylates from alkyl α -hydroxymethacrylates and glycidyl methacrylate”, *J. App. Polym. Sci.*, Vol. 114, pp. 97–106, 2009.
180. Akgun, B. and D. Avci, “Synthesis and evaluations of bisphosphonate-containing monomers for dental materials”, *J. Polym. Sci. A*, Vol. 50, pp. 4854–4863, 2012.

- [181. Akgun, B., E. Savci and D. Avci, "Synthesis and polymerizations of phosphonated-bis(methacrylamide)s for dental applications", *J. Polym. Sci. A*, Vol 50, pp. 801–810, 2012.
182. Bilgici, Z. S., O. Buyukgumus, A. Altin and D. Avci, "Synthesis and polymerizations of novel bisphosphonate-containing methacrylates derived from alkyl α -hydroxymethacrylates", *Polym. Int.*, Vol. 63, pp. 427–434, 2013.
183. Bilgici, Z. S., S. B. Turker and D. Avci, "Novel bisphosphonated methacrylates: synthesis, polymerizations, and interactions with hydroxyapatite", *Macromol. Chem Phys.*, Vol. 214, pp. 2324–2335, 2013.
184. Altin, A., B. Akgun, Z. S. Bilgici, S. B. Turker and D. Avci, "Synthesis, photopolymerization, and adhesive properties of hydrolytically stable phosphonic acid-containing (meth)acrylamides", *J. Polym. Sci. A*, Vol. 52, pp. 511–522, 2014.
185. Guven, M. N., E. Akyol, F. D. Duman, H. Y. Acar, O. Karahan and D. Avci, "Urea dimethacrylates functionalized with bisphosphonate/bisphosphonic acid for improved dental materials", *J. Polym. Sci. A*, Vol. 55, pp. 3195–3204, 2017.
186. Yoshida, Y., B. Van Meerbeek, Y. Nakayama, M. Yoshioka, J. Snauwaert, Y. Abe, P. Lambrechts, G. Vanherle and M. Okazaki, "Adhesion to and decalcification of hydroxyapatite by carboxylic acids", *J Dent Res.*, Vol. 80, pp. 1565-1569, 2001.
187. Song, W., Z. Tang, M. Li, S. Lv, H. Yu, L. Ma, X. Zhuang, Y. Huang and X. Chen "Tunable pH-sensitive poly(β -amino ester)s synthesized from primary amines and diacrylates for intracellular drug delivery", *Macromol. Biosci.*, Vol. 12, pp. 1375–1383, 2012.
188. Plieva, F. M., V. I. Lozinsky, H. Jungvid, B. Mattiasson, I. Y. Galaev and I. N. Savina, "Polymeric cryogels as promising materials of biotechnological interest", *Trends Biotechnol.*, Vol. 21, pp. 445–451, 2003.
189. Okay, O, "Polymeric cryogels macroporous gels with remarkable properties", Vol. 263., *Adv. Polym. Sci.* Vol 263, Springer, Switzerland, 2014.
190. Zhang, L., W. Liu, L. Lin, D. Chen and M. H. Stenzel, "Degradable disulfide core-cross-linked micelles as a drug delivery system prepared from vinyl functionalized

- nucleosides via the RAFT process”, *Biomacromolecules*, Vol. 9, pp. 3321–3331, 2008.
191. Wallin, R. F. and E. Arscott, A practical guide to ISO 10993–5: Cytotoxicity, *Med. Device Diagn. Ind.*, 20, 96–98, 1998.
 192. Liu, Y., Y. Li, D. Keskin and L. Shi, “Poly(β -amino esters): synthesis, formulations, and their biomedical applications”, *Adv. Healthc. Mater.*, Vol. 8, pp. 1–24, 2019.
 193. Li, Y., J. Rodrigues and H. Tomás, “Injectable and biodegradable hydrogels: gelation, biodegradation and biomedical applications”, *Chem. Soc. Rev.*, Vol. 41, pp. 2193–2221, 2012.
 194. Xu, Q., L. Guo, S. A. Y. Gao, D. Zhou, U. Greiser, J. Creagh-Flynn, H. Zhang, Y. Dong, L. Cutlar, F. Wang, W. Liu, W. Wang and W. Wang, “Injectable hyperbranched poly(β -amino ester) hydrogels with on-demand degradation profiles to match wound healing processes”, *Chem. Sci.*, Vol. 9, pp. 2179–2187, 2018.
 195. Xu, Q., M. Venet, W. Wang, J. Creagh-Flynn, X. Wang, X. Li, Y. Gao, D. Zhou, M. Zeng, I. Lara-Sáez, S. A. H. Tai and W. Wang, “Versatile hyperbranched poly(β -hydrazide ester) macromers as injectable antioxidative hydrogels”, *ACS Appl. Mater. Interfaces*, Vol. 10, pp. 39494–39504, 2018.
 196. Ormond, A. B. and H. S. Freeman, “Dye sensitizers for photodynamic therapy”, *Materials*, Vol. 6, pp. 817–840, 2013.
 197. Robertson, C. A., D. H. Evans and H. Abrahamse, “Photodynamic therapy (PDT): A short review on cellular mechanisms and cancer research applications for PDT”, *J. Photochem. Photobiol. B Biol.*, Vol. 96, pp. 1–8, 2009.
 198. Zhang, X., L. Y. Xia, X. Chen, Z. Chen and F. G. Wu, “Hydrogel-based phototherapy for fighting cancer and bacterial infection,” *Sci. China Mater.*, Vol. 60, pp. 487–503, 2017.
 199. Donnelly R.F., D. I. Morrow, M. T. McCrudden, A. Z. Alkilani, E. M. Vicente-Pérez, C. O'Mahony, P. González-Vázquez, P. A. McCarron and A. D. Woolfson, “Hydrogel-forming and dissolving microneedles for enhanced delivery of photosensitizers and precursors”, *Photochem. Photobiol.*, Vol. 90, pp. 641–647, 2014.

200. Fraix, A., R. Gref and S. Sortino, “A multi-photoresponsive supramolecular hydrogel with dual-color fluorescence and dual-modal photodynamic action”, *J. Mater. Chem. B*, Vol. 2, pp. 3443–3449, 2014.
201. Wang, Y., B. Han, R. Shi, L. Pan, H. Zhang, Y. Shen, C. Li, F. Huang and A. Xie, “Preparation and characterization of a novel hybrid hydrogel shell for localized photodynamic therapy”, *J. Mater. Chem. B*, Vol. 1, pp. 6411–6417, 2013.
202. Zhang, H., R. Shi, A. Xie, J. Li, L. Chen, P. Chen, S. Li, F. Huang and Y. Shen, “Novel TiO₂/PEGDA hybrid hydrogel prepared in situ on tumor cells for effective photodynamic therapy”, *ACS Appl. Mater. Interfaces*, Vol. 5, pp. 12317–12322, 2013.
203. Donnelly, R. F., C. M. Cassidy, R. G. Loughlin, A. Brown, M. M. Tunney, M. G. Jenkins and P. A. McCarron, “Delivery of Methylene Blue and meso-tetra (N-methyl-4-pyridyl) porphine tetra tosylate from cross-linked poly(vinyl alcohol) hydrogels: A potential means of photodynamic therapy of infected wounds”, *J. Photochem. Photobiol. B Biol.*, Vol. 96, pp. 223–231, 2009.
204. Fallows, S. J., M. J. Garland, C. M. Cassidy, M. M. Tunney, T. R. R. Singh and R. F. Donnelly, “Electrically-responsive anti-adherent hydrogels for photodynamic antimicrobial chemotherapy”, *J. Photochem. Photobiol. B Biol.*, Vol. 114, pp. 61–72, 2012.
205. Parsons, C., C. P. McCoy, S. P. Gorman, D. S. Jones, S. E. Bell, C. Brady and S. M. McGlinchey, “Anti-infective photodynamic biomaterials for the prevention of intraocular lens-associated infectious endophthalmitis”, *Biomaterials*, Vol. 30, pp. 597–602, 2009.
206. Spagnul, C., J. Greenman, M. Wainwright, Z. Kamil and R. W. Boyle, “Synthesis, characterization and biological evaluation of a new photoactive hydrogel against Gram-positive and Gram-negative bacteria”, *J. Mater. Chem. B*, Vol. 4, pp. 1499–1509, 2016.
207. Dos Santos, A. F., L. F. Terra, R. A. Wailemann, T. C. Oliveira, V. M. Gomes, M. F. Mineiro, F. C. Meotti, A. Bruni-Cardoso, M. S. Baptista and L. Labriola, “Methylene blue photodynamic therapy induces selective and massive cell death in human breast

- cancer cells”, *BMC Cancer*, Vol. 17, pp. 1–15, 2017.
208. Ateş, G. B., A. Ak, B. Garipcan and M. Gülsoy, “Methylene blue mediated photobiomodulation on human osteoblast cells”, *Lasers Med. Sci.*, Vol. 32, pp. 1847–1855, 2017.
209. Lim, E. J., C. H. Oak, J. Heo and Y. H. Kim, “Methylene blue-mediated photodynamic therapy enhances apoptosis in lung cancer cells”, *Oncol. Rep.*, Vol. 30, pp. 856–862, 2013.
210. Koo, H., H. Lee, S. Lee, K. H. Min, M. S. Kim, D. S. Lee, Y. Choi, I. C. Kwon, K. Kim and S. Y. Jeong, “*In vivo* tumor diagnosis and photodynamic therapy via tumoral pH-responsive polymeric micelles”, *Chem. Commun.*, Vol. 46, pp. 5668–5670, 2010.
211. Azizi, N. and M. R. Saidi, “LiClO₄ accelerated Michael addition of amines to α,β -unsaturated olefins under solvent-free conditions”, *Tetrahedron*, Vol. 60, pp. 383–387, 2004.
212. Xu, L. W., J. W. Li, S. L. Zhoua and C. G. Xia, “A green, ionic liquid and quaternary ammonium salt-catalyzed aza-Michael reaction of α,β -ethylenic compounds with amines in water”, *New J. Chem.*, Vol. 28, pp. 183–184, 2004.
213. Chaudhuri, M. K., S. Hussain, M. L. Kantam and B. Neelima, “Boric acid: A novel and safe catalyst for aza-Michael reactions in water”, *Tetrahedron Lett.*, Vol. 46, pp. 8329–8331, 2005.
214. Ranu, B. C. and S. Banerjee, “Significant rate acceleration of the aza-Michael reaction in water”, *Tetrahedron Lett.*, Vol. 48, pp. 141–143, 2007.
215. Abdurrahmanoglu, S., V. Can and O. Okay, “Design of high-toughness polyacrylamide hydrogels by hydrophobic modification”, *Polymer*, Vol. 50, pp. 5449–5455, 2009.
216. Okay, O., “Self-healing hydrogels formed via hydrophobic interactions”, *Adv. Polym. Sci.*, Vol. 268, pp. 101–142, 2015.
217. Calvet, D., J. Y. Wong and S. Giasson, “Rheological monitoring of polyacrylamide

- gelation: Importance of cross-link density and temperature”, *Macromolecules*, Vol. 37, pp. 7762–7771, 2004.
218. Giraldo, J., N. M. Vivas, E. Vila and A. Badia, “Assessing the (a)symmetry of concentration-effect curves”, *Pharmacol. Ther.*, Vol. 95, pp. 21–45, 2002.
219. Tavsanlı, B. and O. Okay, “Mechanically robust and stretchable silk/hyaluronic acid hydrogels”, *Carbohydr. Polym.*, Vol. 208, pp. 413–420, 2019.
220. Creton, C., “50th Anniversary perspective: Networks and gels: Soft but dynamic and tough”, *Macromolecules*, Vol. 50, pp. 8297–8316, 2017.
221. Sobhani, S. and Z. Tashrifi, “Al(OTf)₃ as an efficient catalyst for one-pot synthesis of primary diethyl 1-aminophosphonates under solvent-free conditions”, *Synth. Commun.*, Vol. 39, pp. 120–131, 2009.
222. Bakó, P., T. Novák, K. Ludányi, B. Pete, L. Tőke and G. Keglevich, “D-glucose-based azacrown ethers with a phosphonoalkyl side chain: Application as enantioselective phase transfer catalysts”, *Tetrahedron Asymmetry*, Vol. 10, pp. 2373–2380, 1999.
223. Yoshihara, K., Y. Yoshida, S. Hayakawa, N. Nagaoka, Y. Torii, A. Osaka, K. Suzuki, S. Minagi, B. Van Meerbeek and K. L. Van Landuyt, “Self-etch monomer-calcium salt deposition on dentin”, *J. Dent. Res.*, Vol. 90, pp. 602–606, 2011.
224. Brandrup, J. and E. H. Immergut, *Polymer Handbook*, Wiley-Interscience, New York, US, 1975.
225. Kokubo, T. and H. Takadama, “How useful is SBF in predicting *in vivo* bone bioactivity? ”, *Biomaterials*, Vol. 27, pp. 2907–2915, 2006.
226. Phadke, A., C. Zhang, Y. Hwang and K. Vecchio, “Templated mineralization of synthetic hydrogels for bone-like composite materials: Role of matrix hydrophobicity”, *Biomacromolecules*, Vol. 118, pp. 2060–2068, 2010.
227. Sasaki, S., K. Yataki and H. Maeda, “Effect of the hydrophobicity of chain on Ca²⁺ binding to ionic gels”, Vol. 7463, pp. 796–799, 1998.

228. Plunkett, K. N., M. L. Kraft, Q. Yu and J. S. Moore, "Swelling kinetics of disulfide cross-linked microgels", *Macromolecules*, Vol. 36, pp. 3960–3966, 2003.
229. Phadke, A., C. Zhang, B. Arman, C. C. Hsu, R. A. Mashelkar, A. K. Lele, M. J. Tauber, G. Arya and S. Varghese, "Rapid self-healing hydrogels", *Proc. Natl. Acad. Sci.*, Vol. 109, pp. 4383–4388, 2012.
230. Xu, J. and C. Xiao, "A facile route to obtain an acidic hydrogel containing lactate moieties", *React. Funct. Polym.*, Vol. 74, pp. 67–71, 2014.
231. Li, W., H. Zhao, P. R. Teasdale, R. John and S. Zhang, "Synthesis and characterisation of a polyacrylamide-polyacrylic acid copolymer hydrogel for environmental analysis of Cu and Cd", *React. Funct. Polym.*, Vol. 52, pp. 31–41, 2002.
232. Yetimoğlu, E. K., M. V. Kahraman, Ö. Ercan, Z. S. Akdemir and N. K. Apohan, "N-vinylpyrrolidone/acrylic acid/2-acrylamido-2-methylpropane sulfonic acid based hydrogels: Synthesis, characterization and their application in the removal of heavy metals", *React. Funct. Polym.*, Vol. 67, pp. 451–460, 2007.
233. Johnson, M. T., L. L. Komane, D. D. N'Da and E. W. Neuse, "Polymeric drug carriers functionalized with pairwise arranged hydroxyl and/or carboxyl groups for platinum chelation", *J. Appl. Polym. Sci.*, Vol. 96, pp. 10–19, 2005.
234. Park, S. E., Y. C. Nho, Y. M. Lim and H. Il Kim, "Preparation of pH-sensitive poly(vinyl alcohol-g-methacrylic acid) and poly(vinyl alcohol-g-acrylic acid) hydrogels by gamma ray irradiation and their insulin release behavior", *J. Appl. Polym. Sci.*, Vol. 91, pp. 636–643, 2004.
235. Taşdelen, B., N. Kayaman-Apohan, O. Güven and B. M. Baysal, "Anticancer drug release from poly(N-isopropylacrylamide/itaconic acid) copolymeric hydrogels", *Radiat. Phys. Chem.*, Vol. 73, pp. 340–345, 2005.
236. Wu, D. Q., Y. X. Sun, X. D. Xu, S. X. Cheng, X. Z. Zhang and R. X. Zhuo, "Biodegradable and pH-sensitive hydrogels for cell encapsulation and controlled drug release", *Biomacromolecules*, Vol. 9, pp. 1155–1162, 2008.
237. Tomić, S. L., M. M. Mičić, S. N. Dobić, J. M. Filipović and E. H. Suljovrujić, "Smart

- poly(2-hydroxyethyl methacrylate/itaconic acid) hydrogels for biomedical application”, *Radiat. Phys. Chem.*, Vol. 79, pp. 643–649, 2010.
238. Dadsetan, M., Z. Liu, M. Pumberger, C. V. Giraldo, T. Ruesink, L. Lu and M. J. Yaszemski, “A stimuli-responsive hydrogel for doxorubicin delivery”, *Biomaterials*, Vol. 31, pp. 8051–8062, 2010.
239. Li, Z., Z. Fan, Y. Xu, W. Lo, X. Wang, H. Niu, X. Li, X. Xie, M. Khan and J. Guan, “pH-sensitive and thermosensitive hydrogels as stem-cell carriers for cardiac therapy”, *ACS Appl. Mater. Interfaces*, Vol. 8, pp. 10752–10760, 2016.
240. Filmon, R., F. Grizon, M. F. Baslé and D. Chappard, “Effects of negatively charged groups (carboxymethyl) on the calcification of poly(2-hydroxyethyl methacrylate)”, *Biomaterials*, Vol. 23, pp. 3053–3059, 2002.
241. Grassmann, O. and P. Löbmann, “Biomimetic nucleation and growth of CaCO₃ in hydrogels incorporating carboxylate groups”, *Biomaterials*, Vol. 25, pp. 277–282, 2004.
242. Huang, J., G. Liu, C. Song, E. Saiz and A. P. Tomsia, “Role of molecular chemistry of degradable pHEMA hydrogels in three-dimensional biomimetic mineralization”, *Chem. Mater.*, Vol. 24, pp. 1331–1337, 2012.
243. Liu, C., X. Liu, C. Quan, X. Li, C. Chen, H. Kang, W. Hu, Q. Jiangab and C. Zhang, “Poly(γ -glutamic acid) induced homogeneous mineralization of the poly(ethylene glycol)-co-2-hydroxyethyl methacrylate cryogel for potential application in bone tissue engineering”, *RSC Adv.*, Vol. 5, pp. 20227–20233, 2015.
244. Warren, S. C. and L. J. Mathias, “Synthesis and polymerization of ethyl α -chloromethylacrylate and related derivatives”, *J. Polym. Sci. Part A.*, Vol. 28, pp. 1637–1648, 1990.
245. Gidon, D., D. Aydin and S. Kizilel, “Photocrosslinking of styrene-butadiene-styrene (SBS) networks formed by thiol-ene reactions and their influence on cell survival”, *Biomed. Mater.*, Vol. 10, 2015.
246. Peppas, N. A., H. J. Moyniha and L. M. Lucht, “The structure of highly crosslinked

- poly(2-hydroxyethyl methacrylate) hydrogels”, *J. Biomed. Mater. Res.*, Vol. 19, pp. 397–411, 1985.
247. Migliaresi, C., L. Nicodemo, L. Nicolais and P. Passerini, “Physical characterization of microporous poly(2-hydroxyethyl methacrylate) gels”, *J. Biomed. Mater. Res.*, Vol. 15, pp. 307–317, 1981.
248. Canal, T. and N. A. Peppas, “Correlation between mesh size and equilibrium”, *J. Biomed. Mater. Res.*, Vol. 23, pp. 1183–1193, 1989.
249. Choh, S. Y., D. Cross and C. Wang, “Facile synthesis and characterization of disulfide-cross-linked hyaluronic acid hydrogels for protein delivery and cell encapsulation”, *Biomacromolecules*, Vol. 12, pp. 1126–1136, 2011.
250. Jansen, J. F. G. A., A. A. Dias, M. Dorschu and B. Coussens, “Fast monomers: Factors affecting the inherent reactivity of acrylate monomers in photoinitiated acrylate polymerization”, *Macromolecules*, Vol. 36, pp. 3861–3873, 2003.
251. Lee, T. Y., T. M. Roper, E. S. Jönsson, C. A. Guymon and C. E. Hoyle, “Influence of hydrogen bonding on photopolymerization rate of hydroxyalkyl acrylates”, *Macromolecules*, Vol. 37, pp. 3659–3665, 2004.
252. Zhou, H., Q. Li, T. Y. Lee, C. A. Guymon, E. S. Jönsson and C. E. Hoyle, “Photopolymerization of acid containing monomers: Real-time monitoring of polymerization rates”, *Macromolecules*, Vol. 39, pp. 8269–8273, 2006.
253. Nejadnik, M. R., X. Yang, T. Mimura, Z. T. Birgani, P. Habibovic, K. Itatani, J. A. Jansen, J. Hilborn, D. Ossipov, A. G. Mikos and S. C. Leeuwenburgh, “Calcium-mediated secondary cross-linking of bisphosphonated oligo(poly(ethyleneglycol)fumarate) hydrogels”, *Macromol. Biosci.*, Vol. 13, pp. 1308–1313, 2013.
254. Kemnitz, M., M. Tabatabai, A. Utterodt and H. Ritter, “Phosphonate-containing polymeric networks: Swelling in water controlled by metal ions”, *Macromol. Chem. Phys.*, Vol. 216, pp. 314–320, 2015.
255. Endo, K., K. Murate and T. Otsu, “Living radical polymerization of styrene with

tetramethylene disulfide”, *Macromolecules*, Vol. 25, pp. 5554–5556, 1992.